UNIVERSITY OF OXFORD
DEPARTMENT OF ONCOLOGY

Analysis of nucleotide synthesis and homologous recombination repair in *Schizosaccharomyces pombe*

Elizabeth Jane Blaikley

A thesis presented for the degree of Doctor of Philosophy

Chromosome Integrity Group
Cancer Research UK and Medical Research Council Oxford Institute for Radiation Oncology
Department of Oncology
University of Oxford

Trinity Term 2014

CANCER RESEARCH UK | MRC Medical Research Council

OXFORD INSTITUTE FOR RADIATION ONCOLOGY

Analysis of nucleotide synthesis and homologous recombination repair in *Schizosaccharomyces pombe*

Elizabeth Blaikley
Wolfson College
Department of Oncology

Doctor of Philosophy
University of Oxford
Trinity Term 2014

Nucleotide synthesis is a conserved and highly regulated response to DNA damage, required for the efficient repair of DNA double strand breaks (DSB) by homologous recombination (HR). This is essential to prevent loss of heterozygosity (LOH) and maintain genome stability. The aim of this study was to identify new genes important for HR through roles in damage-induced nucleotide synthesis. A screen was performed to identify *S. pombe* gene deletion strains whose DSB sensitivity was suppressed by deleting the ribonucleotide reductase (RNR) inhibitor *spd1*$^+$ to promote nucleotide synthesis. The screen identified a number of genes including *ddb1*$^+$, *cdt2*$^+$, *rad3*$^+$ and *csn1*$^+$ which have known roles in nucleotide synthesis.

Distinct roles were identified for the DNA damage checkpoint in suppressing LOH. *rad3*$^+$, *rad26*$^+$, *rad17*$^+$ and the *rad9*$^+$, *rad1*$^+$ and *hus1*$^+$ genes encoding the 9-1-1 complex were required for DNA damage-induced nucleotide synthesis through Cdt2 induction to promote Spd1 degradation. The HR repair defect of *rad3* and *rad26* deletion strains was partially suppressed by *spd1*$^+$ deletion. However, the HR repair defect of *rad17*, *rad9*, *rad1* and *hus1* deletion strains was not suppressed. An additional role was confirmed for Rad17 and the 9-1-1 complex in preventing LOH by promoting DSB resection.

A role was identified for the Gcn5 histone acetyl transferase (HAT) protein module, consisting of Gcn5, Ngg1, Ada2 and Sgf29, in suppressing DSB sensitivity by promoting nucleotide synthesis. This was independent of Cdt2 or RNR protein levels. The Gcn5 HAT module was also found to regulate DSB repair pathway choice consistent with previous observations. Deletion of *gcn5*$^+$, *ngg1*$^+$ or *ada2*$^+$ decreased HR and increased non-homologous end joining. Surprisingly, deletion of *spd1*$^+$ in a *gcn5*Δ, *ngg1*Δ or *ada2*Δ background also promoted HR. This predicts a role for nucleotide pools in regulating DSB repair pathway choice.

Eleven other candidates showed repeatable suppression of DSB sensitivity following *spd1*$^+$ deletion. However many of these candidates did not show reduced nucleotide levels. This suggests deleting *spd1*$^+$ may also suppress DSB sensitivity by a different mechanism.

Acknowledgements

Firstly I would like to thank my supervisor Dr Timothy Humphrey for all his support and guidance over the past four years which has enabled me to complete this project. I am most grateful for all his help and encouragement. I would also like to thank the Medical Research Council for funding this project.

I would like to thank all of the members of the Humphrey laboratory past and present for making it such a lovely group to work in where I have made great friends. In particular I would like to thank Carol Walker for all her assistance with the Southern blotting and Sovan Sarkar for his help with proof reading. I would also like to thank Lisa Folkes for the HPLC analysis, the Kearsey group for use of their microscope and High Throughput Genomics at the Oxford Genomics Centre for the whole genome sequencing.

Finally I would like to thank my amazing family for all their love and support.

Declaration

I declare:

The work presented in this thesis is my own, with the exception of the HPLC analysis which was performed by Lisa Folkes, the radioactive steps of Southern blotting which were performed by Carol Walker and whole genome sequencing which was performed by High Throughput Genomics at the Oxford Genomics Centre.

No portion of this work has been previously submitted for another qualification at this, or any other university.

Signed ……..……

Elizabeth Jane Blaikley

Contents

Abstract i
Acknowledgements ii
Declaration iii
Contents iv
List of figures ix
List of tables xi
Nomenclature xii
Abbreviations xiii
Chapter 1 Introduction 1
1.1 MAINTAINING GENOME STABILITY 1
1.2 DNA DOUBLE STRAND BREAKS 2
1.2.1 DNA damage inducing agents 2
1.2.2 Enzymatically induced DSBs 3
1.3 DNA DOUBLE STRAND BREAK REPAIR 4
1.3.1 Non-homologous end joining 4
1.3.2 Homologous recombination 7
1.3.3 Single strand annealing 13
1.3.4 Break-induced replication 13
1.4 A SYSTEM FOR STUDYING DSB REPAIR IN *S. POMBE* 15
1.5 DNA INTEGRITY CHECKPOINTS 18
1.5.1 Sensing DNA damage 20
1.5.2 Transducing the signal 23
1.5.3 Arresting the cell cycle 24
1.6 REGULATION OF NUCLEOTIDE SYNTHESIS 25
1.6.1 Transcriptional regulation of RNR 26
1.6.2 Cullin-RING E3 ubiuitin ligases 27
1.6.3 Regulation of RNR activity by inhibitors 30
1.6.4 Regulation of RNR activity by proteosome degradation 33
1.7 AIMS OF THIS WORK 35
Chapter 2 Methods 36
2.1 GENERAL LABORATORY SUPPLIES 36
2.2 BUFFERS AND SOLUTIONS 37
2.3 MEDIA 39
2.4 PLASMIDS 40

2.5 STRAINS 41
2.5.1 *Escherichia coli* (*E. coli*) strains 41
2.5.2 *Schizosaccharomyces pombe* (*S. pombe*) strains 41
2.6 GROWTH AND STORAGE CONDITIONS 52
2.6.1 Growth and storage of *E. coli* strains 52
2.6.2 Growth and storage of *S. pombe* strains 52
2.7 GENETIC CROSSES 53
2.7.1 Crossing of *S. pombe* strains by free spore analysis 53
2.7.2 Crossing of *S. pombe* strains by tetrad dissection 53
2.7.3 Crossing of *S. pombe* strains in array format 53
2.8 DNA ISOLATION 54
2.8.1 Isolation of plasmid DNA from *E. coli* 54
2.8.2 Isolation of genomic DNA from *S. pombe* for general use 54
2.8.3 Isolation of genomic DNA from *S. pombe* for Southern blotting 54
2.8.4 Isolation of DNA from agarose gels 55
2.8.5 DNA purification by ethanol precipitation 55
2.9 DNA MANIPULATION AND ANALYSIS 55
2.9.1 Standard enzymatic restriction of DNA 55
2.9.2 Enzymatic restriction of DNA for Southern blotting 55
2.9.3 DNA ligation of linearised DNA 56
2.9.4 Polymerase chain reaction (PCR) using Taq DNA polymerase 56
2.9.5 Polymerase chain reaction (PCR) using Phusion™ high fidelity polymerase 56
2.9.6 Quantification of DNA samples 56
2.9.7 DNA sequencing 56
2.9.8 Whole genome sequencing 57
2.9.9 Standard analysis of DNA by gel electrophoresis 57
2.9.10 Analysis of genomic DNA by gel electrophoresis for Southern blotting 57
2.10 DNA TRANSFORMATION 57
2.10.1 Transformation of *E. coli* with DNA 57
2.10.2 Transformation of *S. pombe* with DNA by LiAc method 58
2.11 SOUTHERN BLOT ANALYSIS 58
2.11.1 Transfer of genomic DNA to nitrocellulose membrane 58
2.11.2 Radioactive labelling of probes 58
2.11.3 Southern blotting 59

2.12 ANALYSIS OF DNA DOUBLE STRAND BREAK REPAIR 60
2.12.1 Double strand break (DSB) assay 60
2.12.2 Rapid induction single strand annealing (SSA) assay 61
2.13 ANALYSIS OF CELL VIABILITY 62
2.13.1 Serial dilution assay 62
2.13.2 Screen 62
2.14 MICROSCOPY 62
2.14.1 Light microscopy 62
2.14.2 Fluorescence microscopy 63
2.15 FLUORESCENCE ACTIVATED CELL SORTING (FACS) 63
2.16 PROTEIN EXTRACTION, MANIPULATION AND ANALYSIS 64
2.16.1 TCA protein extraction 64
2.16.2 SDS-PAGE gel electrophoresis 64
2.16.3 Transfer 64
2.16.4 Western blotting 64
2.17 HIGH PERFORMANCE LIQUID CHROMATOGRAPHY (HPLC) NUCLEOTIDE POOL ANALYSIS 65
Chapter 3 A screen to identify genes important for HR through roles in DNA damage-induced nucleotide synthesis **67**
3.1 INTRODUCTION 67
3.2 RESULTS 69
3.2.1 Assembly of a library of DNA damage-sensitive deletion strains 69
3.2.2 The DNA damage-sensitive library was crossed with *spd1*Δ 71
3.2.3 Screen to identify deletion strains with altered DSB sensitivity following *spd1*$^{+}$ deletion 71
3.2.4 Calculating suppression of DSB sensitivity following *spd1*$^{+}$ deletion 73
3.2.5 Preliminary analysis of the screen 78
3.2.6 Identification of candidates with altered DSB sensitivity following *spd1*$^{+}$ deletion 81
3.2.7 Confirmation of the identity of the candidates 85
3.2.8 Confirming suppression of DSB sensitivity following *spd1*$^{+}$ deletion 89
3.2.9 Candidate strains express Cdt2 in response to DSBs 95
3.2.10 Analysis of DSB repair by the candidates 100
3.2.11 Analysis of candidate nucleotide pools 110
3.3 DISCUSSION 114

3.3.1 The DNA damage-sensitive deletion library 114
3.3.2 The identification of deletion strains with altered DSB sensitivity 115
following *spd1*$^{+}$ deletion
3.3.3 Analysis of candidate deletion strains 116
3.3.4 A role for Csn1 in nucleotide synthesis 118
3.3.5 The DSB sensitivity of *arp42*Δ was suppressed by deletion of *spd1*$^{+}$ 119
3.3.6 The DSB sensitivity of *trm112*Δ was suppressed by deletion of *spd1*$^{+}$ 120
3.3.7 The DSB sensitivity of *liz1*Δ was suppressed by deletion of *spd1*$^{+}$ 122
3.3.8 The DSB sensitivity of *pmk1*Δ was suppressed by deletion of *spd1*$^{+}$ 123
3.3.9 The DSB sensitivity of *swi3*Δ was suppressed by deletion of *spd1*$^{+}$ 123
3.3.10 Other candidates 124
3.4 SUMMARY 125
Chapter 4 A role for the DNA damage checkpoint promoting nucleotide synthesis and DSB resection 126
4.1 INTRODUCTION 126
4.2 RESULTS 127
4.2.1 Deletion of *spd1*$^{+}$ suppresses the DSB sensitivity of *rad3*Δ and *rad26*Δ but not 9-1-1 complex gene deletion strains 127
4.2.2 Deletion of *spd1*$^{+}$ suppresses the HR defect of *rad3*Δ and *rad26*Δ 127
4.2.3 Deletion of *spd1*$^{+}$ cannot suppress the HR defect of the 9-1-1 complex gene deletion strains 131
4.2.4 The DNA damage checkpoint is required for DSB-induced accumulation of Cdt2 133
4.2.5 A role for the 9-1-1 complex in DSB resection 136
4.2.6 Investigating the mechanism by which the checkpoint regulates resection 142
4.3 DISCUSSION 146
4.3.1 Deletion of *spd1*$^{+}$ suppresses HR defect of *rad3*Δ and *rad26*Δ 146
4.3.2 Deletion of *spd1*$^{+}$ cannot suppress the HR defect of 9-1-1 complex gene deletion strains 147
4.3.3 A role for the DNA damage checkpoint in DNA damage-induced nucleotide synthesis 147
4.3.4 A role for the 9-1-1 complex in facilitating DSB resection 148
4.3.5 Investigating the mechanism by which the checkpoint regulates resection 149
4.4 SUMMARY 151
Chapter 5 A role for Ngg1 and the Gcn5 HAT protein module promoting 152

nucleotide and synthesis homologous recombination
5.1 INTRODUCTION 152
5.2 RESULTS 155
5.2.1 Deletion of *spd1*$^+$ suppresses the DSB sensitivity and HR defect of *ngg1*Δ ... 155
5.2.2 Deletion of *spd1*$^+$ suppresses the DSB sensitivity and HR defect of 157
Gcn5 HAT module gene deletion strains
5.2.3 Deletion of *ngg1*$^+$ and *gcn5*$^+$ decreases cellular nucleotide pools 162
5.2.4 Exogenous nucleosides suppress the DSB sensitivity of *rad3*Δ, *ngg1*Δ 164
and *gcn5*Δ
5.2.5 Deletion of *ngg1*$^+$ does not affect Cdt2 induction in response to DSB 165
5.2.6 Deletion of *ngg1*$^+$ does not affect RNR protein levels 165
5.2.7 Deletion of *ngg1*$^+$ increases repair by NHEJ and SCC 168
5.2.8 Deletion of *ngg1*$^+$ does not affect the cell cycle during the DSB assay 172
5.2.9 A redundant role for *gcn5*$^+$ in suppressing DSB sensitivity 174
5.3 DISCUSSION 176
5.3.1 A role for the Gcn5 HAT module in DNA damage-induced nucleotide 176
synthesis
5.3.2 A role for the Gcn5 HAT module in DSB repair pathway choice 178
5.3.3 Deletion of *spd1*$^+$ suppresses the HR defect of Gcn5 HAT module 180
deletion strains
5.3.4 Gcn5 and other HATs cooperate to suppress DSB sensitivity 183
5.4 SUMMARY 184
Chapter 6 General Discussion 185
6.1 A role for Csn1 in promoting nucleotide synthesis 187
6.2 A role for the DNA damage checkpoint promoting damage-induced nucleotide 187
synthesis and DSB resection
6.3 A role for Ngg1 and the Gcn5 HAT module promoting nucleotide synthesis and HR .. 188
6.4 Deletion of *spd1*$^+$ promotes HR in *arp42*Δ, *liz1*Δ, and V2-53D9 backgrounds 190
independently of nucleotide synthesis
6.5 Deletion of *spd1*$^+$ suppresses DSB sensitivity in *swi3*Δ, *pmk1*Δ, and *trm112*Δ 191
backgrounds independently of nucleotide synthesis
6.6 Other Candidates 191
6.6 Investigating DSB repair in the context of chromatin 192
References 195
Appendices 211

List of figures

Figure 1.1 Non-homologous end joining in mammalian cells 5
Figure 1.2 Homologous recombination in *S. pombe* 8
Figure 1.3 A bidirectional model for DSB resection in mammalian cells 11
Figure 1.4 Single strand annealing and break-induced replication..... 14
Figure 1.5 The DSB assay..... 16
Figure 1.6 The DNA integrity checkpoints in *S. pombe*..... 21
Figure 1.7 Cullin-RING E3 ubiquitin ligases..... 28
Figure 1.8 Regulation of RNR in *S. pombe* and *S. cerevisiae* by small intrinsically disordered proteins 31
Figure 1.9 DSB-induced nucleotide synthesis promotes efficient HR in *S. pombe*..... 34
Figure 3.1 *S. pombe* haploid deletion library 68
Figure 3.2 Comparison of screens to identify DNA damage-sensitive deletion strains 70
Figure 3.3 PEM-2 high throughput mating 72
Figure 3.4 Overview of the screen..... 74
Figure 3.5 Screen calculations..... 76
Figure 3.6 Preliminary analysis of the screen 79
Figure 3.7 Identification of candidates with altered DNA damage sensitivity following *spd1*$^{+}$ deletion 82
Figure 3.8 Screen strains show both decreased and increased sensitivity to DSBs following *spd1*$^{+}$ deletion 83
Figure 3.9 Confirmation of the identity of candidate gene deletion strains..... 86
Figure 3.10 The identity of V2-53D9 and V2-53C11 could not be confirmed..... 87
Figure 3.11 Whole genome sequencing of V2-53D9 90
Figure 3.12 V2-53D9 corresponds to deletion of *nup132*$^{+}$..... 91
Figure 3.13 Deletion of *spd1*$^{+}$ suppresses the DSB sensitivity of Cul4-Ddb1^{Cdt2} complex members 92
Figure 3.14 Deletion of *spd1*$^{+}$ suppresses the DSB sensitivity of candidate deletion strains..... 93
Figure 3.15 Deletion of *spd1*$^{+}$ cannot reproducibly suppress the DSB sensitivity of of some candidates 94
Figure 3.16 The DSB sensitivity of *rad17*Δ is affected by background markers..... 96
Figure 3.17 DSB-induced nuclear accumulation of Cdt2-YFP..... 97

Figure 3.18 DSB-induced changes in the total levels of Cdt2-YFP for the candidate strains 99
Figure 3.19 Candidate strains showed DSB-induced nuclear accumulation of Cdt2-YFP 101
Figure 3.20 DSB analysis of candidate strains 105
Figure 3.21 DSB analysis of candidate strains and the corresponding *spd1*Δ strains 107
Figure 3.22 *csn1*Δ, *rpp202*Δ, *atp2*Δ and *arp42*Δ have compromised nucleotide pools 112
Figure 3.23 Candidate strains do not have compromised nucleotide pools 113
Figure 4.1 Deletion of *spd1*$^+$ suppresses the DSB sensitivity of *rad3*Δ and *rad26*Δ but not 9-1-1 gene deletion strains 128
Figure 4.2 The identity of the checkpoint deletion strains was confirmed 129
Figure 4.3 Deletion of *spd1*$^+$ suppresses the HR defect of *rad3*Δ and *rad26*Δ..... 130
Figure 4.4 Deletion of *spd1*$^+$ cannot suppress the HR defect of 9-1-1 complex gene deletion strains 132
Figure 4.5 Checkpoint deletion strains did not show DSB-induced nuclear accumulation of Cdt2-YFP 134
Figure 4.6 SSA assay 137
Figure 4.7 The 9-1-1 complex promotes DSB resection..... 138
Figure 4.8 DSB resection in the SSA assay is predominantly Exo1-dependent 143
Figure 5.1 H3K36 chromatin switch regulates DSB repair pathway choice 154
Figure 5.2 Deletion of *spd1*$^+$ suppresses the DSB sensitivity and HR defect of *ngg1*Δ..... 156
Figure 5.3 Screen results for the Gcn5 HAT module gene deletion strains..... 158
Figure 5.4 Deletion of *spd1*$^+$ suppresses the DSB sensitivity and HR defect of Gcn5 HAT module gene deletion strains 161
Figure 5.5 Deletion of *ngg1*$^+$ and *gcn5*$^+$ decreases cellular nucleotide pools..... 163
Figure 5.6 Increasing cellular nucleotide pools suppresses the DSB sensitivity of *rad3*Δ, *gcn5*Δ and *ngg1*Δ 166
Figure 5.7 Deletion of *ngg1*$^+$ does not affect RNR protein levels 167
Figure 5.8 Deletion of *ngg1*$^+$ increases repair by NHEJ..... 169
Figure 5.9 Deletion of *ngg1*$^+$ does not affect DSB induction 171
Figure 5.10 The majority of *ngg1*Δ cells are in G2 at the time of DSB induction 173
Figure 5.11 Deletion of *gcn5*$^+$ increases the DSB sensitivity of other HAT gene deletion strains 175
Figure 5.12 Model of DSB repair pathway regulation by nucleotide synthesis..... 182

List of tables

Table 1.1 Homologous recombination proteins in *S. pombe, S. cerevisiae* and humans.... 7
Table 1.2 Checkpoint proteins in *S. pombe, S. cerevisiae* and humans 19
Table 1.3 RNR subunit compositions in *S. pombe, S. cerevisiae* and humans 26
Table 2.1 Non-minichromosome *S. pombe* strains used in this study 41
Table 2.2 Minichromosome *S. pombe* strains transformed with REP81X plasmids 49
Table 2.3 Minichromosome *S.pombe* strains transformed with REP41X plasmids 51
Table 2.4 Primary antibodies used in this study 65
Table 3.1 Gene ontology (GO) terms of the top candidates 84
Table 6.1 Summary of Results 186

Nomenclature

Schizosaccharomyces pombe

Genes are denoted by lower-case letters in italics. Genes in the wild-type locus given the $^{+}$ suffix e.g. *rad3*$^{+}$. Deletion/null mutants are denoted by Δ e.g. *rad3*Δ. A double colon (::) indicates an insertion into the genome disrupting the gene in question e.g. *rad3::ura4* signifies the *rad3* gene disrupted by *ura4*. Letters and numbers following the gene name identify mutant alleles e.g. *ade6-M210*. Protein names are given an initial capital letter followed by lower-case letters in non-italics e.g. Rad3.

Saccharomyces cerevisiae

Genes are denoted by capital letters in italics e.g. *MEC1*. Deletion/null mutants are indicated by lower-case italics e.g. *mec1* with a suffix designating the allele where necessary e.g. *mre11-D65N*. Protein names are given an initial capital letter followed by lower-case letters in non-italics e.g. Mec1.

Mammalian/human

Genes are denoted by capital letters in italics e.g. *ATM*. Homozygous/heterozygous knockouts are shown as -/- or +/- respectively e.g. ATM -/- and ATM +/-. Protein names are denoted by capital letters in non-italics e.g. ATM.

Abbreviations

°C	degree Celsius
Δ	gene deletion
µg	micrograms
µl	microlitre
µM	micromolar
4-NQO	4-nitroquinoline 1-oxide
9-1-1 complex	Rad9-Rad1-Hus1 complex
A	adenine
ATP	adenosine triphosphate
BIR	break-induced replication
bp	base pairs
BSA	bovine serum albumin
CDK	cyclin-dependent kinase
CFP	cyan fluorescent protein
Ch	chromosome
Ch^{16}	minichromosome 16
CPT	camptothecin
CRL	cullin-RING E3 ubiquitin ligases
dA	deoxyadenosine
DAPI	4', 6-diamidino-2-phenylindole
dATP	deoxyadenosine triphosphate
dC	deoxycytidine
dCTP	deoxycytidine triphosphate
DDR	DNA damage response
dG	deoxyguanosine
dGTP	deoxyguanosine triphosphate
dHJ	double Holliday junction
D loop	displacement loop
*dm*NK	*Drosophila melanogaster* deoxynucleoside kinase
dN	deoxynucleosides
DNA	deoxyribonucleic acid
dNMP	deoxynucleoside monophosphates
dNTP	deoxyribonucleotide triphosphate
DSB	DNA double strand break
dsDNA	double stranded DNA
dT	thymidine
DTT	dithiothreitol
dTTP	deoxythymidine triphosphate
E. coli	*Escherichia coli*
E1	ubiquitin activating enzyme
E2	ubiquitin conjugating enzyme
E3	ubiquitin ligating enzyme
EDTA	ethylenediaminetetraacetic acid
EMM	Edinburgh minimal media
FACS	fluorescence activated cell sorting
FRET	fluorescence resonance energy transfer
g	grams
GC	gene conversion
Gcn5 HAT module	Gcn5-Ada2-Ngg1-Sgf29 histone acetyl transferase module

GFP	green fluorescent protein
GO	gene ontology
H	histidine
HAT	histone acetyl transferase
hENT1	human equilibrative nucleoside transporter 1
HO	*S. cerevisiae* homothallic endonuclease
HPLC	high performance liquid chromatography
HR	homologous recombination
HRP	horse radish peroxidase
HU	hydroxyurea
IR	ionising radiation
Kb	kilobase
kDa	kilodalton
L	leucine
L	litre
LB	lysogeny broth
LMT	low melting temperature
LOH	loss of heterozygosity
M	molar
MBF	Mlu1-box binding factor
MBq	megabecquerel
mg	milligrams
ml	millilitre
mM	millimolar
MMEJ	micro-homology mediated end joining
MMS	methylmethane sulphonate
MQ	Milli-Q® water
MRN	Mre11-Rad50-Nbs1 complex
MTL	mating type locus
NEB	New England Biolabs
ng	nanograms
NHEJ	non-homologous end joining
nm	nanometres
nmt	no message in thiamine
NTP	ribonucleotide triphosphate
OD_{595}	optical density 595 nm
p	p-value for student's T-test
PBS	phosphate buffered saline
PCNA	proliferating cell nuclear antigen
PCR	polymerase chain reaction
PEM-2	*pombe* epistasis mapper 2
PI3K	phosphatidylinositol 3′ kinase
PMG	*pombe* glutamate media
R	arginine
RFC	replication factor C
RNR	ribonucleotide reductase
RPA	replication protein A
rpm	revolutions per minute
S. cerevisiae	*Saccharomyces cerevisiae*
S. pombe	*Schizosaccharomyces pombe*
SCC	sister chromatid conversion
SD	standard deviation

SDS	sodium lauryl sulphate
SDSA	synthesis-dependent strand annealing
SDS-PAGE	sodium lauryl sulphate-polyacrylamide
*sens*Δ	DNA damage sensitive gene deletion strain
SSA	single strand annealing
SSB	single strand break
ssDNA	single stranded DNA
SSPE	saline sodium phosphate EDTA
T	thiamine
TAE	tris acetate EDTA
TCA	trichloroacetic acid
TE	tris EDTA
U	units
U	uracil
Ub	ubiquitin
UV	ultraviolet
V	volts
V1	version 1 *S. pombe* haploid deletion library
V2	version 2 *S. pombe* haploid deletion library
YE6S	yeast extract six supplements
YFM	yeast freezer mix
YFP	yellow fluorescent protein

Chapter 1 Introduction

This thesis presents a study to identify and characterise new genes important for homologous recombination (HR) repair of DNA double strand breaks (DSBs) through roles in damage-induced nucleotide synthesis in *Schizosaccharomyces pombe* (*S. pombe*). Therefore this introduction will focus on the mechanisms of DSB repair and the regulation of nucleotide synthesis.

1.1 MAINTAINING GENOME STABILITY

Genome instability is recognised as a hallmark of cancer, enabling cells to acquire the genetic mutations necessary for tumour progression (Hanahan and Weinberg, 2011). Cancer cells exhibit a wide range of chromosomal aberrations including deletions, truncations, translocations, and amplifications. Whilst many of the resulting genetic mutations are effectively passengers with no benefit to cell fitness, mutant genotypes which confer a selective advantage to the cells can lead to clonal expansion and disease progression (Nik-Zainal *et al.*, 2012; Stephens *et al.*, 2011; Stephens *et al.*, 2009). A selective advantage may be conferred by the activation of oncogenes or by the inactivation of tumour suppressors through loss of heterozygosity (LOH), when the remaining functional allele of a gene is lost (Knudson, 1993; Lasko *et al.*, 1991).

Chromosomal rearrangements and genome instability occur as a result of failure to repair DSBs or incorrectly repaired DSBs, which are considered to be the most dangerous of DNA lesions (Kasparek and Humphrey, 2011). Genome stability is normally maintained by the DNA damage response (DDR) which acts to sense DNA damage, mediate an appropriate cellular response and conduct repair. The DDR integrates both DNA repair pathways and the

DNA integrity checkpoints (Jackson and Bartek, 2009; Ljungman, 2010). Both will be discussed in more detail in this introduction with respect to the repair of DSBs.

As a consequence of their integral role in maintaining genome stability, many DDR genes are considered to be tumour suppressors. Mutation of these genes predisposes to a wide range of cancers and diseases associated with genome instability (Jackson and Bartek, 2009; Kasparek and Humphrey, 2011). Furthermore, many DDR components are highly conserved in eukaryotes (Table 1.1 and Table 1.2). As *S. pombe* can be easily grown and genetically manipulated in the laboratory, it provides a good model for studying the DDR. Using *S. pombe* it has been demonstrated that deletion of genes involved in DSB repair by HR leads to extensive break-induced LOH (Moss *et al.*, 2010; Tinline-Purvis *et al.*, 2009).

1.2 DNA DOUBLE STRAND BREAKS

DSBs are a highly cytotoxic form of DNA damage. DSBs occur during the normal cell cycle as a result of stalled replication forks or the generation of hydroxyl free radicals by metabolism. DSBs are also formed during programmed events such as yeast mating type switching or V(D)J recombination. Alternatively they can be caused by exogenous agents as discussed below (Kasparek and Humphrey, 2011; Mahaney *et al.*, 2009).

1.2.1 DNA damage inducing agents

Ionising radiation (IR) can damage DNA directly through the deposition of energy, or through the generation of hydroxyl radicals. This results in a wide range of DNA damage including DNA single strand breaks (SSB) and damage to the DNA bases or deoxyribose sugars. If two SSBs occur in close proximity, on opposite strands of the DNA helix, this leads to the formation of DSBs which normally have single stranded DNA (ssDNA) overhangs. IR can

also lead to clusters of DNA damage which result in DSBs through failed repair (Dianov *et al.*, 2001; Mahaney *et al.*, 2009; Pfeiffer *et al.*, 2000).

In this study bleocin is used to investigate DSB repair. Bleocin is a member of the bleomycin family of radiomimetics, originally isolated from the bacterium *Streptomyces verticillus*. Bleomycins contain a bithiazole tail which interacts with DNA, a linker region and a metal binding region which catalyses a highly specific free radical attack on the deoxyribose sugar of DNA to generate SSBs. Bleomycins can make a second SSB in close proximity to the first without disassociating from the DNA. This results in both blunt ended DSBs and DSBs with ssDNA overhangs (Chen and Stubbe, 2005; Povirk, 1996).

Other DNA damaging agents mentioned in this study include methyl methane sulphonate (MMS), hydroxyurea (HU), camptothecin (CPT), 4-nitroquinoline 1-oxide (4-NQO) and ultraviolet radiation (UV). MMS is an alkylating agent which causes base mispairing and replication blocks (Beranek, 1990; Lundin *et al.*, 2005). CPT inhibits the unwinding of DNA supercoils by Topoisomerase I and its ability to reseal the DNA nicks generated. The nicks can be converted to DSBs when encountered by the replication fork (Koster *et al.*, 2007; Svejstrup *et al.*, 1991). HU quenches the tyrosyl free radical in the active site of ribonucleotide reductase (RNR). This depletes deoxyribonucleotide triphosphate (dNTP) pools and results in stalled or collapsed replication forks (Bianchi *et al.*, 1986). 4-NQO forms DNA base adducts (Bailleul *et al.*, 1981). UV-induced photolesions include cyclobutane pyrimidine dimers and 6-4 photoproducts (Hannah and Zhou, 2009).

1.2.2 Enzymatically induced DSBs

In contrast to DNA damaging agents, restriction enzymes can generate site-specific DSBs. In this study the *Saccharomyces cerevisiae* (*S. cerevisiae*) homothallic (HO) endonuclease is used to induce a single, site-specific DSB in *S. pombe* in the context of a non-essential

minichromosome (Section 1.4). HO cleaves the 22 bp *MATa* locus to make a staggered DSB with 4 bp 3' overhangs (Nickoloff *et al.*, 1990; Paques and Haber, 1999). In this study HO is expressed under the control of a thiamine repressible promoter *nmt* (no message in thiamine) on a plasmid (Cullen *et al.*, 2007; Moss *et al.*, 2010; Prudden *et al.*, 2003; Tinline-Purvis *et al.*, 2009). DSBs occur 20-24 hours after the removal of thiamine (Prudden *et al.*, 2003).

1.3 DNA DOUBLE STRAND BREAK REPAIR

In eukaryotes DSBs are repaired by two major conserved pathways. Firstly non-homologous end joining (NHEJ), in which the DSBs are re-ligated and secondly homologous recombination (HR) in which a homologous DNA sequence is used as a template for repair.

1.3.1 Non-homologous end joining

NHEJ is the major repair pathway in human cells and is active throughout the cell cycle (Kakarougkas and Jeggo, 2014). In contrast, in yeast NHEJ appears to be restricted to the G1 phase of the cell cycle (Moore and Haber, 1996). Whilst most of the core NHEJ factors are conserved in *S. pombe* others have not been identified. Therefore the pathway will be presented here in respect to human cells.

NHEJ is initiated by the detection of DNA DSBs by the Ku70-Ku80 (Ku) heterodimer (Figure 1.1.A). Ku has a toroidal structure through which it can encircle DNA (Walker *et al.*, 2001). Ku binds to DNA DSB ends with high affinity (Blier *et al.*, 1993; Downs and Jackson, 2004). Following DNA binding, Ku can migrate away from the break site along the DNA (Blier *et al.*, 1993). This allows the recruitment of other NHEJ proteins to the DSB terminus (Yaneva *et al.*, 1997). Ku heterodimers bound to either end of the DSB interact and this is proposed to tether the DNA DSB ends together (Cary *et al.*, 1997). Ku binding also protects the DSB ends from DNA resection (Langerak *et al.*, 2011).

Figure 1.1

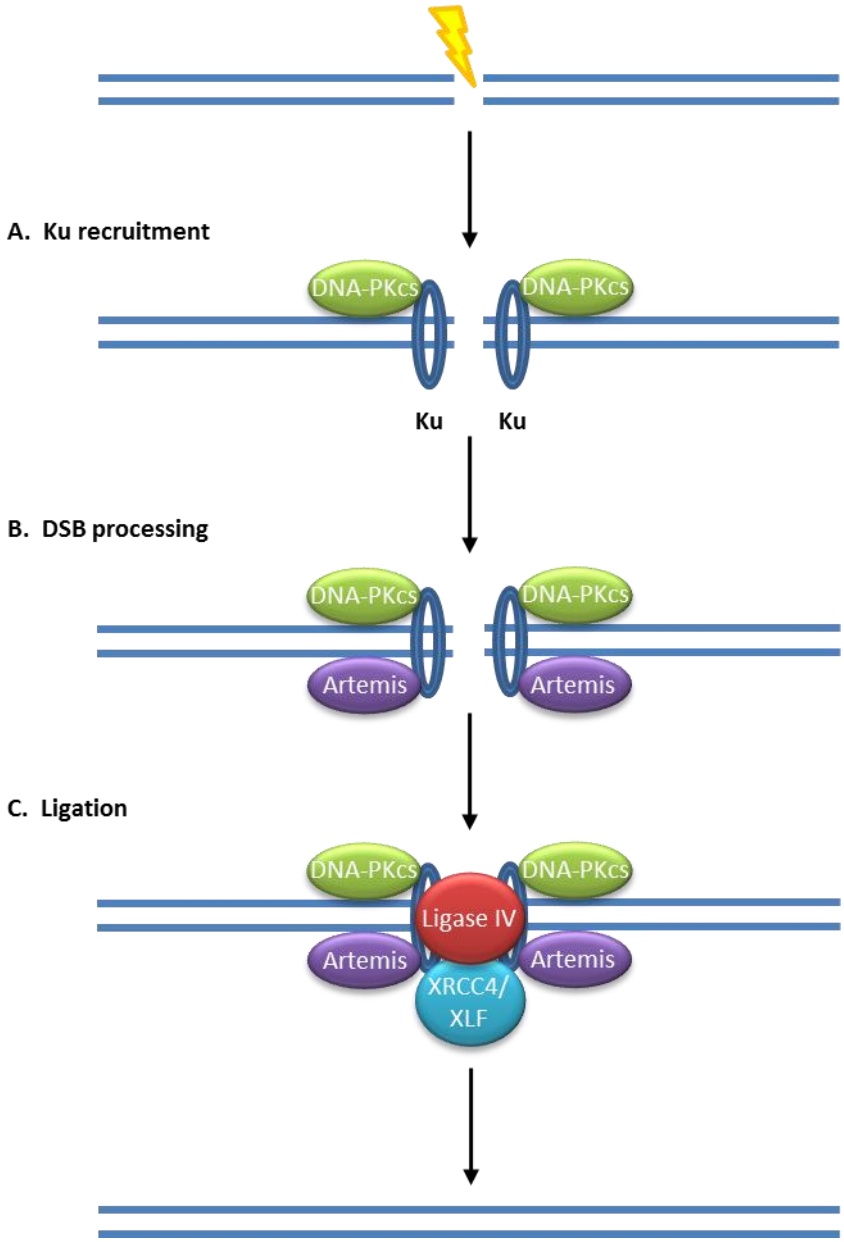


Figure 1.1 Non-homologous end joining in mammalian cells

Schematic of NHEJ in mammalian cells, adapted from Kakarougkas and Jeggo (2014).

(A) NHEJ is initiated by the detection of DSBs by the Ku70-Ku80 (Ku) heterodimer (blue). Ku recruits the kinase DNA-PKcs (green) resulting in its activation.

(B) DNA processing is performed by the exonuclease Artemis (purple) which is activated by DNA-PKcs, the DNA polymerases Pol λ and Pol μ and polynucleotide kinase. Only Artemis is shown for simplicity.

(C) DSB ends are ligated by DNA ligase IV, XRCC4 and XLF (light blue).

Following DNA binding, Ku undergoes conformational changes which allow it to act as a hub for the recruitment of other NHEJ proteins (Lehman *et al.*, 2008). The carboxyl terminus of Ku80 interacts with the kinase DNA-PKcs resulting in its activation (Figure 1.1.A) (Falck *et al.*, 2005; Gottlieb and Jackson, 1993). Active DNA-PK phosphorylates a range of NHEJ proteins including itself (Reddy *et al.*, 2004).

IR induced DSBs are complex and require processing prior to ligation. This processing is performed by the exonuclease Artemis, which is activated by DNA-PKcs (Figure 1.1.B) (Ma *et al.*, 2002); DNA polymerases Pol λ and Pol μ (Mahajan *et al.*, 2002; Nick McElhinny and Ramsden, 2004); and polynucleotide kinase (Chappell *et al.*, 2002). The processing can result in deletions at the break site. Following DNA processing the DSB ends can be ligated, requiring XRCC4, DNA ligase IV and XLF (Figure 1.1.C) (Lieber, 2010).

Alternative end joining pathways also operate when canonical NHEJ is impaired and have been shown to act through micro-homology mediated end joining (MMEJ). These pathways are error prone and result in deletions at the break site (Lieber, 2010).

1.3.2 Homologous recombination

The HR machinery is highly conserved in eukaryotes (Table 1.1). HR is initiated by 5' to 3' resection of DSB ends (Figure 1.2.A). This is an important step in DSB repair pathway choice as resected DNA is no longer a substrate for NHEJ. It is essential that HR only occurs in S and G2 phases of the cell cycle when a sister chromatid can provide a homologous template for repair. Therefore DSB resection is regulated by cyclin-dependent kinase (CDK) activity (Huertas *et al.*, 2008; Ira *et al.*, 2004).

Table 1.1 Homologous recombination proteins in *S. pombe*, *S. cerevisiae* and humans

Role	*S. pombe*	*S. cerevisiae*	Humans
DSB resection	Mre11-Rad50-Nbs1	Mre11-Rad50-Xrs2	MRE11-RAD50-NBS1
	Ctp1	Sae2	CtIP
	Exo1	Exo1	EXO1
	Rqh1-Dna2	Sgs1-Dna2	BLM1-DNA2
ssDNA binding	RPA (large subunit Rad11)	RPA (large subunit Rfa1)	RPA (large subunit RPA70)
Nucleofilament formation	Rad51	Rad51	RAD51
	Rad52	Rad52	RAD52
	Rad55-Rad57	Rad55-Rad57	RAD51B-RAD51C
			RAD51D-XRCC2
			RAD51C-XRCC3
	-	-	BRCA2
	Swi5-Srf1	Sea3-Mei5	SWI5-ME15
DNA synthesis	PCNA	PCNA	PCNA
	Pol δ,	Pol δ,	Pol δ,
	Pol ε	Pol ε	Pol ε
Anti-recombinase	Srs2	Srs2	RTEL
	Fbh1		FBH1
dHJ dissolution	Rqh1-Top3	Sgs1-Top3-Rmi1	BLM-TOPIIIa-RMI1
dHJ resolution	Mus81-Eme1	Mus81-Mms4	MUS81-EME1
	Slx1-Slx4	Slx1-Slx4	SLX1-SLX4
		Yen1	GEN1

Figure 1.2

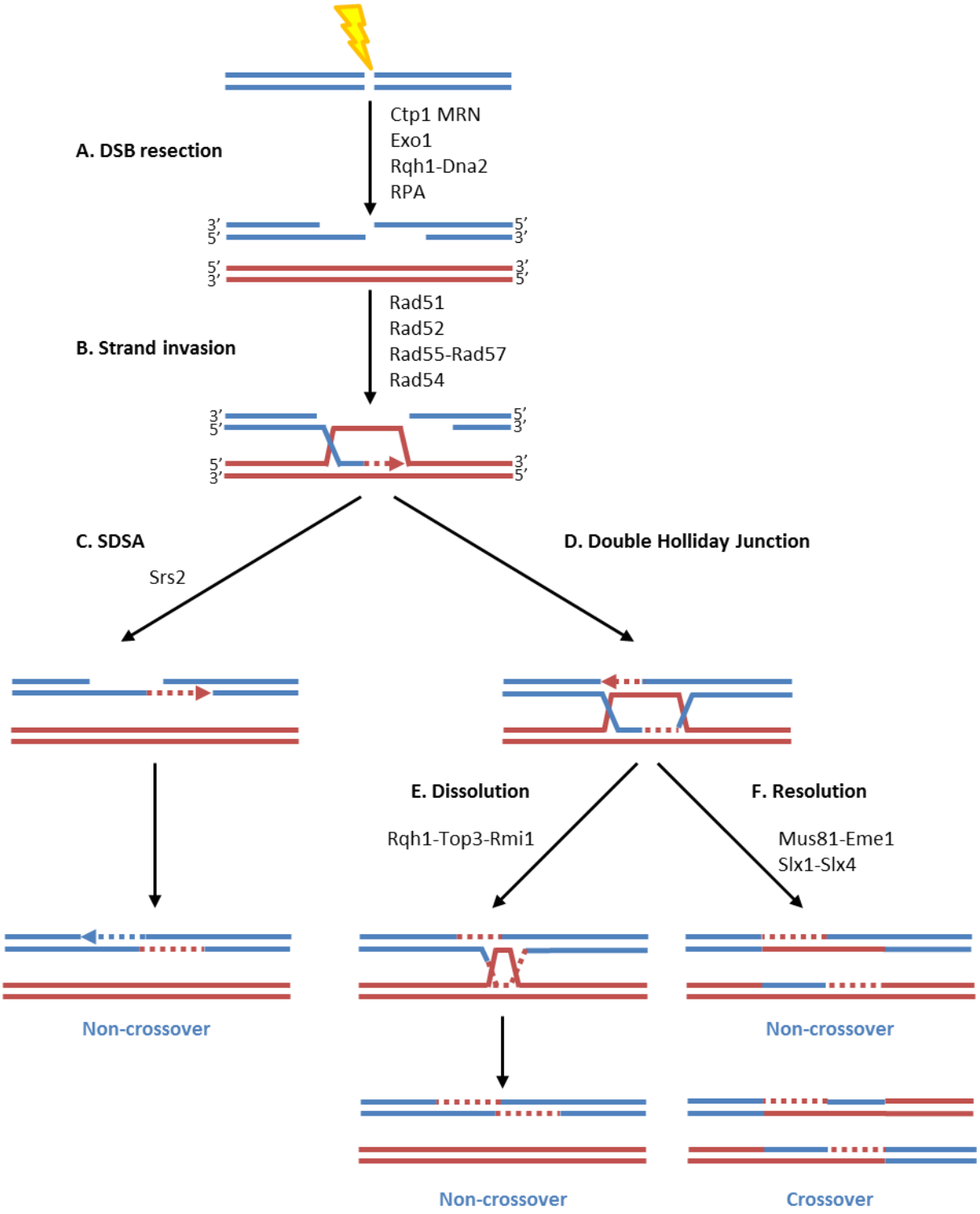

A. DSB resection
Ctp1 MRN
Exo1
Rqh1-Dna2
RPA
B. Strand invasion
Rad51
Rad52
Rad55-Rad57
Rad54
C. SDSA
Srs2
D. Double Holliday Junction
E. Dissolution
Rqh1-Top3-Rmi1
F. Resolution
Mus81-Eme1
Slx1-Slx4
Non-crossover
Non-crossover
Non-crossover
Crossover

Figure 1.2 Homologous recombination in *S. pombe*

Schematic of DSB repair by HR in *S. pombe* adapted from Raji and Hartsuiker (2006) and Daley *et al.* (2014).

(A) HR is initiated by 5'-3' resection of the DSB ends to generate ssDNA which is subsequently coated by replication protein A (RPA). Resection is initiated by the MRN complex (Mre11, Rad50, Nbs1) and Ctp1. Extensive resection is performed by Exo1 or Rqh1-Dna2.

(B) RPA is replaced by Rad51 to from a nucleofilament. This is promoted by Rad52 and Rad55-Rad57. The nucleofilament invades a homologous DNA sequence. Strand invasion is promoted by Rad54.

(C) In the synthesis-dependent strand annealing (SDSA) pathway the invading strand is displaced and anneals back to the second DSB end resulting in non-crossovers. This is promoted by the anti-recombinase Srs2.

(D) Alternatively, following second end capture a double Holliday junction (dHJ) structure forms.

(E) dHJ dissolution involves migration of the junctions followed by decatination catalysed by the Rqh1-Top3-Rmi1 complex (Rmi1 is based on evidence from *S. cerevisiae*). This results in non-crossovers.

(F) dHJ resolution by the endonucleases Mus81-Eme1 and Slx1-Slx4 results in non-crossovers and crossovers.

DSB resection is initiated in *S. pombe* by Ctp1 and the MRN complex consisting of Mre11, Rad50 and Nbs1. Extensive resection is subsequently performed by two parallel pathways, using either the exonuclease Exo1 or the helicase Rqh1 and nuclease Dna2 (Figure 1.2.A) (Langerak *et al.*, 2011). The mechanism by which MRN and Ctp1 initiate resection has been controversial. *In vitro* human MRE11 possesses endonuclease activity and 3'-5' exonuclease activity (Paull and Gellert, 1998).

In *S. pombe* Mre11 nuclease activity and Ctp1 are required for the release of Ku heterodimers from HO-induced DSB ends (Langerak *et al.*, 2011). Similarly, specific inhibition of human MRE11 endonuclease activity results in increased repair of IR-induced DSB by NHEJ (Shibata *et al.*, 2014). The *S. cerevisiae* homologues Mre11 and Sae2 are also required for the release of Spo11 bound oligonucleotides from meiotic DSB ends (Neale *et al.*, 2005).

Garcia *et al.* (2011) investigated the function of *S. cerevisiae* Mre11 in DSB resection using an exonuclease deficient Mre11 mutant. Similarly Shibata *et al.* (2014) developed inhibitors which selectively targeted the exonuclease or endonuclease activities of human MRE11. These studies supported a bidirectional model for resection (Figure 1.3A-B) (Garcia *et al.*, 2011; Shibata *et al.*, 2014). In this model, at blocked DSB ends, a MRN/MRX and CtIP/Sae2-dependent endonuclease creates nicks flanking the DSB, creating sites for bidirectional resection (Figure 1.3.A). The endonuclease was identified as MRE11 in human cells. The MRE11/Mre11 3'-5' exonuclease can then resect from the nick towards the break site, whilst extensive 5'-3' resection moves in the opposite direction (Figure 1.3.B).

The ssDNA generated during DSB resection is bound by replication protein A (RPA) (Figure 1.2.A). RPA protects the resected DNA from nucleolytic cleavage, inhibits MMEJ and the formation of DNA secondary structures (Chen *et al.*, 2013; Deng *et al.*, 2014). RPA coated ssDNA is also important for activation of the DNA damage checkpoint, as will be discussed in Section 1.5 of this intoduction.

Figure 1.3

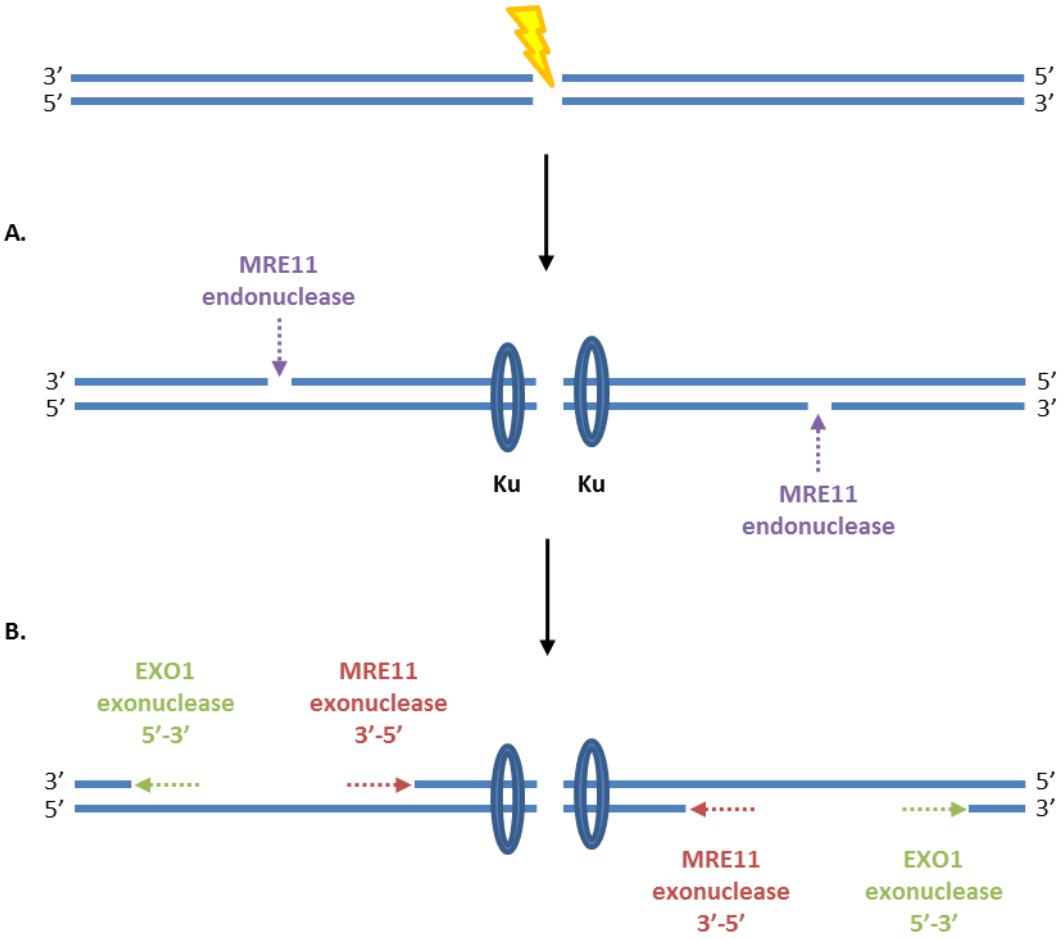


Figure 1.3 A bidirectional model for DSB resection in mammalian cells

A model for DSB resection in mammalian cells, as proposed by Shibata *et al.* (2014).

(A) DSB resection is inhibited by the binding of Ku to DSB ends. Mre11 endonuclease activity initiates resection by creating nicks flanking the DSB.

(B) MRE11 3'-5' exonuclease resects from the nick towards the break site, EXO1 5'-3' exonuclease resects from the nick away from the break site leading to extensive resection.

RPA is replaced by Rad51 to from a nucleofilament (Figure 1.2.B). In yeast Rad52 promotes Rad51 nucleofilament formation (Sung, 1997). However, in humans this function is mainly performed by BRCA2 (Feng *et al.*, 2011; Liu *et al.*, 2010). Yeast Rad51 nucleofilaments are also stabilised by the Rad55-Rad57 heterodimer (Liu *et al.*, 2002b).

The Rad51 nucleofilament searches for homologous DNA (Figure 1.2.B). In *S. cerevisiae* this is facilitated by increased chromosome mobility. At the break site this requires Rad51 whereas a global increase in chromosome mobility requires the DNA damage checkpoint and the INO80 chromatin remodelling complex (Mine-Hattab and Rothstein, 2012; Seeber *et al.*, 2013). Once homology is found, strand invasion generates the displacement loop (D loop). Rad54 stimulates formation of the D loop by stabilising the Rad51 filament (Mazin *et al.*, 2003). Rad54 also promotes Rad51 disassociation (Li *et al.*, 2007). This allows the 3' end of the ssDNA to act as a template for DNA synthesis using the homologous DNA as a template. Nucleotide synthesis is up-regulated in response to DNA damage to promote efficient DNA synthesis during repair, as will be discussed in Section 1.6 of this introduction.

Following DNA synthesis HR can proceed through several genetically distinct sub pathways. In synthesis-dependent strand annealing (SDSA) the newly synthesised strand is displaced and anneals back to the second DSB end (Figure 1.2.C). This results in non-crossovers and is promoted by the helicase Srs2 (Dupaigne *et al.*, 2008). Alternatively the second DSB end can be captured to form a double Holliday junction (dHJ) structure (Figure 1.2.D). dHJs can be repaired in two ways. Firstly dissolution which involves migration of the junctions followed by decatination. This is catalysed by Rqh1-Top3 (Figure 1.2.E) (Ashton *et al.*, 2011). Secondly resolution of dHJs by the endonucleases Mus81-Eme1 and Slx1-Slx4 leads to the formation of crossover and non-crossover products depending on the orientation of cleavage (Figure 1.2.F) (Matos and West, 2014).

1.3.3 Single strand annealing

Single strand annealing (SSA) is a minor HR pathway which results in erroneous repair (Figure 1.4.A) (Raji and Hartsuiker, 2006). HR is initiated normally by DSB resection. However this uncovers homologous sequences either side of the break which can anneal, generating long ssDNA flaps which are cleaved in *S. cerevisiae* by Rad1, the homologue of *S. pombe* Rad16 (Fishman-Lobell and Haber, 1992). This leads to deletion of the DNA between the two homologous sequences. DNA synthesis fills the ssDNA gaps (Raji and Hartsuiker, 2006). Many components of canonical HR including the resection machinery are also used in SSA. However SSA does not require components involved in nucleofilament formation as there is no strand invasion (Ivanov *et al.*, 1996). In this thesis a SSA assay developed by Watson *et al.* (2011) is used to assess DSB resection and will be introduced in Chapter 4.

1.3.4 Break-induced replication

Break-induced replication (BIR) is a HR sub-pathway in which DNA resection, nucleofilament formation and strand invasion are maintained and so BIR requires the canonical HR machinery for these processes. However, in contrast to canonical HR, repair proceeds by DNA replication to the end of the template chromosome (Figure 1.4.B). HR preferentially occurs using a sister-chromatid as a homologous template for repair. However if a homologous chromatid is instead used this can lead to loss of heterozygosity at polymorphic loci between the DSB and the chromosome end (Cullen *et al.*, 2007; Llorente *et al.*, 2008). Furthermore the DNA synthesis associated with BIR is error prone (Deem *et al.*, 2011). BIR occurs at a low frequency in wild-type *S. pombe* cells in the context of repairing a HO endonuclease induced DSB on a non-essential minichromsome (Cullen *et al.*, 2007), but plays a more important role in the repair of collapsed replication fork or uncapped telomeres (Kasparek and Humphrey, 2011; Llorente *et al.*, 2008).

Figure 1.4

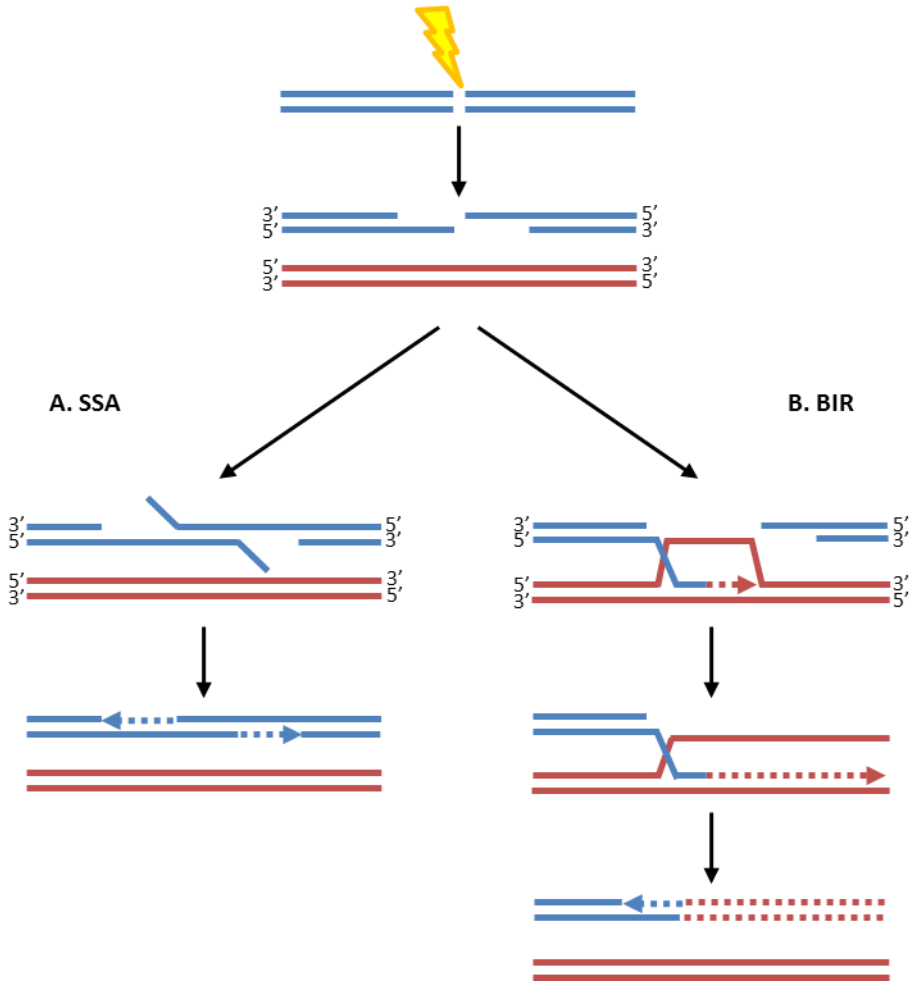


Figure 1.4 Single strand annealing and break-induced replication

Schematic of DSB repair in *S. pombe* by the HR sub pathways single strand annealing (SSA) and break-induced replication (BIR). The figure was adapted from (Heyer *et al.*, 2010).

(A) SSA is initiated by DSB resection. This uncovers homologous sequences either side of the break, which can anneal, generating long ssDNA flaps which are cleaved. The DNA between the two homologous sequences is lost. The ssDNA gaps are filled by DNA synthesis.

(B) BIR is initiated by DSB resection, nucleofilament formation and strand invasion. Repair proceeds by DNA replication to the end of the homologous chromosome. This leads to loss of heterozygosity for all genetic material between the DSB and the chromosome end.

1.4 A SYSTEM FOR STUDYING DSB REPAIR IN *S. POMBE*

In this thesis DSB repair in different *S. pombe* genetic backgrounds is assessed and quantified using a DSB assay (Figure 1.5). This assay utilises Ch^{16}, a 530 kb non-essential minichromosome derived from chromosome III (Ch III) (Niwa *et al.*, 1986). A site-specific DSB can be generated by HO endonuclease at a *MATa* target site on the minichromosome (Prudden *et al.*, 2003). DSB repair events can subsequently be distinguished using genetic markers. Ch^{16}-RMYAH used in this study has previously been described by Tinline-Purvis *et al.* (2009). Ch^{16}-RMYAH contains a *MATa* target site and *hph* gene encoding hygromycin resistance integrated on the right hand arm of the minichromosome. Centromere distal is an *ade6-M216* heteroallele, which is complemented by *ade6-M210* allele on Ch III, and a *his3* marker. On the left hand arm of the minichromosome there is an *arg3* marker.

The assay is performed in two steps. Firstly HO endonuclease is expressed under control of the *nmt* thiamine repressible promoter from a REP81X plasmid. Secondly, following DSB induction, cells are plated onto non-selective media and colonies allowed to form. By replica-plating the colonies onto different selection plates it is possible to accurately quantify the loss of the genetic markers placed on the minichromosome.

In a wild-type background the DSB is efficiently repaired by HR using Ch III as a template. This results in inter-chromosomal gene conversion (GC) and loss of the hygromycin resistance marker adjacent to the break site (Figure 1.5.B). In contrast repair of the DSB by sister chromatid conversion (SSC) results in retention of all minichromosome markers. Direct ligation of the DSB ends by NHEJ also results in retention of all minichromosome markers (Figure 1.5.C). NHEJ and SCC events are indistinguishable from the parental uncut minichromosome. Furthermore if the break site is accurately repaired it can be recut.

Figure 1.5

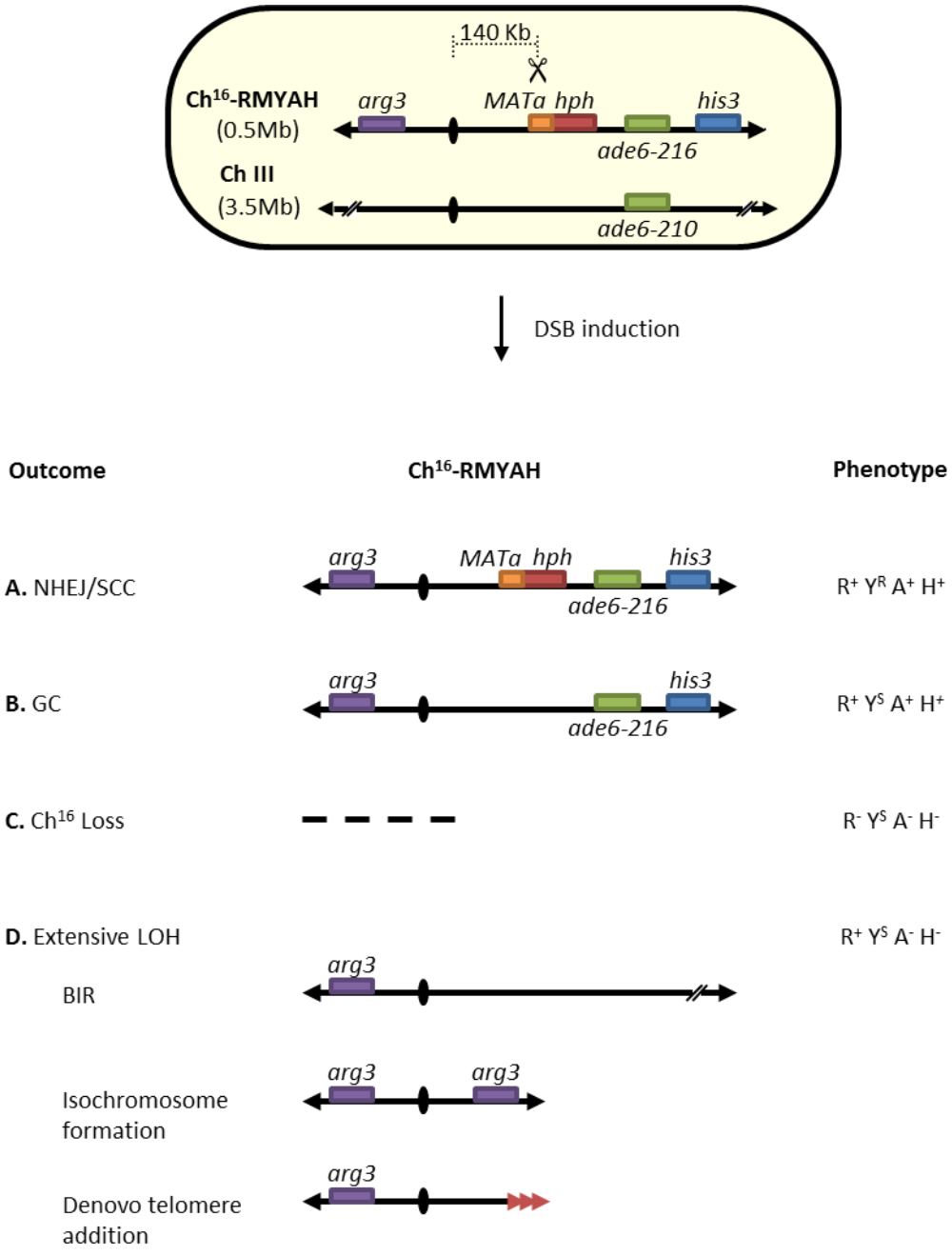

140 Kb
Ch16-RMYAH
(0.5Mb)
arg3
MATa hph
his3
ade6-216
Ch III
(3.5Mb)
ade6-210
DSB induction
Outcome
Ch16-RMYAH
Phenotype
A. NHEJ/SCC
R+ YR A+ H+
B. GC
R+ YS A+ H+
C. Ch16 Loss
R- YS A- H-
D. Extensive LOH
R+ YS A- H-
BIR
Isochromosome formation
Denovo telomere addition

Figure 1.5 The DSB assay

Schematic of a *S. pombe* DSB assay to assess and quantify DSB repair outcomes. This assay was previously described by Tinline-Purvis *et al.* (2009). Ch^{16}-RMYAH is a 530 kb non-essential minichromosome derived from Ch III (Niwa *et al.*, 1986). Ch^{16}-RMYAH contains a *MATa* target site and *hph* gene encoding hygromycin resistance integrated on the right hand arm. Centromere distal is an *ade6-M216* heteroallele, which is complemented by *ade6-M210* allele on Ch III, and a *his3* marker. On the left hand arm there is an *arg3* marker. A site-specific DSB can be generated by HO endonuclease at the *MATa* target site. DSB repair outcomes are quantified by assessing the loss or retention of the genetic markers. The genotype and phenotype used to identify the following repair outcomes are shown:

(A) Non-homologous end joining (NHEJ) and sister chromatid conversion (SCC)

(B) Gene conversion (GC)

(C) Ch^{16} loss

(D) Extensive loss of heterozygosity (LOH), mediated by break-induced replication (BIR), isochomosome formation and *de novo* telomere addition.

The phenotype is presented as follows: R = arginine, Y = hygromycin, A = adenine, H = histindine, $^{+}$ = prototophic, $^{-}$ = auxotrophic, ^{R} = resistant, ^{S} = sensitive.

Generating a DSB within the context of the non-essential minichromosome also allows the study of failed repair events, which would normally be fatal. Ch^{16} loss can be caused by extensive DSB end processing following failed HR (Figure 1.5.C). Extensive LOH is observed as a loss of minichromosome markers centromere-distal to the break site (Figure 1.5.D). HR can facilitate extensive LOH through BIR and allelic crossovers. Extensive resection following failed HR can also cause extensive LOH by facilitating BIR within the centromere which leads to isochromosome formation. Extensive LOH can also be caused by *de novo* telomere addition at the break site (Cullen *et al.*, 2007; Tinline-Purvis *et al.*, 2009).

1.5 DNA INTEGRITY CHECKPOINTS

Acting in conjunction with the DNA repair pathways, cell cycle checkpoints play a key role in maintaining genome stability. In *S. pombe* two major cell cycle checkpoints, collectively known as the DNA integrity checkpoints, are required to maintain genome stability. These are the DNA damage checkpoint, which is activated in response to DNA damage, and the replication checkpoint, which is activated in response to DNA replication stress. *S. pombe* cells spend most of their time in the G2 phase of the cell cycle and both of these checkpoints act at the G2-M cell cycle boundary (Humphrey, 2000).

The DNA damage checkpoint was originally identified as an intracellular signaling pathway which could detect DNA damage and arrest the cell cycle, allowing sufficient time for repair prior to cell division (Weinert and Hartwell, 1989). The checkpoint is now known also to have direct roles in repair (Lydall and Weinert, 1995). The DNA damage checkpoint regulates the transcription of repair genes (Watson *et al.*, 2004), post translational modification of repair proteins (Bashkirov *et al.*, 2000; Morin *et al.*, 2008; Sorensen *et al.*, 2005) and modification of chromatin (Downs *et al.*, 2000).

Of significance to this thesis the DNA damage checkpoint up-regulates nucleotide synthesis. This is discussed in Section 1.6 of this introduction. The checkpoint machinery has also been implicated in DSB resection. Studies in *S. cerevisiae* showed that the 9-1-1 checkpoint complex and Rad24, the homologue of *S. pombe* Rad17, promote resection at uncapped telomeres (Jia *et al.*, 2004; Lydall and Weinert, 1995; Zubko *et al.*, 2004). Deletion of *RAD24* also impairs resection of HO endonuclease-induced DSBs (Aylon and Kupiec, 2003). A role for the DNA damage checkpoint in DSB resection will be addressed in Chapter 4.

The checkpoint machinery is highly conserved between yeast and humans (Table 1.2). In *S. pombe* loss of the DNA damage checkpoint results in defective HR (Blaikley *et al.*, 2014; Moss *et al.*, 2010). As a consequence of this critical role in maintaining genome stability many of the checkpoint genes are tumour suppressors (Zhou and Elledge, 2000).

Table 1.2 Checkpoint proteins in *S. pombe, S. cerevisiae* and humans

Role	*S. pombe*	*S. cerevisiae*	Humans
Sensors			
ATR kinase	Rad3	Mec1	ATR
ATR interacting protein	Rad26	Dcd2	ATRIP
ATM kinase	Tel1	Tel1	ATM
RFC clamp loader	Rad17	Rad24	RAD17
9-1-1 complex	Rad9	Dcd1	RAD9
	Rad1	Rad17	RAD1
	Hus1	Mec3	HUS1
Mediators			
DNA damage checkpoint mediators	Rad4	Dpb11	TOPBP1
	Crb2	Rad9	53BP1
DNA replication checkpoint mediators	Mrc1	Mrc1	Claspin
Effectors			
DNA damage checkpoint effector kinase	Chk1	Chk1	CHK1
DNA replication checkpoint effector kinase	Cds1	Rad53	CHK2

1.5.1 Sensing DNA damage

In *S. pombe* the sensing of DNA damage or replication stress by the checkpoint machinery involves six conserved proteins Rad3, Rad26, Rad17, Rad9, Rad1 and Hus1 (Figure 1.6.A). All six proteins are required for the checkpoints to initiate cell cycle arrest (Humphrey, 2000).

The phosphatidylinositol 3′ kinase-like (PI3K) kinase Rad3, the *S. pombe* homologue of human ATR, is recruited to sites of DNA damage or replication stress by Rad26. Rad26 interacts with RPA bound to single stranded DNA (Cortez *et al.*, 2001; Edwards *et al.*, 1999; Namiki and Zou, 2006; Zou and Elledge, 2003). In human cells a second PI3K, ATM, is also important for sensing DNA damage. ATM is recruited to DNA DSBs by interaction with MRN (Uziel *et al.*, 2003). In contrast to the situation in human cells, Tel1 the *S. cerevisiae* homologue of ATM only plays a minor role in checkpoint activation (Morrow *et al.*, 1995).

Rad9, Rad1 and Hus1 together form the 9-1-1 checkpoint complex. This complex has a toroidal structure that resembles proliferating cell nuclear antigen (PCNA) (Dore *et al.*, 2009; Lindsey-Boltz *et al.*, 2001; Thelen *et al.*, 1999). Rad17 shares homology with the Rfc1 subunit of the heteropentameric replication factor C (RFC) complex (Griffiths *et al.*, 1995). Rad17 forms a complex with the four small RFC subunits (Green *et al.*, 2000; Lindsey-Boltz *et al.*, 2001). Similarly to RFC, which loads PCNA onto DNA during replication, the Rad17-RFC complex recognises ssDNA-dsDNA junctions at sites of DNA damage and loads the 9-1-1 complex onto DNA. This process is dependent on RPA and ATP (Bermudez *et al.*, 2003; Ellison and Stillman, 2003; Zou *et al.*, 2002; Zou *et al.*, 2003).

Figure 1.6

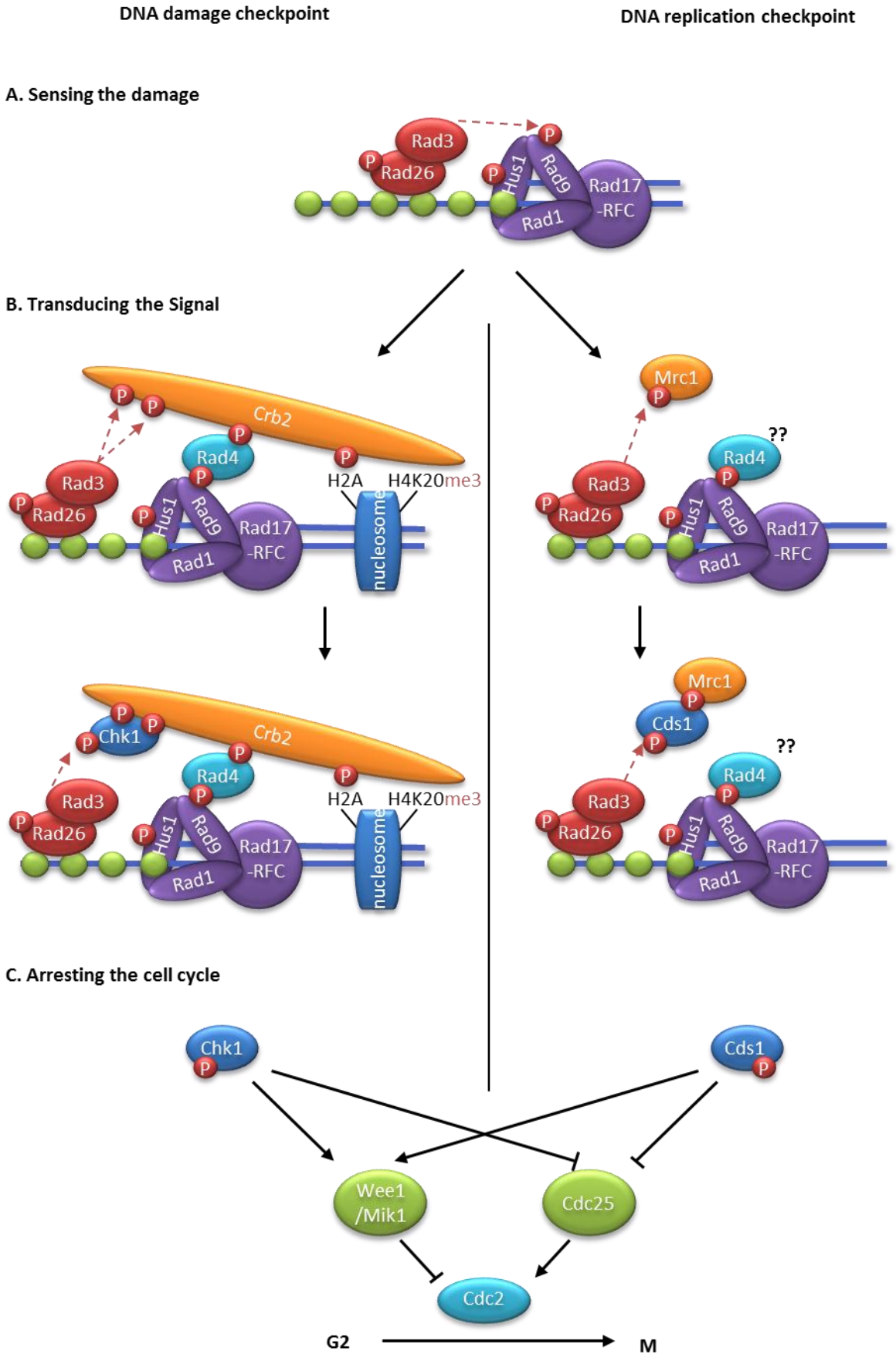

DNA damage checkpoint
DNA replication checkpoint
A. Sensing the damage
Rad3
Rad26
Hus1
Rad9
Rad17
-RFC
Rad1
B. Transducing the Signal
Crb2
Rad4
H2A
H4K20me3
nucleosome
Mrc1
??
Chk1
Cds1
C. Arresting the cell cycle
Wee1
/Mik1
Cdc25
Cdc2
G2
M

Figure 1.6 The DNA integrity checkpoints in *S. pombe*

Schematic of the *S. pombe* DNA integrity checkpoint signaling pathways to arrest the cell cycle. This figure was adapted from Qu *et al.* (2012) and Humphrey (2000).

(A) DNA damage and DNA replication stress are sensed by the DNA damage and DNA replication checkpoints respectively, using the same checkpoint components. Rad26 binds to RPA coated ssDNA and recruits Rad3. The Rad17-RFC complex binds to ssDNA-dsDNA boundaries and recruits the 9-1-1 complex (Rad9, Rad1, Hus1).

(B) The DNA damage and DNA replication checkpoints diverge to transduce the checkpoint signal. To transduce the DNA damage checkpoint signal Rad3 phosphorylates Rad9 allowing the recruitment of Rad4, which is subsequently phosphorylated by Rad3. Crb2 is recruited to sites of DNA damage by interaction with phosphorylated Rad4, phosphorylated H2A and methylated H4K20. Crb2 is phosphorylated by Rad3 allowing the recruitment of Chk1, which is subsequently phosphorylated by Rad3 resulting in Chk1 activation. The DNA replication checkpoint signal is transduced through Mrc1. Mrc1 is phosphorylated by Rad3 and this is required for the recruitment of Cds1. Cds1 is subsequently phosphorylated by Rad3 resulting in Cds1 activation. The role of Rad4 in the DNA replication checkpoint is unclear.

(C) The DNA damage and DNA replication checkpoints both mediate cell cycle arrest at the G2-M cell cycle boundary. In *S. pombe* the G2-M transition is regulated by inhibitory phosphorylation of the CDK Cdc2. Chk1 and Cds1 promote the phosphorylation of Cdc2 by up-regulating the activity of the Cdc2 kinase Mik1 and inhibiting the Cdc2 phosphatase Cdc25.

1.5.2 Transducing the signal

The checkpoint signal is transduced and amplified by the recruitment of effector kinases. In *S. pombe* this is where the DNA damage and DNA replication checkpoints diverge. The DNA damage checkpoint mediates activation of Chk1 whereas the DNA replication checkpoint mediates activation of Cds1 (Figure 1.6.B) (Humphrey, 2000).

Firstly transduction of the DNA damage checkpoint signal will be discussed. Rad3 phosphorylation of the Rad9 carboxyl terminus is required for the interaction of Rad9 with the checkpoint mediator Rad4. This recruitment of Rad4 to sites of DNA damage allows its subsequent interaction with and phosphorylation by Rad3 (Furuya *et al.*, 2004; Qu *et al.*, 2012). In *S. pombe* Rad4 mediates the checkpoint response by acting as a scaffold for protein interactions and, unlike the *S. cerevisiae* homologue Dpb11, is not required for Rad3 activity (Yue *et al.*, 2014).

The DNA damage checkpoint mediator Crb2 is recruited to sites of DNA damage by interaction with modified histones. Following DNA damage Rad3 and to a lesser extent Tel1 are required for phosphorylation of H2A. H2A phosphorylation together with methylation of H4K20 allows Crb2 recruitment (Nakamura *et al.*, 2004; Sanders *et al.*, 2004). The interactions are mediated through the BRCA domain and tandem tudor domains of Crb2 (Botuyan *et al.*, 2006; Du *et al.*, 2006). Crb2 can also be recruited to DNA damage sites independently of histone modifications through interaction of phosphorylated Crb2 with the BRCA domains of Rad4 (Du *et al.*, 2006; Qu *et al.*, 2012).

Recruitment of Crb2 allows its phosphorylation by Rad3. This is subsequently required for its interaction with the checkpoint effector Chk1. Once Chk1 is localised to the site of DNA damage it can be phosphorylated by Rad3 resulting in its activation (Mochida *et al.*, 2004; Qu

et al., 2012). Whilst the *S. cerevisiae* Crb2 homologue Rad9 is also required for Chk1 activation, the human homologue 53BP1 is required for maintenance of checkpoint arrest rather than its initiation (Blankley and Lydall, 2004; Shibata *et al.*, 2010).

The DNA replication checkpoint signal is transduced through Mrc1. Mrc1 is phosphorylated at two sites by Rad3 and this is required for interaction with Cds1. Cds1 can subsequently be phosphorylated by Rad3, resulting in its activation (Xu *et al.*, 2006). Rad4 has also been implicated in the DNA replication checkpoint (Harris *et al.*, 2003; Taricani and Wang, 2006). However, in contrast mutations which abolish most of the checkpoint activity of Rad4 have been shown not to affect Cds1 activation (Yue *et al.*, 2014).

1.5.3 Arresting the cell cycle

The DNA damage and DNA replication checkpoints both mediate cell cycle arrest at the G2-M cell cycle boundary (Figure 1.6.C) (Humphrey, 2000). In *S. pombe* the G2-M transition is regulated by inhibitory phosphorylation of the CDK Cdc2 by Wee1 and Mik1 kinases (Rhind *et al.*, 1997).

The checkpoint effector kinases Chk1 and Cds1 promote the phosphorylation of Cdc2 by up-regulating Mik1 activity (Rhind and Russell, 2001). Chk1 and Cds1 also phosphorylate the Cdc2 phosphatase Cdc25 (Furnari *et al.*, 1997; Zeng *et al.*, 1998). This phosphorylation directly inhibits Cdc25 activity (Furnari *et al.*, 1999). In addition Cdc25 phosphorylation is required for the binding of Cdc25 to Rad24, a member of the 14-3-3 protein family. This interaction mediates Cdc25 export from the nucleus (Lopez-Girona *et al.*, 1999; Zeng and Piwnica-Worms, 1999).

1.6 REGULATION OF NUCLEOTIDE SYNTHESIS

Nucleotide synthesis is a conserved response to DNA damage. Both *S. pombe* and *S. cerevisiae* increase cellular deoxyribonucleotide triphosphate (dNTP) levels in response to DNA damage (Chabes *et al.*, 2003; Hakansson *et al.*, 2006a). Mammalian cells do not show global changes in nucleotide levels following DNA damage (Hakansson *et al.*, 2006b). However, ribonucleotide reductase (RNR), the enzyme which catalyses a critical step in dNTP synthesis, is recruited to DSB in mammalian cells through an interaction with Tip60. This is predicted to increase dNTP levels in the vicinity of the break and is required for efficient repair in G1 and GO phases of the cell cycle when nucleotide levels are low (Niida *et al.*, 2010).

Tight regulation of dNTP levels is required as insufficient supply during DNA replication results in genome instability (Bester *et al.*, 2011). During DSB repair by HR, nucleotide synthesis is also required for efficient gap filling of resected ssDNA. *S. pombe* deletion strains which are defective for damage-induced nucleotide synthesis exhibit high levels of LOH associated with failed HR (Moss *et al.*, 2010). In contrast, excessive nucleotides affect DNA polymerase fidelity resulting in increased mutation rates (Chabes *et al.*, 2003).

RNR catalyses the reduction of ribonucleotide diphosphates (NDPs) to dNDPs. In eukaryotic cells the enzyme is formed from two large subunits and two small subunits (Hofer *et al.*, 2012). RNR subunit composition for yeast and humans is shown in Table 1.3. In human cells a second small subunit, p53R2, is up-regulated in response to DNA damage (Hakansson *et al.*, 2006b). RNR activity is under complex allosteric control by dNTPs and NTPs (Hofer *et al.*, 2012). In addition, RNR activity is regulated during the cell cycle and by the DNA integrity checkpoints (Guarino *et al.*, 2014). This is discussed in the following sections.

Table 1.3 RNR subunit compositions in *S. pombe*, *S. cerevisiae* and humans

RNR subunit	*S. pombe*	*S. cerevisiae*	*Humans*
Large	Cdc22	Rnr1	RRM1
		Rnr3	
Small	Suc22	Rnr2	RRM2
		Rnr4	p53R2

1.6.1 Transcriptional regulation of RNR

In *S. pombe cdc22*$^{+}$ transcription changes during the cell cycle under control of the MBF (Mlu1-box binding factor) transcription factor, with transcription peaking at the G1-S phase boundary (Fernandez Sarabia *et al.*, 1993; Lowndes *et al.*, 1992). MBF-dependent transcription of *cdc22*$^{+}$ is also activated by the DNA replication checkpoint through Cds1 phosphorylation of the MBF inhibitor Yox1 (Gomez-Escoda *et al.*, 2011). However, activation of the DNA damage checkpoint inhibits MBF-dependent transcription as Chk1 phosphorylation of the MBF component Cdc10 results in its release from target genes (Ivanova *et al.*, 2013). In contrast *suc22*$^{+}$ is constitutively expressed throughout the cell cycle. A larger *suc22*$^{+}$ transcript under MBF control is detectable at the G1-S boundary and in response to HU-induced replication stress or UV induced DNA damage (Harris *et al.*, 1996).

In *S. cerevisiae* transcription of *RNR1* is also cell cycle regulated under MBF control (Elledge and Davis, 1990). Up-regulation of transcription in response to DNA damage requires the transcription factor Ixr1 (Tsaponina *et al.*, 2011). In contrast the levels of *RNR2*, *RNR3* and *RNR4* do not change significantly during the cell cycle (Elledge and Davis, 1990; Huang and Elledge, 1997). The transcription of *RNR2*, *RNR3* and *RNR4* is inhibited by Crt1. Crt1 binds to the promoter of these genes and recruits the Sns6-Tup1 co-repressor. Following activation of the DNA damage checkpoint Crt1 is hyperphosphorylated and unable to bind DNA allowing gene expression (Huang *et al.*, 1998; Li and Reese, 2001).

In unperturbed human cells transcription of *RRM1* and *RRM2* takes place mainly in S phase (Bjorklund *et al.*, 1990). However, at the protein level only changes in RRM2 are observed. This is due to proteasome-mediated degradation in G2 and will be discussed in the relevant section below (Chabes and Thelander, 2000). Transcription of an additional small RNR subunit p53R2 is induced in response to DNA damage.

1.6.2 Cullin-RING E3 ubiuitin ligases

Cullin-RING E3 ubiquitin ligases (CRLs) play important roles in the regulation of RNR and so will be introduced here before their role is discussed. The covalent modification of proteins with polyubiquitin chains is a prerequisite for proteins to be recognised and degraded by the proteasome. Ubiquitin is covalently attached to proteins in three steps. Firstly, in an ATP-dependent reaction, the terminal carboxyl group of ubiquitin is covalently attached to an E1 (ubiquitin activating) enzyme. Secondly ubiquitin is transferred to cysteine residue on an E2 (ubiquitin conjugating) enzyme. Thirdly ubiquitin is transferred to a lysine residue on the target protein by an E3 (ubiquitin ligating) enzyme. Chains of ubiquitin can be generated by sequential rounds of attaching ubiquitin to lysine residues within the previous ubiquitin protein (Pickart and Eddins, 2004).

CRLs have a multimeric structure (Figure 1.7.A). Cullin proteins act as scaffolds for assembly of the CRL complex. The carboxyl terminus of each cullin is bound by the ring domain protein Rbx1 which recruits the E2 ubiquitin conjugating enzyme. The amino terminus of each cullin is bound by an adaptor protein. Each cullin has the ability to bind several adaptors which can in turn recruit multiple substrate receptors and substrates. This allows regulation of the degradation of a large number of proteins many of which are involved in DNA repair (Hannah and Zhou, 2009).

Figure 1.7

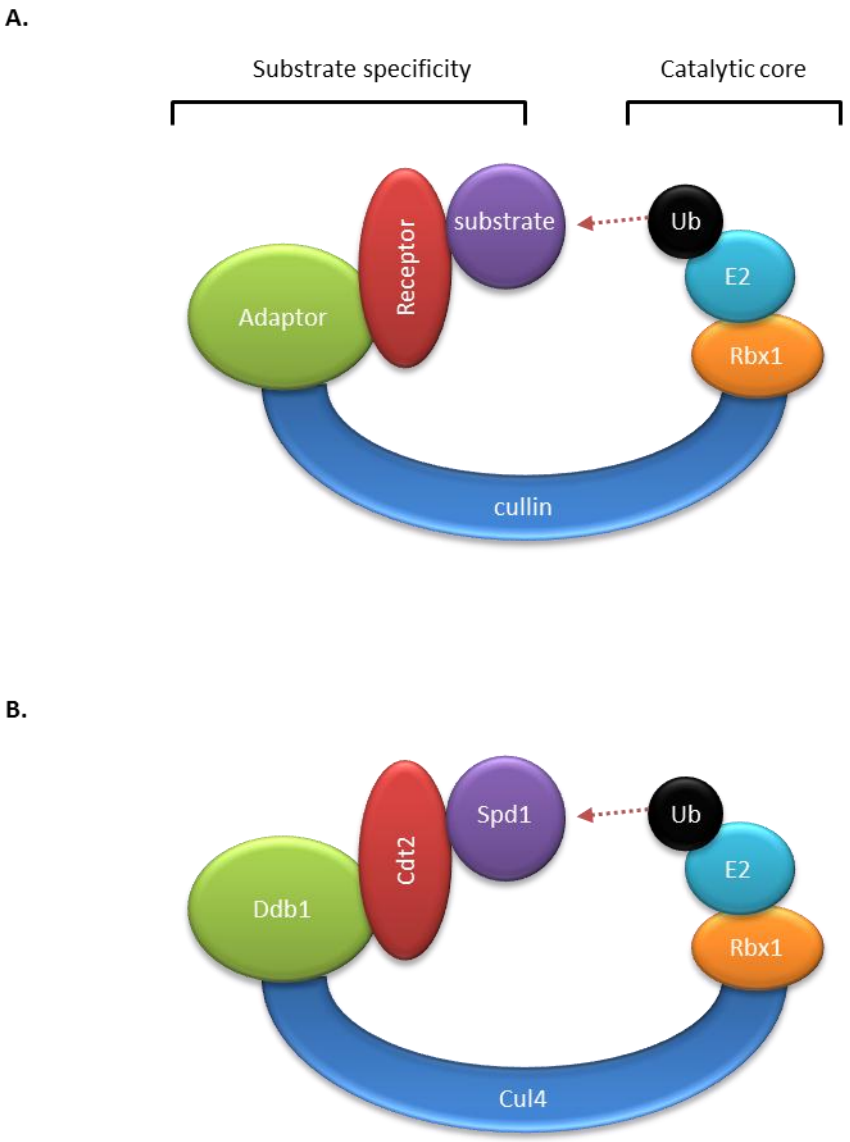


Figure 1.7 Cullin-RING E3 ubiquitin ligases

(A) Cullin (dark blue) acts as a scaffold for assembly of the CRL complex. The carboxyl terminus of cullin assembles the catalytic core by binding Rbx1 (orange) which recruits the E2 ubiquitin conjugating enzyme (light blue). The amino terminus of cullin enables substrate specificity by recruiting specific adaptor proteins (green) which in turn bind specific substrate receptors (red). Following recruitment of the substrate (purple) by the substrate receptor the E2 enzyme transfers ubiquitin (Ub, black) to the substrate.

(B) The Ddb1-Cul4^{Cdt2} CRL complex contains the cullin Cul4 (dark blue), the adaptor Ddb1 (green) and the substrate receptor Cdt2. Cdt2 recruits substrates including Spd1 (purple).

In addition to the availability of substrate receptors, CRL complex activity is regulated by the conjugation of Nedd8 to cullin. Neddylation causes conformational changes in the CRL promoting ubiquitination of CRL substrates (Duda *et al.*, 2008; Saha and Deshaies, 2008). In the absence of neddylation CAND1 binds cullin. In mammalian cells this inhibits the binding of adaptor proteins (Duda *et al.*, 2008; Liu *et al.*, 2002a; Zheng *et al.*, 2002).

Nedd8 is removed from CRLs by the conserved COP9 signalosome. In higher eukaryotes COP9 consists of 8 subunits which are paralogues of the proteasome 19S lid complex subunits (Glickman *et al.*, 1998; Lingaraju *et al.*, 2014; Wei *et al.*, 1998). In lower eukaryotes smaller complexes exist, for example in *S. pombe* COP9 contains 6 subunits, Csn1-5 and Csn7a, none of which are essential for viability (Liu *et al.*, 2003; Zhou *et al.*, 2001). Csn5 is the catalytic subunit containing a metalloprotease motif. Deneddylation is inhibited by the binding of CRL substrates (Cope *et al.*, 2002; Lyapina *et al.*, 2001; Zhou *et al.*, 2001).

Human COP9 is mostly located in the cytosol but also found in the nucleus. Following UV damage the complex shuttles to the nucleus and concurrently CSN1, CSN3 and CSN8 are phosphorylated at ATM/ATR consensus sequences. This is predicted to affect COP9 CRL binding and regulation (Fuzesi-Levi *et al.*, 2014; Matsuoka *et al.*, 2007).

1.6.3 Regulation of RNR activity by inhibitors

In yeast cells a family of small intrinsically disordered proteins are involved in RNR regulation. In *S. pombe* the 14 kDa Spd1 was originally identified as an inhibitor of S phase progression. Overexpression of Spd1 results in cell cycle arrest in G1 and also a DNA replication checkpoint-dependent cell cycle arrest in G2 (Borgne and Nurse, 2000; Woollard *et al.*, 1996). It was predicted that Spd1 directly interfered with replication and Spd1 was subsequently found to be an inhibitor of RNR (Hakansson *et al.*, 2006a; Liu *et al.*, 2003).

Spd1 has been shown to affect both RNR localisation and activity (Figure 1.8.A). Firstly, Spd1 is required for Suc22 nuclear localisation *in vivo* by promoting the import but not the retention of Suc22 into the nucleus. As Cdc22 is normally dispersed throughout the cell, this was predicted to inhibit RNR complex formation in the cytoplasm. However, mutagenesis of Spd1 has shown that the ability of Spd1 to inhibit RNR is independent of its effect on Suc22 localisation (Liu *et al.*, 2003; Nestoras *et al.*, 2010). Secondly, Spd1 interacts directly with Cdc22 *in vitro* to inhibit RNR activity (Hakansson *et al.*, 2006a). Thirdly, Spd1 promotes changes in RNR architecture which allow fluorescence resonance energy transfer (FRET) when Suc22 and Cdc22 are fluorescently tagged. However, the function of this is unclear.

Spd1 is expressed in G1 and G2 phases of the cell cycle and degraded during S phase (Liu *et al.*, 2003; Woollard *et al.*, 1996). Spd1 degradation by the proteasome is dependent on ubiquitination by the Ddb1-Cul4^{Cdt2} E3 ubiquitin ligase complex (Figure 1.7.B) (Liu *et al.*, 2003). This complex is activated by expression of the substrate receptor Cdt2. Cdt2 interacts directly with Ddb1 and recruits Spd1 to the complex for ubiquitination (Liu *et al.*, 2005)

Figure 1.8

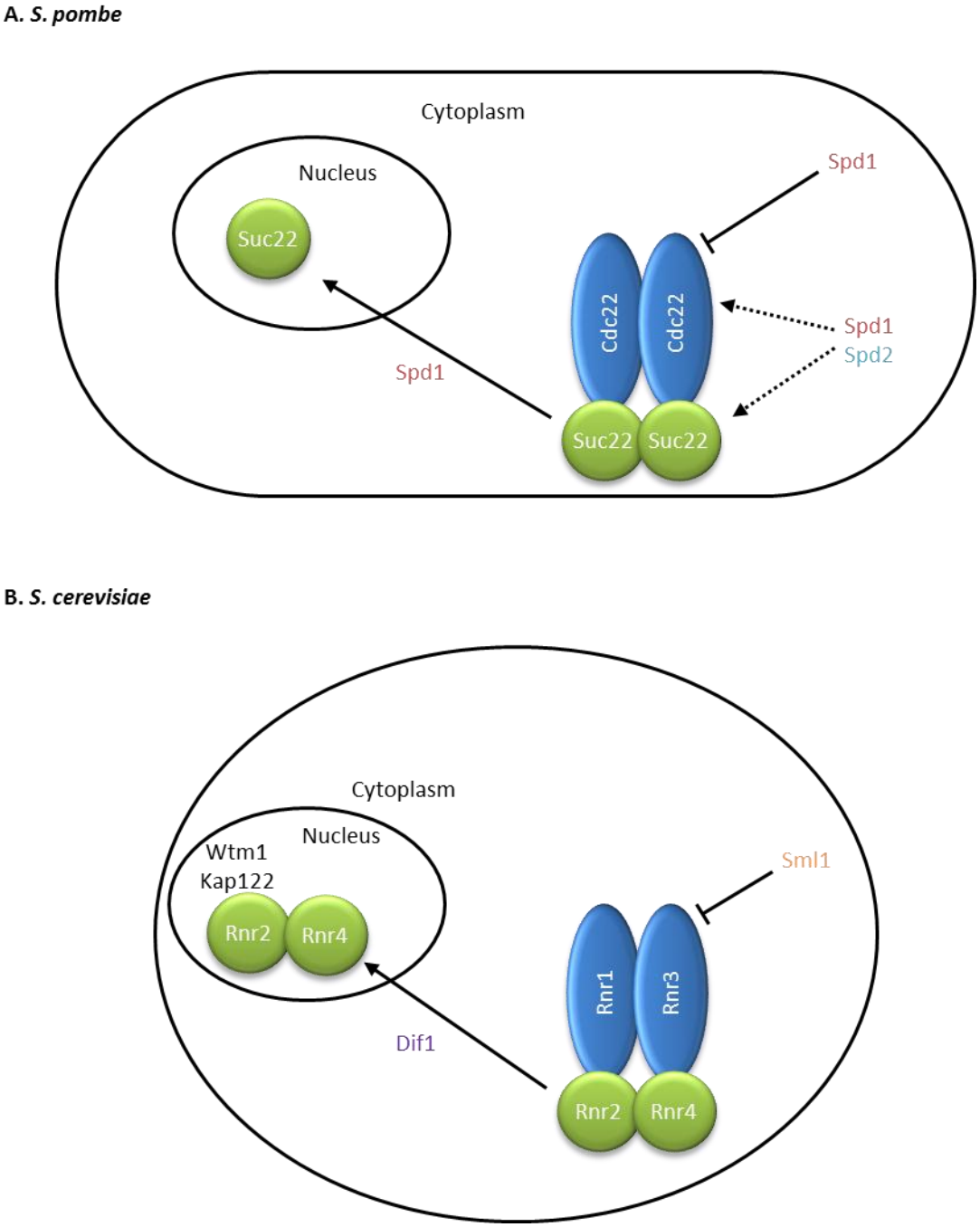


Figure 1.8 Regulation of RNR in *S. pombe* and *S. cerevisiae* by small intrinsically disordered proteins

(A) In *S. pombe* Spd1 interacts directly with Cdc22 to inhibit RNR activity. Spd1 also promotes Suc22 nuclear import. Spd1 and Spd2 promote changes in RNR protein architecture. However, the function of this is unclear.

(B) In *S. cerevisiae* the RNR regulatory functions of *S. pombe* Spd1 are shared by two proteins. Sml1 binds directly to Rnr1 to inhibit RNR activity. Dif1 directly binds Rnr2-Rnr4 complexes and is required for their nuclear import. Their retention in the nucleus is dependent on Wtm1 and Kap122.

Cdt2 expression is regulated by the MBF transcription factor and peaks during S phase (Liu *et al.*, 2005; Yoshida *et al.*, 2003). Cdt2 is expressed in response to HU-induced replication stress dependent on the DNA replication checkpoint components Rad3 and Cds1 (Liu *et al.*, 2005) and in response to DSBs dependent on the DNA damage checkpoint components Rad3 and Chk1 (Moss *et al.*, 2010).

*ddb1*Δ *cdt2*Δ and *rad3*Δ deletion strains are unable to degrade Spd1. Therefore the deletion strains are defective for DNA damage-induced nucleotide synthesis and are sensitive to DNA damage. The damage sensitivity can be partially suppressed by deleting $spd1^{+}$. This is predicted to increase nucleotide pools (Liu *et al.*, 2005; Moss *et al.*, 2010).

Moss *et al.* (2010) demonstrated the importance of DNA damage-induced nucleotide synthesis for HR repair of DSBs. Moss *et al.* (2010) subjected *ddb1*Δ, *cdt2*Δ and *rad3*Δ strains to the DSB assay. All three strains showed reduced repair by HR compared to wild-type. The HR defect was associated with increased levels of LOH and Ch^{16} loss, previously found to result from extensive resection from the break site following failed HR. This was supported by the increased levels of RPA-coated ssDNA observed in a *ddb1*Δ background following DSBs. Deletion of $ku70^{+}$ to promote DSB resection increased the DSB sensitivity of *ddb1*Δ. In contrast, deletion of $exo1^{+}$ to inhibit DSB resection in a *ddb1*Δ *ku70*Δ background partially suppressed the DSB sensitivity. Deletion of $spd1^{+}$ to release RNR inhibition and increase nucleotide pools partially suppressed the HR defect and consequently the DNA damage sensitivity of *ddb1*Δ, *cdt2*Δ and *rad3*Δ strains.

This evidence supported the following model for the role of nucleotide synthesis during HR (Figure 1.9). Activation of Rad3 in response to a DSB up-regulates Cdt2 and activates the Ddb1-$Cul4^{Cdt2}$ complex. Subsequent ubiquitination of Spd1 results in its degradation. This

removes the inhibition of RNR activity and increases nucleotide pools. This provides sufficient nucleotides for efficient post synaptic gap filling during HR repair.

Recently a role was identified for Spd1 in promoting replication stress independently of RNR regulation. Inappropriate expression of Spd1 during S phase in a *ddb1*Δ background results in accumulation of ssDNA and activation of the DNA replication checkpoint. This could be suppressed by deleting *spd1*$^{+}$ but not by increasing nucleotide pools. A second *S. pombe* intrinsically disordered protein Spd2 has also been identified. This protein is also degraded by Ddb1-Cul4^{Cdt2}, required for FRET between Cdc22 and Suc22, but does not affect nucleotide pools (Figure 1.8.A) (Vejrup-Hansen *et al.*, 2014).

In *S. cerevisiae* the RNR regulatory functions of Spd1 are shared by two proteins (Figure 1.8.B). Dif1 binds to Rnr2-Rnr4 complexes and is required for their nuclear import (Lee *et al.*, 2008; Wu and Huang, 2008). Sml1 binds directly to Rnr1 to inhibit RNR activity (Chabes *et al.*, 1999). Dif1 and Sml1 are phosphorylated by Dun1, a kinase downstream of the DNA damage checkpoint. This is required for Dif1 and Sml1 degradation in response to DNA damage (Lee *et al.*, 2008; Wu and Huang, 2008; Zhao and Rothstein, 2002).

1.6.4 Regulation of RNR activity by proteosome degradation

CRL ubiquitin ligases also regulate RNR activity in human cells. Cyclin F is the substrate receptor of the Skp1-Cul1$^{Cyclin\ F}$ E3 ubiquitin ligase complex and is expressed in the G2 phase of the cell cycle. Cyclin F interacts with RRM2 which has been phosphorylated by CDK and recruits it to Skp1-Cul1$^{Cyclin\ F}$ complex. This mediates RRM2 ubiquitination and subsequent degradation. RRM2 degradation in G2 is required to maintain the balance of dNTPs and therefore genome stability. Cyclin F levels decrease in response to DNA damage in an ATR-dependent manner. This is essential for efficient DNA repair (D'Angiolella *et al.*, 2012).

Figure 1.9

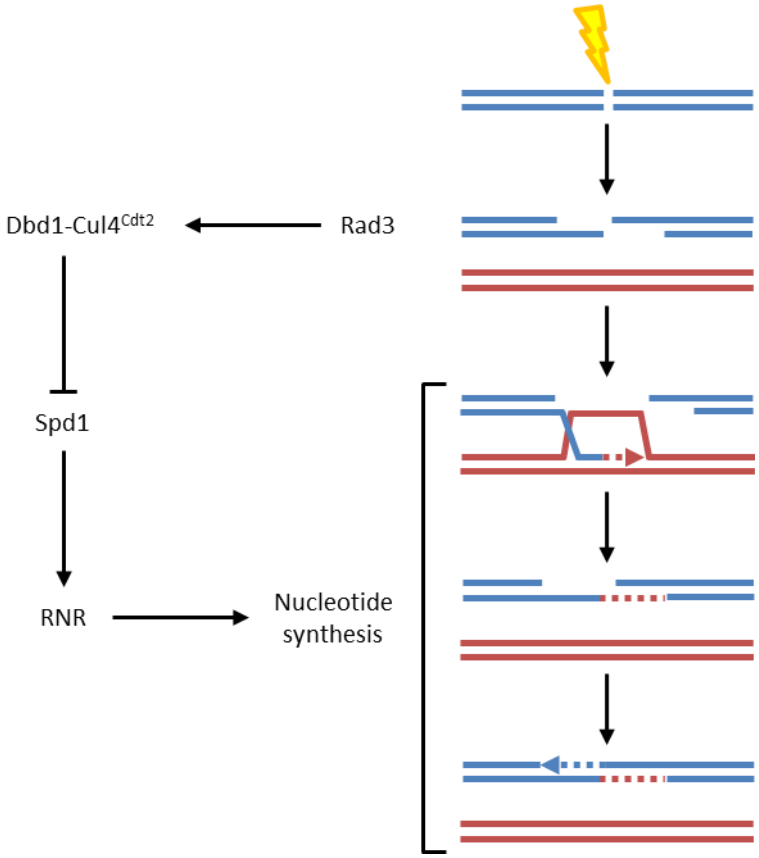


Figure 1.9 DSB-induced nucleotide synthesis promotes efficient HR in *S. pombe*

Figure adapted from Moss *et al.* (2010). Model showing how regulation of RNR activity in response to DSBs promotes nucleotide synthesis and efficient HR. Activation of Rad3 in response to a DSB leads to activation of the Ddb1-Cul4^{Cdt2} complex. Subsequent ubiquitination of Spd1 results in its degradation. This removes Spd1 inhibition of RNR activity and increases nucleotide pools. This provides sufficient nucleotides for efficient post synaptic gap filling during HR repair.

1.7 AIMS OF THIS WORK

Nucleotide synthesis is a conserved and highly regulated response to DNA damage, required for the efficient repair of DNA DSBs by HR. This is essential to prevent LOH and to maintain genome stability. The aim of this project was to identify genes with novel roles in HR through damage-induced nucleotide synthesis. This was investigated by:

- Performing a screen to identify *S. pombe* gene deletion strains showing suppression of DNA DSB sensitivity when the RNR inhibitor *spd1*$^{+}$ was deleted. It was predicted that deleting *spd1*$^{+}$ would promote nucleotide synthesis (Chapter 3).
- Further characterising the role of the DNA damage checkpoint in damage-induced nucleotide synthesis and HR (Chapter 4).
- Further characterising the role of Ngg1 and other components of the Gcn5 HAT protein module in nucleotide synthesis and HR (Chapter 5).

Chapter 2 Methods

2.1 GENERAL LABORATORY SUPPLIES

General laboratory chemicals were purchased from Fisher Scientific, Invitrogen and Sigma-Aldrich. Bleocin and G418 were purchased from Calbiochem. Ampicillin, deoxyribonucleic acid sodium salt (salmon sperm) and RNase A were purchased from Fisher Scientific. Bacterial grade agar was purchased from Formedium. β-glucuronidase, cycloheximide, hygromycin B, typtone and yeast extract, were purchased from Sigma-Aldrich. Zymolyase 20T was purchased from from MP Biomedicals.

DNA grade agarose was purchased from VWR, UltraPure™ agarose from Invitrogen and low melting temperature (LMT) agarose from Sigma-Aldrich. Mini-PROTEAN® TGX™ precast polyacrylamide gels were purchased from Biorad. All DNA ladders, restriction endonucleases, ligases, *Taq* DNA polymerase, and Phusion™ high fidelity DNA polymerase, were obtained from New England Biolabs (NEB). dNTPs were purchased from Thermo Scientific. Oligonucleotides were synthesised by Sigma-Aldrich and are listed in Appendix II.

The following kits were used: Maxi-prep, Mini-prep, QIAquick gel extraction (Qiagen), MasterPure™ Yeast DNA Purification Kit (Epicentre), Amersham ECL™ and ECL plus™ western blotting detection reagents, Amersham megaprime™ DNA labelling system and Illustra ProbeQuant G-50 Micro Columns (GE Healthcare).

The following centrifuges were used during this research: Beckman Coulter Avanti J-26 XP, Beckman Coulter Allegra X-12 R, Eppendorf microcentrifuge 5415D, Eppendorf microcentrifuge 5424 and SciQuip Sigma 1-14 microcentrifuge.

2.2 BUFFERS AND SOLUTIONS

Buffers and solutions provided with commercial kits were used as specified by the manufacturer. Non-commercial buffers and solutions were made using Milli-Q® (MQ) water and autoclaved or filter sterilised. Non-commercial buffers and solutions are listed below:

4', 6-diamidino-2-phenylindole (DAPI) agarose mount

0.1 M tris acetate (pH 8.5), 6 g/L LMT agarose, 1 µg/L DAPI.

Phosphate buffered saline (PBS)

1 PBS tablet per 100 ml MQ water

Tris acetate EDTA (TAE)

40 mM tris base, 20 mM acetic acid, 1 mM EDTA (pH 8.0)

Tris EDTA (TE)

10 mM tris hydrochloric acid (pH 8.0), 1 mM EDTA (pH 8.0)

SP1 solution

1.2 M sorbitol, 50 mM citric acid, 50 mM disodium hydrogen phosphate, 40 mM EDTA (pH 8)

Saline sodium phosphate EDTA (SSPE, pH 7.4)

0.3 M sodium chloride, 20 mM sodium dihydrogen phosphate, 0.2 mM EDTA

Pre-hybridisation buffer

2 × SSPE, 4 g/L bovine serum albumin (BSA, fraction V), 0.25 mg/ml salmon sperm DNA, 3% sodium lauryl sulfate (SDS)

Hybridisation buffer

2 × SSPE, 4 g/L BSA (fraction V), 0.25 mg/ml salmon sperm DNA, 10% dextran sulphate, 3% SDS

Wash buffer (Southern blotting)

0.5%, SSPE, 0.1% SDS

Laemmli solution

100 mM dithiothreitol (DTT), 50 mM tris hydrochloric acid (pH6.8), 10% glycerol, 2% SDS, 0.1%, bromophenol blue

Running buffer

19.2 mM glycine, 2.5 mM tris base, 0.1% SDS

Transfer buffer

9.6 mM glycine, 1.25 mM tris base, 20% methanol

2.3 MEDIA

All media and solutions were dissolved in MQ water and autoclaved or filter sterilised. Agar was added to 2 % for solid media prior to autoclaving.

Lysogeny broth (LB)

0.17 M sodium chloride, 10 g/L tryptone and 10 g/L yeast extract. 100 µg/ml ampicillin was added as required.

Yeast extract six supplements (YE6S)

170 mM glucose, 5 g/L yeast extract plus 225 mg/L of uracil, leucine, histidine, adenine hydrochloride, lysine hydrochloride, arginine hydrochloride. The following drugs were added as required: 500 mg/L G418, 180-240 mg/L hygromycin B and 100 mg/L cycloheximide.

Edinburgh minimal medium (EMM)

110 mM glucose, 93.5 mM ammonium chloride, 15.5 mM di-sodium hydrogen phosphate, 14.7 mM potassium hydrogen phthalate, 1 × salts stock, 1 × vitamins stock and 1 × minerals stock. 150 mg/L of uracil (U), leucine (L), histidine (H), adenine hydrochloride (A), lysine hydrochloride (L) and arginine hydrochloride (R) were added as required. 8 µM thiamine (T) was added as required.

pombe glutamate media (PMG)

110 mM glucose, 20.0 mM L-glutamic acid, 15.5 mM di-sodium hydrogen phosphate, 14.7 mM potassium hydrogen phthalate, 1 × salts stock, 1 × vitamins stock and 1 × minerals stock. 150 mg/L of uracil (U), leucine (L), histidine (H), adenine hydrochloride (A), lysine hydrochloride (L) and arginine hydrochloride (R) were added as required. 8 µM thiamine (T) was added as required.

SPAS mating media

55.5 mM glucose, 7.3 mM potassium di-hydrogen phosphate, 1 × vitamin stock and 45 mg/L uracil, leucine, histidine, adenine hydrochloride, lysine hydrochloride, arginine hydrochloride.

50 × salts stock

0.67 M potassium chloride, 0.26 M magnesium chloride, 14.1 mM disodium sulphate and 5.0 mM calcium chloride.

1000 × vitamins stock

55.5 mM inositol, 8.1 mM nicotinic acid, 4.2 mM pantothenic acid and 40.8 µM biotin.

10000 × minerals stock

80.9 mM boric acid, 47.6 mM citric acid, 23.7 mM manganese sulphate, 13.9 mM zinc sulphate, 7.4 mM iron (III) chloride, 6.0 mM potassium iodide, 2.5 mM molybdic acid, 1.6 mM copper sulphate.

Yeast freezer mix (YFM)

1:1 ratio of YE6S and glycerol.

2.4 PLASMIDS

Appendix III contains the details of plasmids used in this study.

2.5 STRAINS

2.5.1 *Escherichia coli (E. coli)* strains

DH5α^{TM} (F- φ80*lacZ*Δ*M15*Δ(*lacZYA-argF*)U169 *recA1 endA1 hsdR17* (rk-, mk+) *phoA supE44 thi-1 gyrA96 relA1* λ-) *E. coli* from Invitrogen was used in this study.

2.5.2 *Schizosaccharomyces pombe (S. pombe)* strains

Non-minichromosome *S. pombe* strains used in this study are listed in Table 2.1.

Minichromosome *S. pombe* strains used in this study are listed in Table 2.2 and Table 2.3

Table 2.1 Non-minichromosome *S. pombe* strains used in this study

Strain	Genotype	Source
2093	*ade6-D1 arg3-D4 his3-D1 leu1-32 ura4-D18 h*$^+$	Lab stock
2094	*ade6-D1 arg3-D4 his3-D1 leu1-32 ura4-D18 h*$^-$	Lab stock
212	*972 h*$^-$	Lab stock
213	*975 h*$^+$	Lab stock
6958	***cdc22-CFP-kanMX*** *ade6-704 leu1-32 ura4-D18 h*$^+$	S. Kearsey
7919	***suc22-GFP*** *ada6-704, leu1-32, ura4-D18 h*$^-$	J. Wing
6188	***spd1::ura4 mat1_m-cyhS smt0 rpl42::cyhR(sP56Q)*** *ade6- arg3-D4 leu1-32 ura4-D18 h*$^-$	Lab stock
4355	***spd1::hph*** *ade6- arg3-D4 his3-D1 leu1-32 ura4-D18 h*$^-$	Lab stock
8440	***ura4::adh-dmNK-NAT-adh-hENT1*** *ura4-aim h*$^+$	E. Hartsuiker
7184	***urg1::urg1*** **P-HO LE_L-HOcs-*his3*+-EU_R** *his3-D1 leu1-32 ura4-D18 h*$^-$	A. Watson
7910	***ada2::kanMX*** *ade6- arg3-D4 his3-D1 leu1-32 ura4-D18 h*$^+$	This study
7914	***ada2::kanMX spd1::hph*** *ade6- arg3-D4 his3-D1 leu1-32 ura4-D18 h*$^-$	This study

Strain	Genotype	Source
7918	***ada2::kanMX spd1::ura4*** *ade6- arg3-D4 his3-D1 leu1-32 ura4-D18 h*$^{+}$	This study
8205	***alp14::kanMX*** *ade6- arg3-D4 his3-D1 leu1-32 ura4-D18 h*$^{-}$	This study
7281	***alp14::kanMX cdt2-YFP-hph*** *ade6- ura4-D18 leu1-32 h*$^{-}$	This study
8248	***alp14::kanMX spd1::hph*** *ade6- arg3-D4 his3-D1 leu1-32 ura4-D18 h*$^{-}$	This study
7351	***arp42::kanMX*** *ade6- arg3-D4 his3-D1 leu1-32 ura4-D18 h*$^{+}$	This study
7282	***arp42::kanMX cdt2-YFP-hph*** *ade6- ura4-D18 leu1-32 h*$^{-}$	This study
7302	***arp42::kanMX spd1::hph*** *ade6- arg3-D4 his3-D1 leu1-32 ura4-D18 h*$^{-}$	This study
7232	***arp42::kanMX spd1::ura4*** *ade6- arg3-D4 his3-D1 leu1-32 ura4-D18 h*$^{-}$	This study
8199	***atp2::kanMX*** *ade6- arg3-D4 his3-D1 leu1-32 ura4-D18 h*$^{-}$	This study
7269	***atp2::kanMX cdt2-YFP-hph*** *ade6- ura4-D18 leu1-32 h*$^{+}$	This study
7238	***atp2::kanMX spd1::hph*** *ade6- arg3-D4 his3-D1 leu1-32 ura4-D18 h*$^{+}$	This study
8240	***cdt2::kanMX*** *ade6-D1 arg3-D4 his3-D1 leu1-32 ura4-D18 h*$^{+}$	This study
8246	***cdt2::kanMX spd1::hph*** *ade6- arg3-D4 his3-D1 leu1-32 ura4-D18 h*$^{+}$	This study
7165	***cdt2-YFP-hph*** *ade6-M216 ura4-D18 leu1-32 h*$^{+}$	This study
7197	***cdt2-YFP-hph*** *ade6-M216 ura4-D18 leu1-32 h*$^{-}$	This study
7403	***csn1::kanMX*** *ade6- arg3-D4 his3-D1 leu1-32 ura4-D18 h*$^{-}$	This study
7272	***csn1::kanMX cdt2-YFP-hph*** *ade6- his3-D1 leu1-32 ura4-D18 h*$^{+}$	This study
8209	***csn1::kanMX spd1::hph*** *ade6- arg3-D4 his3-D1 leu1-32 ura4-D18 h*$^{-}$	This study
7401	***csn1::kanMX spd1::ura4*** *ade6- arg3-D4 his3-D1 leu1-32 ura4-D18 h*$^{-}$	This study
3738	***ddb1::kanMX*** *ade6-D1 arg3-D4 his3-D1 leu1-32 ura4-D18 h*$^{-}$	Lab stock
7317	***ddb1::kanMX cdt2-YFP-hph*** *ade6- his3-D1 leu1-32 ura4-D18 h*$^{-}$	This study
8208	***ddb1::kanMX spd1::hph*** *ade6- arg3-D4 his3-D1 leu1-32 ura4-D18 h*$^{+}$	This study

Strain	Genotype	Source
8390	***eaf6::kanMX*** *ade6- arg3-D4 his3-D1 leu1-32 ura4-D18 h*$^{-}$	This study
8398	***eaf6::kanMX gcn5::kanMX*** *ade6- arg3-D4 his3-D1 leu1-32 ura4-D18 h*$^{-}$	This study
8387	***eaf7::kanMX*** *ade6- arg3-D4 his3-D1 leu1-32 ura4-D18 h*$^{-}$	This study
8395	***eaf7::kanMX gcn5::kanMX*** *ade6- arg3-D4 his3-D1 leu1-32 ura4-D18 h*$^{-}$	This study
8382	***elp3::kanMX*** *ade6- arg3-D4 his3-D1 leu1-32 ura4-D18 h*$^{+}$	This study
8391	***elp3::kanMX gcn5::kanMX*** *ade6- arg3-D4 his3-D1 leu1-32 ura4-D18 h*$^{+}$	This study
8610	***exo1::kanMX urg1::urg1 P-HO LE_L-HOcs-his3+-EU_R*** *his3-D1 leu1-32 ura4-D18 h*$^{-}$	This study
8044	***exo1::ura4 urg1::urg1 P-HO LE_L-HOcs-his3+-EU_R*** *his3-D1 leu1-32 ura4-D18 h*$^{-}$	This study
8304	***gcn5::kanMX*** *ade6- arg3-D4 his3-D1 leu1-32 ura4-D18 h*$^{-}$	This study
8303	***gcn5::kanMX*** *ade6- arg3-D4 his3-D1 leu1-32 ura4-D18 h*$^{+}$	This study
7912	***gcn5::kanMX spd1::hph*** *ade6- arg3-D4 his3-D1 leu1-32 ura4-D18 h*$^{+}$	This study
8410	***gcn5::kanMX spd1::ura4*** *ade6- arg3-D4 his3-D1 leu1-32 ura4-D18 h*$^{+}$	This study
8570	***gcn5::kanMX ura4::adh-dmNK-NAT-adh-hENT1*** *ura4-aim h*$^{+}$	This study
5465	***hat1::kanMX*** *ade6- arg3-D4 his3-D1 leu1-32 ura4-D18 h*$^{+}$	Lab stock
8389	***hat1::kanMX*** *ade6- arg3-D4 his3-D1 leu1-32 ura4-D18 h*$^{+}$	This study
8397	***hat1::kanMX gcn5::kanMX*** *ade6- arg3-D4 his3-D1 leu1-32 ura4-D18 h*$^{-}$	This study
7334, 8296	***hus1::kanMX*** *ade6- arg3-D4 his3-D1 leu1-32 ura4-D18 h*$^{-}$	This study
7174	***hus1::kanMX cdt2-YFP-hph*** *ade6- his3-D1 leu1-32 ura4-D18 h*$^{-}$	This study
8195	***hus1::kanMX spd1::hph*** *ade6- arg3-D4 his3-D1 leu1-32 ura4-D18 h*$^{-}$	This study
7402	***hus1::kanMX spd1::ura4*** *ade6- arg3-D4 his3-D1 leu1-32 ura4-D18 h*$^{-}$	This study
4455	***ku70::ura4*** *ade6- arg3-D4 his3-D1 leu1-32 ura4-D18*$^{-}$*h*$^{-}$	Lab stock

Strain	Genotype	Source
7352	***liz1::kanMX*** *ade6- arg3-D4 his3-D1 leu1-32 ura4-D18 h*$^{+}$	This study
7274	***liz1::kanMX cdt2-YFP-hph*** *ade6- his3-D1 leu1-32 ura4-D18 h*$^{-}$	This study
7244	***liz1::kanMX spd1::hph*** *ade6- arg3-D4 his3-D1 leu1-32 ura4-D18 h*$^{+}$	This study
7473	***liz1::kanMX spd1::ura4*** *ade6- arg3-D4 his3-D1 leu1-32 ura4-D18 h*$^{-}$	This study
7442, 8343	***ngg1::kanMX*** *ade6- arg3-D4 his3-D1 leu1-32 ura4-D18 h*$^{-}$	This study
7907, 8344	***ngg1::kanMX*** *ade6- arg3-D4 his3-D1 leu1-32 ura4-D18 h*$^{+}$	This study
8464	***cdc22-CFP-kanMX ngg1::kanMX*** *ade6- leu1-32 ura4-D18 h*	This study
8466	***suc22-GFP ngg1::kanMX*** *ade6- leu1-32 ura4-D18 h*	This study
7296	***ngg1::kanMX cdt2-YFP-hph*** *ade6- leu1-32 ura4-D18 h*$^{-}$	This study
7911	***ngg1::kanMX spd1::hph*** *ade6- arg3-D4 his3-D1 leu1-32 ura4-D18 h*$^{-}$	This study
7462	***ngg1::kanMX spd1::ura4*** *ade6- arg3-D4 his3-D1 leu1-32 ura4-D18 h*$^{-}$	This study
8569	***ngg1::kanMX ura4::adh-dmNK-NAT-adh-hENT1*** *ura4-aim h*$^{-}$	This study
8384	***nrc1::kanMX*** *ade6- arg3-D4 his3-D1 leu1-32 ura4-D18 h*$^{+}$	This study
8412	***nrc1::kanMX gcn5::kanMX*** *ade6- arg3-D4 his3-D1 leu1-32 ura4-D18 h*$^{+}$	This study
8236	***nse6::kanMX*** *ade6- arg3-D4 his3-D1 leu1-32 ura4-D18 h*$^{-}$	This study
7263	***nse6::kanMX cdt2-YFP-hph*** *ade6- ura4-D18 leu1-32 h*$^{-}$	This study
8241	***nse6::kanMX spd1::hph*** *ade6- arg3-D4 his3-D1 leu1-32 ura4-D18 h*$^{+}$	This study
8386	***nto1::kanMX*** *ade6- arg3-D4 his3-D1 leu1-32 ura4-D18 h*$^{-}$	This study
8394	***nto1::kanMX gcn5::kanMX*** *ade6- arg3-D4 his3-D1 leu1-32 ura4-D18 h*$^{-}$	This study
8565	***pab1::kanMX*** *ade6- arg3-D4 his3-D1 leu1-32 ura4-D18 h*$^{+}$	This study
7278	***pab1::kanMX cdt2-YFP-hph*** *ade6- ura4-D18 leu1-32 h*$^{+}$	This study

Strain	Genotype	Source
8611	***pab1::kanMX spd1::hph*** *ade6- arg3-D4 his3-D1 leu1-32 ura4-D18 h*$^{-}$	This study
7349	***pmk1::kanMX*** *ade6- arg3-D4 his3-D1 leu1-32 ura4-D18 h*$^{-}$	This study
7273	***pmk1::kanMX cdt2-YFP-hph*** *ade6- ura4-D18 leu1-32 h*$^{-}$	This study
8210	***pmk1::kanMX spd1::hph*** *ade6- arg3-D4 his3-D1 leu1-32 ura4-D18 h*$^{-}$	This study
7399	***pmk1::kanMX spd1::ura4*** *ade6- arg3-D4 his3-D1 leu1-32 ura4-D18 h*$^{-}$	This study
7333	***rad1::kanMX*** *ade6- arg3-D4 his3-D1 leu1-32 ura4-D18 h*$^{-}$	This study
7173	***rad1::kanMX cdt2-YFP-hph*** *ade6- leu1-32 ura4-D18 h*$^{-}$	This study
8249	***rad1::kanMX spd1::hph*** *ade6- arg3-D4 his3-D1 leu1-32 ura4-D18 h*$^{+}$	This study
7476	***rad1::kanMX spd1::ura4*** *ade6- arg3-D4 his3-D1 leu1-32 ura4-D18 h*$^{-}$	This study
7331	***rad17::kanMX*** *ade6- arg3-D4 his3-D1 leu1-32 ura4-D18 h*$^{-}$	This study
7171	***rad17::kanMX cdt2-YFP-hph*** *ade6- his3-D1 leu1-32 ura4-D18 h*$^{+}$	This study
7794	***rad17::kanMX spd1::hph*** *ade6- arg3-D4 his3-D1 leu1-32 ura4-D18 h*$^{-}$	This study
7472	***rad17::kanMX spd1::ura4*** *ade6- arg3-D4 his3-D1 leu1-32 ura4-D18 h*$^{-}$	This study
8040, 8049	***rad17::ura4 urg1::urg1 P-HO LE_L-HOcs-his3+-EU_R*** *his3-D1 leu1-32 ura4-D18 h*$^{+}$	This study
7330	***rad26::kanMX*** *ade6- arg3-D4 his3-D1 leu1-32 ura4-D18 h*$^{-}$	This study
7170	***rad26::kanMX cdt2-YFP-hph*** *ade6- leu1-32 ura4-D18 h*$^{-}$	This study
8194	***rad26::kanMX spd1::hph*** *ade6- arg3-D4 his3-D1 leu1-32 ura4-D18 h*$^{+}$	This study
7471	***rad26::kanMX spd1::ura4*** *ade6- arg3-D4 his3-D1 leu1-32 ura4-D18 h*$^{-}$	This study
7329	***rad3::kanMX*** *ade6- arg3-D4 his3-D1 leu1-32 ura4-D18 h*$^{-}$	This study
7169	***rad3::kanMX cdt2-YFP-hph*** *ade6- leu1-32 ura4-D18 h*$^{-}$	This study
8295	***rad3::kanMX spd1::hph*** *ade6- arg3-D4 his3-D1 leu1-32 ura4-D18 h*$^{+}$	This study
7475	***rad3::kanMX spd1::ura4*** *ade6- arg3-D4 his3-D1 leu1-32 ura4-D18 h*$^{-}$	This study

Strain	Genotype	Source
8568	***rad3::kanMX ura4::adh-dmNK-NAT-adh-hENT1*** *ura4-aim* h^+	This study
8092, 8093	***rad3::ura4 exo1::ura4 urg1::urg1 P-HO LE_L-HOcs-his3+-EU_R*** *his3-D1 leu1-32 ura4-D18* h^-	This study
8091	***rad3::ura4 urg1::urg1*** **P-HO LE_L-HOcs-*his3*+-EU_R** *his3-D1 leu1-32 ura4-D18* h^+	This study
7414	***rad9::kanMX*** *ade6- arg3-D4 his3-D1 leu1-32 ura4-D18* h^+	This study
7172	***rad9::kanMX cdt2-YFP-hph*** *ade6- leu1-32 ura4-D18* h^+	This study
7146	***rad9::kanMX spd1::hph*** *ade6- arg3-D4 his3-D1 leu1-32 ura4-D18* h^-	This study
7415	***rad9::kanMX spd1::ura4*** *ade6- arg3-D4 his3-D1 leu1-32 ura4-D18* h^-	This study
8050	***rad9::ura4 urg1::urg1 P-HO LE_L-HOcs-his3+-EU_R*** *his3-D1 leu1-32 ura4-D18* h^+	This study
8203	***rpp202::kanMX*** *ade6- arg3-D4 his3-D1 leu1-32 ura4-D18* h^+	This study
7279	***rpp202::kanMX cdt2-YFP-hph*** *ade6- ura4-D18 leu1-32* h^+	This study
8211	***rpp202::kanMX spd1::hph*** *ade6- arg3-D4 his3-D1 leu1-32 ura4-D18* h^+	This study
8388	***rtt109::kanMX*** *ade6- arg3-D4 his3-D1 leu1-32 ura4-D18* h^-	This study
8396	***rtt109::kanMX gcn5::kanMX*** *ade6- arg3-D4 his3-D1 leu1-32 ura4-D18* h^+	This study
7909	***sgf29::kanMX*** *ade6- arg3-D4 his3-D1 leu1-32 ura4-D18* h^+	This study
7913	***sgf29::kanMX spd1::hph*** *ade6- arg3-D4 his3-D1 leu1-32 ura4-D18* h^-	This study
8292	***sod2::kanMX*** *ade6- arg3-D4 his3-D1 leu1-32 ura4-D18* h^+	This study
7268	***sod2::kanMX cdt2-YFP-hph*** *ade6- ura4-D18 leu1-32* h^-	This study
8293	***sod2::kanMX spd1::hph*** *ade6- arg3-D4 his3-D1 leu1-32 ura4-D18* h^+	This study
8612	***SPAC806.05::kanMX*** *ade6- arg3-D4 his3-D1 leu1-32 ura4-D18 h*	This study
7298	***SPAC806.05::kanMX cdt2-YFP-hph*** *ade6- ura4-D18 leu1-32* h^-	This study
8613	***SPAC806.05::kanMX spd1::hph*** *ade6- arg3-D4 his3-D1 leu1-32 ura4-D18* h^+	This study

Strain	Genotype	Source
8614	***SPBC21C3.12c::kanMX*** *ade6- arg3-D4 his3-D1 leu1-32 ura4-D18 h*$^{+}$	This study
7297	***SPBC21C3.12c::kanMX cdt2-YFP-hph*** *ade6- ura4-D18 leu1-32 h*$^{+}$	This study
8615	***SPBC21C3.12c::kanMX spd1::hph*** *ade6- arg3-D4 his3-D1 leu1-32 ura4-D18 h*$^{+}$	This study
7441	***SPBC557.02c::kanMX*** *ade6- arg3-D4 his3-D1 leu1-32 ura4-D18 h*$^{-}$	This study
7295	***SPBC557.02c::kanMX cdt2-YFP-hph*** *ade6- his3-D1 leu1-32 ura4-D18 h*$^{-}$	This study
8244	***SPBC557.02c::kanMX spd1::hph*** *ade6- arg3-D4 his3-D1 leu1-32 ura4-D18 h*$^{+}$	This study
7602	***SPBC557.02c::kanMX spd1::ura4*** *ade6- arg3-D4 his3-D1 leu1-32 ura4-D18 h*$^{+}$	This study
7440	***swi3::kanMX*** *ade6- arg3-D4 his3-D1 leu1-32 ura4-D18 h*$^{-}$	This study
7283	***swi3::kanMX cdt2-YFP-hph*** *ade6- ura4-D18 leu1-32 h*$^{-}$	This study
8213	***swi3::kanMX spd1::hph*** *ade6- arg3-D4 his3-D1 leu1-32 ura4-D18 h*$^{-}$	This study
7474	***swi3::kanMX spd1::ura4*** *ade6- arg3-D4 his3-D1 leu1-32 ura4-D18 h*$^{-}$	This study
7348	***trm112::kanMX*** *ade6- arg3-D4 his3-D1 leu1-32 ura4-D18 h*$^{-}$	This study
7275	***trm112::kanMX cdt2-YFP-hph*** *ade6- ura4-D18 leu1-32 h*$^{+}$	This study
7245	***trm112::kanMX spd1::hph*** *ade6- leu1-32 ura4-D18 h*$^{+}$	This study
7600	***trm112::kanMX spd1::ura4*** *ade6- arg3-D4 his3-D1 leu1-32 ura4-D18 h*$^{+}$	This study
8566	***trt1::kanMX*** *ade6- arg3-D4 his3-D1 leu1-32 ura4-D18 h*$^{+}$	This study
7265	***trt1::kanMX cdt2-YFP-hph*** *ade6- ura4-D18 leu1-32 h*$^{-}$	This study
8567	***trt1::kanMX spd1::hph*** *ade6- arg3-D4 his3-D1 leu1-32 ura4-D18 h*$^{+}$	This study
8198	***uge1::kanMX*** *ade6- arg3-D4 his3-D1 leu1-32 ura4-D18 h*$^{+}$	This study
7267	***uge1::kanMX cdt2-YFP-hph*** *ade6- ura4-D18 leu1-32 h*$^{+}$	This study
8294	***uge1::kanMX spd1::hph*** *ade6- arg3-D4 his3-D1 leu1-32 ura4-D18 h*$^{-}$	This study
8200	***vam7::kanMX*** *ade6- arg3-D4 his3-D1 leu1-32 ura4-D18 h*$^{+}$	This study

Strain	Genotype	Source
7270	***vam7::kanMX cdt2-YFP-hph*** *ade6- his3-D1 leu1-32 ura4-D18 h*$^{+}$	This study
8207	***vam7::kanMX spd1::hph*** *ade6- arg3-D4 his3-D1 leu1-32 ura4-D18 h*$^{+}$	This study
8201	***vps16::kanMX*** *ade6- arg3-D4 his3-D1 leu1-32 ura4-D18 h*$^{-}$	This study
7271	***vps16::kanMX cdt2-YFP-hph*** *ade6- ura4-D18 leu1-32 h*$^{+}$	This study
7242	***vps16::kanMX spd1::hph*** *ade6- arg3-D4 his3-D1 leu1-32 ura4-D18 h*$^{+}$	This study
8383	***yaf9::kanMX*** *ade6- arg3-D4 his3-D1 leu1-32 ura4-D18 h*$^{-}$	This study
8392	***yaf9::kanMX gcn5::kanMX*** *ade6- arg3-D4 his3-D1 leu1-32 ura4-D18 h*$^{-}$	This study

Table 2.2 Minichromosome *S. pombe* strains transformed with REP81X plasmids

Strain	Genotype	Parent	pREP 81X	pREP81X-HO
2654[1], 7332	*ade6-M210 arg3-D4 his3-D1 leu1-32 ura4-D18* **Ch[16]-RMYAH**	-	4125[2]	4104,4121, 4122[2]
7924-7926	***ada2::kanMX*** *ade6-M210 arg3-D4 his3-D1 leu1-32 ura4-D18* **Ch[16]-RMYAH**	7910	7987	7988-7990
7927-7929	***ada2::kanMX spd1::ura4*** *ade6-M210 arg3-D4 his3-D1 leu1-32 ura4-D18* **Ch[16]-RMYAH**	7918	8057	8058-8060
7636-7638	***arp42::kanMX*** *ade6-M210 arg3-D4 his3-D1 leu1-32 ura4-D18* **Ch[16]-RMYAH**	7351	8622	8623-8625
7624-7626	***arp42::kanMX spd1::ura4*** *ade6-M210 arg3-D4 his3-D1 leu1-32 ura4-D18* **Ch[16]-RMYAH**	7756	7756	7757-7759
7526-7528	***csn1::kanMX*** *ade6-M210 arg3-D4 his3-D1 leu1-32 ura4-D18* **Ch[16]-RMYAH**	7403	7596	7597-7599
7578-7580	***csn1::kanMX spd1::ura4*** *ade6-M210 arg3-D4 his3-D1 leu1-32 ura4-D18* **Ch[16]-RMYAH**	7401	7426	7593-7595
8318-8320	***gcn5::kanMX*** *ade6-M210 arg3-D4 his3-D1 leu1-32 ura4-D18* **Ch[16]-RMYAH**	8304	8349	8350-8352
8456-8458	***gcn5::kanMX spd1::ura4*** *ade6-M210 arg3-D4 his3-D1 leu1-32 ura4-D18* **Ch[16]-RMYAH**	8410	8459	8460-8461
5544-5546[1]	***hat1::kanMX*** *ade6-M210 arg3-D4 his3-D1 leu1-32 ura4-D18* **Ch[16]-RMYAH**	5465[3]	5626[3]	5623-5625[3]
8626	***hat1::kanMX gcn5::kanMX*** *ade6-M210 arg3-D4 his3-D1 leu1-32 ura4-D18* **Ch[16]-RMYAH**	8397	8627	8628-8630
7342-7344	***hus1::kanMX*** *ade6-M210 arg3-D4 his3-D1 leu1-32 ura4-D18* **Ch[16]-RMYAH**	7334	7431	7432-7434
7523-7525	***hus1::kanMX spd1::ura4*** *ade6-M210 arg3-D4 his3-D1 leu1-32 ura4-D18* **Ch[16]-RMYAH**	7402	8086	8087-8089
5301-5303[2]	***ku70::ura4*** *ade6-M210 arg3-D4 his3-D1 leu1-32 ura4-D18* **Ch[16]-RMYAH**	4455[4]	5352[2]	5348, 5349,5351[2]
7500-7502	***liz1::kanMX*** *ade6-M210 arg3-D4 his3-D1 leu1-32 ura4-D18* **Ch[16]-RMYAH**	7352	7573	7574-7576

Strain	Genotype	Parent	pREP 81X	pREP81X-HO
7627-7629	***liz1::kanMX spd1::ura4*** *ade6-M210 arg3-D4 his3-D1 leu1-32 ura4-D18* **Ch^{16}-RMYAH**	7473	7639	7640-7642
7480-7482	***ngg1::kanMX*** *ade6-M210 arg3-D4 his3-D1 leu1-32 ura4-D18* **Ch^{16}-RMYAH**	7442	7513	7514-7516
8315-8317	***ngg1::kanMX ku70::ura4*** *ade6-M210 arg3-D4 his3-D1 leu1-32 ura4-D18* **Ch^{16}-RMYAH**	7907, 5301	8345	8346-8348
8404-8405	***ngg1::kanMX ku70::ura4 spd1::ura4*** *ade6-M210 arg3-D4 his3-D1 leu1-32 ura4-D18* **Ch^{16}-RMYAH**	7581, 8315	8406	8407-8409
7581-7583	***ngg1::kanMX spd1::ura4*** *ade6-M210 arg3-D4 his3-D1 leu1-32 ura4-D18* **Ch^{16}-RMYAH**	7462	7610	7611-7613
7506-7508	***pmk1::kanMX*** *ade6-M210 arg3-D4 his3-D1 leu1-32 ura4-D18* **Ch^{16}-RMYAH**	7349	7549	7550-7552
7691-7693	***pmk1::kanMX spd1::ura4*** *ade6-M210 arg3-D4 his3-D1 leu1-32 ura4-D18* **Ch^{16}-RMYAH**	7399	7694	7695-7697
7477-7479	***rad1::kanMX*** *ade6-M210 arg3-D4 his3-D1 leu1-32 ura4-D18* **Ch^{16}-RMYAH**	7333	7493	7494-7496
7503-7505	***rad1::kanMX spd1::ura4*** *ade6-M210 arg3-D4 his3-D1 leu1-32 ura4-D18* **Ch^{16}-RMYAH**	7476	7545	7546-7548
7361-7363	***rad17::kanMX*** *ade6-M210 arg3-D4 his3-D1 leu1-32 ura4-D18* **Ch^{16}-RMYAH**	7331	7427	7428-7430
7520-7522	***rad17::kanMX spd1::ura4*** *ade6-M210 arg3-D4 his3-D1 leu1-32 ura4-D18* **Ch^{16}-RMYAH**	7472	7565	7566-7568
7339-7341	***rad26::kanMX*** *ade6-M210 arg3-D4 his3-D1 leu1-32 ura4-D18* **Ch^{16}-RMYAH**	7330	7423	7424-7426
7542-7544	***rad26::kanMX spd1::ura4*** *ade6-M210 arg3-D4 his3-D1 leu1-32 ura4-D18* **Ch^{16}-RMYAH**	7471	7584	7585-7587
7336-7338	***rad3::kanMX*** *ade6-M210 arg3-D4 his3-D1 leu1-32 ura4-D18* **Ch^{16}-RMYAH**	7329	7419	7420-7422
7517-7519	***rad3::kanMX spd1::ura4*** *ade6-M210 arg3-D4 his3-D1 leu1-32 ura4-D18* **Ch^{16}-RMYAH**	7475	7561	7562-7564
7497-7499	***rad9::kanMX*** *ade6-M210 arg3-D4 his3-D1 leu1-32 ura4-D18* **Ch^{16}-RMYAH**	7414	7588	7589-7591

Strain	Genotype	Parent	pREP 81X	pREP81X-HO
7443-7745	***rad9::kanMX spd1::ura4*** *ade6-M210 arg3-D4 his3-D1 leu1-32 ura4-D18* **Ch^{16}-RMYAH**	7415	7463	7464-7466
7603-7605	***SPBC557.02c::kanMX*** *ade6-M210 arg3-D4 his3-D1 leu1-32 ura4-D18* **Ch^{16}-RMYAH**	7441	7606	7607-7609
7630-7632	***SPBC557.02c::kanMX spd1::ura4*** *ade6-M210 arg3-D4 his3-D1 leu1-32 ura4-D18* **Ch^{16}-RMYAH**	7602	7647	7648-7649
7486-7488	***swi3::kanMX*** *ade6-M210 arg3-D4 his3-D1 leu1-32 ura4-D18* **Ch^{16}-RMYAH**	7440	7509	7510-7512
7633-7635	***swi3::kanMX spd1::ura4*** *ade6-M210 arg3-D4 his3-D1 leu1-32 ura4-D18* **Ch^{16}-RMYAH**	7474	7643	7644-7646
7732-7734	***trm112::kanMX*** *ade6-M210 arg3-D4 his3-D1 leu1-32 ura4-D18* **Ch^{16}-RMYAH**	7348	8353	8354-8356
7735-7737	***trm112::kanMX spd1::ura4*** *ade6-M210 arg3-D4 his3-D1 leu1-32 ura4-D18* **Ch^{16}-RMYAH**	7600	7738	7739-7741

Ch^{16}-RMYAH genotype: Ch^{16} *yps1::arg3^{+} rpm1::MATa-hph ade6-M216 cid2::his3^{+}*

Strains were made during this study except where indicated: made by [1]J. Cullen, [2]J. Moss, [3]R. Deegan, [4]laboratory stock.

The parental strain is the auxotrophic gene deletion strain subsequently crossed with a strain containing Ch^{16}-RMYAH.

Table 2.3 Minichromosome *S.pombe* strains transformed with REP41X plasmids

Strain	Genotype	Parent	pREP4 1X	pREP41X-HO
2654[1]	*ade6-M210 arg3-D4 his3-D1 leu1-32 ura4-D18* **Ch^{16}-RMYAH**	-	8400	8401-8403
8315-8317	***ngg1::kanMX ku70::ura4*** *ade6-M210 arg3-D4 his3-D1 leu1-32 ura4-D18* **Ch^{16}-RMYAH**	7907,5301	8357	8358-8360

Ch^{16}-RMYAH genotype: Ch^{16} *yps1::arg3^{+} rpm1::MATa-hph ade6-M216 cid2::his3^{+}*

Strains were made during this study except where indicated: made by [1]J. Cullen.

The parental strain is the auxotrophic gene deletion strain subsequently crossed with a strain containing Ch^{16}-RMYAH.

2.6 GROWTH AND STORAGE CONDITIONS

2.6.1 Growth and storage of *E. coli* strains

E. coli, transformed with plasmid DNA were plated onto LB containing 100 µg/ml ampicillin agar plates and incubated overnight at 37°C. Individual colonies were inoculated into liquid LB containing 100 µg/ml ampicillin and grown overnight at 300 rpm, 37°C in preparation for mini and maxi preps according to the manufactures instructions (Qiagen). *E. coli* were stored permanently at -80°C in Nunc cryo-tubes containing 1 ml saturated culture and 1 ml glycerol.

2.6.2 Growth and storage of *S. pombe* strains

Yeast strains were cultured and stored as described by (Moreno *et al.*, 1991). Yeast strains were grown on nutrient rich YE6S media, or on selective EMM or PMG media with the appropriate amino acid supplements. Strains were grown for 2-3 days on agar plates at 32°C then stored at room temperature. Liquid cultures were inoculated with a loop of cells from fresh agar plates and grown overnight at 250 rpm, 32°C, unless otherwise stated. The absorbance at 595 nm (optical density, OD_{595}) was measured using a Pharmacia Biotech Ultraspec 2000 to determine the concentration of cells in liquid culture. An OD_{595} of 0.1 is equivalent to approximately 2×10^6 cells/ml. Unless stated, cultures were maintained in mid-exponential growth between OD_{595} 0.1 and 0.5. Yeast strains were stored permanently at -80°C in Nunc cryo-tubes containing 1 ml of YE6S and 1 ml of YFM media.

2.7 GENETIC CROSSES

2.7.1 Crossing of *S. pombe* strains by free spore analysis

1 µl loops of two strains with opposite mating types (h+ / h-) were streaked onto SPAS mating media, mixed with 10 µl MQ water and incubated for 2-3 days at 25ºC. Asci were observed by light microscopy. 1 µl loop of cells was resuspended in 1/200 dilution β-glucuronidase and incubated overnight at 25ºC or for 5 hours at 37°C. Serial dilutions were plated onto YE6S and colonies replica plated onto appropriate selective media.

2.7.2 Crossing of *S. pombe* strains by tetrad dissection

1 µl loops of two strains of opposite mating types (h+ / h-) were streaked onto SPAS mating media, mixed with 10 µl MQ water and incubated for 2-3 days at 25ºC. Asci were observed by light microscopy. A 1 µl loop of cells was resuspended in 500 µl MQ water and 10 µl streaked along the side of a YE6S plate. Asci were selected and positioned on the plate using an MSM micro-manipulator (Singer Instruments). The plates were incubated at overnight at 16°C or for approximately 1 hour at 32°C to break down the asci walls. The spores of each asci were separated using the micro manipulator and the plates incubated at 32°C until visible colonies had formed. Colonies were replicated onto appropriate selective media.

2.7.3 Crossing of *S. pombe* strains in array format

ROTOR© (Singer Instruments) was used for high throughput pinning of yeast strains in array format. A 40 ml saturated culture of an *spd1*Δ PEM-2 strain was spotted onto EMM + LARH in 96 array format. The DNA damage sensitive library (see Chapter 3) was revived on YE6S + G418 in 96 array format. Both were incubated for 3 days at 32ºC. The PEM-2 and library arrays were combined on SPAS plates and incubated for 4 days at 25ºC. Cells were pinned to YE6S plates and incubated for 1 day at 32ºC to allow colonies to form. Colonies were pinned onto YE6S + cycloheximide and incubated for 2 days at 32ºC. Colonies were finally pinned onto plates selective for both the PEM-2 and library strains' deletion markers.

2.8 DNA ISOLATION

2.8.1 Isolation of plasmid DNA from *E. coli*

Mini and Maxi preps of single transformed colonies were performed according to the manufacturer's (Qiagen) instructions. Plasmids were confirmed by restriction digest (Section 2.9.1) and the DNA concentration analysed (Section 2.9.6).

2.8.2 Isolation of genomic DNA from *S. pombe* for general use

Genomic DNA was isolated from saturated cultures using the MasterPure^{TM} Yeast DNA Purification Kit (Epicentre) according to the manufacturer's instructions. The DNA concentration was analysed (Section 2.9.6).

2.8.3 Isolation of genomic DNA from *S. pombe* for Southern blotting

Cells from a 50 ml log phase culture of OD_{595} 0.3-0.5 were pelleted at 2100 g for 5 minutes and washed twice with MQ water. The cells were resuspended in 1 ml SP1 solution containing 2.5 mg/ml zymolyase and incubated for 1 hour at 37°C. Light microscopy was used to confirm loss of cellular refractivity on addition of 2% SDS to an equal volume of cellular solution. Cells were pelleted for 10 seconds at 17000 g and the supernatant discarded. The cells were resuspended in 550 µl TE buffer containing 1% SDS and incubated for 1 hour at 65°C. 175 µl 5 M potassium acetate was added and the samples transferred to ice. The samples were centrifuged at 17000 g for 15 minutes at 4°C. 500 µl of the supernatant was retained and added to an equal volume of propan-2-ol. Samples were incubated for 1-24 hours at -20ºC. Nucleic acids were pelleted at 17000 g for 15 minutes at 4°C and the pellet washed with 70% ethanol. The pellet was resuspended in 350 µl of TE containing 50 µg/ml RNase A and incubated for 10 minutes at 65°C, inverting the tube after 5 minutes. 300 µl phenol/chloroform/isoamyl alcohol 25:24:1 solution was added, the samples mixed by

vortexing for 20 seconds and centrifuged at 17000 g for 10 minutes. The aqueous layer was retained. Phenol/chloroform extraction was repeated. The DNA was pelleted at 17000 g for 10 minutes, washed with 70% ethanol and resuspended in 50 µl 1 × TE.

2.8.4 Isolation of DNA from agarose gels

DNA was extracted from 0.5% TAE UltraPure™ agarose gels containing using QIAquick gel extraction kit (Qiagen) according to the manufacturer's instructions.

2.8.5 DNA purification by ethanol precipitation

A 2:1 ratio of 100% ethanol plus a 1:10 ratio of 3M sodium acetate was added to the polymerase chain reaction (PCR) product. DNA was precipitated for 30 minutes at -80ºC or overnight at -20ºC. DNA was pelleted at 17000 g for 30 minutes, washed with 70% ethanol and resuspended in TE buffer.

2.9 DNA MANIPULATION AND ANALYSIS

2.9.1 Standard enzymatic restriction of DNA

Digests were performed in 50 µl with 1 × Reaction buffer (NEB), 1 × BSA, ~0.5 µg DNA and 5 U restriction enzyme (NEB). Reactions were incubated for 2 hours at 37°C.

2.9.2 Enzymatic restriction of DNA for Southern blotting

Digests were performed in 30 µl with 1 × Reaction buffer 3 (NEB), 1 × BSA, 30 µg genomic DNA, 25 U *PvuI* restriction enzyme (NEB) and 25 U *NruI* restriction enzyme (NEB). Reactions were incubated overnight at 37°C. Digestion was confirmed by observing the smearing pattern resolved by gel electrophoresis (Section 2.9.9)

2.9.3 DNA ligation of linearised DNA

Ligations were carried out in 20 µl containing: 30 ng linear DNA vector, 10 × molar excess of linear DNA insert, 1 × T4 DNA ligase buffer with ATP and 400 U T4 DNA ligase (NEB). Reactions were incubated overnight at 37ºC. An additional 400 U of T4 DNA ligase were added and the reaction incubated for a further 6 hours at 37ºC.

2.9.4 Polymerase chain reaction (PCR) using Taq DNA polymerase

50 µl reaction mixtures contained 1 × standard Taq buffer, 200 µM dNTPs, 2.5 U Taq polymerase (NEB), 2 µM forward and reverse primers (synthesised by Sigma), and 50 ng genomic DNA. Typical PCR reaction conditions were: 94°C for 3 minutes, 30 × (94°C for 15 seconds, annealing temperature for 30 seconds, 72°C for 2 minutes), 72°C for 7 minutes.

2.9.5 Polymerase chain reaction (PCR) using Phusion™ high fidelity polymerase

50 µl reaction mixtures contained 1 × Phusion™ high fidelity PCR master mix with high fidelity buffer (NEB), 0.5 µM forward and reverse primers (synthesised by Sigma) and 50 ng of genomic DNA. Typical PCR reaction conditions were: 98°C for 1 minute, 30 × (98°C for 10 seconds, annealing temperature for 20 seconds, 72°C for 2 minutes), 72°C for 7min.

2.9.6 Quantification of DNA samples

DNA concentration was quantified using a Nanodrop 1000 spectrophotometer (Thermo Scientific).

2.9.7 DNA sequencing

Sanger sequencing of PCR amplified DNA was performed by Source BioScience plc (www.lifesciences.sourcebioscience.com). Sequencing data was viewed using SnapGene®

software from GSL Biotech (snapgene.com) and Bioedit sequence alignment editor from Tom Hall, Ibis Biosciences (www.mbio.ncsu.edu/bioedit/bioedit.html).

2.9.8 Whole genome sequencing

Whole genome sequencing was performed by High throughput genomics group, Oxford genomics centre. Sequencing data was viewed using integrative genomics viewer from (Robinson *et al.*, 2011; Thorvaldsdottir *et al.*, 2013) (http://www.broadinstitute.org/igv/).

2.9.9 Standard analysis of DNA by gel electrophoresis

Linear DNA was resolved using a 1% agarose, 1 × TAE, 0.5 µg/ml ethidium bromide gel.

2.9.10 Analysis of genomic DNA by gel electrophoresis for Southern blotting

Restriction enzyme digested genomic DNA (Section 2.9.2) was resolved using a 0.5% UltraPure^{TM} agarose, 1 × TAE gel subjected to 70 V for 30 minutes, followed by 20 V for 15 hours.

2.10 DNA TRANSFORMATION

2.10.1 Transformation of *E. coli* with DNA

150 µl of $CaCl_2$ competent DH5α^{TM} cells were incubated on ice for 10 minutes, mixed with 200 ng plasmid DNA, heat shocked for 45 seconds at 42ºC and returned to ice for 10 minutes. 1 ml LB media was added and the cells incubated for 30 minutes at 37ºC. Cells were pelleted at 17000 g for 2 minutes and resuspended in 150 µl LB media. Serial dilutions were spread onto LB plates supplemented with 100 µg/ml ampicillin and incubated overnight at 37ºC to select for transformants.

2.10.2 Transformation of *S. pombe* with DNA by LiAc method

Cells from a 50 ml log phase culture were pelleted at 900 g for 2 minutes, washed in MQ water and then 100 mM lithium acetate. Cells were resuspended in 100 mM lithium acetate to a final volume of 400 µl. Cells from 50 µl samples were pelleted at 17000 g and the lithium acetate removed. 240 µl 50% polyethylene glycol, 36 µl 1 M lithium acetate, 10 µl 10 mg/ml single stranded DNA and 74 µl DNA in MQ H_2O , the sample mixed by vortexing and incubated for 1 hour at 32ºC. Cells were heat shocked for 30 minutes 42ºC, pelleted at 1500 g washed twice in MQ water and resuspended in 300 µl MQ water. 150 µl was plated onto media selective for transformants and incubated for 2 days at 32ºC.

2.11 SOUTHERN BLOT ANALYSIS

2.11.1 Transfer of genomic DNA to nitrocellulose membrane

The agarose gel containing DNA (Section 2.9.10) was washed for 15 minutes in MQ water then in 0.4 M NaOH, 1 M NaCl for 45 minutes. The DNA was transferred to nitrocellulose membrane (Gene screen plus ™, PerkinElmer) by the downward capillary method, washed in 2 × SSPE solution and crosslinked to the membrane (Spectrolinker™ XL-1500 UV Cross linker, 120 mJ/cm^2). Membranes were stored at 4°C.

2.11.2 Radioactive labelling of probes

DNA probes were amplified by PCR using Phusion™ high fidelity polymerase (NEB), cleaned by ethanol precipitation, analysed by gel electrophoresis and sequenced a described in this chapter. Probe A was amplified using primers 1044 and 1045, probe B using primers 650 and 651. The radioactive steps of Southern blotting were performed by Carol Walker (Department of Oncology, University of Oxford). The radioactive probe labelled with deoxycytidine 5'-triphosphate, [alpha-^{32}P] was synthesised using Amersham megaprime

DNA labelling system (GE healthcare) according to the manufacturer's instructions using 3 µl (1.11 MBq) deoxycytidine 5'-triphosphate, [alpha-^{32}P], 1 ng of a molecular weight marker ladder probe and either 400 ng of probe A or 200 ng probe B. Radioactive probe was separated from unincorporated nucleotides using Illustra ProbeQuant G-50 Micro Columns (GE healthcare) according to the manufacturer's instructions. The probe was boiled for 5 minutes immediately before use.

2.11.3 Southern blotting

The membrane was incubated in 10 ml pre-hybridisation buffer for 1 hour at 65°C in a Hybaid mini lab oven, then in 10 ml hybridisation buffer containing deoxycytidine 5'-triphosphate, [alpha-^{32}P] labelled probe B and molecular weight marker ladder probe, overnight, at 65°C. The membrane was washed briefly with wash buffer (0.5%, SSPE, 0.1% SDS) at room temperature three times. The membrane was then washed with wash buffer for 20 minutes at 65°C and the process repeated to reduce non-specific binding. The blot was exposed to a phosphor screen (Bio-rad) overnight and visualised using a Personal Molecular Imager^{TM} and Quantity One software (Bio-rad). To strip, the membrane was immersed in boiling water and SDS added to 1%. The membrane was incubated in the Hybaid mini lab oven for 30 minutes at room temperature. The stripping was repeated until only background levels of radiation were detected. The hybridisation was then repeated deoxycytidine 5'-triphosphate, [alpha-^{32}P] labelled probe A and molecular weight marker ladder probe.

2.12 ANALYSIS OF DNA DOUBLE STRAND BREAK REPAIR

2.12.1 Double strand break (DSB) assay

For wild-type and each deletion mutant, three independently isolated Ch^{16}-RMYAH strains were obtained and transformed with pREP81X-HO (p28) or pREP41X-HO (p206) plasmids. In addition one Ch^{16}-RMYAH strain was transformed with either the control plasmid, pREP81X (p40) or pREP41X (p39) to allow analysis of break independent events.

The strains were woken on EMM + UT media. This is selective for the minichromosome and plasmid markers. Thiamine will inhibit HO endonuclease expression. The strains were grown for 2-3 days at 32°C. The strains were streaked onto YE6S + hygromycin to select for the *MATa* site on the minichromosome and grown overnight at 32°C.

The assay was performed at 250 rpm, 32°C. Strains were inoculated into 10 ml EMM + UT, (selective for the minichromosome and plasmid) and grown overnight. Cultures were diluted to OD_{595} 0.1 and grown for a further 3 hours. Cells were pelleted at 900 g for 2 minutes and washed twice with 20 ml PBS. The pellets were resuspended in EMM + RAHU (selective for the plasmid but not the minichromosome markers) containing no thiamine to allow expression of HO endonuclease and break induction. Cultures were maintained in exponential growth phase for 48 hours. After 48 hours the cells were plated onto 3 × YE6S plates, such that ~200 colonies were present per plate, and incubated at 32°C for 3 days. The plates were replica plated onto EMM + LAHUT, EMM + LRHUT, EMM + LRAUT and YE6S + G418.

The percentage of colonies which had undergone repair by non-homologous end joining or sister chromatid conversion (NHEJ/SCC) (hygromycin resistant colonies), repair by interchromosomal gene conversion (GC) (hygromycin sensitive colonies minus A- colonies), minichromosome loss (Ch^{16} loss) (R- colonies) and loss of heterozygosity (LOH) (A- colonies

minus R- colonies) were calculated. Spontaneous levels of GC, Ch^{16} loss and LOH, calculated from the blank plasmid controls, were subtracted from the levels observed following break induction to calculate the final levels of break-dependent outcomes. Statistical significance was calculated using the student T-test. For strains carrying REP41X plasmids, the levels of repair events at 0 hours were subtracted from the 48 hour results.

Appendix IV lists all DSB assay results presented in this thesis.

2.12.2 Rapid induction single strand annealing (SSA) assay

All EMM liquid media used in this experiment was autoclaved separately to the ammonium chloride component and the two solutions combined once cool. All solid media was autoclaved following the standard protocol.

Induction strains were woken on EMM + LT two days prior to starting the experiment. The assay was performed at 270 rpm, 32°C. Each strain was inoculated into 100 ml of EMM + L to OD_{595} 0.05-0.10 and incubated for 3 hours. The starter cultures were added to a total volume of 400 ml EMM + L and incubated overnight to reach OD_{595} 0.4-0.5. Cells were pelleted at 1700 g, for 10 min, at 10°C and resuspended in 400 ml EMM + LH. Uracil was added to a final concentration of 0.3 mg/ml to start the induction. 50 ml samples were taken at 0, 30, 60, 120, 180 and 360 minutes and treated with sodium azide, at a final concentration of 0.1%, on ice. Cells were pelleted at 2100 g for 5 minutes, washed with MQ water and the pellets stored at -80°C until ready for DNA extraction. For each time point cells were plated onto two EMM + LHT plates such that ~ 200 colonies were present per plate. Plates were incubated at 32°C until visible colonies had formed and then replica plated onto EMM + LT plates. This allowed quantification of the percentage of cells which had cleaved *MATa* sites (colonies which have become H-). A 360 time point was also obtained for cells grown in EMM + LH in the absence of uracil (no induction, 360-OFF).

2.13 ANALYSIS OF CELL VIABILITY

2.13.1 Serial dilution assay

OD_{595} 0.2 log phase cultures were serial diluted fivefold in MQ water. 8 µl of each dilution was spotted onto YE6S and appropriate selective media. The plates were incubated at 32°C for 3 days.

2.13.2 Screen

ROTOR© robot (Singer Instruments) was used for high through put pinning of yeast strains in array format. DNA damage sensitive deletion strains (*sens*Δ) were woken on YE6S + G418. *sens*Δ *spd1*Δ strains were woken on PMG + LARH + G418. The strains were grown for 3 days at 32°C. Two colonies of each strain were pinned onto YE6S and YE6S + 0.1 µg/ml bleocin. The plates were incubated at 32°C for 48 hours. Plates were photographed using an SP imager (S & P robotics inc) and the size of each colony analysed using colony imager software (S & P robotics inc). Colony sizes were used to determine the effect of *spd1*$^{+}$ deletion on the bleocin sensitivity of each strain as discussed in Chapter 3.

2.14 MICROSCOPY

2.14.1 Light microscopy

Cells were viewed using a Nikon Eclipse E400 microscope with 10 × and 50 × objectives. Cells growing on agar plates were streaked out using a sterile toothpick. 10 µl of cells growing in liquid culture were placed onto a microscope slide with a coverslip.

2.14.2 Fluorescence microscopy

100 ml log phase overnight cultures were diluted to OD_{595} 0.1 and incubated at 250 rpm, for 3 hours, at 32°C. The cultures were split into two 50 ml cultures, the first left untreated and the second treated with 1 µg/ml bleocin. Cultures were incubated at 250 rpm, for 1 hour, at 26°C. 10 ml samples were removed, washed with 1 ml MQ water and fixed by addition of 1ml 100% methanol for 6 minutes on ice. Cells were stored in 100% acetone at -20°C. Fluorescence microscopy was performed on the same day as fixing the cells. 10 µl of cells were spread on a microscope slide. Cells were rehydrated, stained with DAPI and mounted using either 8 µl of DAPI agarose mount or ProLong® Gold antifade reagent with DAPI (Invitrogen). Coverslip were added and the slides placed at 4°C to dry. Slides were examined using a 100 × objective on a Zeiss Axioplan 2ie microscope, Hamamatsu Orca ER camera and micromanager software (Edelstein *et al.*, 2010).

2.15 FLUORESCENCE ACTIVATED CELL SORTING (FACS)

10 ml samples of log phase cultures were pelleted for 2 minutes at 900 g, the supernatant discarded and the cells fixed with 5 ml 100% ethanol. The fixed cells were pelleted for 2 minutes at 900 g, washed with 5 ml 10 mM EDTA (pH 8.0), resuspended in 0.5 ml 10 mM EDTA (pH 8.0) containing 0.1 mg/ml RNase A and incubated overnight at 37°C. Samples were stored at -20°C until needed for FACS analysis. Immediately prior to analysis 0.5 ml 10mM EDTA pH 8.0 containing 2 µM Sytox Green was added to each sample and the samples sonicated for 20 seconds at amplitude 10 (Branson Digital Sonifier). Samples were processed using FACS Scan machine (Becton Dickinson), Cell Quest Pro software and WinMDI 2.9 software.

2.16 PROTEIN EXTRACTION, MANIPULATION AND ANALYSIS

2.16.1 TCA protein extraction

The cells were resuspended in 100 µl 20% TCA and add 400 µl of 425-600 µm glass beads. The mixture was vortexed for 15 minutes at 4°C. 900 µl of 5% TCA were added and the mixture vortexed for 10 seconds. 800 µl of the solution was removed from the glass beads and centrifuged at 900 g for 10 minutes. The supernatant was discarded and the pellet resuspended in 250 µl Laemmli solution. The sample was boiled for 3 minutes and centrifuged at 900 g for 10 minutes. The protein supernatant was transfer to a new microfuge tube.

2.16.2 SDS-PAGE gel electrophoresis

The protein samples were boiled for 3 minutes and loaded onto PROTEAN TGX 4-20% precast minigels (Biorad). Gel were subjected to 100 V for 2 hours in running buffer.

2.16.3 Transfer

Gels were subjected to wet transfer onto nitrocellulose membrane at 80 V for 1 hour in transfer buffer. The membrane was stained with Ponceau to check the transfer and loading.

2.16.4 Western blotting

The membranes were blocked by immersion 5% skim milk (Fluka Analytical) for 1 hour at room temperature. The membranes were incubated in 5% skim milk containing primary antibodies using the conditions detailed in Table 2.4. Membranes were washed 3 times in 1 × PBS, 0.1% Tween and incubated in 5% skim milk containing 1:10000 anti-mouse horseradish peroxidase (HRP) conjugate antibody (Promega W402B) for 1 hour at room temperature. The washing steps were repeated and the proteins visualised using Amersham ECL or ECL plus (GE healthcare) were used for chemiluminescent detection according to the manufacturer's

instructions. The results were visualised using Fuji Medical X-Ray film 100 NIF (Fuji Film) and a SRX-101A developer (Konica Minolta).

Table 2.4 Primary antibodies used in this study

Antibody	Source	Dilution	Conditions
α-tubulin	Sigma Aldrich (T5168)	1:10000	1 hour at room temperature
GFP	Roche (11814460001)	1:500-1000	overnight at 4°C

2.17 HIGH PERFORMANCE LIQUID CHROMATOGRAPHY (HPLC) NUCLEOTIDE POOL ANALYSIS

Cells were extracted using a method similar to (Moss *et al.*, 2010), based on a method described in (Decosterd *et al.*, 1999). 100 ml cultures were grown to OD_{595} 0.4. The cultures were split into two 50 ml samples, the first untreated and the second treated with 2 µg/ml bleocin and incubated at 250 rpm, for 2 hours, at 26°C. The cell density was calculated using a haemocytometer and 2×10^8 cells harvested by centrifugation for 2 minutes at 900 g. The samples were washed with 250 µl 20% glucose and resuspended in 50 µl 10% TCA and quickly frozen at -80°C.

HPLC analysis was performed by Lisa Folkes (Department of Oncology, University of Oxford). The extracted samples were defrosted, vortexed and centrifuged at 19,000 g for 1 minute. 10 µl of supernatant was diluted in 40 µl Synergy water. The TCA was extracted using a method modified from Khym (1975) by the addition of an equal volume (50 µl) of Freon (1,1,2-trichlorotrifluorethane):trioctylamine (4:1). 10 µl of the aqueous upper layer was injected for analysis. Samples were analysed using HPLC with absorbance detection (Waters 2695 equipped with a photodiode array detector (Waters 2996)), monitoring at 250 nm. Separation was achieved using an Ace (3 µM, 3 x 125 mm) column maintained at 30°C with

eluent A (10 mM potassium dihydrogen phosphate, 10 mM tetrabutylammonium hydrogen sulphate, 10% methanol, pH 6.9) and eluent B (50 mM potassium dihydrogen phosphate, 6 mM tetrabutylammonium hydrogen sulphate, 30 % methanol, pH 7), using a flow rate of 0.6 ml/minute, a gradient of 25-80% B over 20 minutes, and a 25 minute run time. Nucleotides were identified by comparison with the absorbance spectra and retention times of commercially available standards.

Chapter 3 A screen to identify genes important for HR through roles in DNA damage-induced nucleotide synthesis

3.1 INTRODUCTION

An estimated 66% of *S. pombe* genes are conserved with vertebrates including many genes involved in DNA repair pathways (Wood *et al.*, 2012). As *S. pombe* can be easily grown and genetically manipulated in the laboratory, it provides a good model for studying the DNA damage response. The Bioneer Corporation (Korea) developed a library of haploid *S. pombe* gene deletion strains. In each strain a single gene was systematically replaced with a *kanMX* cassette encoding G418 resistance (Kim *et al.*, 2010) (Figure 3.1). Version 1 (V1) of the library contained 2662 deletion strains representing 63% of the non-essential genome. This was expanded in version 2 (V2) to 93%. The library has allowed the identification of a large number of DNA damage-sensitive strains with predicted roles in DNA repair (Deshpande *et al.*, 2009; Moss, 2011).

Nucleotide synthesis is a conserved and highly regulated response to DNA damage required for the efficient repair of DSBs by HR. Moss *et al.* (2010) previously identified a role for Rad3 in DSB-induced nucleotide synthesis. In response to DSBs Rad3 activates the Ddb1-Cul4^{Cdt2} ubiquitin ligase complex dependent degradation of the RNR inhibitor Spd1 to increase nucleotide pools. *rad3*Δ *cdt2*Δ and *ddb1*Δ strains are sensitive to DSBs and have impaired HR. This can be suppressed by deleting *spd1*$^{+}$ to increase nucleotide pools.

The aim of this chapter was to identify DNA damage-sensitive deletion strains with novel roles in HR through damage-induced nucleotide synthesis. This was investigated by screening for strains whose DNA damage sensitivity was suppressed by deletion of *spd1*$^{+}$.

Figure 3.1

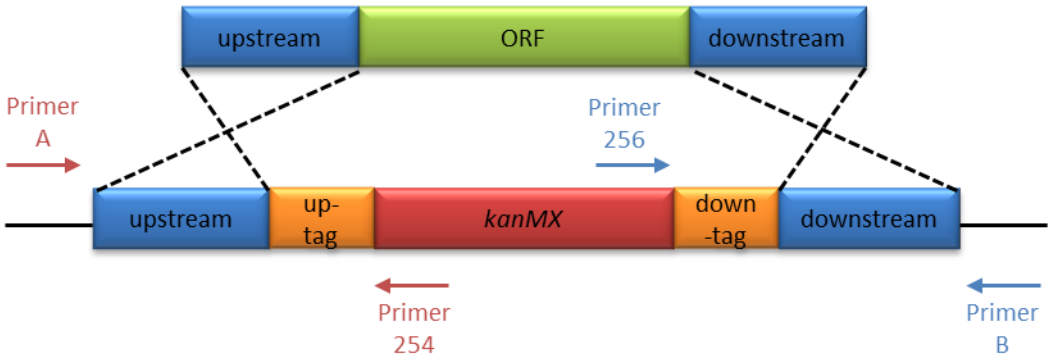


Figure 3.1 *S. pombe* haploid deletion library

A library of haploid gene deletion strains was obtained from Bioneer Corporation (Korea). Non-essential genes were systematically replaced with a deletion cassette encoding G418 resistance (red). The resistance gene was flanked by sequences containing 20 base pair barcodes unique to each deleted gene (orange). Upstream and downstream homologous regions were used to target the cassette by recombination (blue). The position of PCR primers used to confirm gene deletion are indicated (arrows).

3.2 RESULTS

3.2.1 Assembly of a library of DNA damage-sensitive deletion strains

To identify genes involved in DNA damage-induced nucleotide synthesis a comprehensive library of DNA damage-sensitive deletion strains was required. To our knowledge, at the time of analysis, two screens for DNA damage sensitivity including DSB sensitivity had been performed using the V1 *S. pombe* haploid deletion library (Deshpande *et al.*, 2009; Moss, 2011).

In a screen performed in the Humphrey laboratory, library strain colonies were pinned onto plates treated with the radiomimetic bleomycin or the alkylating agent MMS. Each strain's ability to form colonies was qualitatively assessed. The screen identified 34 deletion strains sensitive to bleomycin, 32 sensitive to MMS and 130 sensitive to both (Moss, 2011).

An independent screen was performed by Deshpande et al. (2009). This screen differed as the library strains were pinned from liquid cultures onto plates treated with increasing concentrations of one of five DNA damaging agents to give a semi-quantitative measurement of DNA damage sensitivity. The agents used included IR, MMS, HU, CPT and 4-NQO. The screen isolated 229 deletion strains which were sensitive to one or more of the agents. 5 strains were identified as sensitive to IR, 15 to MMS and 17 to both agents. The two screens together identified a total of 353 strains. However, only 72 strains (20.3%) were in common (Figure 3.2.A). Deshpande *et al.* (2009) identified far fewer IR and MMS sensitive gene deletion strains however the majority of these were also identified by our laboratory (Figure 3.2.B-C).

Figure 3.2

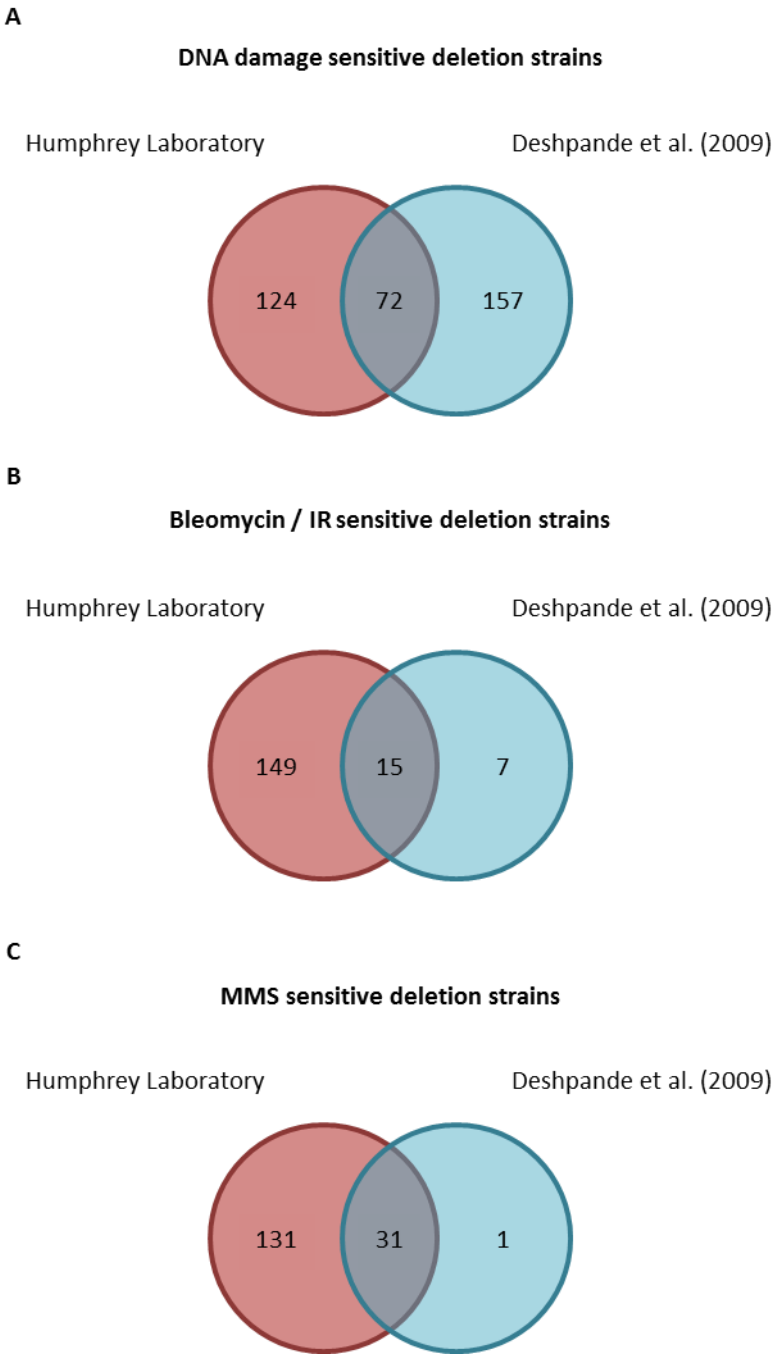


Figure 3.2 Comparison of screens to identify DNA damage-sensitive deletion strains

Venn diagram representations of the DNA damage-sensitive deletion strains identified by the Humphrey laboratory (Moss, 2011) and Deshpande *et al.* (2009) comparing: **(A)** the total number of DNA damage-sensitive deletion strains identified; **(B)** bleomycin and IR sensitive deletion strains; **(C)** MMS sensitive deletion strains.

The two libraries were pooled to form a new library of 350 DNA damage-sensitive strains. For simplicity, strains from this library will be referred to as *sens*Δ. Strains were sourced, where possible, from the V2 deletion library as it was expected to be more accurate. 8 strains were excluded from further analysis as they could not be woken.

3.2.2 The DNA damage-sensitive library was crossed with *spd1*Δ

The library of DNA damage-sensitive deletion strains was crossed with *spd1*Δ using the *pombe* epistasis mapper 2 (PEM-2) method developed by Roguev et al. (2007). This method allows the high throughput mating of yeast strains in array format by providing selection from meiotic progeny of double mutants of a single mating type. In addition the method provides selection against surviving parental and diploid cells in the population. The method is outlined in Figure 3.3.

By performing the PEM-2 mating in duplicate 314 of the DNA damage-sensitive library strains were successfully crossed to *spd1*Δ and double deletion mutants isolated. A further 25 double deletion strains were isolated by free spore analysis to give a total of 339 strains, covering 98.2% of the library.

3.2.3 Screen to identify deletion strains with altered DSB sensitivity following *spd1*$^+$ deletion

The DNA damage-sensitive deletion library and corresponding *sens*Δ *spd1*Δ strains were screened for strains exhibiting altered sensitivity following loss of *spd1*$^+$. To detect small differences in sensitivity a quantitative measurement of colony fitness was used.

Figure 3.3

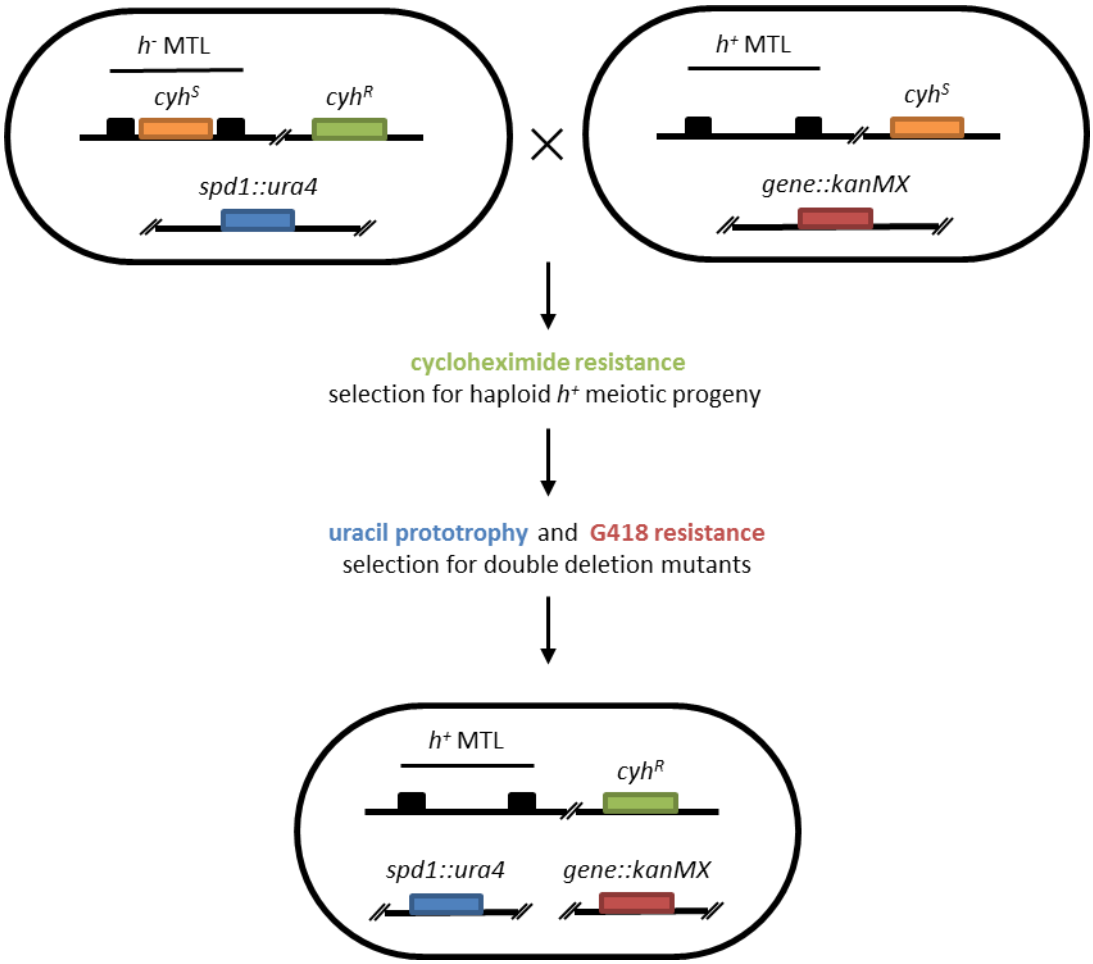


Figure 3.3 PEM-2 high throughput mating

Schematic of the PEM-2 method used to cross *spd1*Δ with the DNA damage-sensitive library, as previously described by Roguev et al. (2007). An *rpl42* allele conferring recessive cycloheximide resistance (cyh^R) was introduced at the *rpl42* locus and a cycloheximide sensitive allele (cyh^S) at the h^- mating type locus (MTL) of the *spd1*Δ strain (top left). The strain was mated with h^+ library strains (top right) and haploid h^+ progeny selected with cycloheximide. Double deletion strains were isolated by selecting for the gene deletion markers (bottom).

The libraries were revived on media selective for the deletion markers. Two *sens*Δ and two *sens*Δ *spd1*Δ colonies for each gene deletion were replica pinned, in array format, onto control plates or plates treated with 0.1 µg/ml bleocin (Figure 3.4.A). At 48 hours the plates were photographed and final colony sizes quantified using an SP imager (Figure 3.4.B). Three strains previously characterised by Moss et al (2010), *rad3*Δ *cdt2*Δ and *ddb1*Δ, exhibited clear bleocin sensitivity compared to wild-type and increased colony fitness following *spd1*$^{+}$ deletion (Figure 3.4.C).

The screen was repeated 5 times and anomalous data from faulty replica plating discarded. 26 strains did not form detectable colonies during the screen and a further 9 strains were excluded due to high variability between repeats. Final colony size data was successfully collected for 304 strains corresponding to 88.1% of the DNA damage-sensitive library. 98.4% of the strains were represented by ≥3 data repeats and 41.4% by 4-5 data repeats.

3.2.4 Calculating suppression of DSB sensitivity following *spd1*$^{+}$ deletion

The aim of the screen was to identify DNA damage sensitive strains whose sensitivity was suppressed by deleting *spd1*$^{+}$. Comparing the colony size of *sens*Δ and *sens*Δ *spd1*Δ strains on bleocin treated plates gives a measure of suppression. However, colony size is also influenced by strain fitness as seen under control conditions. Therefore, to specifically measure suppression of DNA damage sensitivity, the ratio of *sens*Δ *spd1*Δ to *sens*Δ colony size on bleocin treated plates was compared with the ratio of *sens*Δ *spd1*Δ to *sens*Δ colony size on control plates. A schematic for these calculations is shown in Figure 3.5.

Figure 3.4

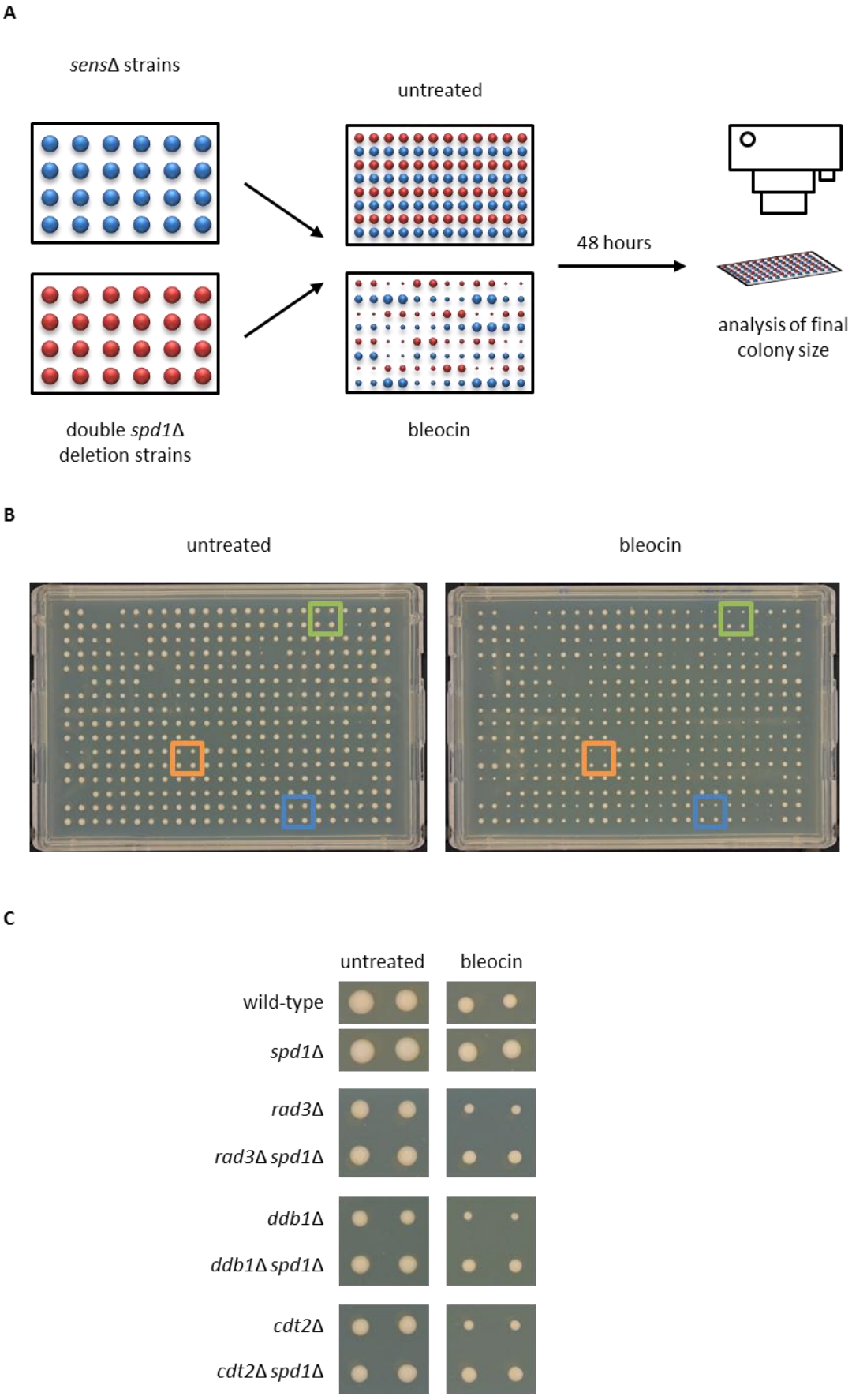

A
sensΔ strains
untreated
48 hours
analysis of final colony size
double spd1Δ deletion strains
bleocin
B
untreated
bleocin
C
untreated
bleocin
wild-type
spd1Δ
rad3Δ
rad3Δ spd1Δ
ddb1Δ
ddb1Δ spd1Δ
cdt2Δ
cdt2Δ spd1Δ

Figure 3.4 Overview of the screen

(A) Schematic of the screen. *sens*Δ strains were woken on YE6S + G418 and *sens*Δ *spd1*Δ strains on PMG + LARH + G418. Two colonies of each strain were pinned in array format onto YE6S and YE6S + 0.1 µg/ml bleocin and incubated at 32°C. At 48 hours the plates were photographed using an SP imager and colony sizes measured (S & P robotics inc).

(B) Example YE6S and YE6S + 0.1 µg/ml bleocin screen plates photographed at 48 hours. *rad3*Δ colonies are highlighted in orange, *ddb1*Δ in green and *cdt2*Δ in blue. For each gene the top two colonies represent the single deletion strain and the bottom two the corresponding *spd1*Δ strain.

(C) Example wild-type, *spd1*Δ, *rad3*Δ, *rad3*Δ *spd1*Δ, *ddb1*Δ, *ddb1*Δ *spd1*Δ, *cdt2*Δ, and *cdt2*Δ *spd1*Δ colonies photographed after 48 hours growth on YE6S or YE6S + 0.1 µg/ml bleocin.

Figure 3.5

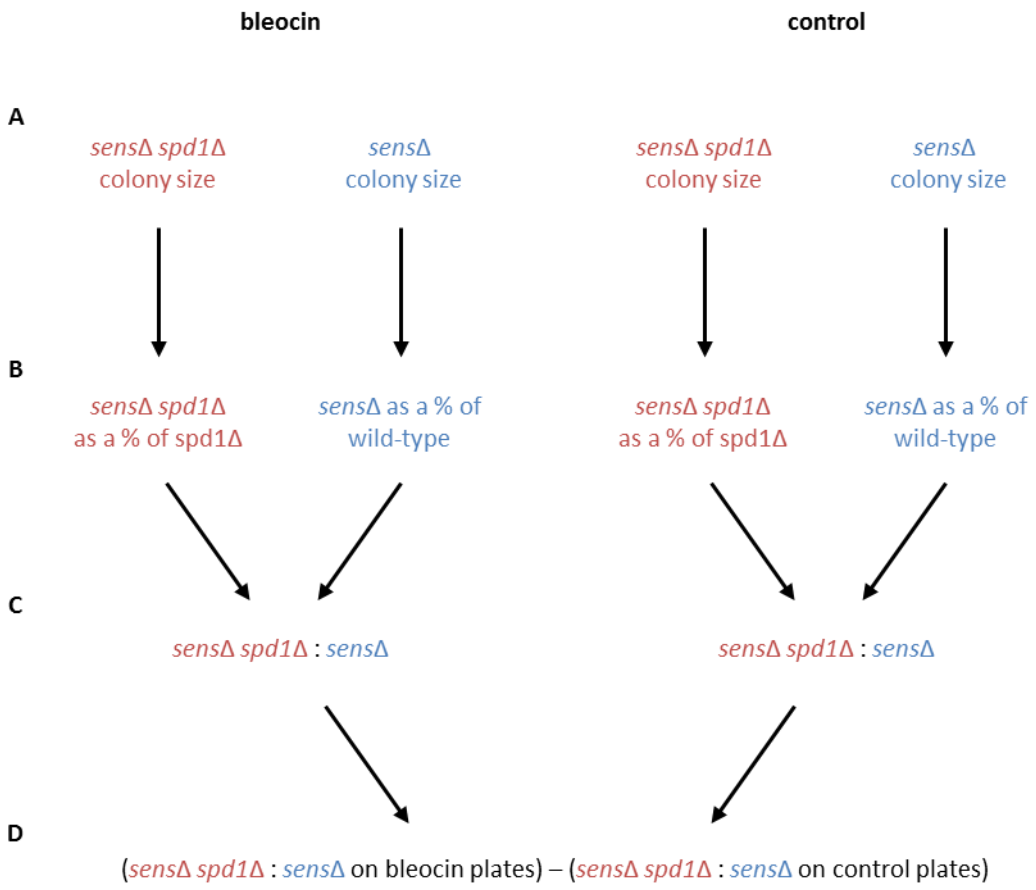


Figure 3.5 Screen calculations

(A) After 48 hours of growth the size of *sens*Δ colonies on control plates, *sens*Δ colonies on bleocin treated plates, *sens*Δ *spd1*Δ colonies on control plates, and *sens*Δ *spd1*Δ colonies on bleocin treated plates were measured.

(B) *sens*Δ colony sizes were calculated as a percentage of wild-type and *sens*Δ *spd1*Δ colony sizes as a percentage *spd1*Δ for each particular experiment.

(C) The ratios of *sens*Δ *spd1*Δ : *sens*Δ colony size on bleocin treated plates and the ratios of *sens*Δ *spd1*Δ : *sens*Δ colony size on control plates were calculated.

(D) The difference between the ratios in (C) was calculated

Four sets of measurements were obtained from the screen: the final colony size of *sens*Δ strains on control plates, the final colony size of *sens*Δ strains on bleocin treated plates, the final colony size of *sens*Δ *spd1*Δ strains on control plates, and the final colony size of *sens*Δ *spd1*Δ strains bleocin treated plates (Figure 3.5.A). Final colony size measurements were also obtained for two control strains, wild-type and *spd1*Δ, under control and bleocin conditions.

To correct for differences between screen repeats each *sens*Δ colony size was calculated as a percentage of wild-type for each particular experiment. Each *sens*Δ *spd1*Δ colony size was calculated as a percentage *spd1*Δ for each particular experiment (Figure 3.5.B). *spd1*Δ was chosen here instead of wild-type as an *spd1*Δ single deletion strain grows better than wild-type under both bleocin and control conditions. *sens*Δ *spd1*Δ colony sizes were not calculated as a percentage of the appropriate *sens*Δ strains as a stable denominator was required to reduce noise within the analysis.

The ratio of *sens*Δ *spd1*Δ to *sens*Δ colony size on bleocin treated plates was obtained to assess the effect of *spd1*Δ on strain fitness under damage conditions. It was important to determine whether any effect on colony growth conferred by *spd1*Δ was specific to bleocin conditions, and so the ratio of *sens*Δ *spd1*Δ to *sens*Δ colony size on control plates was obtained to assess the effect of *spd1*Δ on general strain fitness (Figure 3.5.C). The difference between the ratios was used to measure the specific effect of *spd1*Δ on the DNA damage sensitivity of each strain (Figure 3.5.D).

3.2.5 Preliminary analysis of the screen

As discussed in Section 3.2.4 *sens*Δ colony sizes were calculated as a percentage of wild-type and *sens*Δ *spd1*Δ colony sizes as a percentage *spd1*Δ in each experiment (Figure 3.5.B). Mean values were obtained for each strain. Similar average standard errors of the mean were obtained for *sens*Δ strains on control plates (6.4%), *sens*Δ strains on bleocin treated plates (10.5%), *sens*Δ *spd1*Δ strains on control plates (4.4%) and *sens*Δ *spd1*Δ strains on bleocin treated plates (10.5%) (Appendix V).

*sens*Δ colony sizes on control plates were plotted against *sens*Δ colony sizes on bleocin treated plates to compare strain fitness and bleocin sensitivity (Figure 3.6.A). Large differences were observed in bleocin sensitivity of the *sens*Δ strains. The final colony size of *sens*Δ strains on bleocin treated plates ranged from 12% to 165% (standard deviation (SD) = 28.5%) of wild-type size under the same conditions, with 164 strains growing less well than wild-type. Encouragingly 82% of strains with average colony sizes less than 60% of wild-type under bleocin conditions were annotated as DSB sensitive by Moss (2011) or Deshpande *et al.* (2009). However, only 46% of all strains growing less well than wild-type were annotated as DSB sensitive. Unexpectedly 140 strains had average colony sizes equal to or greater than wild-type on bleocin treated plates. 46% of these strains were annotated as DSB sensitive.

The size of *sens*Δ colonies on control plates had a smaller size range from 40% to 112% (SD = 13%) of wild-type on these plates (Figure 3.6.A). This indicates a moderate range of strain fitness. The bleocin sensitivity of the *sens*Δ strains did not correlate with colony fitness on control plates suggesting DSB sensitivity was largely independent of strain fitness.

Figure 3.6

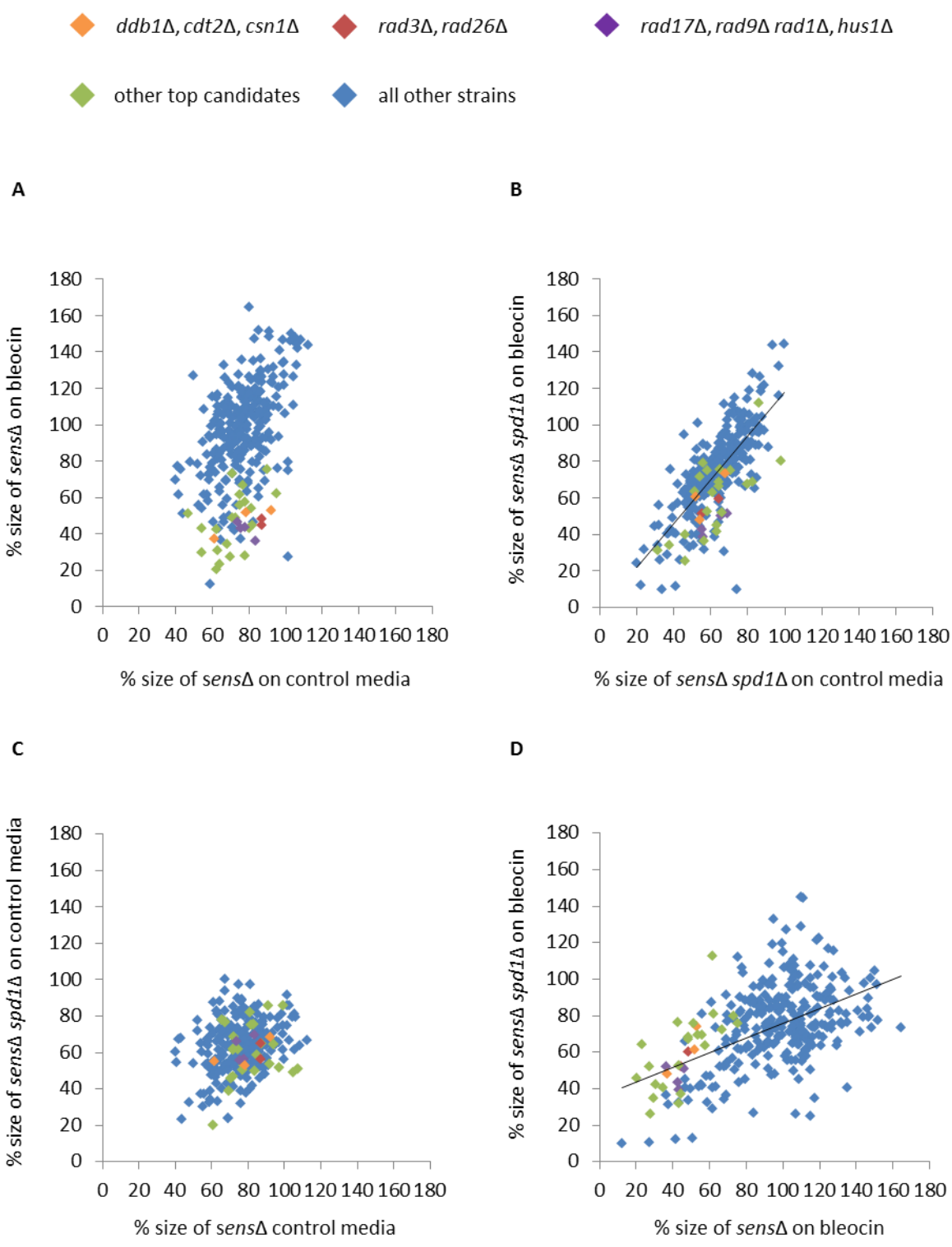

ddb1Δ, cdt2Δ, csn1Δ
rad3Δ, rad26Δ
rad17Δ, rad9Δ rad1Δ, hus1Δ
other top candidates
all other strains
A
% size of sensΔ on bleocin
% size of sensΔ on control media
B
% size of sensΔ spd1Δ on bleocin
% size of sensΔ spd1Δ on control media
C
% size of sensΔ spd1Δ on control media
% size of sensΔ control media
D
% size of sensΔ spd1Δ on bleocin
% size of sensΔ on bleocin

Figure 3.6 Preliminary analysis of the screen

Colonies were grown for 48 hours, the size of *sens*Δ colonies calculated as a percentage of wild-type and the size of *sens*Δ *spd1*Δ as a percentage of *spd1*Δ. Mean values are presented and error bars indicate ± standard error. On all graphs *ddb1*Δ *cdt2*Δ and *csn1*Δ are highlighted in orange, *rad3*Δ and *rad26*Δ in red and 9-1-1 complex deletion strains in purple. All other candidates selected for further study are highlighted in green.

(A) Colony size of *sens*Δ strains grown on YE6S plotted against the colony size of the same strains grown on YE6S + 0.1 µg/ml bleocin.

(B) Colony size of *sens*Δ *spd1*Δ strains grown on YE6S plotted against the colony size of the same strains grown on YE6S + 0.1 µg/ml bleocin.

(C) Colony size of *sens*Δ strains plotted against the colony size of *sens*Δ *spd1*Δ strains both grown on YE6S.

(D) Colony size of *sens*Δ strains plotted against the colony size of *sens*Δ *spd1*Δ strains both grown on YE6S + 0.1 µg/ml bleocin.

*sens*Δ *spd1*Δ colony sizes on control plates were plotted against *sens*Δ *spd1*Δ colony sizes on bleocin treated plates to compare strain fitness and bleocin sensitivity (Figure 3.6.B). *sens*Δ *spd1*Δ colonies grown on control media ranged in size from 20% to 100% (SD = 14%) of *spd1*Δ under the same conditions. The same strains grown on bleocin treated plates had an increased range of sizes from 10% to 145% (SD = 23%) of *spd1*Δ under the same conditions. In contrast to the *sens*Δ strains the normal colony fitness of the *sens*Δ *spd1*Δ strains was positively correlated with bleocin sensitivity (R^2 = 0.56). This suggested that *spd1*Δ was having DSB-independent effects on colony growth.

No correlation was observed between the fitness of *sens*Δ and *sens*Δ *spd1*Δ strains in the absence of bleocin (Figure 3.6.C). A weak correlation was observed between the bleocin sensitivity of of *sens*Δ and *sens*Δ *spd1*Δ strains (Figure 3.6.D). This suggested that whilst the *sens*Δ strain deletion impacts on the bleocin sensitivity of *sens*Δ *spd1*Δ strains, *spd1*Δ is also having an independent and varied effect.

3.2.6 Identification of candidates with altered DSB sensitivity following *spd1*$^+$ deletion

The aim of the screen was to identify deletion strains with altered DSB sensitivity when *spd1*$^+$ was deleted to increase nucleotide pools. As discussed in Section 3.2.4, it was important to study the effect of *spd1*Δ on DSB sensitivity independently of effects on normal strain growth. Therefore the ratio of *sens*Δ *spd1*Δ to *sens*Δ colony sizes was calculated for the control and bleocin conditions (Figure 3.5). The ratios are compared in Figure 3.7 and the differences between them presented in Figure 3.8 as a measure of suppression of DSB sensitivity.

Figure 3.7

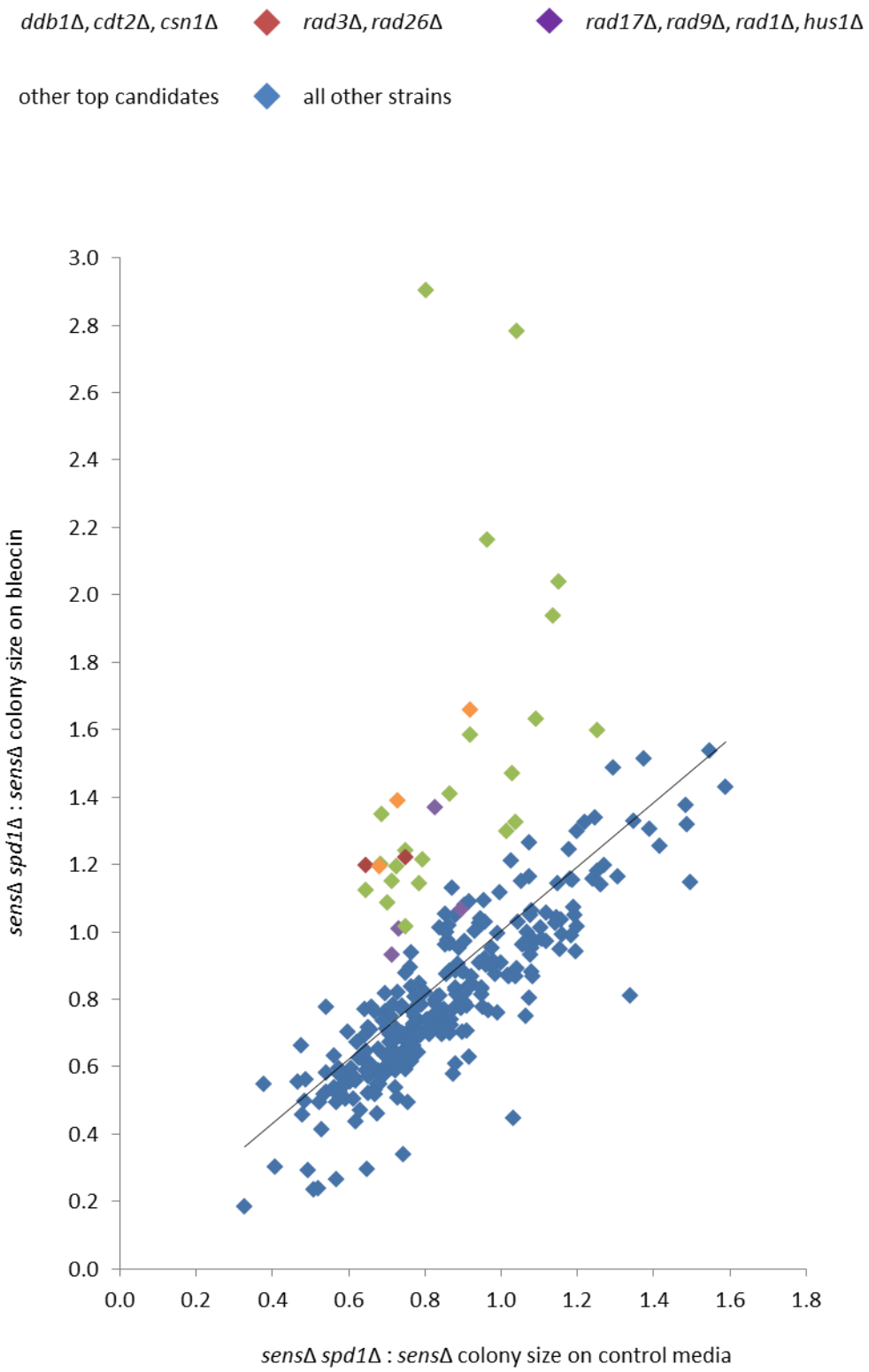


Figure 3.7 Identification of candidates with altered DNA damage sensitivity following *spd1*$^{+}$ deletion

The ratio of the size of *sens*Δ *spd1*Δ colonies to *sens*Δ colonies grown for 48 hours on YE6S plates was plotted against the same ratio when the colonies were grown on YE6S + 0.1 µg/ml bleocin (see figure 3.5 for the calculations). *ddb1*Δ *cdt2*Δ and *csn1*Δ are highlighted in orange, *rad3*Δ and *rad26*Δ in red, and *rad17*Δ, *rad9*Δ, *rad1*Δ and *hus1*Δ in purple. All other candidates selected for further study are highlighted in green.

Figure 3.8

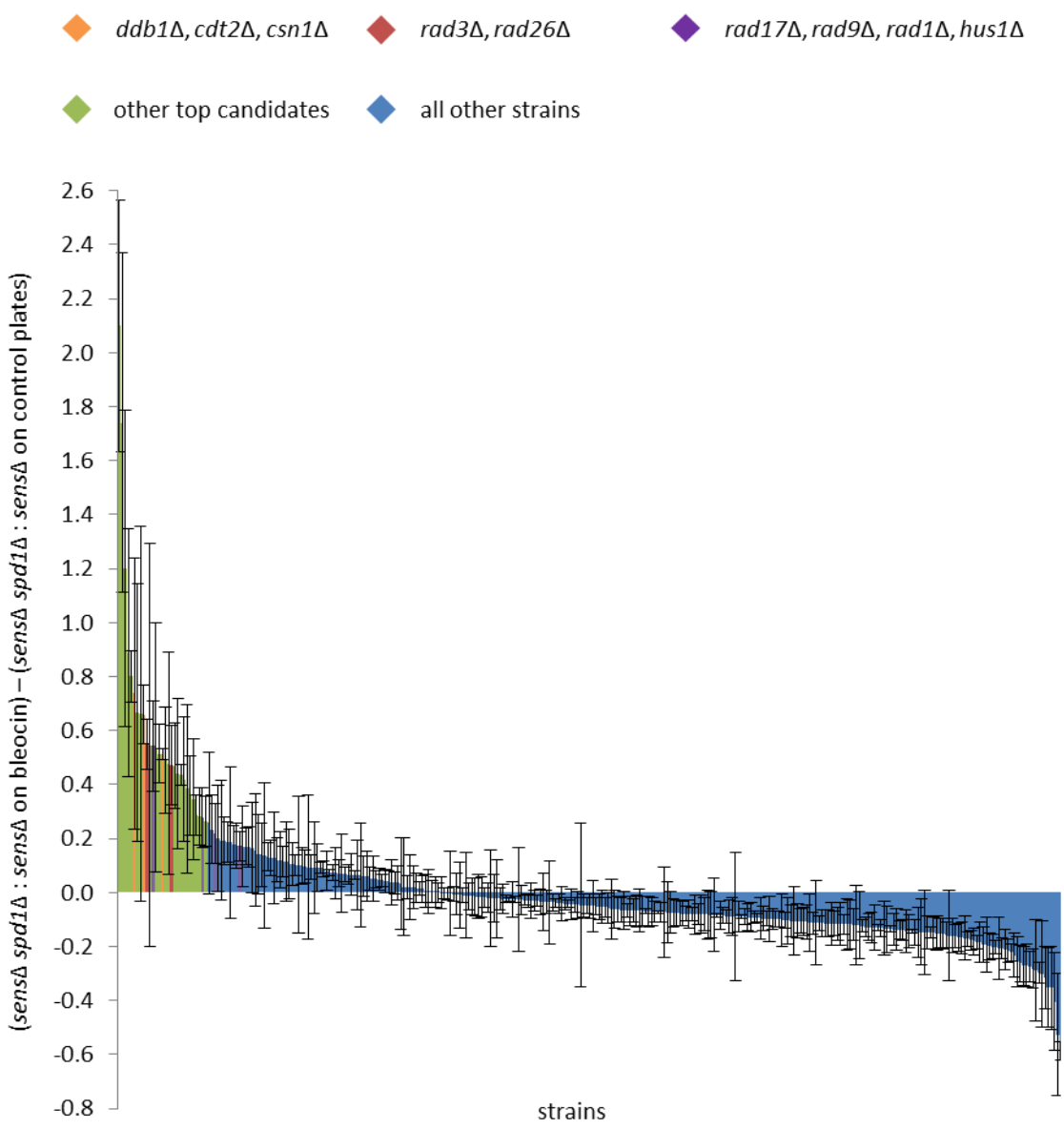


Figure 3.8 Screen strains show both decreased and increased sensitivity to DSBs following *spd1*$^{+}$ deletion

The difference between the ratios in Figure 3.7: ((*sens*Δ *spd1*Δ : *sens*Δ colony size on bleocin) – (*sens*Δ *spd1*Δ : *sens*Δ colony size on control plates)) is presented as a measure of altered sensitivity to DSBs when *spd1*$^{+}$ is deleted. For an explanation of the calculations see Figure 3.5. Positive values represent increased DSB resistance and negative values represent increased DSB sensitivity. *ddb1*Δ *cdt2*Δ and *csn1*Δ are highlighted in orange, *rad3*Δ and *rad26*Δ in red and *rad17*Δ, *rad9*Δ, *rad1*Δ and *hus1*Δ in purple. All other candidates selected for further study are highlighted in green.

The ratios demonstrate a weak positive correlation. This suggests that *spd1*Δ has DSB independent effects on strain fitness (Figure 3.7). The 29 strains with largest positive difference between the ratios were selected as candidates for further study (Figure 3.8, Table 3.1). These strains show a larger suppression of DNA damage sensitivity by *spd1*Δ than predicted by the line of best fit (Figure 3.7). The candidates were amongst the most bleocin sensitive *sens*Δ strains (Figure 3.6.A) but the corresponding *sens*Δ *spd1*Δ strains show highly variable bleocin sensitivity (Figure 3.6.B).

Table 3.1 Gene ontology (GO) terms of the top candidates

Gene	Name	GO term
SPAC1486.01	*sod2*	transport
SPAC222.12c	*atp2*	transport
SPCC594.06c	*vam7*	transport
SPAC824.05	*vps16*	transport
SPBC2G2.01c	*liz1*	transport
SPAC9E9.08	*rad26*	DNA damage checkpoint
SPAC664.07c	*rad9*	DNA damage checkpoint
SPBC216.05	*rad3*	DNA damage checkpoint
SPAC1952.07	*rad1*	DNA damage checkpoint
SPAC11E3.08c	*nse6*	DNA repair
SPAC644.14c	*rhp51*	DNA repair
SPAC3H8.05c	*mms1*	DNA repair
SPBC21C3.12c	-	unknown
SPBC557.02c	-	unknown
SPAC806.05	-	unknown
SPAC23D3.09	*arp42*	chromatin remodelling
SPBC28F2.10c	*ngg1*	chromatin remodelling
SPBC23G7.15c	*rpp202*	translation
SPAC31A2.02	*trm112*	translation
SPCC895.07	*alp14*	cell morphogenesis
SPAC227.07c	*pab1*	cell morphogenesis
SPBC30D10.04	*swi3*	DNA replication
SPBC119.08	*pmk1*	stress response
SPBC29A3.14c	*trt1*	telomere maintenance
SPBP35G2.08c	*air1*	RNA metabolism
SPBC365.14c	*uge1*	metabolism

The candidate genes were involved in a wide range of cellular processes (Table 3.1). Notably the candidates included *rad3*$^{+}$, *cdt2*$^{+}$ and *ddb1*$^{+}$ previously characterised by Moss *et al.* (2010); *csn1*$^{+}$ a member of the signalosome complex associated with Cul4-Ddb1^{Cdt2} (Liu *et al.*, 2005); and *rad26*$^{+}$, *rad9*$^{+}$ and *rad1*$^{+}$ checkpoint proteins although *rad1*$^{+}$ was only marginally included in this group. The role of the DNA damage checkpoint is presented separately in Chapter 4.

3.2.7 Confirmation of the identity of the candidates

As the deletion library occasionally contains errors, the identity of the candidates was confirmed. PCR amplification was performed using DNA extracted from the deletion strains, a forward primer specific to the region upstream of each deleted gene and a reverse primer specific to the deletion cassette. The identity of 21 candidates was confirmed (Figure 3.9) however a PCR product was not detected for *SPBC557.02c*Δ, *SPBC21C3.12c*Δ, *atp2*Δ or *sod2*Δ.

Further analysis of the strains annotated as *SPBC557.02c*Δ and *SPBC21C3.12c*Δ confirmed that the annotated genes were not deleted (Figure 3.10.A-B). From this point the strains will be referred to by their Bioneer V2 deletion library codes. V2-53D9 for *SPBC557.02c*Δ and V2-53C11 for *SPBC21C3.12c*Δ. The sequence of the strains up-tag and down-tag barcodes corresponded to deletion of *npp106*$^{+}$ for V2-53D9 and *elf1*$^{+}$ for V2-53C11 (Figure 3.10.C).

Figure 3.9

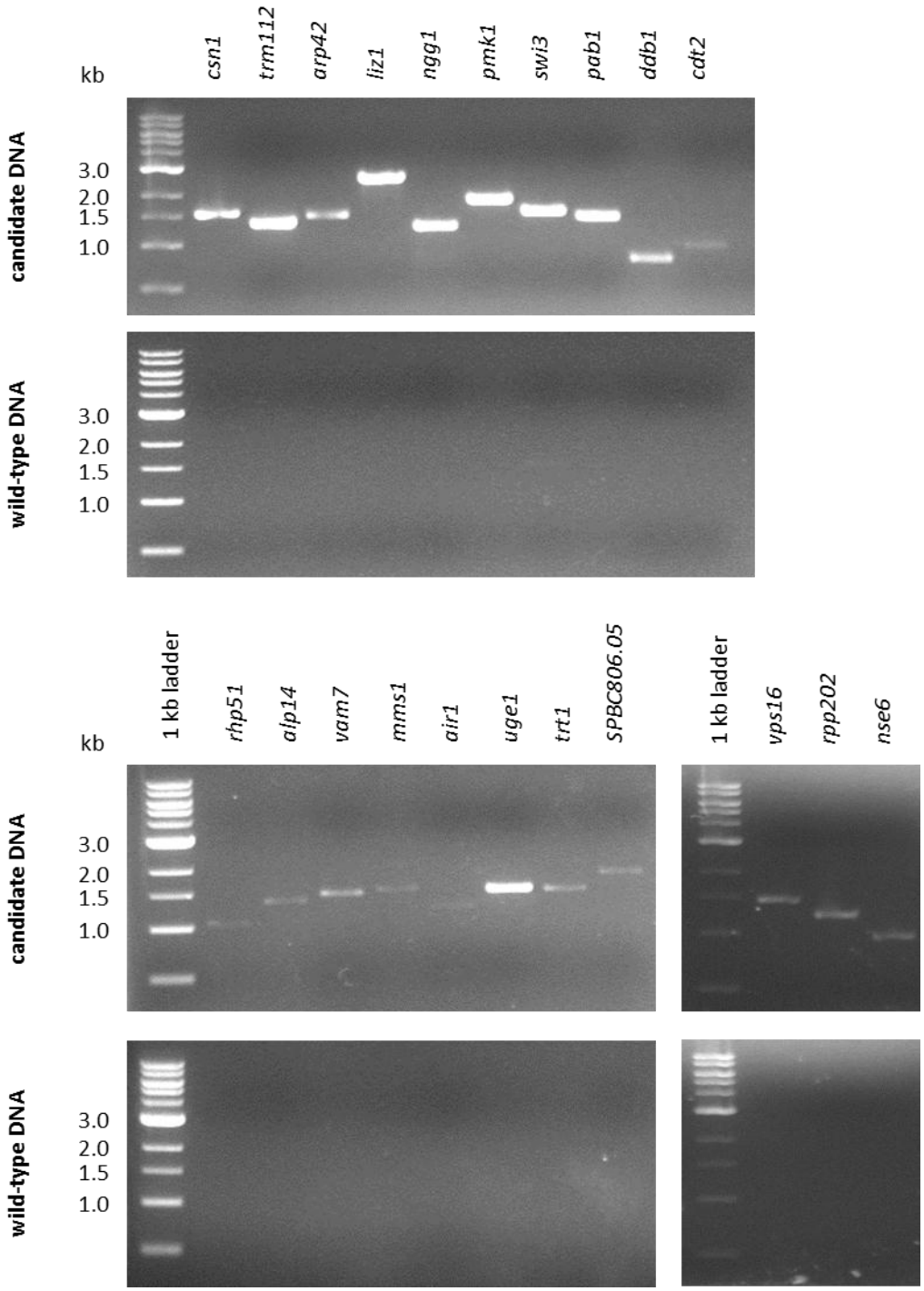
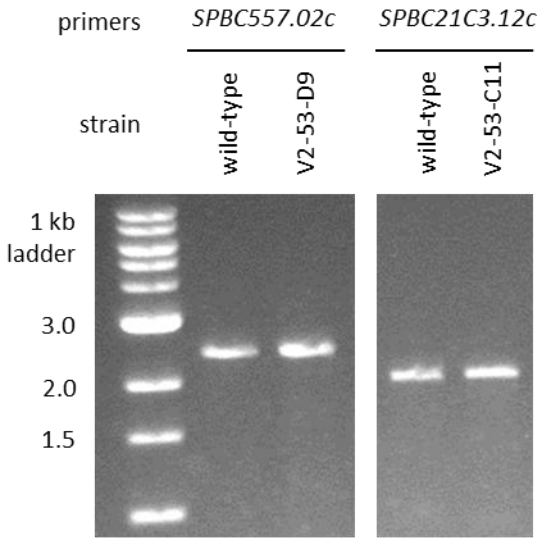


Figure 3.9 Confirmation of the identity of candidate gene deletion strains

PCR was performed using a forward primer specific to the sequence upstream of the gene deletion (primer A, Figure 3.1) and a reverse primer specific to the gene deletion cassette (primer 254, Figure 3.1). The detection of a band when deletion strain DNA was used as a template and the absence when wild-type DNA was used confirms gene deletion.

Figure 3.10

A



B

V2-53-D9

```
  1 ATGGAT-AAAAAAATCGCAGATTTGCTTCAAGAGCTTCAAAGCTCCTCCA   49
    |||||| ||||||||||||||||||||||||||||||||||||||||||||
  1 ATGGATAAAAAAAATCGCAGATTTGCTTCAAGAGCTTCAAAGCTCCTCCA   50

 50 ACGTAACGAGTAATCAGCTTGAAAATGTAGACAAATCATCCATCCCTCTA   99
    ||||||||||||||||||||||||||||||||||||||||||||||||||||
 51 ACGTAACGAGTAATCAGCTTGAAAATGTAGACAAATCATCCATCCCTCTA  100

100 TCGAAGGCTCGGAAACCCTCTGATTTTGAGTTGAACAATTCTATAGAGGA  149
    ||||||||||||||||||||||||||||||||||||||||||||||||||||
101 TCGAAGGCTCGGAAACCCTCTGATTTTGAGTTGAACAATTCTATAGAGGA  150

150 CGCAGAAAAAATTAAAACCTATCCCGCTGCCTTGAGGTACATCTTTGCCC  199
    ||||||||||||||||||||||||||||||||.|||||||||||||...|
151 CGCAGAAAAAATTAAAACCTATCCCGCTGCNTTGAGGTACATCTTTNNNC  200

200 TAAATTCCCGCCATCCCGAAAAGTTACAAAAATTAAGAAAGATGAAGGCT  249
    |||||||||||||||||.||||.||.|||||||||||.|||||||
201 TAAATTCCCGCCATCCCGANAAGTNACCAAAATTAAGAAAGNTGAAGGCT  250

250 ATGCAGGAACGTC-AAGAGCGCAACTGGTCTCTGGAACGGCA-GCGGCTA  297
    |||||.|||||| ||||||||||.|.||||.|.||||||.| ||||||
251 ATGCAAGAACGTCNAAGAGCGCAANTNGTCTNTNGAACGGNAGGCGGCTA  300

298 GTTCAA-CATTTTGAGTCGAAAACTAAGCTTCAAGAAATACTGAAACCGC  346
    |||||| ||||..|||||||||.|||||||||||||....|||||||||
301 GTTCAANCATTNNGAGTCGAAAANTAAGCTTCAAGAANNNNTGAAACCGC  350

347 TTTCCTCCGACCCTAAATTGAAACAACCGTCCAATTGTCTTAATGACCAG  396
    |||||||||.||||.|||||||||||||||.|||||||||||||||||||
351 TTTCCTCCGNCCCTTAATTGAAACAACCGTNCAATTGTCTTAATGACCAG  400

397 ACCAACAATGATTCCGCTCAAACTTTAGATGACAATAGGGCTTTACAAGA  446
    ||||||.|||||||||||||||||||||||||||||||||||||||.|||
401 ACCAACCATGATTCCGCTCAAACTTTAGATGACAATAGGGCTTTACNAGA  450

447 ATTTGATGAACAAGTGGTACAATTGACAAACAGGATGTACAAA-GAACAG  495
    |||||||||||||||||||||||||||||||||||||||||| ||||||
451 ATTTGATGAACAAGTGGTACAATTGACAAACAGGATGTACAAANGAACAG  500

496 CTTGCAATCCTTGCAGACCTGAAGATACCATTGTTTTTGTCAGTGAATAA  545
    |||||||||..|||||||||||||||||||.|||||||||||||||||||
501 CTTGCAATCNNTGCAGACCTGAAGATACCATNGTTTTTGTCAGTGAATAA  550

546 TGATGAAGAGTTATCTGAAGATCAGAAGCGCCTCTTACAATTGTTACAGG  595
    ||||||||||||||||||||||||||||||||||||||||||||||||||||
551 TGATGAAGAGTTATCTGAAGATCAGAAGCGCCTCTTACAATTGTTACAGG  600

596 ATCTCCTTGGAGCCTAA    612
    |||||||||||||||||
601 ATCTCCTTGGAGCCTAA    617
```

V2-53-C11

```
  1 ATGTTGTTACCATTGAAAG--AATCACTGG-AATCTACTTTAGCTAACGT   47
    |||||||||||||||||.  |||||||| ||||||||||||||||.|||
  1 ATGTTGTTACCATTGAAANGAAATCACTGGAAATCTACTTTAGCTANCGT   50

 48 TGCTAAAAATGAGACACTTTTCGTTGCTTATCTTGCTTCT-GTTGATCCT   96
    ||||||||||||||||||||||||||||||||||||||| |||||||||
 51 TGCTAAAAATGAGACACTTTTCGTTGCTTATCTTGCTTCTGGTTGATCCT  100

 97 CGTACTAAACAGCCTTGGTGTCCAACGGTTCGTGCGGCTTTGCCTCTCTT  146
    ||||||||||||.|.|||||||||||||||||||||||||||||||||||
101 CGTACTAAACAGCNTGGGTGTCCAACGGTTCGTGCGGCTTTGCCTCTCTT  150

147 TAACAATGCCTTTAATAGCTCTAAAAAGCTCAATGTTGTCCATGTCTATG  196
    |.|||||||||||||||||||||||||||||||||||||||||||||||||
151 TNACAATGCCTTTAATAGCTCTAAAAAGCTCAATGTTGTCCATGTCTATG  200

197 TTGGCAACATGCCTCAATGGAAAACACCCACACAATGAATTTCGAGTGAAA  246
    ||||||||||.|||||||||||||||||||||||||||||||||||||||
201 TTGGCAACATNCCTCAATGGAAAACACCCACACAATGAATTTCGAGTGAAA  250

247 TTTGGTATCAGTGCAGTCCCCCACTTTAGGTAAATATACTCGAGACGCCCA  296
    ||||||||||||||||||||||||||||||||||||||||||||||||||||
251 TTTGGTATCAGTGCAGTCCCCCACTTTAGGTAAATATACTCGAGACGCCCA  300

297 AGGAAATCTTAAAACCTCATTACTGGTAGATTATGACTGCCTTGACGCCA  346
    ||||||||||||||||||||||||||||||||||||||||||||||||||||
301 AGGAAATCTTAAAACCTCATTACTGGTAGATTATGACTGCCTTGACGCCA  350

347 ACAAGTTTTCAAAGTTTATCGACATATAA    375
    ||||||||||||||||||||||||||||
351 ACAAGTTTTCAAAGTTTATCGACATATAA    379
```

C

Strain	Uptag Barcode	Downtag Barcode	Gene
V2-53D9	CGACCGACCAAAGCGAACAA	CCTCTCACCGCCCTCGCACT	*npp106*
V2-53C11	TTTTGTGTTCGGTGGCGTCC	GCCCCCATCCCCGACCTATT	*elf1*

Figure 3.10 The identity of V2-53D9 and V2-53C11 could not be confirmed

(A) PCR amplification from wild-type, V2-53D9 and V2-53C11 genomic DNA using primers specific to sequences upstream and downstream of the annotated deletions (primer A and B, Figure 3.1).

(B) PCR products from (A) were sequenced and aligned with the corresponding wild-type sequences obtained Pombase (www.pombase.org) using Nucleotide BLAST (NCBI)

(C) The unique up-tag and down-tag barcodes of the strains' deletion cassettes were amplified by PCR and sequenced.

As V2-53D9 was a promising candidate, the strain was selected for whole genome sequencing. The sequence of *SPBC557.02c*$^{+}$ (Figure 3.11.A) and *npp106*$^{+}$ (Figure 3.11.B) indicated that these genes were intact however the entire coding region of *nup132*$^{+}$ was deleted (Figure 3.11.C). PCR analysis confirmed that in both V2-53D9 and V2-9B9 (annotated as *nup132*Δ) *nup132*$^{+}$ had been replaced with a deletion cassette (Figure 3.12.A). As a *nup132* deletion strain was not present in the V1 deletion library its DNA damage sensitivity was not previously addressed. Serial spot dilutions on plates treated with bleocin demonstrated that, whilst V2-53D9 is sensitive to DSBs, V2-9B9 is not (Figure 3.12.B).

3.2.8 Confirming suppression of DSB sensitivity following *spd1*$^{+}$ deletion

To confirm that the candidates were sensitive to DSBs and that this sensitivity could be suppressed by *spd1*Δ, the *sens*Δ candidates and the corresponding *sens*Δ *spd1*Δ strains were subjected to a serial dilution assay. The assay was firstly performed with strains from the screen and then repeated using strains independently constructed from V2 library strains and *spd1::hph*.

The previously characterised Ddb1-Cul4^{Cdt2} complex deletion strains *cdt2*Δ and *ddb1*Δ were sensitive to bleocin and this was partially suppressed by *spd1*Δ as expected (Moss *et al.*, 2010). The same was observed for deletion of *csn1*$^{+}$, encoding a component of the signalosome associated with Ddb1-Cul4^{Cdt2} (Liu *et al.*, 2005) (Figure 3.13). A further 11 candidates also showed repeatable suppression of bleocin sensitivity by *spd1*Δ (Figure 3.14). However, 8 strains only showed suppression by *spd1*Δ with the screen strains and 3 strains showed no suppression (Figure 3.15.A-B).

Figure 3.11

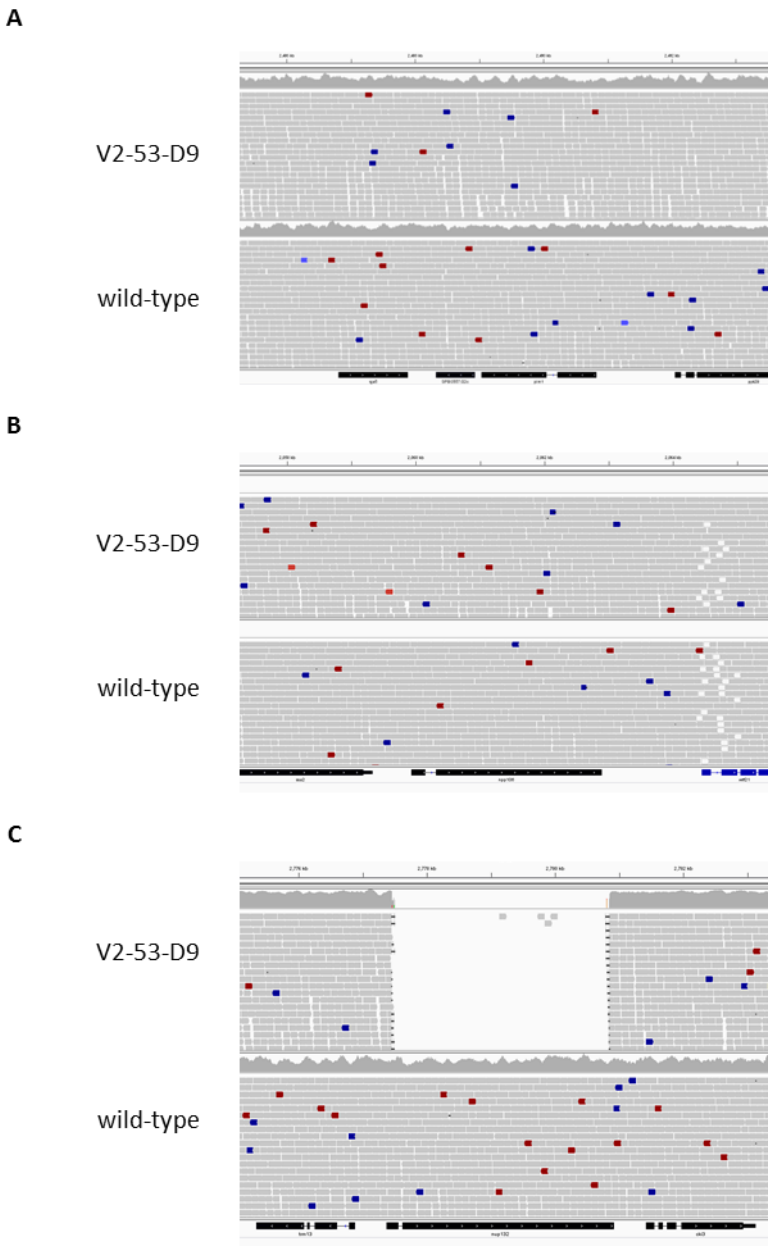


Figure 3.11 Whole genome sequencing of V2-53D9

Whole genome sequencing of wild-type and V2-53D9 strains was performed by High Throughput Genomics, Oxford Genomics Centre. The following genomic loci are shown **(A)** *SPBC557.02c*$^{+}$, **(B)** *npp106*$^{+}$, *and* **(C)** *nup132*$^{+}$.

Figure 3.12

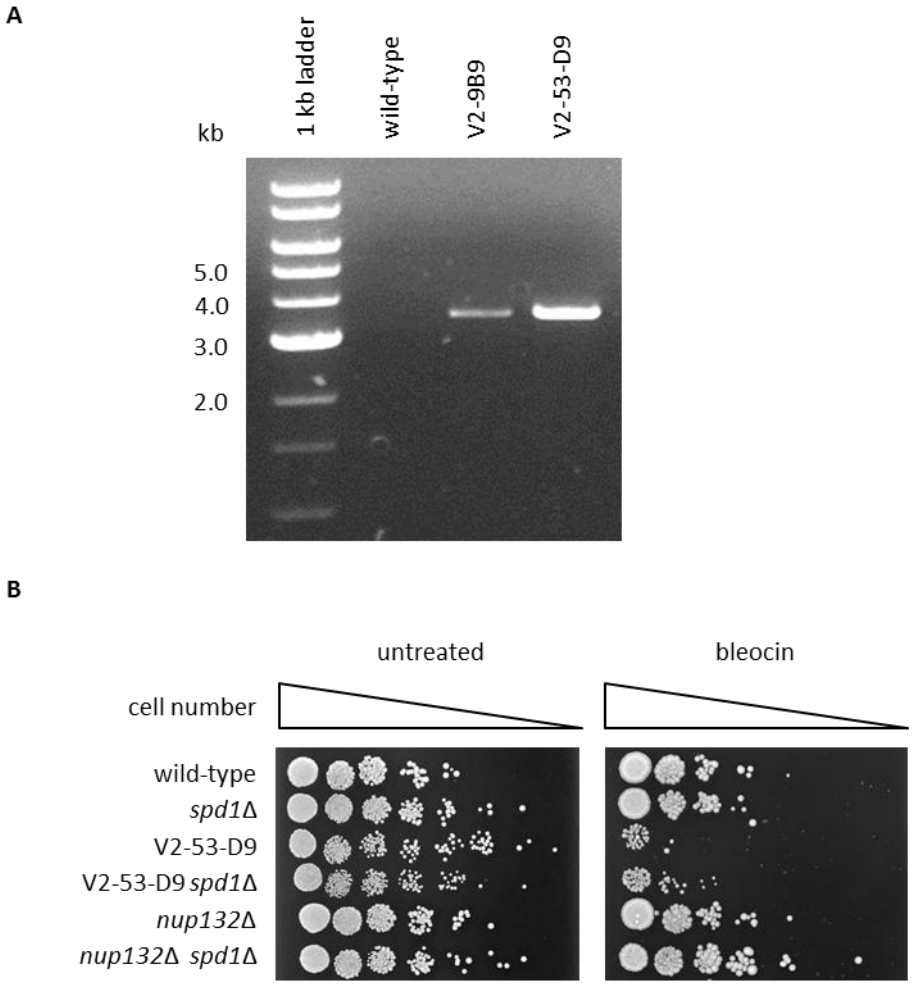


Figure 3.12 V2-53D9 corresponds to deletion of *nup132*$^{+}$

(A) PCR was performed using a forward primer specific to upstream of *nup132*$^{+}$ (primer A, Figure 3.1) and a reverse primer specific to the deletion cassette (primer 254, Figure 3.1). The detection of a band using V2-53D9 and *nup132*Δ (V2-9B9) DNA as a template and the absence using wild-type DNA confirmed *nup132*Δ deletion.

(B) Fivefold serial dilutions of wild-type, *spd1*Δ, V2-53D9, V2-53D9 *spd1*Δ, *nup132*Δ and *nup132*Δ *spd1*Δ spotted onto YE6S and YE6S + 0.2 µg/ml bleocin.

Figure 3.13

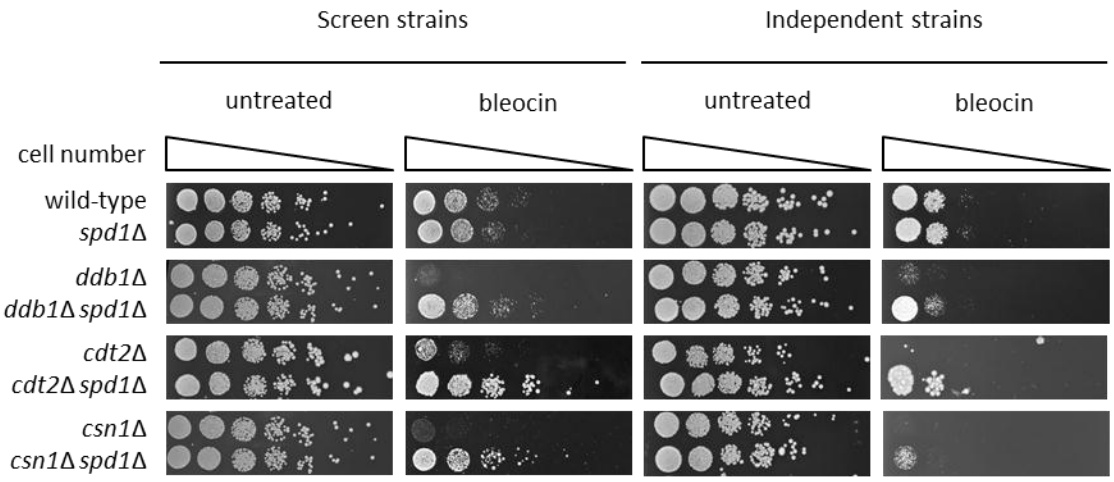


Figure 3.13 Deletion of *spd1*$^{+}$ suppresses the DSB sensitivity of Cul4-Ddb1^{Cdt2} complex members

Fivefold serial dilutions of wild-type, *spd1*Δ, *ddb1*Δ, *ddb1*Δ *spd1*Δ, *cdt2*Δ, *cdt2*Δ *spd1*Δ, *csn1*Δ, and *csn1*Δ *spd1*Δ, spotted onto YE6S and YE6S + 0.2 µg/ml bleocin. Serial dilutions on the left were performed with screen strains and on the right using independently constructed auxotrophic strains.

Figure 3.14

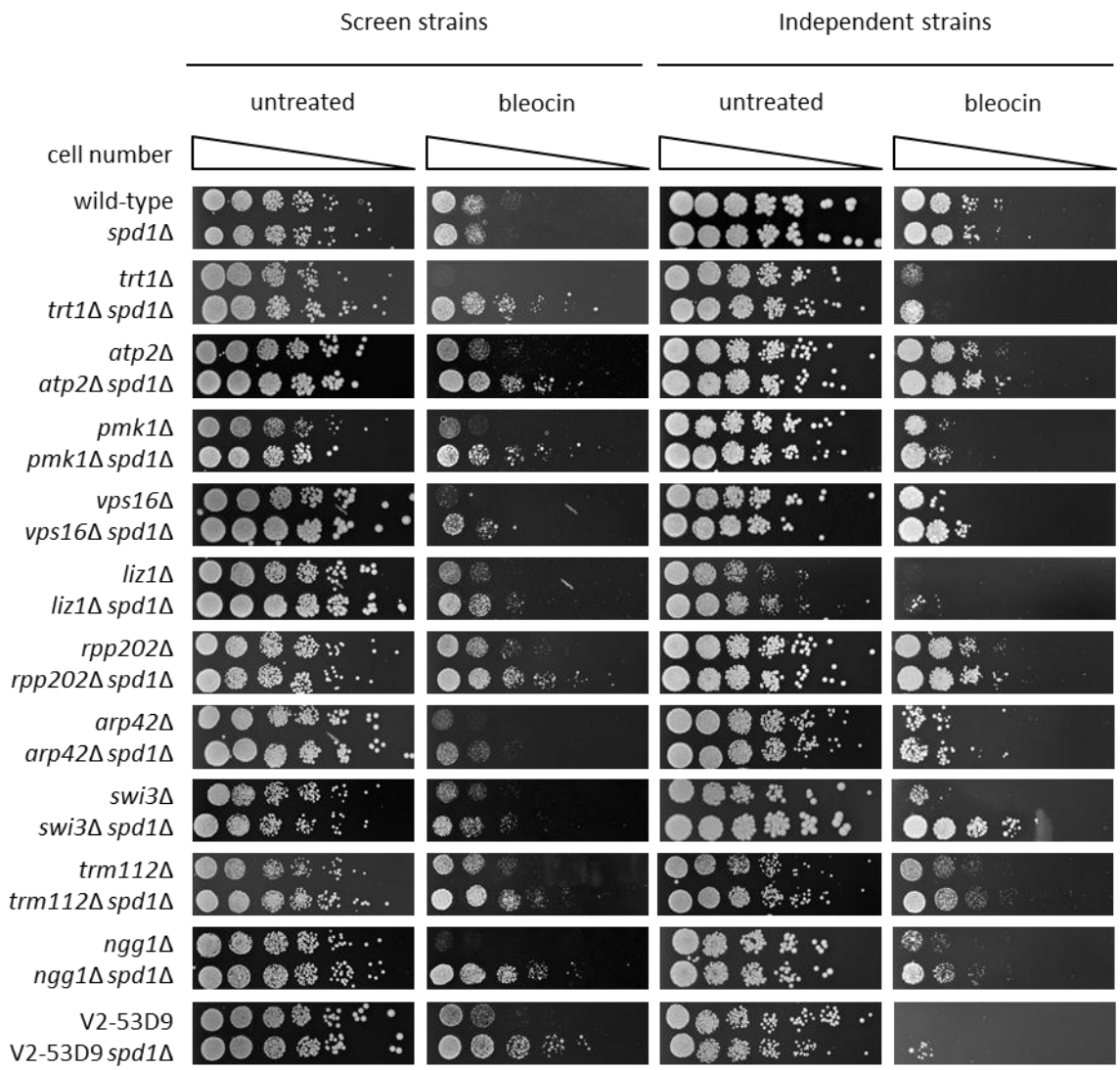


Figure 3.14 Deletion of *spd1*$^{+}$ suppresses the DSB sensitivity of candidate deletion strains

Candidates represented in this figure showed repeatable suppression of bleocin sensitivity by *spd1*Δ. Fivefold serial dilutions of wild-type, *spd1*Δ, *sens*Δ candidates and the corresponding *sens*Δ *spd1*Δ strains spotted onto YE6S and YE6S + 0.2 µg/ml bleocin. Serial dilutions on the left were performed with screen strains and on the right using independent auxotrophic strains. An auxotrophic *trm112*Δ *spd1*Δ could not be selected and so the *trm112*Δ and *trm112*Δ *spd1*Δ strains are prototrophic for arginine and histidine.

Figure 3.15

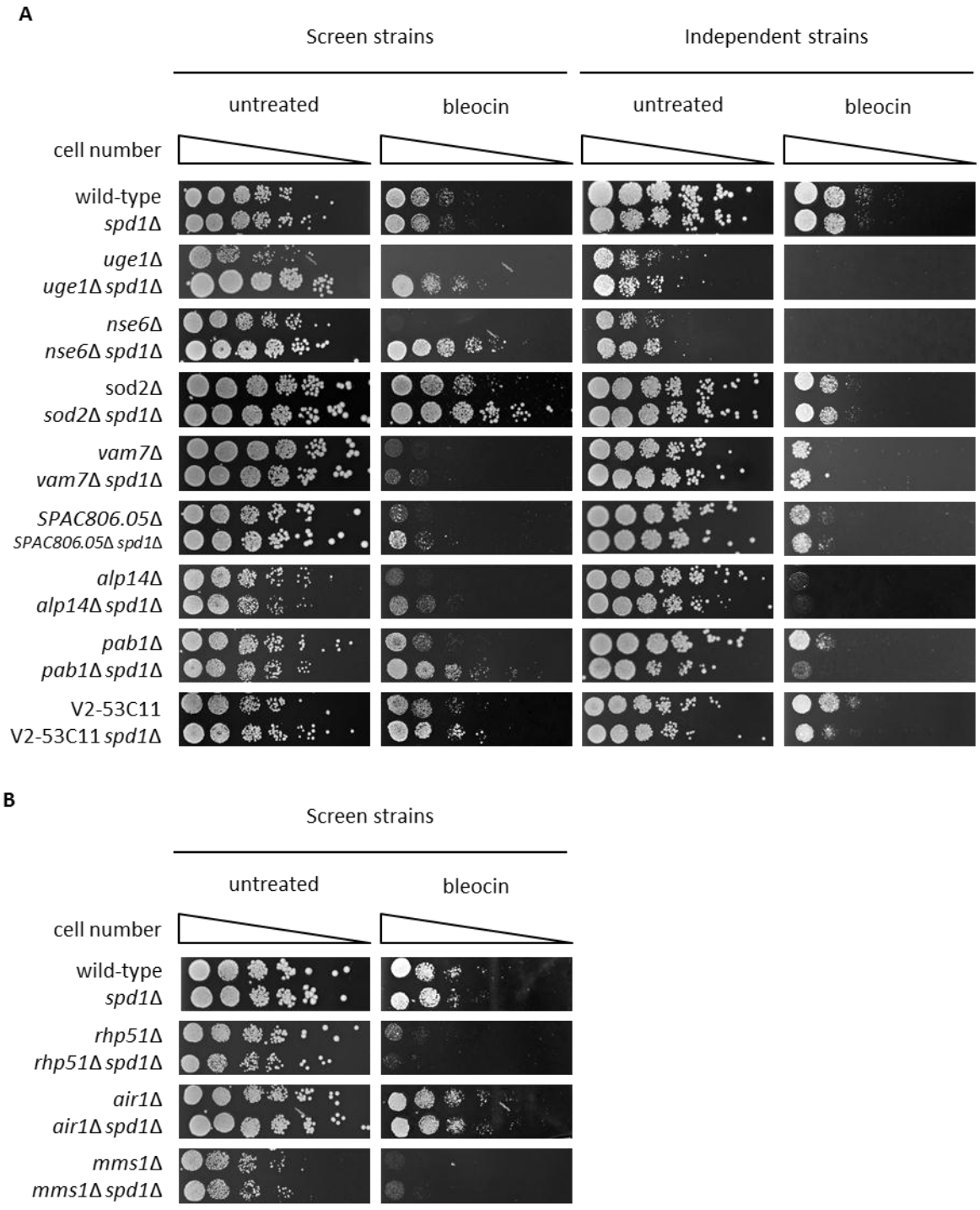


Figure 3.15 Deletion of *spd1*$^{+}$ cannot reproducibly suppress the DSB sensitivity of some candidates

(A) Fivefold serial dilutions of wild-type, *spd1*Δ, *sens*Δ candidates and the corresponding *sens*Δ *spd1*Δ strains spotted onto YE6S and YE6S + 0.2 µg/ml bleocin. Serial dilutions on the left were performed with screen strains and serial dilutions on the right using independently constructed auxotrophic strains. Candidates represented in this figure only showed suppression of bleocin sensitivity by *spd1*Δ using the screen strains.

(B) Fivefold serial dilutions of wild-type, *spd1*Δ, *sens*Δ candidates and the corresponding *sens*Δ *spd1*Δ strains spotted onto YE6S and YE6S + 0.2 µg/ml bleocin. The DSB sensitivity of candidates represented in this figure could not be supressed.

A possible cause for the differences between the bleocin sensitivity of the screen strains and the independent strains observed in Figure 3.15 was the background markers of the strains. The independent strains were auxotrophic for leucine (*leu1-32*), adenine (*ade6-*), uracil (*ura4-D18*), histidine (*his3-D1*) and arginine (*arg3-D4*) (all background markers). In contrast the DNA damage-sensitive library strains were only auxotrophic for leucine, adenine and uracil and following crossing to the PEM-2 *spd1::ura4* strain became auxotrophic only for leucine and adeneine with variable histidine auxotrophy.

It was found that background markers can have subtle but reproducible effects on bleocin sensitivity (Figure 3.16.A-B). For example *rad17*Δ and *rad17*Δ *spd1*Δ auxotrophic strains (*rad17::kanMX, spd1::hph, leu1-32, ade6-, ura4-D18, his3-D1, arg3-D4*) were sensitive to bleocin but prototrophy for uracil ($ura4^+$), arginine ($arg3^+$) or adenine ($ade6^+$) caused small decreases in sensitivity.

3.2.9 Candidate strains express Cdt2 in response to DSBs

Rad3 activates the Ddb-$Cul4^{Cdt2}$ ubiquitin ligase complex in response to DSBs by inducing expression of Cdt2 which recruits Spd1 for ubiquitination (Liu *et al.*, 2005; Moss *et al.*, 2010). It was investigated by fluorescence microscopy and western blotting whether other candidates were also required for damage-induced accumulation of Cdt2 tagged with yellow fluorescent protein (Cdt2-YFP). As Cdt2 is also expressed during S phase only mononuclear cells were studied (Liu *et al.*, 2005; Moss *et al.*, 2010).

In the absence of exogenous DNA damage 7.2% of mononuclear wild-type cells had a visible nuclear accumulation of Cdt2-YFP. Following 1 hour treatment with bleocin this increased 7.6 fold to 54.3% of cells (Figure 3.17.A-B). There was also an increase in total cellular Cdt2-YFP levels (Figure 3.18).

Figure 3.16

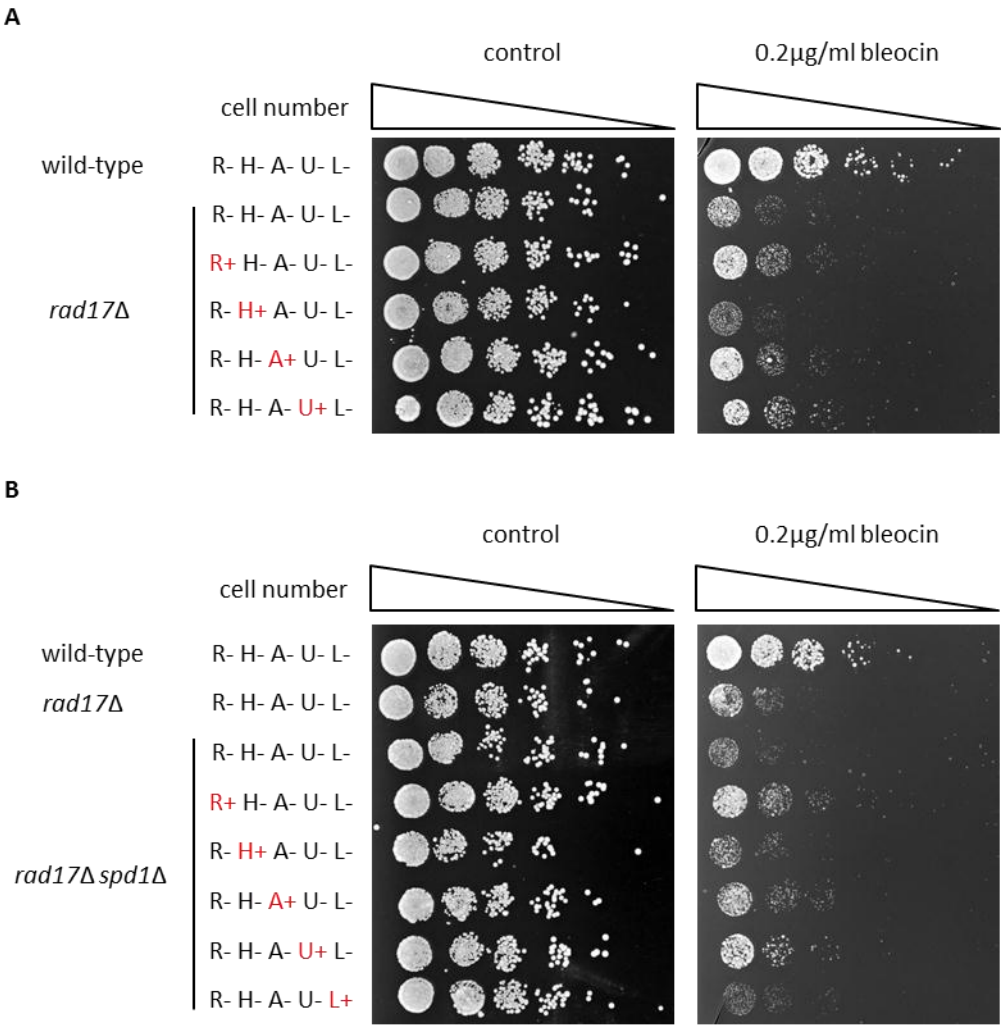


Figure 3.16 The DSB sensitivity of *rad17*Δ is affected by background markers

(A) Fivefold serial dilutions of wild-type and *rad17::kanMX* spotted onto YE6S and YE6S + 0.2 µg/ml bleocin.

(B) Fivefold serial dilutions of wild-type, *rad17::kanMX* and *rad17::kanMX spd1::hph* spotted onto YE6S and YE6S + 0.2 µg/ml bleocin.

All strains were auxotrophic except where noted. Prototrophy is recorded in red as (+). R = Arginine, H = histidine, A = adenine U = uracil and L = leucine.

Figure 3.17

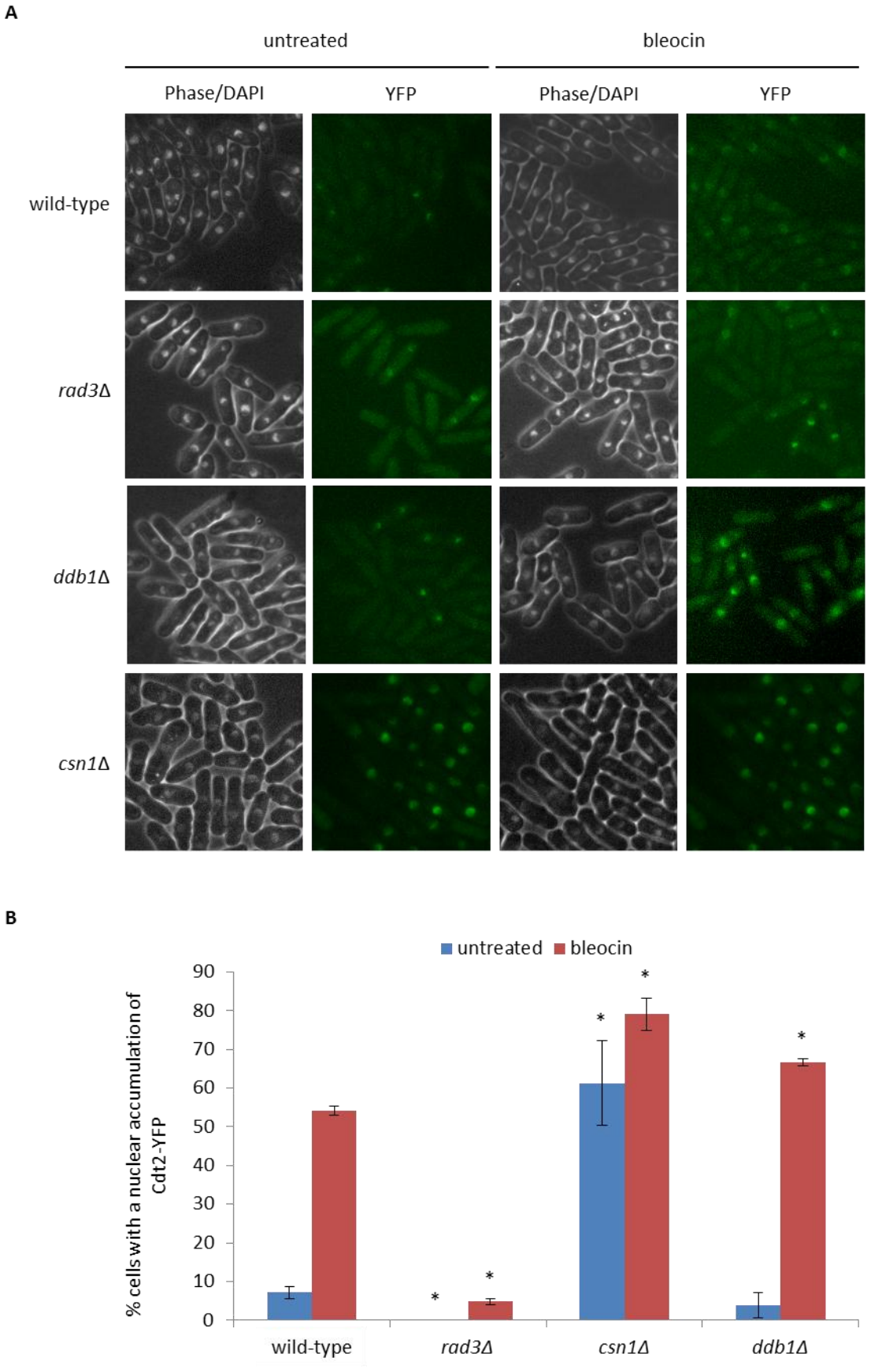

A
untreated
bleocin
Phase/DAPI
YFP
Phase/DAPI
YFP
wild-type
rad3Δ
ddb1Δ
csn1Δ
B
untreated
bleocin
% cells with a nuclear accumulation of Cdt2-YFP
90
80
70
60
50
40
30
20
10
0
wild-type
rad3Δ
csn1Δ
ddb1Δ

Figure 3.17 DSB-induced nuclear accumulation of Cdt2-YFP

(A) Methanol fixed asynchronous Cdt2-YFP wild-type, *rad3*Δ, *ddb1*Δ and *csn1*Δ cells grown in in YE6S or YE6S + 1 μg/ml bleocin for 1 hour. 100× Phase-DAPI and YFP fluorescence microscopy images are shown.

(B) Quantitation of the percentage mononuclear cells observed in (A) with a nuclear Cdt2-YFP accumulation. Approximately 100 cells per sample were scored. Mean scores ± standard errors for three independent repeats are shown.

Figure 3.18

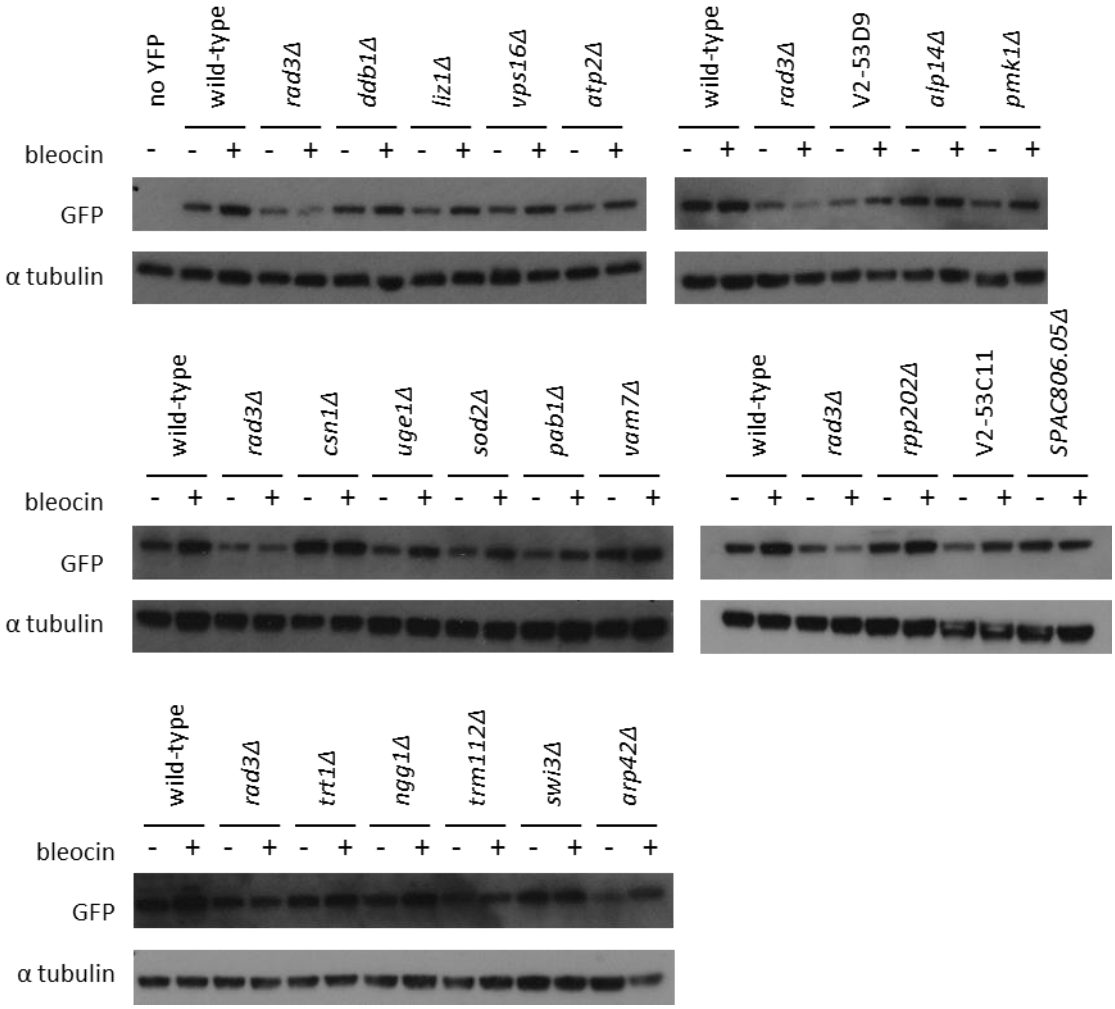


Figure 3.18 DSB-induced changes in the total levels of Cdt2-YFP for the candidate strains

Western blot analysis of total Cdt2-YFP levels for wild-type, *rad3*Δ and candidate gene deletion strains grown in the presence or absence of 2 μg/ml bleocin for 1 hour. Cdt2-YFP was detected using an anti-green fluorescent protein (GFP) antibody. An α tubulin loading control was used.

As expected, very few mononuclear *rad3*Δ cells had a visible nuclear Cdt2-YFP either in the presence (0.0%, p compared to wild-type ≤0.01) or absence of bleocin (4.9% p compared to wild-type ≤0.01). (Figure 3.17.A-B). No increase in total cellular Cdt2-YFP was observed in response to bleocin treatment (Figure 3.18).

In the absence of damage *ddb1*Δ showed no significant differences in the number of untreated cells with nuclear Cdt2-YFP compared to wild-type (3.9%, p = 0.55). Following bleocin treatment this increased to 66.6%, significantly higher than wild-type (p = <0.01) (Figure 3.17.A-B) However, only a wild-type increase in total Cdt2-YFP levels was detectable (Figure 3.18). In contrast *csn1*Δ showed significantly increased visible Cdt2-YFP compared to wild-type both in the presence an absence of bleocin (Figure 3.17.A-B). High total levels of Cdt2-YFP were also observed both in the presence and absence of bleocin (Figure 3.18).

The novel candidates were also able to express Cdt2-YFP in response to DNA damage. However, notably induction of Cdt2-YFP in response to DNA damage was compromised in a *trm112*Δ background. Also in a *swi3*Δ background high levels of Cdt2-YFP were observed both in the presence and absence of bleocin (Figure 3.18 and Figure 3.19.A-B).

3.2.10 Analysis of DSB repair by the candidates

To investigate the role of the candidates in DSB repair the deletion strains were subjected to a DSB assay (Figure 1.5). In this assay 69.2% of wild-type cells repair by GC, 4.0% repair by NHEJ/SCC, 16.8% undergo Ch^{16} loss and 7.3% undergo LOH. *spd1*Δ had significantly increased levels of GC (77.1%, p < 0.01) and significantly reduced levels of NHEJ/SCC (2.0%, p = 0.03) and LOH (7.3%, p = 0.02) compared to wild-type. No significant change was observed in the levels of Ch^{16} loss (13.7%, p = 0.08) (Figure 3.20).

Figure 3.19.A (page 1 of 3)

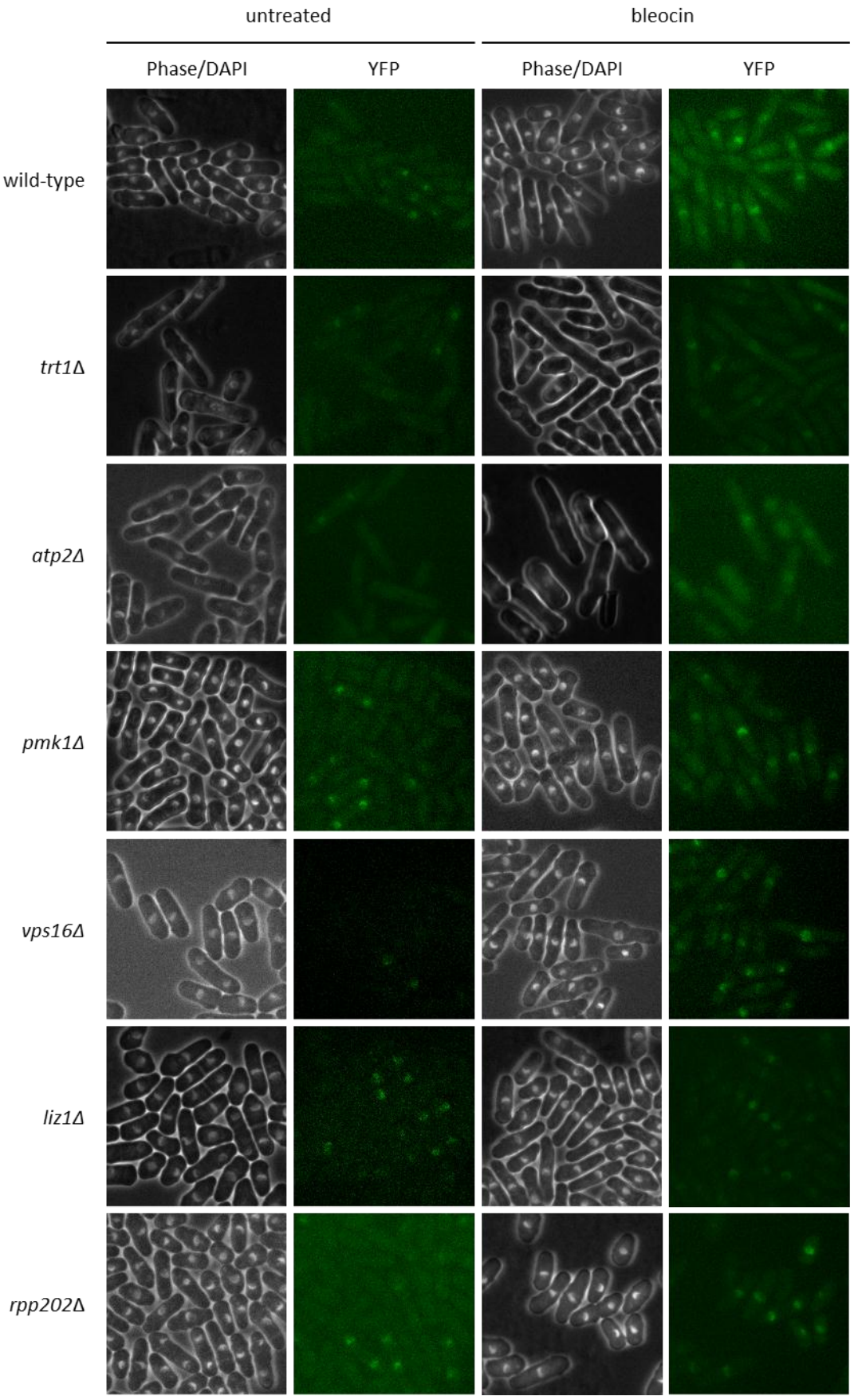


Figure 3.19.A (page 2 of 3)

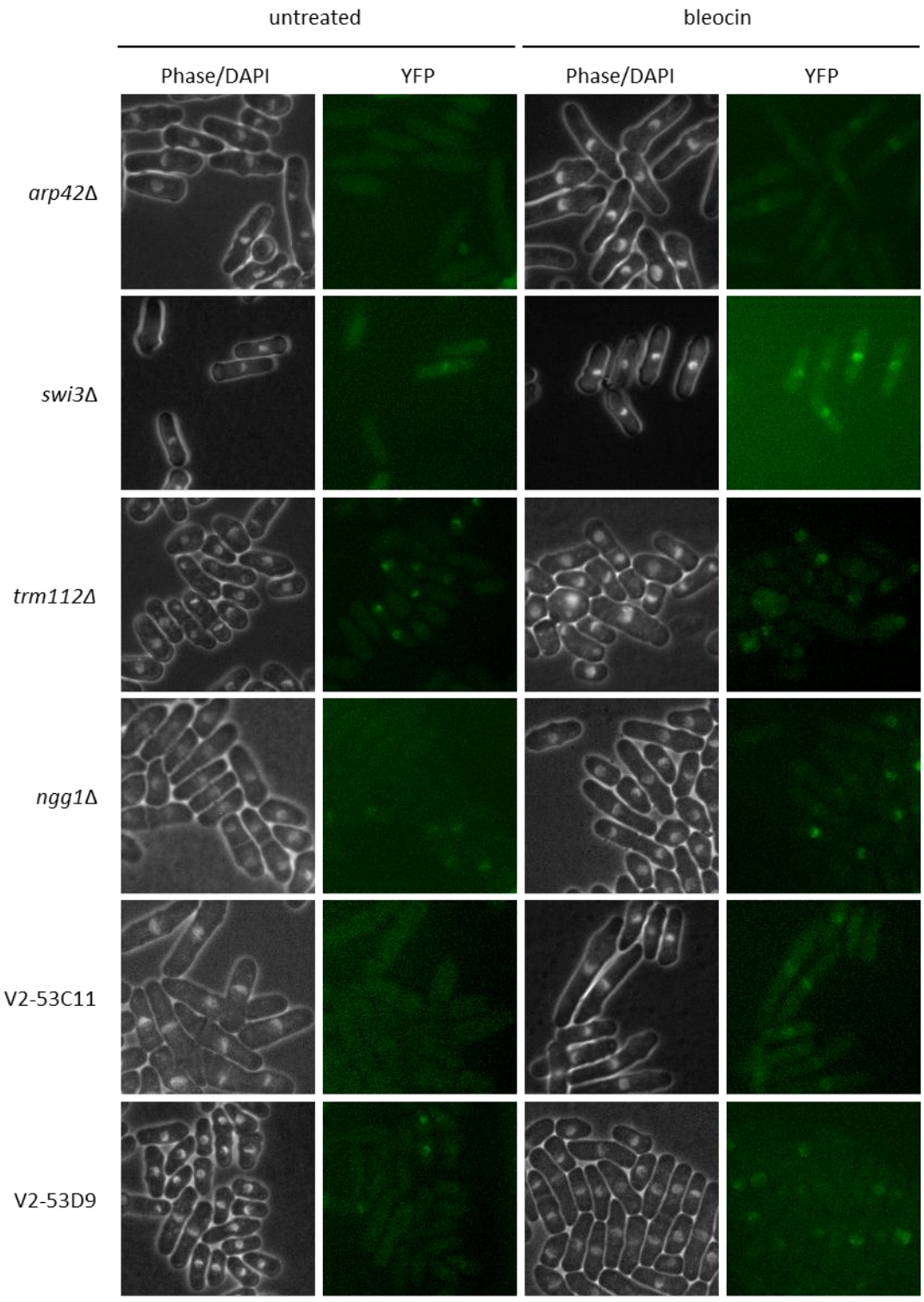


Figure 3.19.A (page 3 of 3)

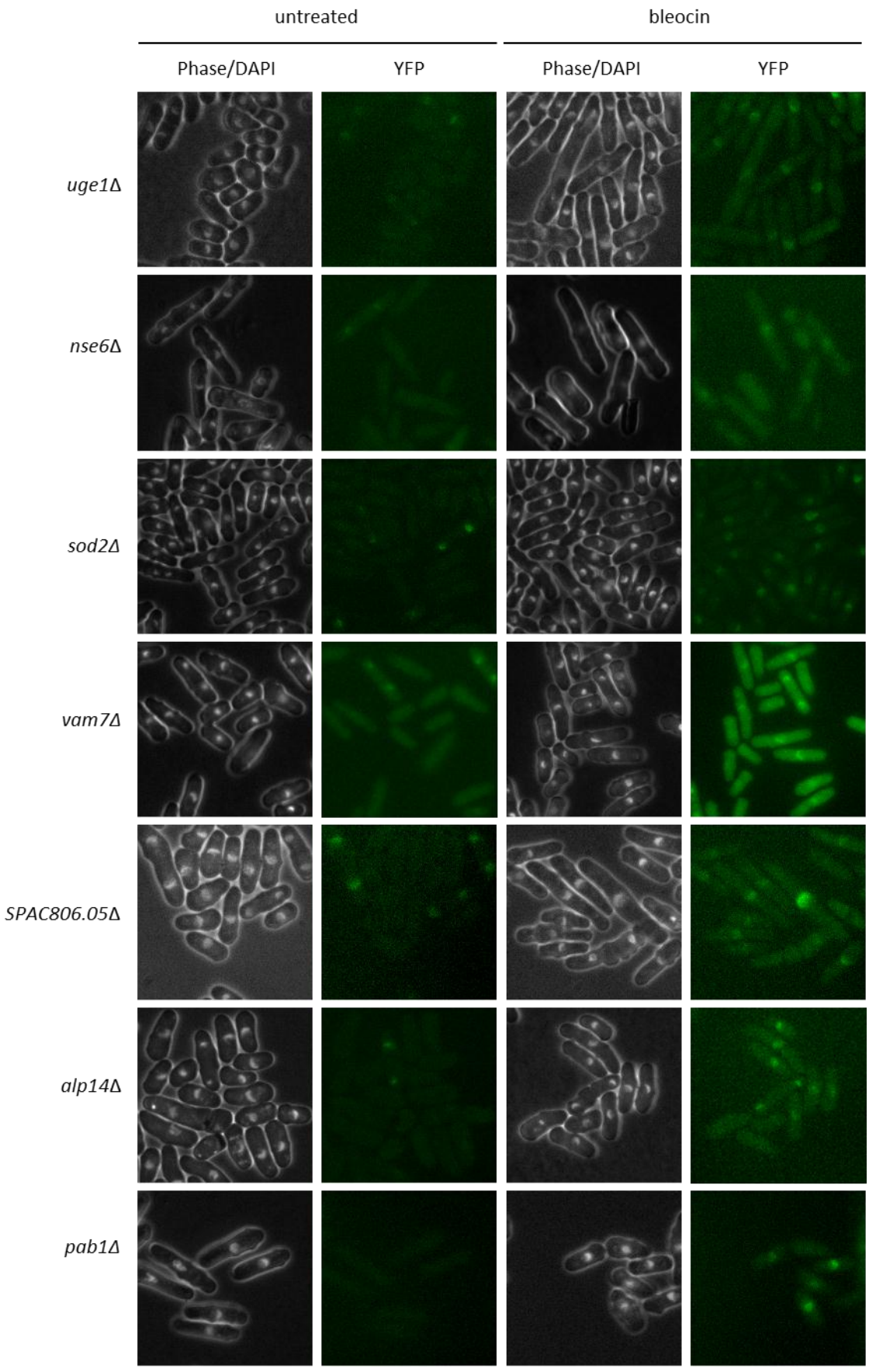


Figure 3.19.B

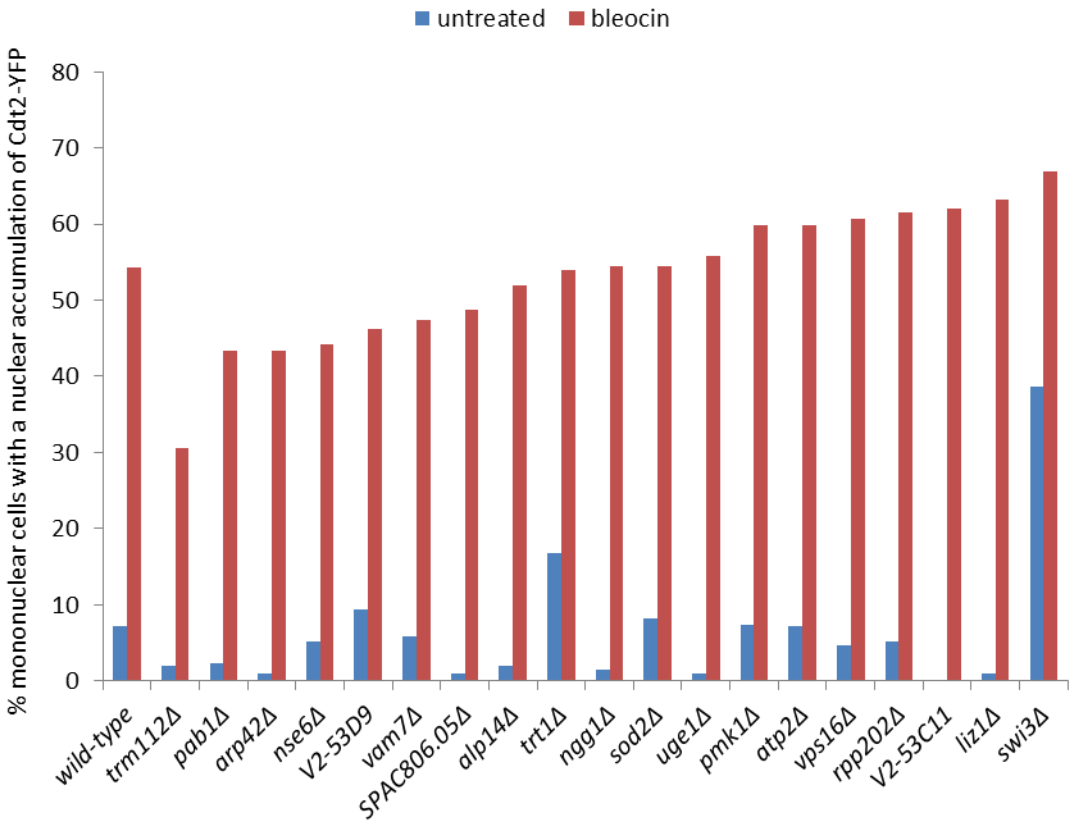


Figure 3.19 Candidate strains showed DSB-induced nuclear accumulation of Cdt2-YFP

(A) Methanol fixed asynchronous Cdt2-YFP wild-type, and candidate gene deletion strains grown in in YE6S (untreated) or YE6S + 1 µg/ml bleocin for 1 hour. 100× Phase-DAPI and YFP fluorescence microscopy images are shown.

(B) Quantitation of the percentage mononuclear cells observed in (A) with a nuclear Cdt2-YFP accumulation. Approximately 100 cells per sample were scored (N.B. approximately 40 cells per sample were scored for *nse6*Δ)

Figure 3.20

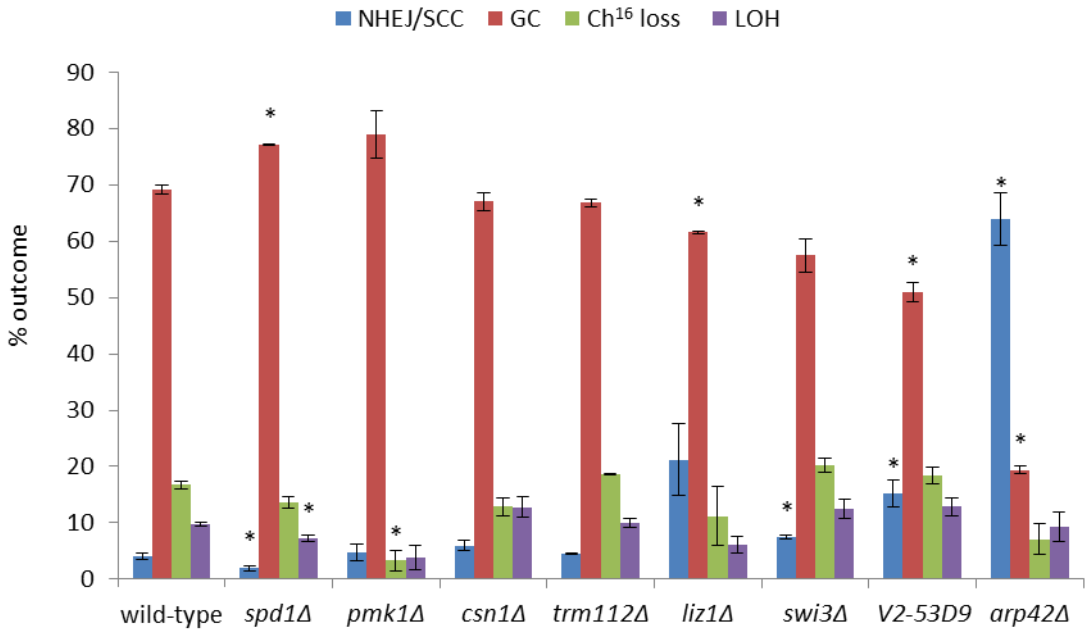


Figure 3.20 DSB analysis of candidate strains

DSB assay analysis of wild-type and *spd1*Δ, *pmk1*Δ, *csn1*Δ, *trm112*Δ, *liz1*Δ, s*wi3*Δ V2-53D9 and *arp42*Δ. The percentage NHEJ/SCC, GC, LOH and Ch^{16} loss events are shown. Mean values ± standard errors are presented for three independent repeats. Mean values for *trm112*Δ are presented for two independent repeats. Asterisk (*****) represents a significant difference to wild-type.

The candidates *trm112*Δ and *pmk1*Δ both had similar repair profiles to wild-type (Figure 3.20). *trm112*Δ showed no significant difference to wild-type in the levels of GC (66.8%, p = 0.19), NHEJ/SCC (4.6%, p = 0.19), Ch^{16} loss (18.6%, p = 0.25), or LOH (10.0%, p = 0.19). *pmk1*Δ showed no significant difference to wild-type in the levels of GC (78.9%, p = 0.15), NHEJ/SCC (4.8%, p = 0.66), or LOH (3.8%, p = 0.50). However, the levels Ch^{16} loss (3.3%, p = 0.03) were significantly reduced. Deletion of *spd1*$^+$ in either background had no significant effect on repair (Figure 3.21.A-B).

*csn1*Δ also had a repair profile similar to wild-type however deletion of *spd1*$^+$ in this background dramatically increased the efficiency of HR repair. In a *csn1*Δ background no significant difference was observed in the levels of GC (67.0%, p =0.32), NHEJ/SCC (5.9%, p = 0.16) Ch^{16} loss (12.9%, p = 0.12), or LOH (13.7%, p = 0.08) compared to wild-type (Figure 3.20). Deletion of *spd1*$^+$ significantly increased GC (91.4%, p < 0.01) and significantly reduced NHEJ/SCC (0.9%, p = 0.02), Ch^{16} loss (3.7%, p = 0.03) and LOH (3.6%, p = 0.02) compared to *csn1*Δ alone (Figure 3.21.C).

*liz1*Δ had significantly decreased GC (61.6%, p < 0.01). No significant change was observed in the levels of NHEJ/SCC (21.2%, p = 0.11), Ch^{16} loss (13.7%, p = 0.08) or LOH (7.3%, p = 0.02) compared to wild-type (Figure 3.20). Deletion of *spd1*$^+$ significantly increased GC (67.5%, p = 0.05) compared to *liz1*Δ alone (Figure 3.21.D).

Figure 3.21 (page 1 of 3)

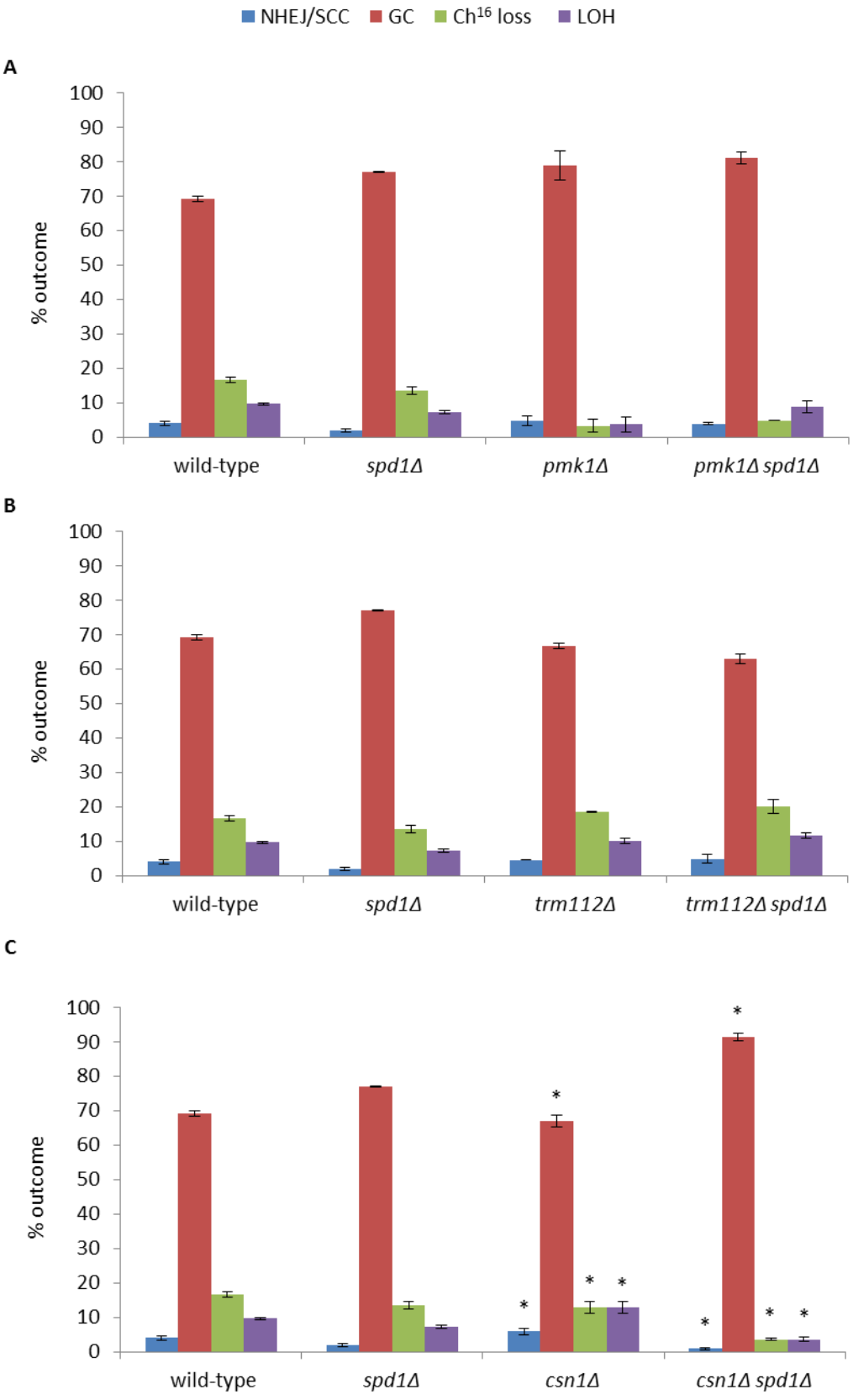


Figure 3.21 (page 2 of 3)

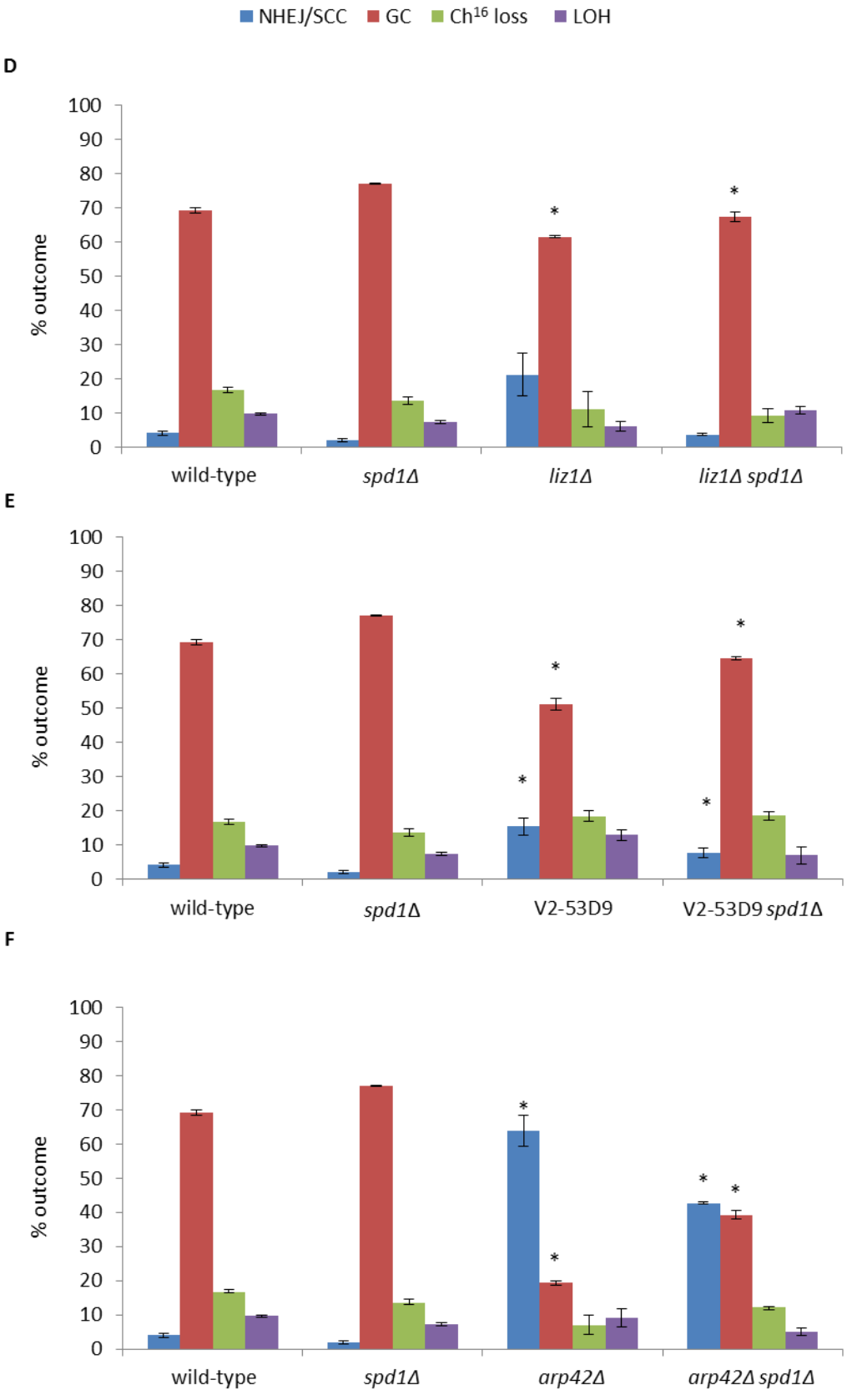


Figure 3.21 (page 3 of 3)

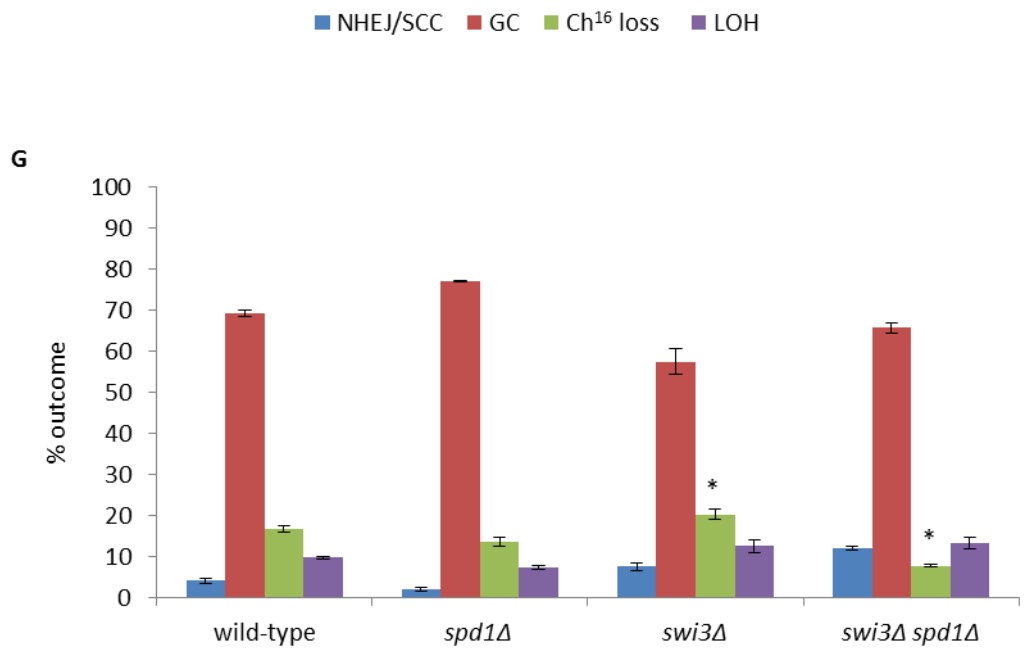


Figure 3.21 DSB analysis of candidate strains and the corresponding *spd1*Δ strains

DSB assay analysis of:

(A) wild-type, *spd1*Δ, *pmk1*Δ and *pmk1*Δ *spd1*Δ

(B) wild-type, *spd1*Δ, *csn1*Δ and *csn1*Δ *spd1*Δ

(C) wild-type, *spd1*Δ, *trm112*Δ and *trm112*Δ *spd1*Δ

(D) wild-type, *spd1*Δ, *liz1*Δ and *liz1*Δ *spd1*Δ

(E) wild-type, *spd1*Δ, V2-53D9 and V2-53D9 *spd1*Δ

(F) wild-type, *spd1*Δ, *arp42*Δ and *arp42*Δ *spd1*Δ

(G) wild-type, *spd1*Δ, *swi3*Δ and *swi3*Δ *spd1*Δ

The percentage NHEJ/SCC, GC, LOH and Ch^{16} loss events are shown. Mean values ± standard errors are presented for three repeats. Mean values for *trm112*Δ and *arp42*Δ *spd1*Δ are presented for two independent repeats. Asterisk (*****) represents a significant difference between the *sens*Δ and corresponding *sens*Δ *spd1*Δ strains.

V2-53D9 had significantly decreased levels of GC (51.0%, $p < 0.01$) and significantly increased levels of NHEJ/SCC (15.3%, $p < 0.01$) compared to wild-type with no significant change observed in the levels of Ch^{16} loss (18.4%, $p = 0.35$) or LOH (12.9%, $p = 0.12$) (Figure 3.20). Deletion of *spd1*$^+$ significantly increased GC (64.4%, $p < 0.01$) and decreased NHEJ/SCC (7.6%, $p < 0.01$) compared to V2-53D9 alone (Figure 3.21.E).

A much more pronounced exchange between repair by GC and NHEJ/SCC was observed for *arp42*Δ. *arp42*Δ had dramatically decreased levels GC (19.4%, $p < 0.01$) and increased levels of NHEJ/SCC (64.0%, $p = 0.01$) compared to wild-type. No significant difference was observed in the levels of Ch^{16} loss (7.1%, $p = 0.06$) or LOH (9.2%, $p = 0.86$) compared to wild-type (Figure 3.20). Deletion of *spd1*$^+$ significantly increased GC (39.3%, $p = 0.02$) and decreased NHEJ/SCC (42.8% $p = 0.04$) compared to *arp42*Δ alone (Figure 3.21.F).

There was no significant difference in the levels of GC (57.5%, $p = 0.05$), Ch^{16} loss (20.2%, $p = 0.08$) or LOH (12.5%, $p = 0.23$) in a *swi3*Δ background compared to wild-type. However NHEJ/SCC was significantly increased (7.5%, $p < 0.01$) compared to wild-type (Figure 3.20). The only significant change following *spd1*$^+$ deletion in this background was significantly decreased Ch^{16} loss (7.8%, $p < 0.01$) (Figure 3.21.G).

3.2.11 Analysis of candidate nucleotide pools

To confirm whether the candidate genes are involved in DNA damage-induced nucleotide synthesis, log phase cultures of a wild-type strain and the candidate deletion strains were grown in the presence or absence of bleocin to induce DSBs. The levels of dNTPs were measured by HPLC and normalised to wild-type in the absence of bleocin treatment. An example chromatogram showing the output of HPLC analysis for a wild-type strain is shown in Appendix VI.

In a wild-type background treatment with bleocin increased the levels of all four dNTPs (Figure 3.22.A-B). The levels of deoxycytidine triphosphate (dCTP) and deoxyadenosine triphosphate (dATP) increased 2.0 fold, the levels of deoxythymidine triphosphate (dTTP) increased 1.7 fold and the levels of deoxyguanosine triphosphate (dGTP) increased 1.5 fold. A *rad3*Δ strain is known to have compromised DNA damage-induced dNTP synthesis (Moss *et al.*, 2010). In the absence of bleocin *rad3*Δ had similar levels of dNTPs compared to wild-type (Figure 3.22.A). However bleocin did not induce nucleotide synthesis in this background (Figure 3.22.B).

*csn1*Δ had reduced levels of all four dNTPs compared to wild-type both in the presence and absence of bleocin. *pmk1*Δ had reduced levels only of dCTP compared to wild-type both in the presence and absence of bleocin. In the absence of bleocin *rpp202*Δ showed similar levels of dNTPs compared to wild-type. However, following bleocin treatment induction of dCTP, dATP and dTTP was reduced compared to wild-type. Following bleocin treatment *atp2*Δ and *arp42*Δ had reduced levels only of dCTP compared to wild-type (Figure 3.22.A-B). The other candidates did not have compromised nucleotide pools either in the presence or absence of bleocin (Figure 3.23.A-B).

Figure 3.22

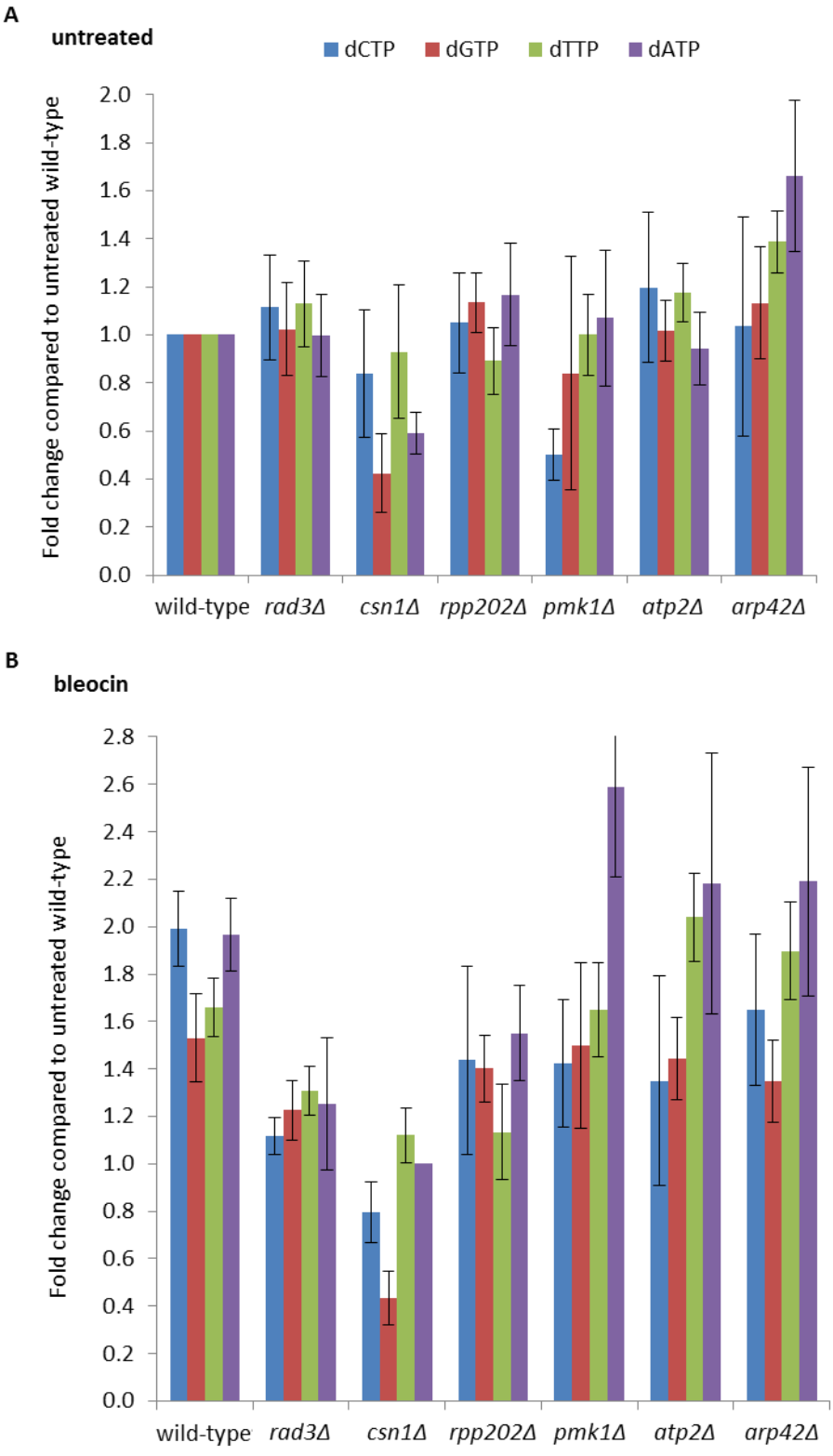


Figure 3.22 *csn1*Δ, *rpp202*Δ, *atp2*Δ and *arp42*Δ have compromised nucleotide pools

HPLC analysis nucleotide levels for wild-type, *rad3*Δ, *csn1*Δ, *rpp202*Δ, *atp2*Δ and *arp42*Δ grown for 2 hours in **(A)** YE6S **(B)** YE6S + 2 µg/ml bleocin. Mean values are presented as a percentage of wild-type in the absence of bleocin and ± standard errors are indicated. A minimum of 3 independent repeats were performed. Due to detection problems only one dATP measurement was made for *csn1*Δ in (B). HPLC analysis was performed by Lisa Folkes (Department of Oncology, University of Oxford).

Figure 3.23

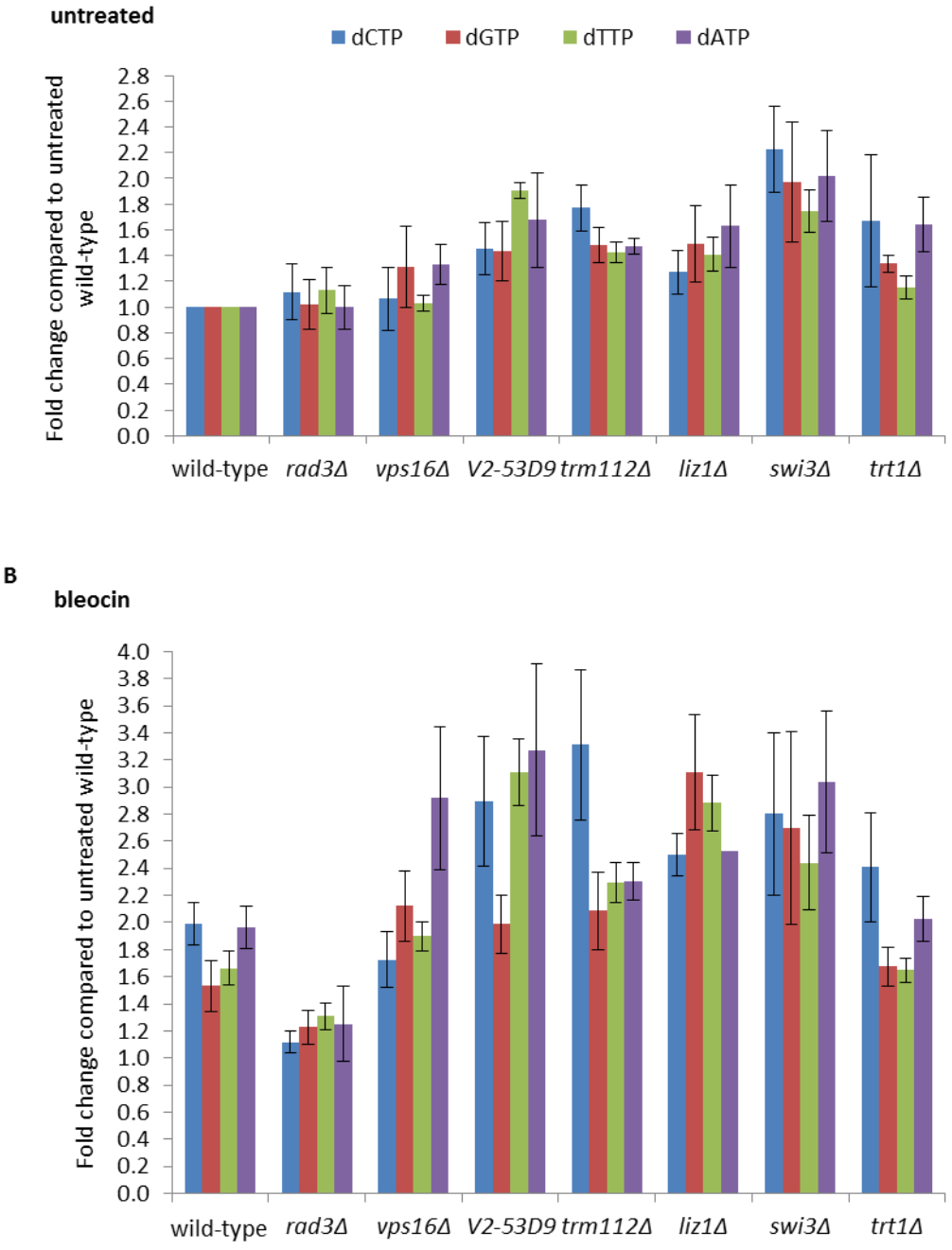


Figure 3.23 Candidate strains do not have compromised nucleotide pools

HPLC analysis nucleotide levels for wild-type, *rad3*Δ, *vps16*Δ, *pmk1*Δ, V2-53D9, *trm112*Δ, *liz1*Δ, *swi3*Δ, and *trt1*Δ grown for 2 hours in **(A)** YE6S **(B)** YE6S + 2 µg/ml bleocin. Mean values are presented as a percentage of wild-type in the absence of bleocin and ± standard errors are indicated. A minimum of 3 independent repeats were performed. Due to detection problems only one dATP measurement was made for *liz1*Δ in (B). HPLC analysis was performed by Lisa Folkes (Department of Oncology, University of Oxford).

3.3 DISCUSSION

In this chapter the results of a screen to identify genes involved in DNA repair through damage-induced nucleotide synthesis are presented. This was investigated by screening for *S. pombe* deletion strains whose DSB sensitivity was suppressed by deletion of *spd1*$^{+}$ to promote nucleotide synthesis. The screen successfully identified a number of candidates showing repeatable suppression of DSB sensitivity when *spd1*$^{+}$ was deleted. The role of these genes in DSB repair and nucleotide synthesis was investigated. From these candidates DNA damage checkpoint genes and *ngg1*$^{+}$ involved in histone acetylation were chosen for further study and the results for these candidates are presented separately in Chapter 4 and Chapter 5.

3.3.1 The DNA damage-sensitive deletion library

A library of 350 DNA damage-sensitive deletion strains was compiled from strains identified by Moss (2011) and Deshpande *et al.* (2009) in screens of the V1 *S. pombe* haploid deletion library (Figure 3.2). Differences between the strains identified by the two groups were partly due to the different DNA damaging agents used, but also because strain sensitivity was assessed in different ways (Moss, 2011) (Figure 3.2). These factors also explain the differences in DSB sensitivity of the strains observed in this project. This suggests that the screens most accurately identify strains with acute DSB sensitivity.

The V1 library only provides 63% coverage of the *S. pombe* non-essential genome. Subsequent to the analysis presented in this chapter, the V2 library, providing 93% coverage, was screened firstly for strains sensitive to MMS, bleomycin and CPT using a similar colony based approach (Kasparek, 2013) and secondly for bleocin sensitivity using a quantitative approach based on the deep sequencing of deletion cassette barcodes (Humphrey laboratory, unpublished data). The latter adopted an approach used previously with both *S. pombe* and

S. cerevisiae deletion libraries (Han *et al.*, 2010; Smith *et al.*, 2009). These screens would provide more comprehensive libraries of DSB sensitive strains for future analysis.

3.3.2 The identification of deletion strains with altered DSB sensitivity following *spd1*$^+$ deletion

96% of the DNA damage sensitive strains were successfully crossed with *spd1*Δ (Figure 3.3) and 87% were successfully screened for altered DSB sensitivity when *spd1*$^+$ was deleted (Figure 3.4-3.8). The screen identified two groups of deletion strains, those with decreased DSB sensitivity when *spd1*$^+$ is deleted and those with increased DSB sensitivity when *spd1*$^+$ is deleted (Figure 3.7-3.8).

Quantitative analysis of *sens*Δ and *sens*Δ *spd1*Δ colony size in the presence and absence of bleocin was used to assess the effect of *spd1*Δ on the bleocin sensitivity of each *sens*Δ strain (Figure 3.4). Whilst several methods of calculating differences in bleocin sensitivity could have been used, the approach presented in Figure 3.5 is validated by the identification of *rad3*Δ, *cdt2*Δ, *ddb1*Δ and *csn1*Δ within the top 10% of strains showing suppression of DSB sensitivity when *spd1*$^+$ was deleted (Figure 3.7, Figure 3.8 and Figure 3.13). These results are supported by independent observations (Liu *et al.*, 2005; Moss *et al.*, 2010). The suppression of DSB sensitivity by *spd1*Δ was also confirmed by spot dilution for 19 out of 22 candidate strains analysed in this chapter (Figure 3.13, Figure 3.14 and Figure 3.15).

Unexpectedly *sens*Δ strains were identified which grew better than wild-type under bleocin conditions as well as *sens*Δ *spd1*Δ strains which grew better than *spd1*Δ (Figure 3.6.A-D). This may have been caused by differences in the genetic background of the strains which can effect bleocin sensitivity (Figure 3.16).

37 strains were not analysed in the screen either due to poor growth or because a double mutant with *spd1*Δ could not be produced (Appendix V). It would be expected that deletion of genes involved in the DNA damage response would compromise genome stability and strain fitness. Variations between replica measurements also made it difficult to apply statistical significance to the results and resulted in the removal of 9 strains from the screen analysis (Appendix V). The final size of each colony was influenced not only by the strains fitness but also by the number of inoculated cells, competition for space and nutrients, variations in drug activity and the ability of the software to accurately detect colony boundaries (Lawless *et al.*, 2010). Additional screen repeats could improve the error of results. It has also been proposed that measuring the exponential growth rate of colonies could provide a better indication of fitness (Lawless *et al.*, 2010).

3.3.3 Analysis of candidate deletion strains

The top 29 deletion strains showing suppression of DSB sensitivity when *spd1*$^{+}$ was deleted in the screen were selected for validation (Table 3.1). This included four checkpoint deletion strains assessed separately in Chapter 4. Of the remaining 25 deletion strains, the identity of 21 was confirmed by PCR. However, two strains contained incorrectly inserted deletion cassettes and two strains require further characterisation (Figure 3.9 to Figure 3.12). Errors are known to exist in the V1 library and it appears some persist in the V2 library (Han *et al.*, 2010; Moss, 2011). In addition the deletion cassette barcode for V2-53D9 did not correspond to the gene deleted. Studies of *S. cerevisiae* deletion libraries found an estimated 20-30% of barcode sequences deviated from those annotated (Eason *et al.*, 2004; Smith *et al.*, 2009). Incorrect barcodes were also identified in the *S. pombe* V1 deletion library (Han *et al.*, 2010).

Of the 25 candidates assessed in this chapter, 22 showed the suppression of DSB sensitivity by *spd1*Δ when the screen strains were subjected to serial dilution assays. However, when

independent strains were constructed this was reduced to 14 candidates (Figure 3.13 to Figure 3.15). It was found that the strains genetic background, in particular the ability to synthesise uracil, adenine and histidine had subtle effects on DSB sensitivity (Figure 3.16).

A role in DSB repair and nucleotide synthesis was investigated for the candidates showing repeatable suppression of DSB sensitivity when *spd1*$^{+}$ was deleted and is discussed in the following sections. The roles of the DNA damage checkpoint genes and *ngg1*$^{+}$ are presented separately in Chapters 4 and 5. Unexpectedly many of the candidates did not have reduced nucleotide pools compared to wild-type either in the presence or absence of DSBs. These candidates included *trm112*Δ, *liz1*Δ, swi3Δ, *vps16*Δ, *trt1*Δ, V2-53D9 and V2-53C11. An explanation consistent with these results would be that Spd1 is playing an additional role in suppressing DSB sensitivity independently of promoting nucleotide synthesis.

Subsequent to this screen Fleck *et al.* (2013) identified a role for Spd1 in promoting replication stress independently of RNR regulation. They found that inappropriate expression of Spd1 during S phase in a *ddb1*Δ background results in accumulation of ssDNA and replication checkpoint activation. This was not just caused by reduced nucleotide pools as the phenotype could be suppressed by *spd1*Δ but not by increasing nucleotide pools using *cdc22-D57N*. They proposed that Spd1 perturbs replication through an unknown pathway.

The candidates *ngg1*Δ, *arp42*Δ, *liz1*Δ and V2-53D9 also showed a switch from repair by GC to NHEJ/SCC which could be rescued by *spd1*Δ. In further studies of these candidates it would be important firstly to confirm whether this was an indirect effect of an altered cell cycle, an artefact of the experiment, or a direct biological effect. Secondly it would be important to investigate whether *spd1*Δ mediates this switch through nucleotide pools or an alternative mechanism. This is discussed further in Chapter 5 with respect to *ngg1*Δ.

3.3.4 A role for Csn1 in nucleotide synthesis

Csn1 is a component of the conserved COP9 signalosome. A *csn1*Δ strain was sensitive to DSBs (Figure 3.13) and had reduced nucleotide pools both in the presence and absence of DNA damage (Figure 3.22). The DSB sensitivity was partially supressed by deleting *spd1*$^{+}$ to increase nucleotide pools (Figure 3.13). This evidence is consistent with a role for Csn1 in nucleotide synthesis and was expected as Csn1 is required for the ubiquitination of Spd1 by Ddb1-Cul4^{Cdt2} (Liu *et al.*, 2005; Liu *et al.*, 2003).

Three COP9 subunits, *csn1*Δ, *csn3*Δ and *csn7*Δ, were present in the V1 library however only *csn1*Δ was identified as damage-sensitive (Deshpande *et al.*, 2009; Moss, 2011). Mundt et al. (2002) previously showed that *csn1*Δ and *csn2*Δ were IR and UV sensitive whereas *csn4*Δ and *csn5*Δ had wild-type phenotypes. It should also be investigated whether the DSB sensitivity of *csn2*Δ is suppressed by *spd1*Δ. As all 4 subunits are required for Cul1 deneddylation, Csn1 is predicted to have an additional function in Spd1 ubiquitination (Mundt *et al.*, 2002).

Deletion of *csn1*$^{+}$ resulted in high levels of Cdt2-YFP compared to wild-type both in the presence and absence of bleocin (Figure 3.17 and Figure 3.18). In human cells Cdt2 is signalled for degradation by Cul4A-Ddb1^{Cdt2} autoubiquitination and also ubiquitination by the Cul1-Skp1^{FBXO11} complex (Abbas *et al.*, 2013a; Abbas *et al.*, 2013b; Rossi *et al.*, 2013). As COP9 is required for Spd1 degradation it may also be required for Cdt2 degradation (Liu *et al.*, 2003). It is also possible that high levels of Cdt2 are expressed in a *csn1*Δ strain in response to an accumulation of endogenous DNA damage.

Moss et al (2010) analysed the repair of *ddb1*Δ and *cdt2*Δ using the DSB assay. Both strains showed reduced repair by GC and increased LOH and Ch^{16} loss compared to wild-type. Unexpectedly *csn1*Δ had a DSB repair profile similar to wild-type (Figure 3.20). This

contrasts with the DSB sensitivity of *csn1*Δ and reflects the complex role of COP9 in regulating the degradation of many proteins. *csn1*Δ *spd1*Δ had significantly increased levels of GC compared to wild-type (Figure 3.21.C). A similar hyper-recombinant phenotype has been observed for *mrc1*Δ and *cds1*Δ replication checkpoint deletion strains (Blaikley *et al.*, 2014). These phenotypes may be related as the inability to degrade Spd1 results in activation of the replication checkpoint (Fleck *et al.*, 2013).

3.3.5 The DSB sensitivity of *arp42*Δ was suppressed by *spd1*Δ

In this study *arp42*Δ was identified as DSB sensitive consistent with the observations of Moss (2011). This DSB sensitivity was partially suppressed by deletion of *spd1*Δ independently of an effect on Cdt2 (Figure 3.14, Figure 3.18 and Figure 3.19). The DSB sensitivity of *arp42*Δ was also associated with a dramatic switch in repair pathway choice from GC to NHEJ/SCC. This was also partially suppressed by *spd1*Δ (Figure 3.20 and Figure 3.21.F). In future studies it would be important to confirm whether this outcome is due to NHEJ, SCC or reduced DSB induction and whether it is an artefact of an altered cell cycle. Arp42 may be involved in DNA damage-induced nucleotide synthesis as dCTP levels were reduced compared to wild-type in an *arp42*Δ background. However the same was not observed for the other dNTPs.

Arp42 is a member of the *S. pombe* SWI/SNF and RSC nucleosome remodelling complexes involved in transcription. Deletion of *arp42*$^{+}$ showed that the protein is not required for formation of the complexes but is important for the complexes function under stress conditions (Monahan *et al.*, 2008). Components of the *S. cerevisiae* RSC have been shown to be required for nucleosome sliding at DSB to promote both resection and NHEJ but were not required for transcription of RNR subunits (Chambers *et al.*, 2012; Liang *et al.*, 2007). In *S. cerevisiae* the RSC also promotes HO accessibility to *MATa* which may have implications for the DSB assay (Kent *et al.*, 2007). SWI/SNF-dependent remodelling at the break site has also been shown to be important for HR (Chai *et al.*, 2005).

3.3.6 The DSB sensitivity of *trm112*Δ was suppressed by deletion of *spd1*$^{+}$

In this study *trm112*Δ was confirmed to be mildly sensitive to DSBs, consistent with prior observations (Deshpande *et al.*, 2009; Moss, 2011). This DSB sensitivity was partially suppressed by *spd1*Δ (Figure 3.14). *trm112*Δ was found to have impaired Cdt2-YFP induction in response to DSB (Figure 3.18 and Figure 3.19) which is required for Spd1 degradation (Liu *et al.*, 2003). These results suggested a role for Trm112 in facilitating efficient DSB repair by damage-induced nucleotide synthesis. However *trm112*Δ did not have reduced nucleotide pools compared to wild-type (Figure 3.23) and was able to efficiently repair a single targeted DSBs by HR (Figure 3.21.B).

Trm112 is evolutionarily conserved (Heurgue-Hamard *et al.*, 2006; Purushothaman *et al.*, 2005) and studies in *S. cerevisiae* have shown Trm112 to be required for the activity of methyltransferase proteins involved in many aspects of translation. In *S. cerevisiae* Trm112 transiently binds and stabilises the methyltransferase Bud23 required for 40S ribosomal subunit biogenesis. This loss of interaction is responsible for most of the *trm112*Δ growth defect (Figaro *et al.*, 2012; Sardana and Johnson, 2012; White *et al.*, 2008). Trm112 also interacts with the methyltransferases Nop2 and Rcm1 resulting in smaller effects on large (60S) ribosomal subunit biogenesis (Sardana and Johnson, 2012). In addition Trm112 binds and stabilises the methyltransferase Mtq2, allowing methylation of a conserved GCQ motif of eRF1 protein termination factor (Heurgue-Hamard *et al.*, 2005; Heurgue-Hamard *et al.*, 2006). These interactions would have global effects on translation.

S. cerevisiae Trm112 also plays a direct role in DNA damage-induced nucleotide synthesis through its requirement for Trm9 methyltransferase activity (Mazauric *et al.*, 2010). *trm9*Δ is sensitive to DNA damage (Begley *et al.*, 2002; Bennett *et al.*, 2001). Trm9 methylates the wobble base position of arginine and glutamic acid tRNA to enhance the translation of mRNA

transcripts over-represented with specific arginine and glutamic acid codons (Begley *et al.*, 2007; Kalhor and Clarke, 2003). Bioinformatic sequence analysis found that many DDR genes are enriched with these codons including the RNR subunits Rnr1 and Rnr3 which have reduced protein levels in a *trm9*Δ strain. The DNA damage sensitivity of *trm9*Δ can be suppressed by promoting nucleotide synthesis by either overexpressing Rnr1 or by deleting the RNR inhibitor Sml1 (Begley *et al.*, 2007; Patil *et al.*, 2012).

The elevated nucleotide pools in an *S. pombe trm112*Δ suggest that any effect of Trm112 on RNR translation is not functionally relevant. As *trm112*Δ reduced Cdt2 induction it would be interesting to investigate whether Trm112 promotes DSB survival either through global effects on translation or a targeted response. Subtle effects on translation may only compromise HR when multiple DSBs are induced, for example by in bleocin treatment.

A conserved role for Trm112 in the DDR is supported by evidence in humans. The human homologue of Trm9 (ALKBH8), which coimmunoprecipitates with the human homologue of Trm112 (HSPC152), possesses methyltransferase activity and catalyses the final steps of tRNA wobble base modification (Fu *et al.*, 2010; van den Born *et al.*, 2011). ALKBH8 is up-regulated in response to DNA damage in an ATM-dependent manner and improves the survival of bleomycin and MMS treatment (Fu *et al.*, 2010). ALKBH8 is overexpressed in bladder cancer and is associated with invasion and disease progression (Shimada *et al.*, 2009).

3.3.7 The DSB sensitivity of *liz1*Δ was suppressed by deletion of *spd1*$^{+}$

Liz1 is an active plasma membrane transporter of the vitamin pantothenate, a coenzyme A (CoA) precursor required for fatty acid biosynthesis. *liz1*Δ was included in the screen as Deshpande *et al.* (2009) found it to be sensitive to the RNR inhibitor HU, consistent with the observations of Moynihan and Enoch (1999). In this study *liz1*Δ was also confirmed to be sensitive to bleocin. The bleocin sensitivity of *liz1*Δ was partially suppressed *spd1*Δ (Figure 3.14). However deletion of *liz1*$^{+}$ did not affect Cdt2 expression or reduce nucleotide pools (Figure 3.18, Figure 3.19 and Figure 3.23).

Stolz et al. (2004) found that, in the presence of HU, *liz1*Δ shows slow growth and aberrant mitosis independently of an effect on DNA replication or the checkpoint. These phenotypes can be rescued by the addition of pantothenate. In the absence of *liz1*$^{+}$ pantothenate must be synthesised from uracil. Uracil is also a nucleotide precursor and cells are unable to synthesise sufficient uracil to support both pathways. A model was proposed where, in the absence of RNR activity, the concentrations of its substrates CTP and UTP increase. This inhibits uracil synthesis via a negative feedback mechanism and, in turn, also inhibits pantothenate synthesis. (Han *et al.*, 2010; Stolz *et al.*, 2004).

Although *spd1*Δ would be predicted to promote RNR activity and have the opposite effect on uracil synthesis, this is difficult to reconcile with suppression of the DSB sensitivity of the independent *liz1*Δ strain by *spd1*Δ as these strains were auxotrophic and uracil was provided in the media. The DSB assay profile of *liz1*Δ showed significantly decreased GC compared to wild-type which could be suppressed by *spd1*Δ (Figure 3.20 and Figure 3.21.D).

3.3.8 The DSB sensitivity of *pmk1*Δ was suppressed by deletion of *spd1*$^+$

*pmk1*Δ was included in the screen as Deshpande et al. (2009) identified it as sensitive to CPT and HU. In this study *pmk1*Δ was also confirmed to be sensitive to bleocin and this sensitivity was suppressed by *spd1*Δ (Figure 3.14). Pmk1 is the MAPK in the cell integrity MAPK pathway activated in response to cell wall stress, osmotic stress, oxidative stress and glucose deprivation, allowing cell adaptation (Madrid *et al.*, 2006; Toda *et al.*, 1996; Zaitsevskaya-Carter and Cooper, 1997). Broadus and Gould (2012) found that, in addition to the checkpoint machinery, Pmk1 contributes to relocalisation of Clp1 from the nucleolus to the nucleoplasm for cell cycle arrest following genotoxic stress with H_2O_2.

It is predicted that *pmk1*Δ is sensitive to bleocin as it helps protect the cell from genotoxic and oxidative damage. Consistent with a role independent from DNA repair a *pmk1*Δ strain was able to efficiently repair single induced DSB by HR (Figure 3.20 and Figure 3.21.A). Therefore *spd1*Δ may suppress *pmk1*Δ DSB sensitivity through a mechanism independent of up-regulating nucleotide synthesis to allow efficient HR (Fleck *et al.*, 2013). However the levels of dCTPs were reduced in a *pmk1*Δ background compared to wild-type both in untreated cells and in response to DSBs (Figure 3.22).

3.3.9 The DSB sensitivity of *swi3*Δ was suppressed by deletion of *spd1*$^+$

Swi3 and Swi1 together form the conserved replication fork protection complex (Gotter *et al.*, 2007; Noguchi *et al.*, 2004). Swi1 associates with chromatin during S phase through its DDT domain, recruits Swi3 and travels with the replication fork (Noguchi *et al.*, 2012; Noguchi *et al.*, 2004). The complex is important for the stabilisation of stalled replication forks through recruitment of replication checkpoint mediator Mrc1 to chromatin and activation of the replication checkpoint effector Cds1 (Noguchi *et al.*, 2003; Noguchi *et al.*, 2004; Shimmoto *et*

al., 2009; Tanaka *et al.*, 2010). In the absence of functional Swi3-Swi1 lesions associated with collapsed replication forks accumulate (Noguchi *et al.*, 2003; Noguchi *et al.*, 2004).

In this study *swi3*Δ was identified as bleocin sensitive (Figure 3.14). DNA damage during S phase would be predicted to have catastrophic effects in a *swi3*Δ background as the DNA replication checkpoint cannot be activated (Noguchi *et al.*, 2003; Noguchi *et al.*, 2004; Shimmoto *et al.*, 2009; Tanaka *et al.*, 2010). The high levels of Cdt2 foci observed even in the absence of DNA damage are predicted to be caused by an accumulation of DNA lesions associated with collapsed replication forks (Figure 3.18 and Figure 3.19.A-B). *spd1*Δ partially suppressed the DSB sensitivity of a *swi3*Δ and this was associated with a decrease in LOH resulting from failed HR (Figure 3.14, Figure 3.21.G). Nucleotide pools were elevated in a *swi3*Δ background, suggesting that *spd1*Δ may be acting through a different mechanism (Figure 3.23.A-B). A role has been identified for Spd1 in promoting replication stress independently of RNR regulation (Fleck *et al.*, 2013). It should also be confirmed whether the elevated nucleotide pools were caused by a high proportion of S phase cells.

3.3.10 Other candidates

The DSB sensitivity of *trt1*Δ, *vps16*Δ and V2-53D9 could be suppressed by deleting *spd1*Δ (Figure 3.14). However nucleotide pools were not reduced in these backgrounds (Figure 3.23). In V2-53D9 the DSB sensitivity was associated with a switch in repair pathway choice from GC to NHEJ, which could also be suppressed by *spd1*Δ (Figure 3.20 and Figure 3.21.E). However it would be important to confirm this is not due to reduced DSB induction or an altered cell cycle. V2-53D9 was found to contain a deletion of $nup132^{+}$. The strain identity requires further analysis as a second *nup132*Δ strain was not DSB sensitive (Figure 3.12). Nup132 is a component of the *S. pombe* nuclear pore complex (Asakawa *et al.*, 2014). The nuclear pore has been implicated in DSB repair in *S. cerevisiae* (Horigome *et al.*, 2014).

The DSB sensitivity of *atp2*Δ was suppressed by *spd1*Δ (Figure 3.14). *atp2*Δ had reduced DNA damage-induced levels of dCTP but not other nucleotides compared to wild-type (Figure 3.22). *rpp202*Δ was not DSB sensitive however *spd1*Δ further increased strain fitness (Figure 3.14). Damage-induced nucleotide levels were reduced compared to wild-type (Figure 3.22). In a future study it would be interesting to investigate DSB repair in these backgrounds.

3.4 SUMMARY

In this chapter a quantitative, colony-based screen was performed to identify *S. pombe* gene deletion strains whose DSB sensitivity was suppressed by deleting the RNR inhibitor *spd1*$^{+}$. This was predicted to identify genes important for HR through roles in damage-induced nucleotide synthesis.

- The top 29 candidate deletion strains showing suppression of DSB sensitivity following *spd1*$^{+}$ deletion were selected for validation.
- The top candidates included *ddb1*Δ, *cdt2*Δ, *rad3*Δ and *csn1*Δ which have known roles in damage-induced nucleotide synthesis.
- The validation and further study of 4 DNA damage checkpoint deletion strains: *rad3*Δ, *rad26*Δ, *rad9*Δ and *rad1*Δ are presented in Chapter 4.
- The validation and further study of *ngg1*Δ are presented in Chapter 5.
- 11 other candidates showed repeatable suppression of DSB sensitivity following *spd1*$^{+}$ deletion. These candidates did not show reduced nucleotide levels associated with a defect in HR. This suggests deleting Spd1 may also suppress DSB sensitivity by a different mechanism.

Chapter 4 A role for the DNA damage checkpoint promoting nucleotide synthesis and DSB resection

4.1 INTRODUCTION

The DNA damage checkpoint is important for many aspects of the DDR. In *S. pombe* Rad3 promotes the nucleotide synthesis required for efficient DSB repair by HR. In response to DNA damage Rad3 activates the Ddb-Cul4^{Cdt2} complex which ubiquitinates Spd1. This signals Spd1 for proteasome degradation and promotes RNR activity (Liu *et al.*, 2005; Moss *et al.*, 2010). Rad3 is recruited to sites of DNA damage by Rad26 (Edwards *et al.*, 1999; Zou and Elledge, 2003). The screen presented in Chapter 3 identified *rad3*Δ and *rad26*Δ, amongst the top candidates exhibiting suppression of DSB sensitivity when *spd1*$^{+}$ was deleted.

Rad9 and Rad1 together with Hus1 form the 9-1-1 checkpoint complex recruited to DNA damage by Rad17-RFC (Bermudez *et al.*, 2003; Lindsey-Boltz *et al.*, 2001). *rad17*Δ and *hus1*Δ were not identified as top candidates exhibiting suppression of DSB sensitivity when *spd1*$^{+}$ was deleted, although *rad1*Δ was marginally included in this group (Figure 3.8). To assess the DSB dependence of any suppression conferred by *spd1*Δ the ratios of *sens*Δ *spd1*Δ to *sens*Δ colony size under control and bleocin conditions were compared (Figure 3.5). *rad17*Δ, *rad1*Δ, and *hus1*Δ clustered close to the line of best fit. In contrast *rad9*Δ was identified in the screen as a top candidate with similar levels of suppression of DSB sensitivity by *spd1*Δ as *rad3*Δ and *rad26*Δ (Figure 3.7 and Figure 3.8).

The aim of this chapter was to investigate the role of the DNA damage checkpoint in damage-induced nucleotide synthesis and HR. Some data presented in this chapter has recently been published in Blaikley *et al.* (2014) as indicated in the figure legends. All work presented in this chapter was carried out by Elizabeth Blaikley except where indicated.

4.2 RESULTS

4.2.1 Deletion of *spd1*$^{+}$ suppresses the DSB sensitivity of *rad3*Δ and *rad26*Δ but not 9-1-1 complex gene deletion strains

To confirm whether *spd1*Δ could suppress the DSB sensitivity of the other checkpoint genes, the deletion strains were subjected to a serial dilution assay. Auxotrophic strains were used in this study as background markers can affect bleocin sensitivity (Figure 3.16). *spd1*Δ partially suppressed the bleocin sensitivity of *rad3*Δ and *rad26*Δ (Figure 4.1). However, *spd1*Δ could not suppress the bleocin sensitivity of *rad17*Δ, *rad9*Δ, *rad1*Δ or *hus1*Δ (Figure 4.1). Since the V2 deletion library is known to have erroneous strains (Figure 3.10 to Figure 3.12), the validity of each checkpoint strain was confirmed by PCR (Figure 4.2).

4.2.2 Deletion of *spd1*$^{+}$ suppresses the HR defect of *rad3*Δ and *rad26*Δ

A DSB assay has previously been used to demonstrate that the HR defect of a *rad3*Δ strain was partially suppressed by *spd1*Δ Moss *et al.* (2010). These results were confirmed (Figure 4.3). As expected, *rad3*Δ had significantly reduced GC (17.0%, $p < 0.01$) and significantly increased Ch^{16} loss (45.2%, $p < 0.01$), LOH (29.9%, $p = 0.01$), and NHEJ/SCC (7.7%, $p = 0.01$) compared to wild-type. This HR defect was partially suppressed by *spd1*Δ. *rad3*Δ *spd1*Δ showed significantly increased GC (36.8%, $p < 0.01$) and significantly decreased LOH (20.6%, $p = 0.05$) and NHEJ/SCC (1.8% $p < 0.01$) compared to *rad3*Δ. Levels of Ch^{16} loss were also reduced but not significantly (38.4%, $p = 0.18$).

Figure 4.1

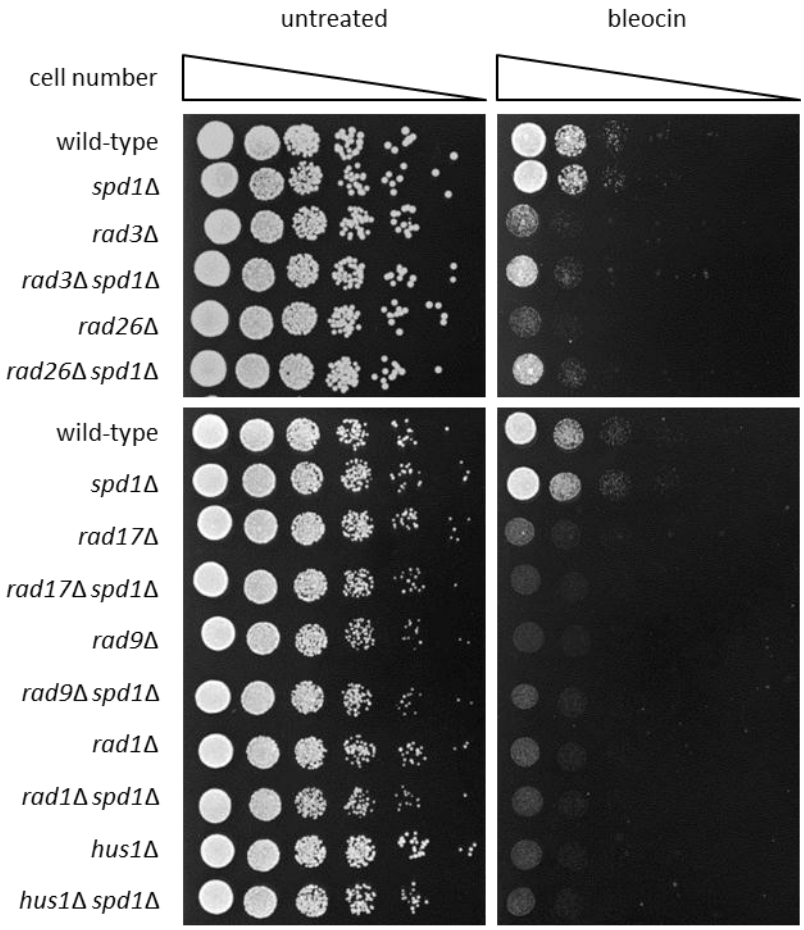


Figure 4.1 Deletion of *spd1*$^{+}$ suppresses the DSB sensitivity of *rad3*Δ and *rad26*Δ but not 9-1-1 gene deletion strains

(A) Fivefold serial dilutions of auxotrophic wild-type, *spd1*Δ, *rad3*Δ, *rad3*Δ *spd1*Δ, *rad26*Δ and *rad26*Δ *spd1*Δ spotted onto YE6S (untreated) and YE6S + 0.2 μg/ml bleocin.

(B) Fivefold serial dilutions of auxotrophic wild-type, *spd1*Δ, *rad17*Δ, *rad17*Δ *spd1*Δ, *rad9*Δ, *rad9*Δ *spd1*Δ, *rad1*Δ, *rad1*Δ *spd1*Δ, *hus1*Δ and *hus1*Δ *spd1*Δ spotted onto YE6S (untreated) and YE6S + 0.2 μg/ml bleocin

The data presented in this figure was published in Blaikley *et al.* (2014).

Figure 4.2

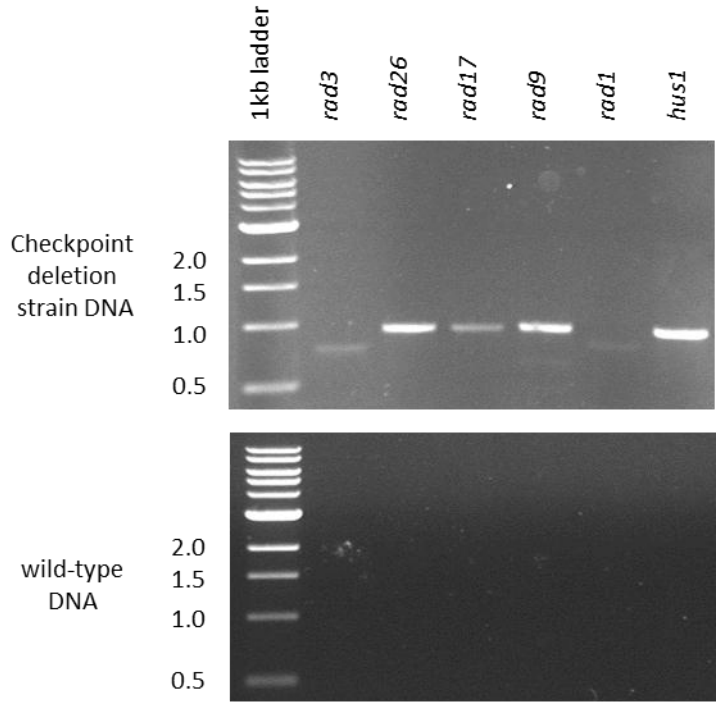


Figure 4.2 The identity of the checkpoint deletion strains was confirmed

PCR was performed using a forward primer specific to the sequence upstream of the gene deletion (primer A, Figure 3.1) and a reverse primer specific to the gene deletion cassette (primer 254, Figure 3.1). The detection of a band when deletion strain DNA was used as a template and the absence when wild-type DNA was used confirms gene deletion.

Figure 4.3

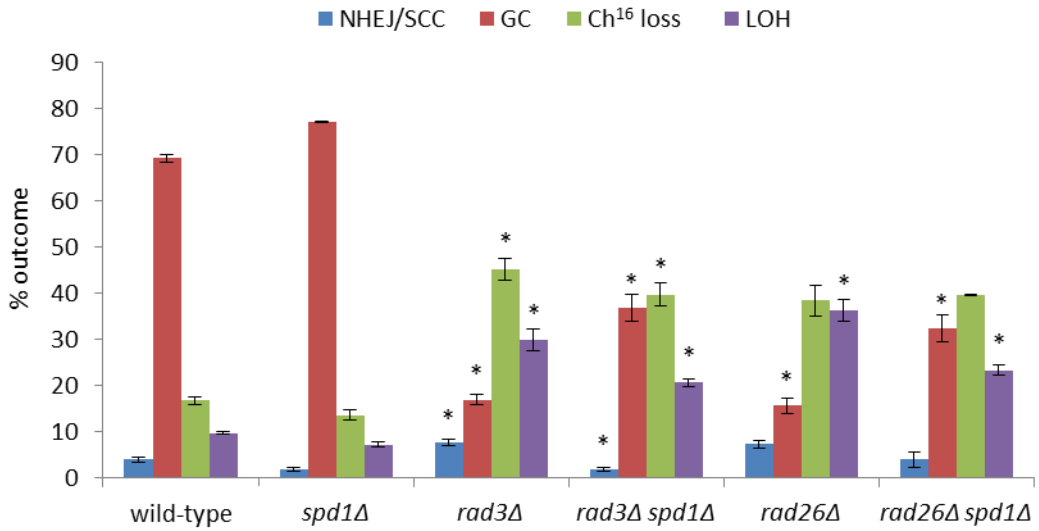


Figure 4.3 Deletion of *spd1*$^{+}$ suppresses the HR defect of *rad3*Δ and *rad26*Δ

DSB assay analysis of wild-type, *spd1*Δ, *rad3*Δ, *rad3*Δ *spd1*Δ, *rad26*Δ and *rad26*Δ *spd1*Δ. The percentage NHEJ/SCC, GC, LOH and Ch^{16} loss events are shown. Mean values ± standard errors are presented for three independent repeats. Asterisk (*****) represents a significant difference between the *checkpoint*Δ and corresponding *checkpoint*Δ *spd1*Δ. Some of the data presented in this figure was published in Blaikley *et al.* (2014)

The HR defect of *rad26*Δ could also be suppressed by *spd1*Δ (Figure 4.3). The repair profile of *rad26*Δ showed no significant difference with that of *rad3*Δ. *rad26*Δ had significantly reduced GC (15.6%, $p < 0.01$) and significantly increased Ch^{16} loss (38.4%, $p = 0.02$), LOH (36.3%, $p = 0.01$), and NHEJ/SCC (7.4% $p = 0.03$) compared to wild-type. Deletion of $spd1^+$ in a *rad26*Δ background resulted in a significant increase in GC (32.4% $p = 0.02$) and a reduction in LOH (23.4%, $p = 0.75$) compared to *rad26*Δ alone. There were no significant changes in Ch^{16} loss (39.6%, $p = 0.02$) or NHEJ/SCC (4.0% $p = 0.17$) compared to *rad26*Δ. These results support a role for Rad3 and Rad26 in facilitating efficient HR by promoting nucleotide synthesis.

4.2.3 Deletion of $spd1^+$ cannot suppresses the HR defect of the 9-1-1 complex gene deletion strains

*rad17*Δ, *rad9*Δ, *rad1*Δ and *hus1*Δ strains have a unique DSB repair profile compared to other deletion strains with defective HR (Moss, 2011). For the purpose of this study this was confirmed (Figure 4.4). GC was significantly reduced for *rad17*Δ (32.3%, $p < 0.01$), *rad9*Δ (34.7%, $p < 0.01$), *rad1*Δ (41.1%, $p < 0.01$) and *hus1*Δ (38.1%, $p = 0.01$) compared to wild-type. Notably Ch^{16} loss was also significantly reduced for *rad17*Δ (1.3%, $p < 0.01$), *rad9*Δ (1.0%, $p < 0.01$), *rad1*Δ (0.2%, $p < 0.01$) and *hus1*Δ (1.4%, $p < 0.01$) compared to wild-type. In contrast LOH was greatly increased for *rad17*Δ (61.2%, $p < 0.01$), *rad9*Δ (57.4%, $p < 0.01$), *rad1*Δ (54.8%, $p = 0.01$) and *hus1*Δ (56.6%, $p < 0.01$) compared to wild-type. No significant changes in the levels of NHEJ/SCC were observed.

Figure 4.4

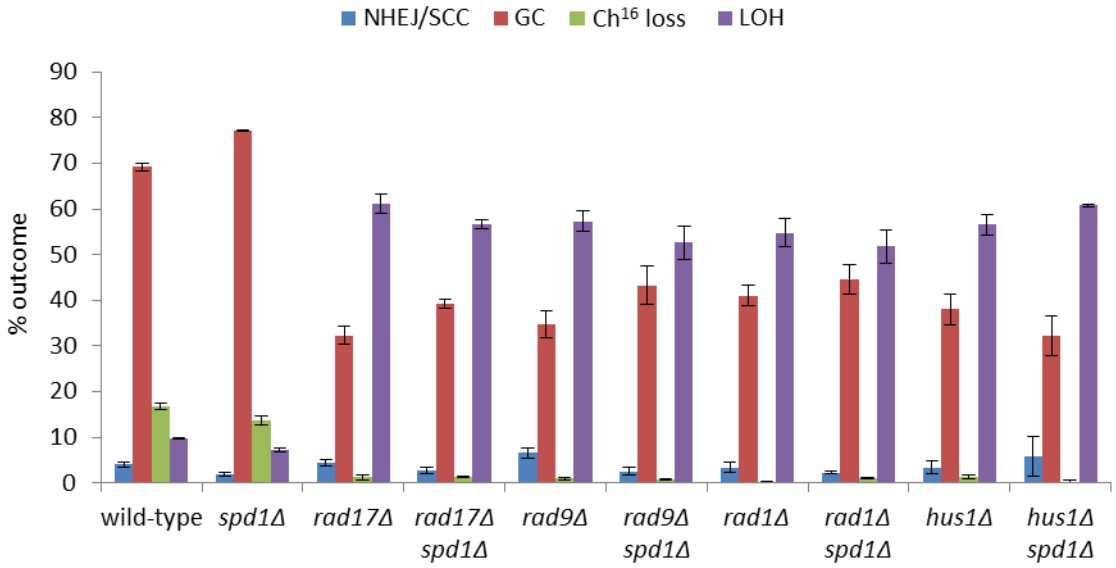


Figure 4.4 Deletion of *spd1*$^{+}$ cannot suppress the HR defect of 9-1-1 complex gene deletion strains

DSB assay analysis of wild-type, *spd1*Δ, *rad17*Δ, *rad17*Δ *spd1*Δ, *rad9*Δ, *rad9*Δ *spd1*Δ, *rad1*Δ, *rad1*Δ *spd1*Δ, *hus1*Δ and *hus1*Δ *spd1*Δ. The percentage NHEJ/SCC, GC, LOH and Ch^{16} loss events are shown. Mean values ± standard errors are presented for three independent repeats. Some of the data presented in this figure was published in Blaikley *et al.* (2014)

Deletion of *spd1*$^{+}$ could not suppress the HR defect or increased LOH observed for *rad17*Δ, *rad9*Δ, *rad1*Δ and *hus1*Δ (Figure 4.4). No significant change was observed in the levels of GC for *rad17*Δ *spd1*Δ (39.2%, p = 0.22), *rad9*Δ *spd1*Δ (43.3%, p = 0.18), *rad1*Δ *spd1*Δ (44.6%, p = 0.43) and *hus1*Δ *spd1*Δ (32.2%, p = 0.36) compared to the parental checkpoint deletion strains. No significant change was observed in the levels of Ch^{16} loss for *rad17*Δ *spd1*Δ (1.13%, p = 0.99), *rad9*Δ *spd1*Δ (0.75%, p = 0.53), *rad1*Δ *spd1*Δ (1.02%, p = 0.10) and *hus1*Δ *spd1*Δ (0.02%, p = 0.15) compared to the parental checkpoint deletion strains. In addition no significant change was observed in the high levels of LOH observed for *rad17*Δ *spd1*Δ (56.63%, p = 0.21), *rad9*Δ *spd1*Δ (52.69%, p = 0.35), *rad1*Δ *spd1*Δ (51.81%, p = 0.57) and *hus1*Δ *spd1*Δ (60.84% $P < 0.21$) compared to the parental checkpoint deletion strains.

4.2.4 The DNA damage checkpoint is required for DSB-induced accumulation of Cdt2

Rad3 activates Ddb-Cul4^{Cdt2} in response to DSBs by inducing expression of Cdt2 which recruits Spd1 for ubiquitination (Liu *et al.*, 2005; Moss *et al.*, 2010). As the HR defect of 9-1-1 complex deletion strains could not be suppressed by *spd1*Δ, it was investigated whether the DNA damage checkpoint in general was required for DSB-induced Cdt2 accumulation.

As for *rad3*Δ, no significant DSB-induced nuclear accumulation of Cdt2-YFP was observed for the other checkpoint gene deletion strains by fluorescence microscopy (Figure 4.5.A-B). In the absence of exogenous DNA damage a significantly reduced percentage of *rad26*Δ (1.3%, p = 0.02), *rad9*Δ (0.0%, p = 0.00) and *rad1*Δ (0.7%, p = 0.01) cells had visible nuclear Cdt2-YFP compared to wild-type (7.2%). A percentage of Cdt2-YFP positive nuclei comparable to wild-type was observed for *rad17*Δ (4.0%, p = 0.42) and *hus1*Δ (3.9%, p = 0.14). In response to bleocin treatment no significant increase in the percentage of Cdt2-YFP positive nuclei was detected for *rad26*Δ (4.4%, p = 0.13), *rad17*Δ (1.7%, p = 0.54), *rad9*Δ (1.7%, p = 0.19), *rad1*Δ (2.6%, p = 0.23) or *hus1*Δ (2.4%, p = 0.54) compared to untreated.

Figure 4.5

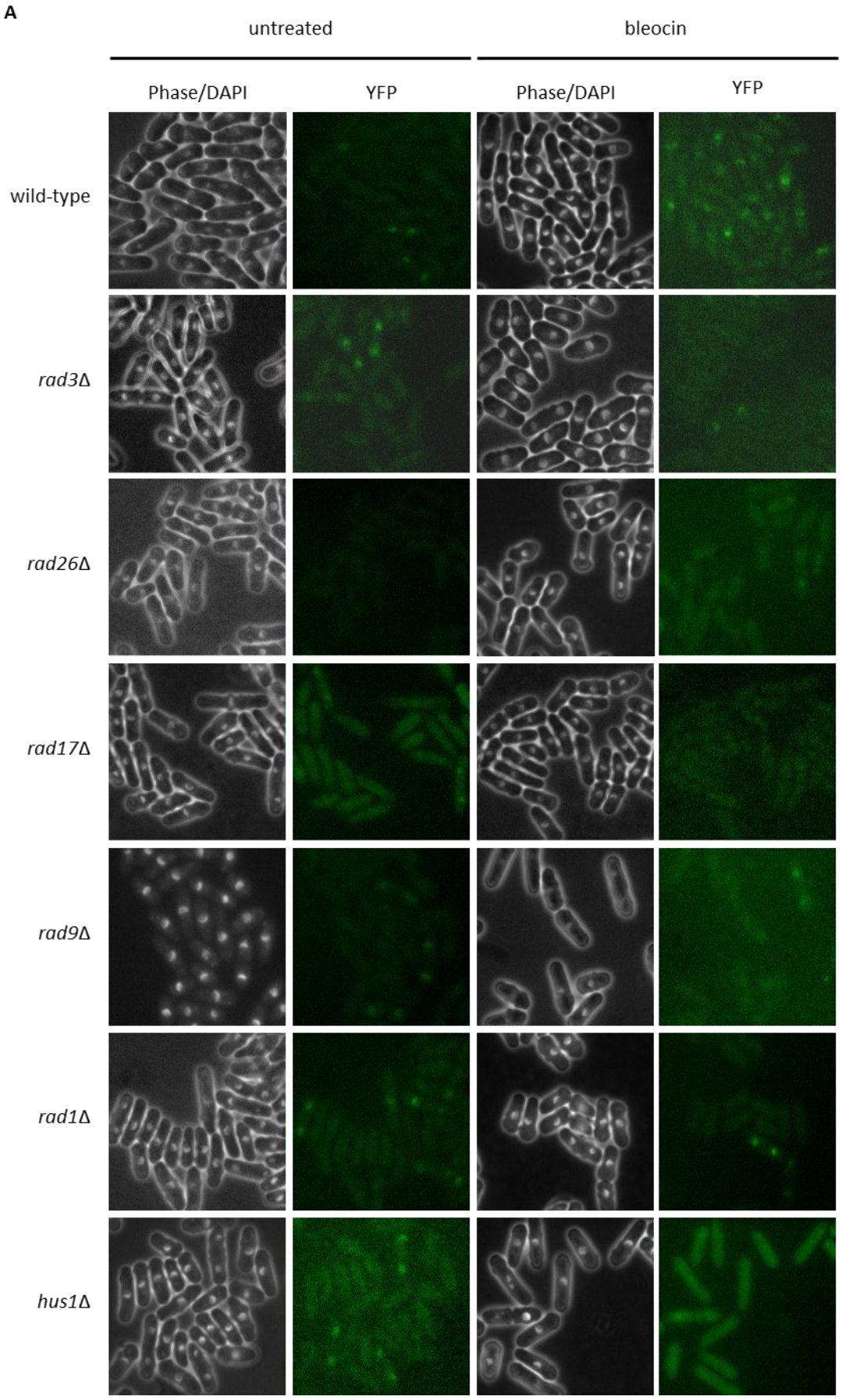

A
untreated
bleocin
Phase/DAPI
YFP
Phase/DAPI
YFP
wild-type
rad3Δ
rad26Δ
rad17Δ
rad9Δ
rad1Δ
hus1Δ

Figure 4.5 continued

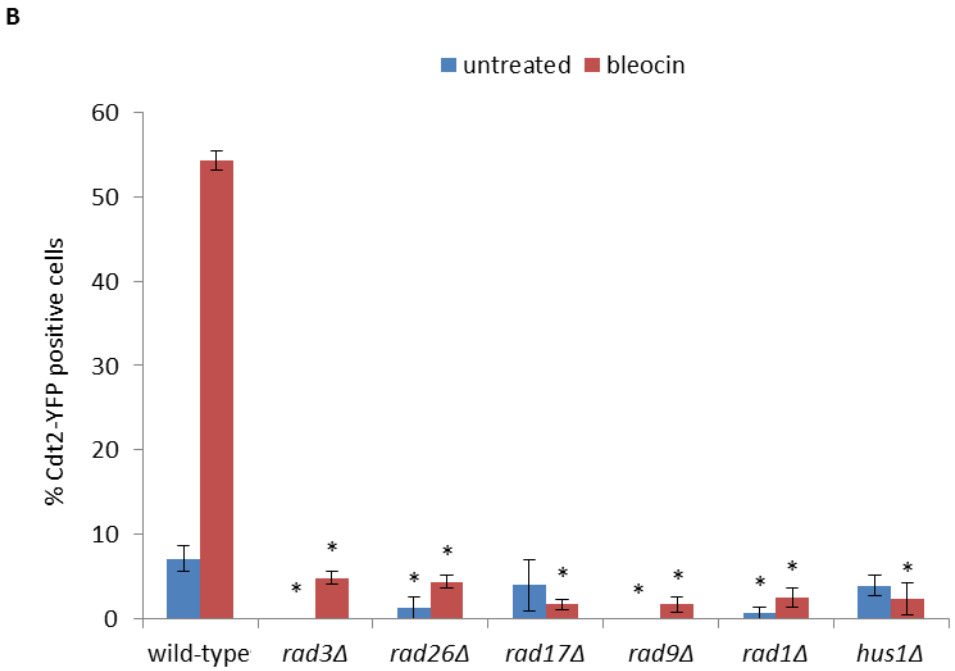


Figure 4.5 Checkpoint deletion strains did not show DSB-induced nuclear accumulation of Cdt2-YFP

(A) Methanol fixed asynchronous Cdt2-YFP wild-type, *rad3*Δ, *rad26*Δ, *rad17*Δ, *rad9*Δ, *rad1*Δ and *hus1*Δ cells grown in YE6S (untreated) or YE6S + 1 µg/ml bleocin for 1 hour. 100× Phase-DAPI and YFP fluorescence microscopy images are shown.

(B) Quantitation of the percentage mononuclear cells observed in (A) with a nuclear Cdt2-YFP accumulation. A Approximately 100 cells per sample were scored. Mean scores ± standard errors are shown for three independent repeats.

The data presented in this figure was published in Blaikley *et al.* (2014).

4.2.5 A role for the 9-1-1 complex in DSB resection

The results presented suggest that whilst Rad3, Rad26 and the 9-1-1 complex all are important for DNA damage-induced nucleotide synthesis, the 9-1-1 complex also has an additional function in HR which cannot be suppressed by deleting *spd1*$^{+}$ to increase nucleotide pools. The role of the DNA damage checkpoint in regulating DSB resection was investigated using a SSA assay developed by Watson et al (2011) (Figure 4.6).

The SSA construct was integrated onto chromosome I and incorporated a *his3* gene containing a HO-endonuclease cut-site. Cleavage of the cut-site generates a DSB resulting in histidine auxotrophy. Subsequent DSB resection is required to uncover 500 base pairs of homology in two truncated *LEU2* genes allowing repair by SSA. To assess the time taken for SSA to occur, HO-endonuclease was expressed from the *urg1* promoter at the *urg1* locus allowing rapid and robust DSB-induction upon the addition of uracil (Watson *et al.*, 2011).

Strains were grown overnight in EMM + L. This selected against premature DSB induction as cleavage of the HO cut-site within the *his3* gene caused histidine auxotrophy and cell death in this medium. Cells were resuspended in either EMM + LH (DSB-OFF) or EMM + LHU (DSB-ON) to induce DSBs. At intervals following HO induction genomic DNA was extracted, digested with *PvuI* and *NruI* and subjected to Southern blotting.

The membranes were hybridised with probe B to analyse the kinetics of repair by observing the loss of a 6.2 kb pre-SSA fragment and the appearance of a 3.1 kb band post SSA (Figure 4.7.A left and Figure 4.7.B). The intensity of the 6.2 kb and 3.1 kb bands was calculated as percentage of the total band intensity (sum of the 6.2 kb and 3.1 kb bands) for each lane.

Figure 4.6

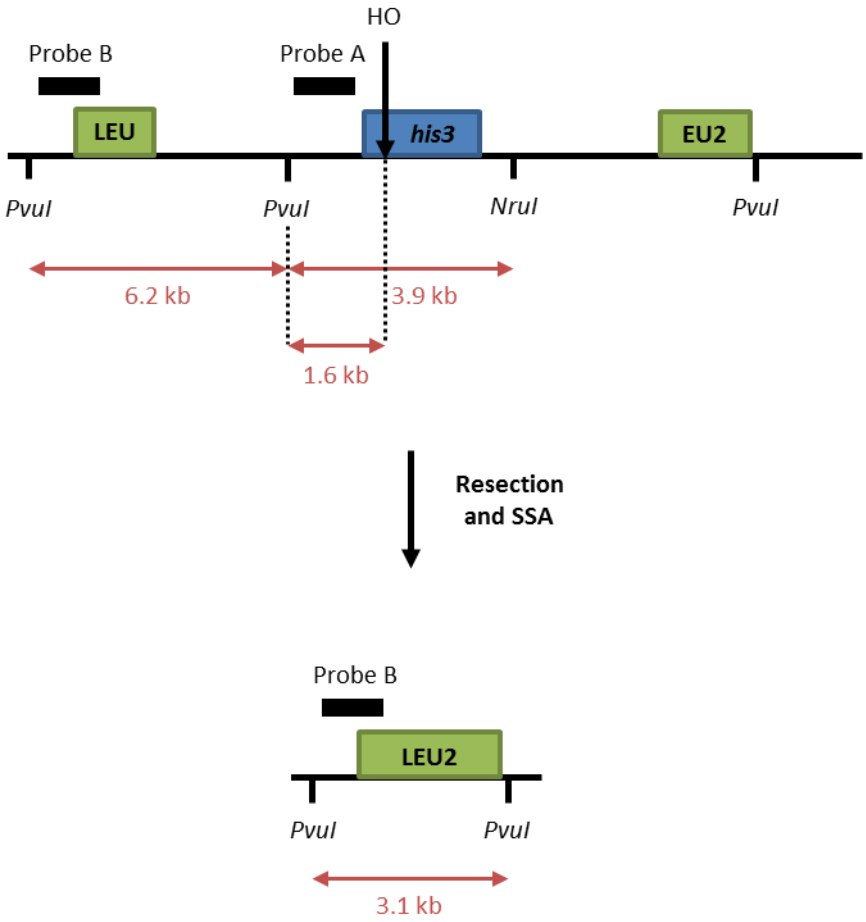


Figure 4.6 SSA assay

Schematic of the SSA assay described previously by Watson et al (2011). Cleavage of a HO recognition sequence at the start of the *his3* ORF leads to histidine auxotrophy. Resection of the DSB uncovers regions of homology in two truncated LEU2 genes. This allows SSA and loss of the intervening sequence. At intervals following HO induction genomic DNA is extracted, digested with *PvuI* and *NruI* (cleavage sites are indicated) and subjected to Southern blotting. The positions of probe A, to detect SSA, and probe B, to detect HO cleavage, are shown as are the lengths of the fragments detected pre and post-SSA.

Figure 4.7

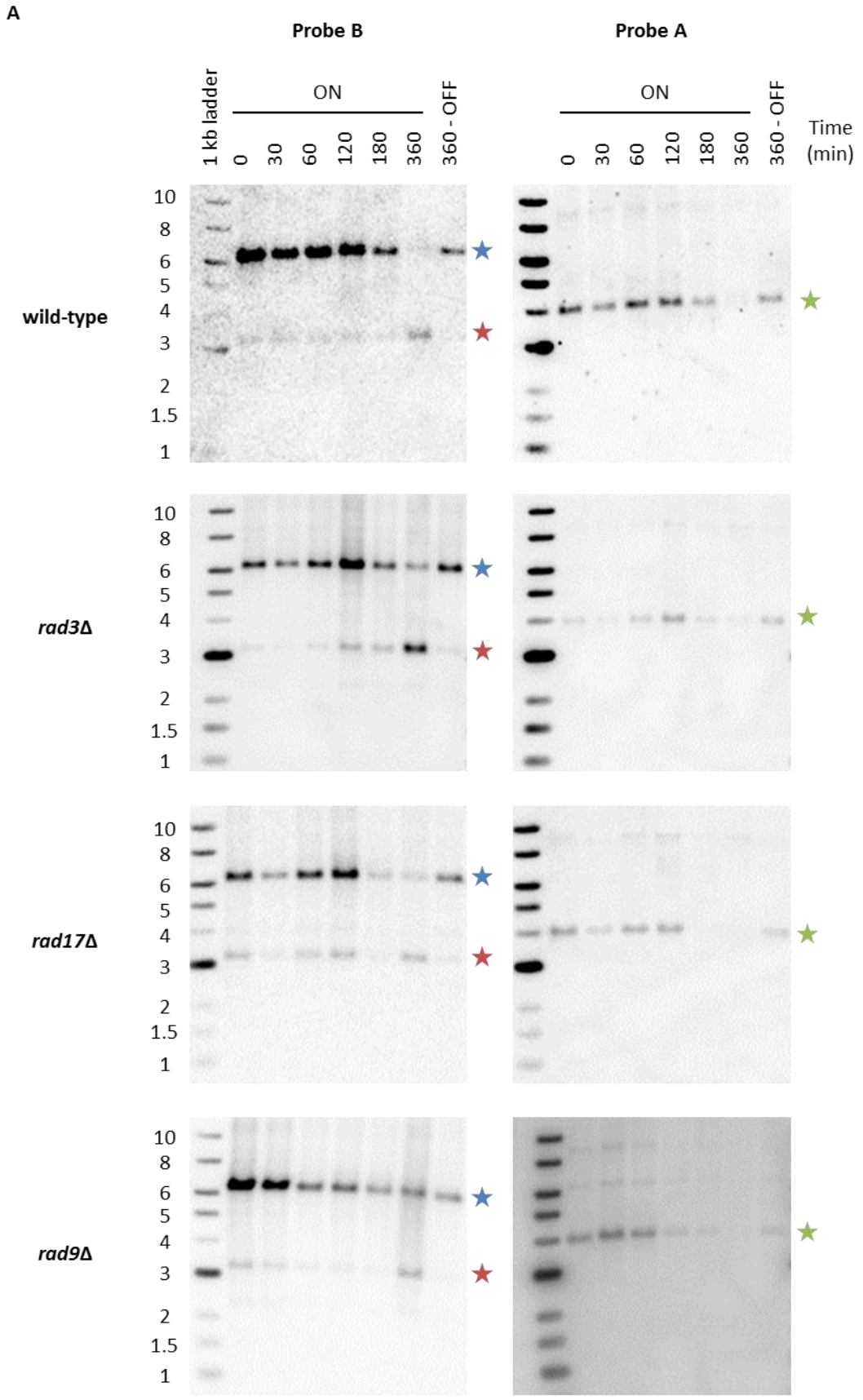
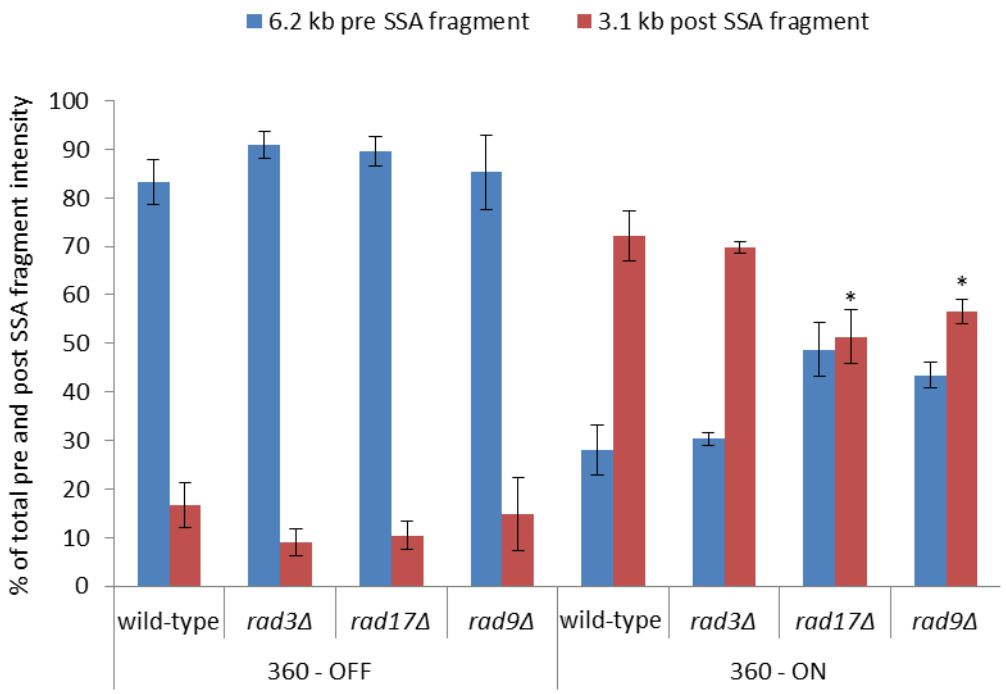

A
Probe B
Probe A
1 kb ladder
ON
ON
0
30
60
120
180
360
360 - OFF
0
30
60
120
180
360
360 - OFF
Time (min)
wild-type
rad3Δ
rad17Δ
rad9Δ
10
8
6
5
4
3
2
1.5
1

Figure 4.7 continued

B



C

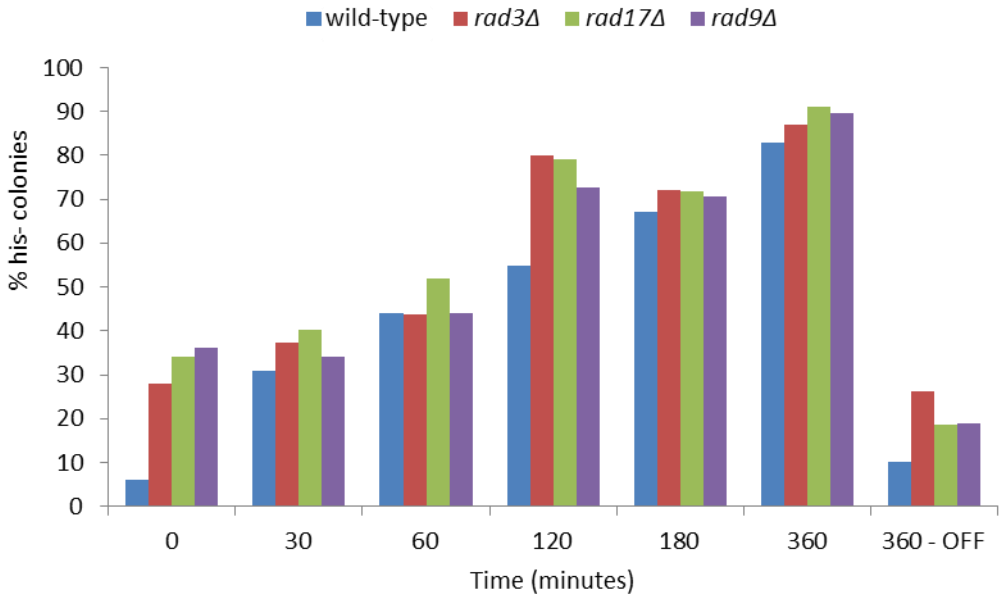


Figure 4.7 The 9-1-1 complex promotes DSB resection

(A) Southern Blot analysis of the SSA assay (Figure 4.6) for wild-type, *rad3*Δ, *rad17*Δ and *rad9*Δ strains. The membranes were hybridised with probe B (left) to detect a 6.2 kb pre-SSA fragment (blue) and a 3.1 kb post-SSA fragment (red). Probe A (right) was used to detect loss of a 3.9 kb fragment (green) following HO cleavage. 360 OFF refers to no HO induction.

(B) Quantification of Probe B band intensities at 360 minutes for wild-type, *rad3*Δ, *rad17*Δ and *rad9*Δ strains. Band intensities were quantified using Quantity One (Bio-rad) and normalised by calculating the intensities of 6.2 kb pre-SSA band and 3.1 kb post-SSA band as a percentage of the total for these bands at each time point. Mean values are presented for three independent repeats including the blots in (A). Error bars indicate ± standard error, asterisk (*****) represents a significant difference to wild-type.

(C) Colony assay observing loss of the *his3* marker following HO induction for wild-type, *rad3*Δ, *rad17*Δ and *rad9*Δ strains. The results shown correspond to the inductions analysed by Southern blotting in (A).

Some of the data presented in this figure was published in Blaikley *et al.* (2014). The radioactive steps of Southern blotting were carried out by Carol Walker (Department of Oncology, University of Oxford).

In a wild-type background, in the absence of DSB induction (360-OFF), 83.3% of the band intensity was attributed to the pre-SSA fragment and only 16.7% to the post SSA fragment, a result of leaky induction. There was no significant difference for the checkpoint mutants with the pre-SSA fragment contributing 90.9% for *rad3*Δ ($p = 0.22$), 89.6% for *rad17*Δ ($p = 0.30$) and 85.2% for *rad9*Δ ($p = 0.84$) (Figure 4.7.A left and Figure 4.7.B).

DSB induction for 360 minutes in a wild-type background (360-ON) resulted in almost complete loss of the pre-SSA fragment and formation of a strong post-SSA fragment band representing 72.1% of the total band intensity. No significant difference was observed in a *rad3*Δ background, with the post-SSA fragment representing 69.7% of the total band intensity ($p = 0.69$) (Figure 4.7.A left and Figure 4.7.B). This is consistent with both wild-type and *rad3*Δ strains performing efficient DSB resection and SSA.

In contrast, following DSB induction in a *rad17*Δ background for 360 minutes, a significantly weaker post-SSA band formed compared to wild-type representing 51.3% ($p = 0.04$) of the band intensity. The 360 minute post-SSA band was also reduced in a in a *rad9*Δ background representing 56.5% of the total band intensity ($p = 0.05$). (Figure 4.7.A left and Figure 4.7.B). This is consistent with reduced resection and SSA in *rad17*Δ and *rad9*Δ backgrounds.

Cleavage of the HO cut-site within the histidine gene caused histidine auxotrophy. DSB induction was followed using a colony assay to observe loss of the histidine marker. The assay was performed using cells collected at the same time as the samples subjected to Southern blotting. Wild-type, *rad3*Δ, *rad17*Δ and *rad9*Δ strains showed similar kinetics of DSB formation (Figure 4.7.C). At 180 minutes after adding of uracil roughly 70% of colonies had lost the histidine marker and by 360 minutes this reached 90%. In the absence of HO induction with uracil (360-OFF) only 10-20% loss of the histidine marker was observed.

To further confirm consistent DSB induction, the membranes were re-hybridised with probe A which detects a 3.9 kb fragment prior to its cleavage with HO (Figure 4.7.A, right). Following DSB induction in a wild-type background loss of the 3.9 kb fragment was observed between 180 and 360 minutes. However, the band was not lost in the absence of induction (360-OFF). A similar pattern was observed for *rad3*Δ, *rad17*Δ and *rad9*Δ.

4.2.6 Investigating the mechanism by which the checkpoint regulates resection

Tinline-Purvis (in Blaikley *et al.*, 2014) found the DSB assay profile of *rad3*Δ *rad17*Δ or *exo1*Δ *rad17*Δ to be epistatic with that of *rad17*Δ alone with low levels of GC and Ch^{16} loss coupled with dramatically increased levels of LOH compared to wild-type. Furthermore the DSB assay profile of *rad3*Δ *exo1*Δ was similar to that of *rad17*Δ. This suggested that Rad3 and Exo1 may function in the same pathway as Rad17 to prevent LOH. This was further investigated using the SSA assay (Figure 4.6) (Watson *et al.*, 2011).

The membranes were firstly hybridised with probe B to analyse the kinetics of repair (Figure 4.8.A left and Figure 4.8.B). In the absence of DSB induction (360-OFF), no significant difference to wild-type was observed in the percentage band intensity attributed to the pre-SSA fragment for either *exo1*Δ (94.5% $p = 0.09$) or *rad3*Δ *exo1*Δ (94.0% for $p = 0.10$). DSB induction (360-ON) in an *exo1*Δ background caused no significant change in the contribution of the pre-SSA fragment compared to 360-OFF (86.5% $p = 0.50$) indicating no detectable SSA had occurred. In contrast, following DSB induction (360-ON) in a *rad3*Δ *exo1*Δ the background, a weak but significantly increased post-SSA band was detected compared to 360-OFF in this background, representing 29.3% of the total band intensity ($p = 0.01$).

Figure 4.8

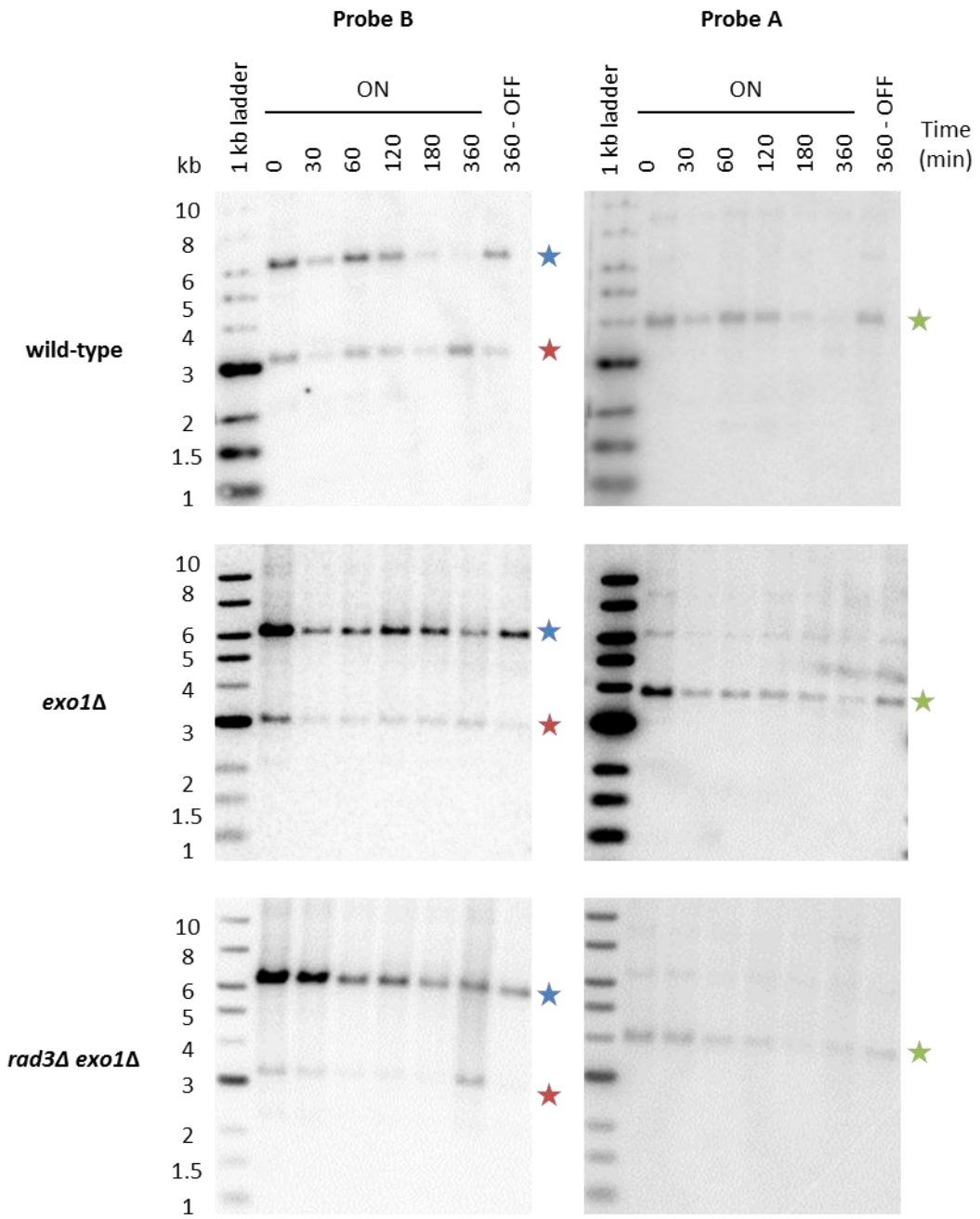

Probe B
Probe A
1 kb ladder
ON
0
30
60
120
180
360
360 - OFF
Time (min)
kb
10
8
6
5
4
3
2
1.5
1
wild-type
exo1Δ
rad3Δ exo1Δ

Figure 4.8

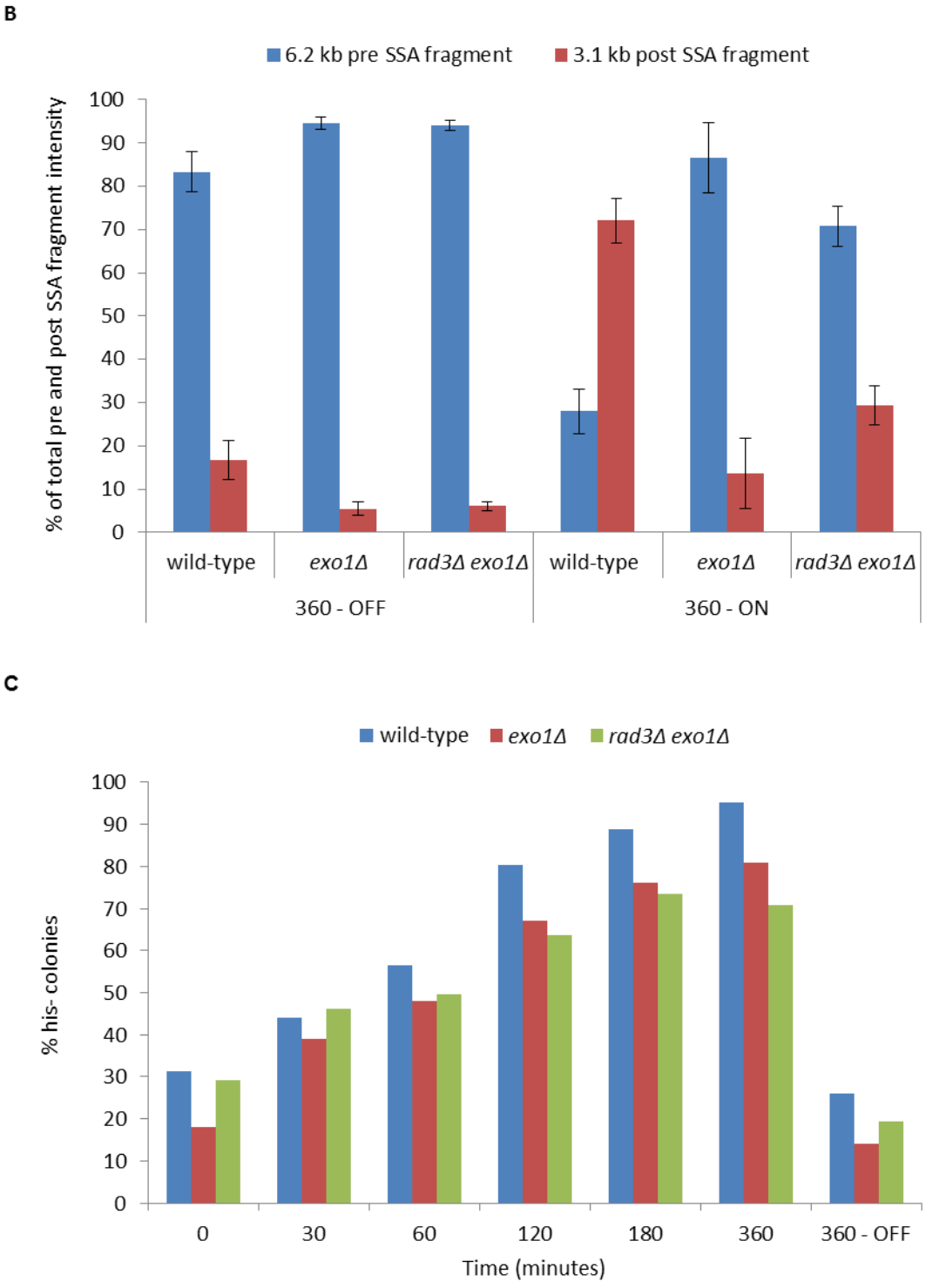

B
6.2 kb pre SSA fragment
3.1 kb post SSA fragment
% of total pre and post SSA fragment intensity
100
90
80
70
60
50
40
30
20
10
0
wild-type
exo1Δ
rad3Δ exo1Δ
wild-type
exo1Δ
rad3Δ exo1Δ
360 - OFF
360 - ON
C
wild-type
exo1Δ
rad3Δ exo1Δ
% his- colonies
100
90
80
70
60
50
40
30
20
10
0
0
30
60
120
180
360
360 - OFF
Time (minutes)

Figure 4.8 DSB resection in the SSA assay is predominantly Exo1-dependent

(A) Southern Blot analysis of the SSA assay (Figure 4.6) for wild-type, *exo1*Δ and *exo1*Δ *rad3*Δ strains. The membranes were hybridised with probe B (left) to detect a 6.2 kb pre-SSA fragment (blue) and a 3.1 kb post-SSA fragment (red). Probe A (right) was used to detect loss of a 3.9 kb fragment (green) following HO cleavage. 360 OFF refers to no HO induction.

(B) Quantification of Probe B band intensities at 360 minutes for wild-type, *exo1*Δ and *exo1*Δ *rad3*Δ strains. Band intensities were quantified using Quantity One (Bio-rad) and normalised by calculating the intensities of 6.2 kb pre-SSA band and 3.1 kb post-SSA band as a percentage of the total for these bands at each time point. Mean values are presented for three independent repeats including the blots in (A). Error bars indicate ± standard error, aasterisk (*****) represents a significant difference to wild-type.

(C) Colony assay observing loss of the *his3* marker following HO induction for wild-type, *exo1*Δ and *exo1*Δ *rad3*Δ strains. The results shown correspond to the inductions analysed by Southern blotting in (A).

The radioactive steps of Southern blotting were carried out by Carol Walker (Department of Oncology, University of Oxford).

The colony assay to observe loss of the histidine marker suggested DSB induction in the *exo1*Δ and *rad3*Δ *exo1*Δ backgrounds was reduced compared wild-type (Figure 4.8.C). 360 minutes following the addition of uracil 81% of *exo1*Δ and 72% of *rad3*Δ *exo1*Δ colonies were auxotrophic for histidine compared to 95% of wild-type colonies. The membranes were hybridised with probe A to further assess DSB induction (Figure 4.8.A, right). Whereas following DSB induction in a wild-type background loss of the 3.9 kb fragment was observed between 180 and 360 minutes, a reduced but detectable 3.9 kb band remained at 360 minutes for *exo1*Δ and *rad3*Δ *exo1*Δ.

4.3 DISCUSSION

The results presented in this chapter provide evidence for a general role of the DNA damage checkpoint in mediating DNA damage-induced nucleotide synthesis by inducing an accumulation of nuclear Cdt2. Evidence is also provided for an additional role of the 9-1-1 complex in mediating DSB resection.

4.3.1 Deletion of *spd1*$^{+}$ suppresses HR defect of *rad3*Δ and *rad26*Δ

*rad3*Δ and *rad26*Δ both exhibited sensitivity to DSBs and significantly impaired HR associated with high levels of Ch^{16} loss and LOH (Figure 4.1 and Figure 4.3). This confirms previous observations and demonstrates the importance of the DNA damage checkpoint in maintaining genome stability (Tinline-Purvis in Blaikley *et al.*, 2014; Moss *et al.*, 2010). Moss *et al.* (2010) previously showed that the DNA damage sensitivity and HR defect of *rad3*Δ could be suppressed by *spd1*Δ because Rad3 is required for DNA damage-induced degradation of Spd1 (Liu *et al.*, 2005; Moss *et al.*, 2010). The comparable suppression of the *rad26*Δ phenotype by *spd1*Δ was expected as Rad26 is required for the recruitment of Rad3 to

sites of DNA damage and Rad3 activity (Cortez *et al.*, 2001; Edwards *et al.*, 1999; Zou *et al.*, 2003).

4.3.2 Deletion of *spd1*$^+$ cannot suppress the HR defect of 9-1-1 complex gene deletion strains

The very low levels of Ch^{16} loss and high levels of LOH exhibited by *rad17*Δ, *rad9*Δ, *rad1*Δ and *hus1*Δ strains are unique amongst gene deletion strains identified to have compromised HR using DSB assay (Moss, 2011). The HR defect and DSB sensitivity of *rad17*Δ, *rad9*Δ, *rad1*Δ and *hus1*Δ could not be suppressed by *spd1*Δ (Figure 4.1 and Figure 4.4).In the screen presented in Chapter 3, low levels of suppression of *rad1*Δ, *rad17*Δ and *hus1*Δ DSB sensitivity by *spd1*Δ were observed (Figure 3.5 and Figure 3.6). This suppression was greatly reduced compared to that of *rad3*Δ and *rad26*Δ and the data presented in this chapter suggests it was not significant. In addition the results of the screen were influenced by the effect of background markers on the DSB sensitivity of a strain (Figure 3.15). The substantial error in the screen final colony size measurements may also help to explain the anomalous suppression of *rad9*Δ DSB sensitivity by *spd1*Δ in the screen.

4.3.3 A role for the DNA damage checkpoint in DNA damage-induced nucleotide synthesis

rad3$^+$, *rad26*$^+$, *rad17*$^+$, *rad9*$^+$, *rad1*$^+$ and *hus1*$^+$ were all required for Cdt2 accumulation in response to bleocin treatment and therefore for the degradation of Spd1 in response to DSB (Figure 4.5). This provided evidence for a general role of the DNA damage checkpoint in promoting nucleotide synthesis in response to DNA damage. It also suggested the 9-1-1 complex was playing an additional role in HR, the lack of which could not be suppressed by increasing nucleotide pools.

4.3.4 A role for the 9-1-1 complex in facilitating DSB resection

Studies in *S. cerevisiae* have provided evidence that the 9-1-1 complex and Rad24, the homologue of *S. pombe* Rad17, promote resection at uncapped telomeres (Jia *et al.*, 2004; Lydall and Weinert, 1995; Zubko *et al.*, 2004). Deletion of *RAD24* also impairs resection of HO endonuclease-induced DSBs (Aylon and Kupiec, 2003). The unique DSB repair profile of *rad17*Δ, *rad9*Δ, *rad1*Δ and *hus1*Δ strains showed very low levels of Ch^{16} loss. As Ch^{16} loss occurs as a result of extensive resection from the break site (Tinline-Purvis *et al.*, 2009), it was investigated whether the *S. pombe* 9-1-1 complex also promotes DSB resection.

The role of the DNA damage checkpoint in regulating DSB resection was investigated using a SSA assay developed by Watson et al (2011) (Figure 4.6). To monitor SSA annealing over time, this assay relies on rapid and robust HO expression from the *urg1* promoter to induce DSBs. DSB induction was found to be delayed compared to the original report (Figure 4.7.C and Figure 4.8.C). In all backgrounds approximately 70% loss of the histidine marker was observed 180 minutes after the addition of uracil opposed to 98% loss observed at 120 minutes by Watson *et al.* (2011). The background levels of histidine marker loss were also high, reaching 36% in a *rad9*Δ background (Figure 4.7.C and Figure 4.8.C). This contrasts with 9% loss observed by Watson *et al.* (2011) in a wild-type background. Control of the *urg1* promoter is complex and leakiness could be improved in future experiments by adding arginine to inhibit premature expression (Watson *et al.*, 2013). Despite these difficulties the comparable DSB induction observed in wild-type, *rad3*Δ, *rad17*Δ and *rad9*Δ backgrounds, as well as the repeatable SSA results for these strains, justify the use of this system.

Using the SSA assay wild-type and *rad3*Δ strains showed efficient resection and SSA in 360 minutes. However, *rad17*Δ and *rad9*Δ showed reduced SSA (Figure 4.7.A left and Figure 4.7.B). This provides evidence that, in addition to promoting nucleotide synthesis, the

S. pombe 9-1-1 complex plays a role in HR by promoting DSB resection. This plausibly explains why the HR defect of 9-1-1 complex gene deletion strains cannot be suppressed by *spd1*Δ. The 9-1-1 complex gene deletion strains showed high levels of LOH mediated by isochromosome formation (Tinline-Purvis in Blaikley *et al.*, 2014). Isochromsomes arise from extensive resection following failed HR leading to BIR within the centromere (Tinline-Purvis *et al.*, 2009). It is hypothesised that the reduced efficiency of resection in *rad17*Δ and *rad9*Δ backgrounds may promote isochromosome formation by stabilising BIR intermediates within the centromeric repeats. This demonstrates the importance of efficient DSB resection in maintaining genome stability.

Subsequent to publishing these results Tsang *et al.* (2014) provided evidence that *S. pombe* checkpoint proteins are also involved in regulating resection in the context of collapsed replication forks. Replication forks were arrested at RTS1 sequences integrated into the *ura4* gene and required recombination mediated restart. DNA resection was assessed by using Chip to detect RPA, Rad51 and Rad52 bound to ssDNA. Consistent with the evidence presented in this chapter for Rad17 and Rad9 promoting DSB resection, Rad17 and Rad9 were found to promote resection at the arrested fork. However, Rad3 was found to inhibit resection at the arrested fork. This may reflect differential regulation of DNA resection at DSBs and replication forks or an issue with the sensitivity of the SSA assay. This point could be addressed by adding additional time points between 180 and 360 minutes.

4.3.5 Investigating the mechanism by which the checkpoint regulates resection

Using the SSA developed by Watson *et al.* (2011), no detectable SSA was observed in a *exo1*Δ background up to 360 minutes after DSB induction (Figure 4.8.A left and Figure 4.8.B). This suggests that, when using the SSA assay in a wild-type background, most if not all extensive DSB resection was performed by Exo1 and that the 9-1-1 complex

promotes Exo1-dependent resection. However, DSB induction was slightly reduced in this background. This may have delayed SSA (Figure 4.8.B-C). The dependence on Exo1 contrasts with the situation in the DSB assay where efficient GC is achieved in an *exo1*Δ background (Tinline-Purvis in Blaikley *et al.*, 2014). However, the DSB assay assessed repair 48 hours following HO induction from a weak *nmt* promoter. In *S. pombe* extensive resection can be performed by Exo1 and Dna2-Rqh1 (Langerak *et al.*, 2011). Ngo *et al.* (2014) proposed that *S. cerevisiae* Exo1 and Dna2-Sgs1 have different abilities to resect through chromatin structures which may also contribute to the differences observed in these assays.

In support of a conserved role for the 9-1-1 complex in promoting Exo1-dependent DNA resection, Tsang *et al.* (2014) found that *S. pombe* Rad17 and Rad9 also promoted Exo1-dependent resection at arrested replication forks. Ngo *et al.* (2014) found that binding of the human 9-1-1 complex to DNA *in vitro* stimulated both EXO1 and DNA2 mediated resection of DNA structures mimicking both DSBs and replication forks. Evidence suggested the 9-1-1 complex stimulated resection by increasing the local concentration of the endonucleases. Ngo *et al.* (2014) also found that the *S. cerevisiae* 9-1-1 complex stimulated *in vivo* the binding of Exo1 and Dna2-Sgs1 to uncapped telomeres despite no direct interaction being detected between the nucleases and the 9-1-1 complex. They hypothesised that the 9-1-1 complex may promote changes in chromatin to aid nuclease loading.

Small but significant levels of SSA were detected at 360 minutes after DSB induction in a *rad3*Δ *exo1*Δ background. This suggests that, in the absence of Exo1, Rad3 inhibits Exo1 independent extensive resection mediated by Rqh1-Dna2. *S. cerevisiae* Mec1, the homologue of *S. pombe* Rad3, is required for the inhibitory phosphorylation of Exo1 (Morin *et al.*, 2008) and also phosphorylates Dna2 in response to DNA damage, although the significance is not clear (Chen *et al.*, 2011).

4.4 SUMMARY

In this chapter the role of the DNA damage checkpoint in DNA damage-induced nucleotide synthesis and HR was investigated. The results presented provide evidence that:

- Rad3, Rad26, Rad17 and the 9-1-1 complex are required for DNA damage-induced nucleotide synthesis through the induction of Cdt2 to promote Spd1 degradation.
- The DSB sensitivity and HR defect of *rad3*Δ and *rad26*Δ is suppressed by deleting *spd1*$^{+}$ to promote nucleotide synthesis.
- In contrast, the DSB sensitivity and HR defect of *rad17*Δ, *rad9*Δ, *rad1*Δ and *hus1*Δ is not suppressed by deleting *spd1*$^{+}$ to promote nucleotide synthesis.
- The 9-1-1 complex has an additional role in DNA DSB repair by promoting Exo1-dependent DSB resection.
- In the absence of Exo1, Rad3 inhibits Exo1-independent DSB resection.

Chapter 5 A role for Ngg1 and the Gcn5 HAT protein module promoting nucleotide synthesis and homologous recombination

5.1 INTRODUCTION

The screen presented in Chapter 3 identified *ngg1*Δ as a candidate showing suppression of DSB sensitivity when *spd1*$^{+}$ was deleted to increase nucleotide pools (Table 3.1). Ngg1 is a component of a conserved histone acetyl transferase (HAT) module (Balasubramanian *et al.*, 2002; Lee *et al.*, 2011; Spedale *et al.*, 2012). In this chapter the role of Ngg1 and the HAT module in nucleotide synthesis and DSB repair is further investigated. The HAT module and its associated complexes are first introduced here as this is relevant to the results presented.

In *S. cerevisiae* the HAT module is associated with three protein complexes: the SAGA, SILK and ADA complexes (Eberharter *et al.*, 1999; Lee *et al.*, 2010; Pray-Grant *et al.*, 2002). The SAGA complex is broadly conserved from yeast to humans and in *S. cerevisiae* contains 21 subunits arranged into functionally independent modules which cooperate to promote transcription (Lee *et al.*, 2010; Spedale *et al.*, 2012; Sterner *et al.*, 1999).

Gcn5 is the catalytic subunit of the HAT module (Brownell *et al.*, 1996). However, the subunits Ada2 and Ngg1 are additionally required for the Gcn5-dependent acetylation of nucleosomes (Balasubramanian *et al.*, 2002). Gcn5 has been shown to acetylate histones residues including H3K9, H3K14, H3K18, H3K23 and H3K36 (Balasubramanian *et al.*, 2002; Grant *et al.*, 1997; Morris *et al.*, 2007). Gcn5 HAT activity is required for the expression of stress response genes in both *S. pombe* and *S. cerevisiae* (Johnsson *et al.*, 2006; Xue-Franzen *et al.*, 2010). In *S. pombe* Gcn5 acetylates nucleosomes at the promoters and coding regions of stress response genes resulting in nucleosome eviction, thus promoting transcriptional elongation (Johnsson *et al.*, 2009; Sanso *et al.*, 2011).

The fourth member of the HAT domain is Sgf29 (Lee *et al.*, 2011; Sanders *et al.*, 2002). Sgf29 binds to H3K4me2-me3 via conserved tandem Tudor domains (Bian *et al.*, 2011; Vermeulen *et al.*, 2010) Sgf29 promotes Gcn5 HAT activity and TATA binding protein recruitment in *S. cerevisiae* (Bian *et al.*, 2011; Shukla *et al.*, 2012).

S. pombe Gcn5 also has a role in DSB repair. A *gcn5*Δ strain is unable to acetylate histone H3K36 (Morris *et al.*, 2007) and consequently has increased levels of H3K36me3 (Pai *et al.*, 2014). Pai *et al.* (2014) showed that a *gcn5*Δ strain exhibited reduced DSB repair by GC compared to wild-type, associated with increased repair by NHEJ. Conversely a *set2*Δ strain was unable to methylate H3K36 resulting in increased H3K36ac. *set2*Δ exhibited increased HR and reduced NHEJ compared to wild-type. Investigation of the mechanism by which H3K36 modification regulated repair pathway choice found that *gcn5*Δ reduced chromatin accessibility and DSB resection whereas the opposite was observed for *set2*Δ.

A model was proposed where Gcn5-dependent H3K36 acetylation results in open chromatin, increased DSB resection and HR. Set2-dependent H3K36 methylation results in closed chromatin, reduced DSB and promotes NHEJ (Figure 5.1) (Pai *et al.*, 2014). Modification of H3K36 was found to be cell cycle regulated with H3K36 acetylation peaking in S/G2 phases of the cell cycle when a sister chromatid is available as a template for HR (Pai *et al.*, 2014).

Previous studies have also suggested roles for Gcn5 in HR. Tamburini and Tyler (2005) showed that in *S. cerevisiae* Gcn5 is recruited to DSBs where it acetylates histones during HR. Lee *et al.* (2010) showed that following a DSB in human cells Gcn5 associates with nucleosomes containing γ-H2AX and acetylates H3 in these nucleosomes allowing further recruitment of SWI/SNF to stimulate γ-H2AX formation. Oishi *et al.* (2006) showed that human GCN5 may interact with BRCA1 and that its HAT activity is required for BRCA1-dependent transcription.

Figure 5.1

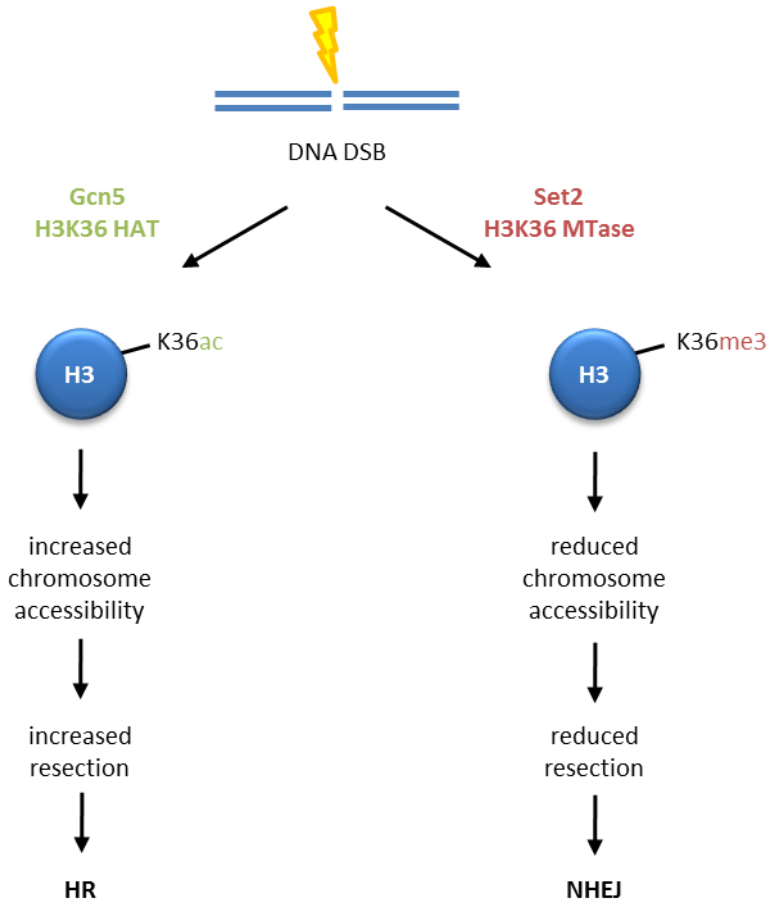


Figure 5.1 H3K36 chromatin switch regulates DSB repair pathway choice

Figure adapted from Pai *et al.* (2014). Gcn5-dependent H3K36 acetylation at the break site results in open chromatin, increased DSB resection and HR. Set2-dependent H3K36 methylation at the break site results in closed chromatin, reduced DSB which promotes NHEJ.

5.2 RESULTS

5.2.1 Deletion of *spd1*$^+$ suppresses the DSB sensitivity and HR defect of *ngg1*Δ

The sensitivity of *ngg1*Δ to bleocin and suppression of this phenotype by *spd1*Δ was confirmed using a serial dilution assay (Figure 3.14 and Figure 5.2.A). This suggested a role for Ngg1 in DNA damage-induced nucleotide synthesis.

To test whether the sensitivity of *ngg1*Δ to bleocin was caused by a defect in DSB repair, a *ngg1*Δ strain was subjected to the DSB assay (Figure 1.5, Figure 5.2.B). The repair profile of *ngg1*Δ displayed a significant decrease in GC compared to wild-type (50.3%, $p = 0.03$). However, this was not associated with an increase in the assay outcomes associated with failed HR. In fact significant reductions in the levels of Ch^{16} loss (7.5%, $p = 0.01$) and LOH (7.0%, $p < 0.01$) were observed compared to wild-type. There was instead a significant increase in repair by NHEJ/SCC (34.9% $p = 0.01$) compared to wild-type.

Deletion of *spd1*$^+$ in an *ngg1*Δ background partially suppressed the strains HR defect (Figure 5.2.B). *ngg1*Δ *spd1*Δ had significantly increased levels of GC (66.1%, $p = 0.04$) compared to *ngg1*Δ. This was associated with significantly decreased levels of NHEJ/SCC (18.75%, $p = 0.05$) compared to *ngg1*Δ. No significant change was observed in the levels of Ch^{16} loss (9.0%, $p = 0.43$) or LOH (6.0%, $p = 0.40$) compared to *ngg1*Δ.

Figure 5.2

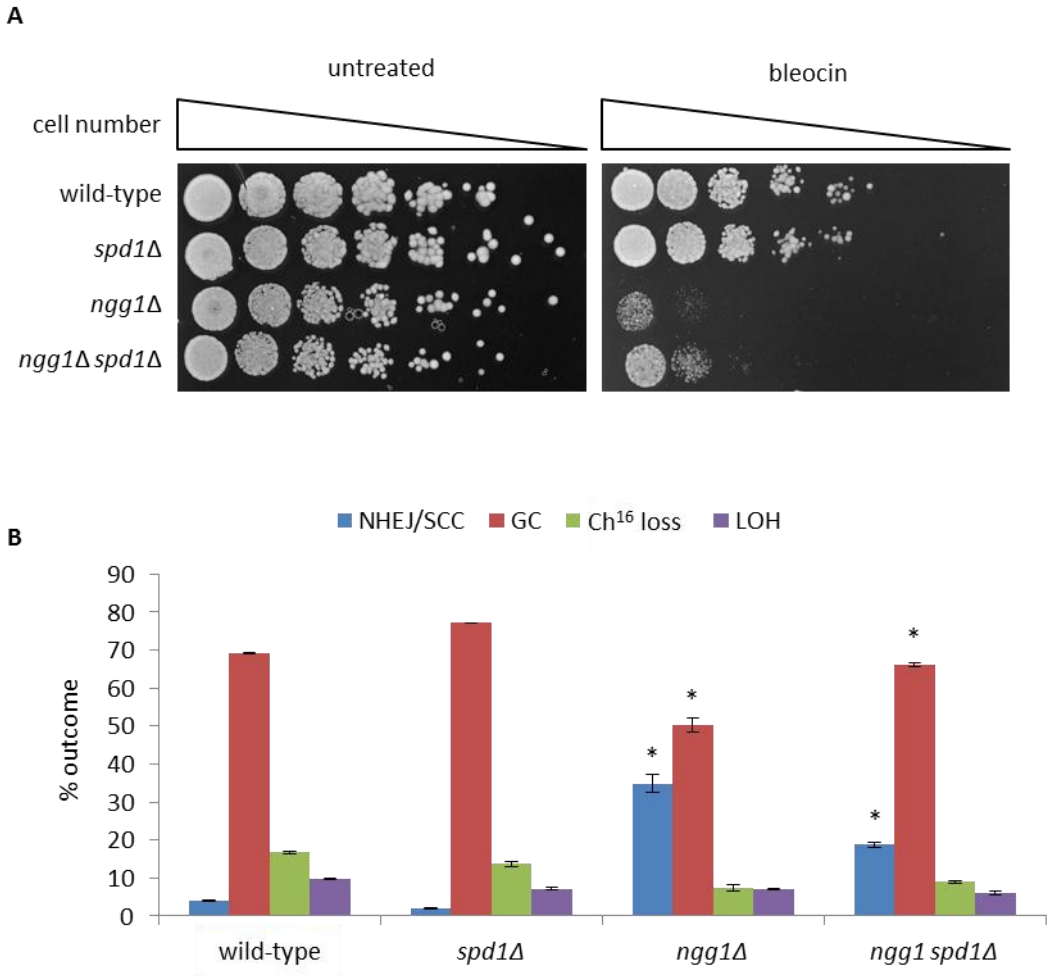


Figure 5.2 Deletion of *spd1*$^{+}$ suppresses the DSB sensitivity and HR defect of *ngg1*Δ

(A) Fivefold serial dilutions of wild-type, *spd1*Δ, *ngg1*Δ and *ngg1*Δ *spd1*Δ were spotted onto YE6S and YE6S + 0.2 µg/ml bleocin. Serial dilutions were performed using auxotrophic strains.

(B) DSB assay analysis of wild-type and *spd1*Δ, *ngg1*Δ and *ngg1*Δ *spd1*Δ. The percentage NHEJ/SCC, GC, LOH and Ch^{16} loss events are shown. Mean values ± standard errors are presented for three repeats. Asterisk (*****) represents a significant difference between *ngg1*Δ and *ngg1*Δ *spd1*Δ.

5.2.2 Deletion of *spd1*$^{+}$ suppresses the DSB sensitivity and HR defect of Gcn5 HAT module gene deletion strains

Ngg1 is a component of the Gcn5 HAT module which also contains Gcn5, Ada2 and Sgf29 (Horiuchi *et al.*, 1995; Lee *et al.*, 2011). *gcn5*Δ and *ada2*Δ were also included in the library screened for deletion strains showing suppression of DSB sensitivity when *spd1*$^{+}$ was deleted.

In addition to *ngg1*Δ the screen identified both *gcn5*Δ and *sgf29*Δ as mildly DSB sensitive (Figure 5.3.A). Bleocin treatment reduced the average *ngg1*Δ colony size from 95% to 62% of wild-type, the average *gcn5*Δ colony size from 102% to 80% of wild-type and the average *sgf29*Δ colony size from 86% to 65% of wild-type. SAGA complex SPT domain mutants *spt3*Δ and *spt8*Δ as well as DUB domain mutant *sgf73*Δ were also included in the screen however they were not found to be DSB sensitive.

As discussed in Section 3.2.4, to analyse the effect of *spd1*Δ on deletion strain DSB sensitivity independently of effects on strain fitness the ratio of *sens*Δ *spd1*Δ to *sens*Δ colony sizes was calculated under both control and bleocin conditions and compared (Figure 3.5). As observed for *ngg1*Δ the ratio of *sens*Δ *spd1*Δ to *sens*Δ colony size for both *gcn5*Δ and *ada2*Δ was greater under bleocin conditions, indicating specific suppression of bleocin sensitivity by *spd1*Δ (Figure 5.3.B). However, these differences were not large enough for selection for further study in Chapter 3 (Figure 5.3.C). *gcn5*Δ was ranked at 38 and *ada2*Δ at 42.

Figure 5.3

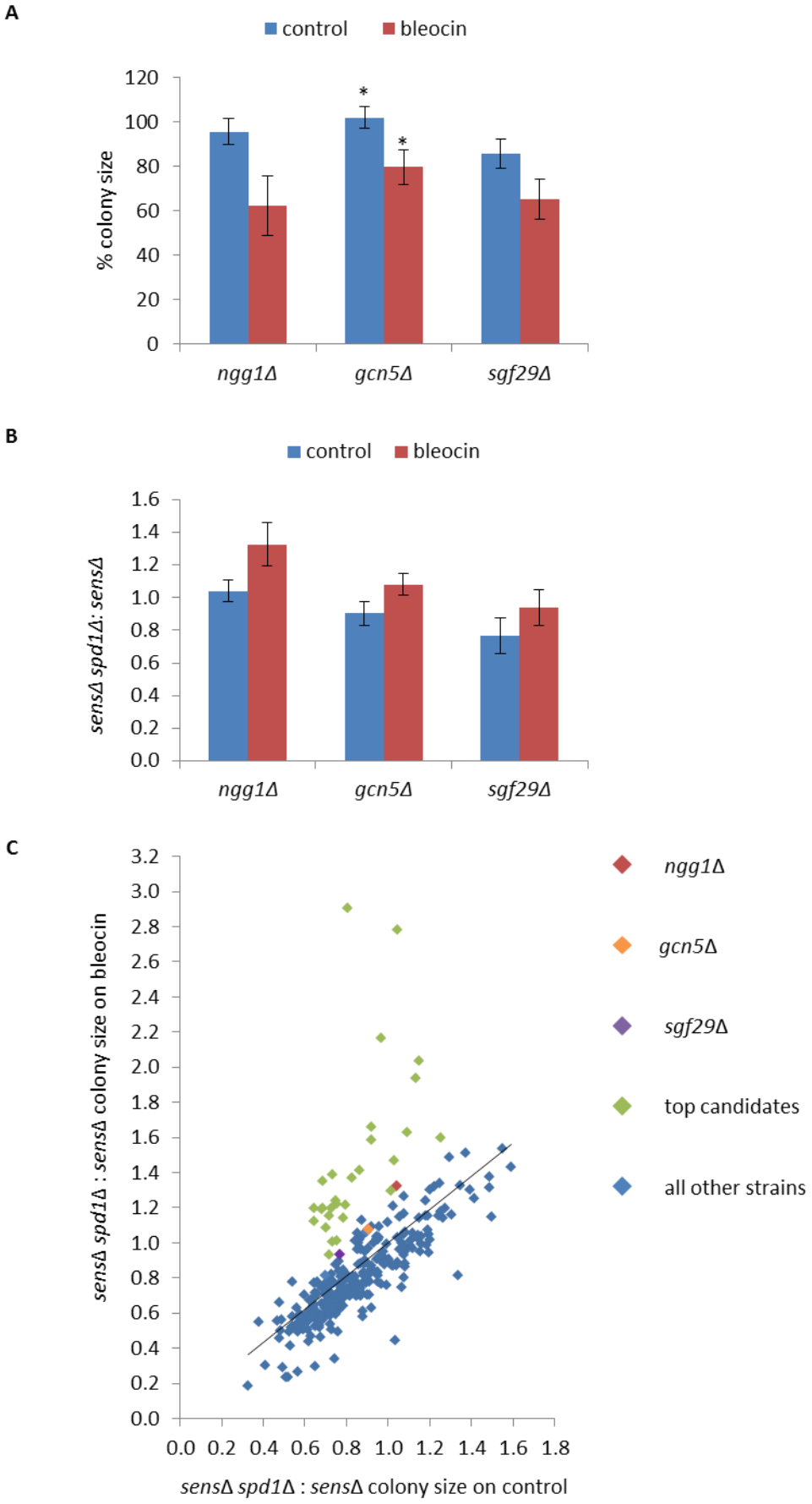

A
control
bleocin
% colony size
120
100
80
60
40
20
0
*
*
ngg1Δ
gcn5Δ
sgf29Δ
B
control
bleocin
sensΔ spd1Δ: sensΔ
1.6
1.4
1.2
1.0
0.8
0.6
0.4
0.2
0.0
ngg1Δ
gcn5Δ
sgf29Δ
C
sensΔ spd1Δ : sensΔ colony size on bleocin
3.2
3.0
2.8
2.6
2.4
2.2
2.0
1.8
1.6
1.4
1.2
1.0
0.8
0.6
0.4
0.2
0.0
0.0 0.2 0.4 0.6 0.8 1.0 1.2 1.4 1.6 1.8
sensΔ spd1Δ : sensΔ colony size on control
ngg1Δ
gcn5Δ
sgf29Δ
top candidates
all other strains

Figure 5.3 Screen results for the Gcn5 HAT module gene deletion strains

In the screen colonies were grown for 48 hours, the size of *sens*Δ colonies calculated as a percentage of wild-type and the size of *sens*Δ *spd1*Δ as a percentage of *spd1*Δ.

(A) Colony size of *ngg1*Δ, *gcn5*Δ and *ada2*Δ strains grown on YE6S and YE6S + 0.1 µg/ml bleocin. Mean values are presented and error bars indicate ± standard error. Asterisk (*) represents a significant difference between untreated and bleocin conditions.

(B) Screen results are presented for *ngg1*Δ, *gcn5*Δ and *ada2*Δ. The ratio of the size of *sens*Δ *spd1*Δ colonies to *sens*Δ colonies grown on YE6S and on YE6S + 0.1 µg/ml bleocin is shown (see Figure 3.5 for the calculations). Mean values are presented and error bars indicate ± standard error.

(C) The ratio of the size of *sens*Δ *spd1*Δ colonies to *sens*Δ colonies on YE6S plates was plotted against the same ratio when the colonies were grown on YE6S + 0.1µg/ml bleocin (see Figure 3.5 for the calculations). *ngg1*Δ is highlighted in red, *gcn5*Δ in orange, *sgf29*Δ in purple, other candidates selected for further study in green and all other strains in blue.

To confirm whether *spd1*Δ could suppress the DSB sensitivity of *gcn5*Δ, *ada2*Δ and *sgf29*Δ, the double mutant strains were constructed and subjected to a serial dilution assay. As the background markers of a strain can affect bleocin sensitivity auxotrophic strains were used (Figure 3.16). *spd1*Δ partially supressed the bleocin sensitivity of *gcn5*Δ, *ada2*Δ and*sgf29*Δ (Figure 5.4.A).

The DSB assay repair profile for a *gcn5*Δ strain had been independently determined in the laboratory and resembled the repair profile *ngg1*Δ, exhibiting reduced GC and increased NHEJ/SCC compared to wild-type (Pai *et al.*, 2014). For the purpose of this study this was confirmed. *ada2*Δ was also subjected to the DSB assay to assess whether this phenotype was a general feature of Gcn5 HAT module gene deletion strains (Figure 5.4.B).

GC was significantly reduced compared to wild-type in both *gcn5*Δ (43.7%, $p = 0.01$) and *ada2*Δ (52.6%, $p = 0.01$), backgrounds. This was associated with significant increase in NHEJ/SCC for both *gcn5*Δ (45.1%, $p = 0.01$) and *ada2*Δ (39.1%, $p < 0.01$) compared to wild-type. Ch^{16} loss was significantly reduced for *gcn5*Δ (6.2%, $p = 0.01$) and *ada2*Δ (9.0%, $p < 0.01$) compared to wild-type. LOH was also significantly reduced for *gcn5*Δ (4.9%, $p < 0.01$) and *ada2*Δ (6.1%, $p = 0.02$) compared to wild-type.

Figure 5.4

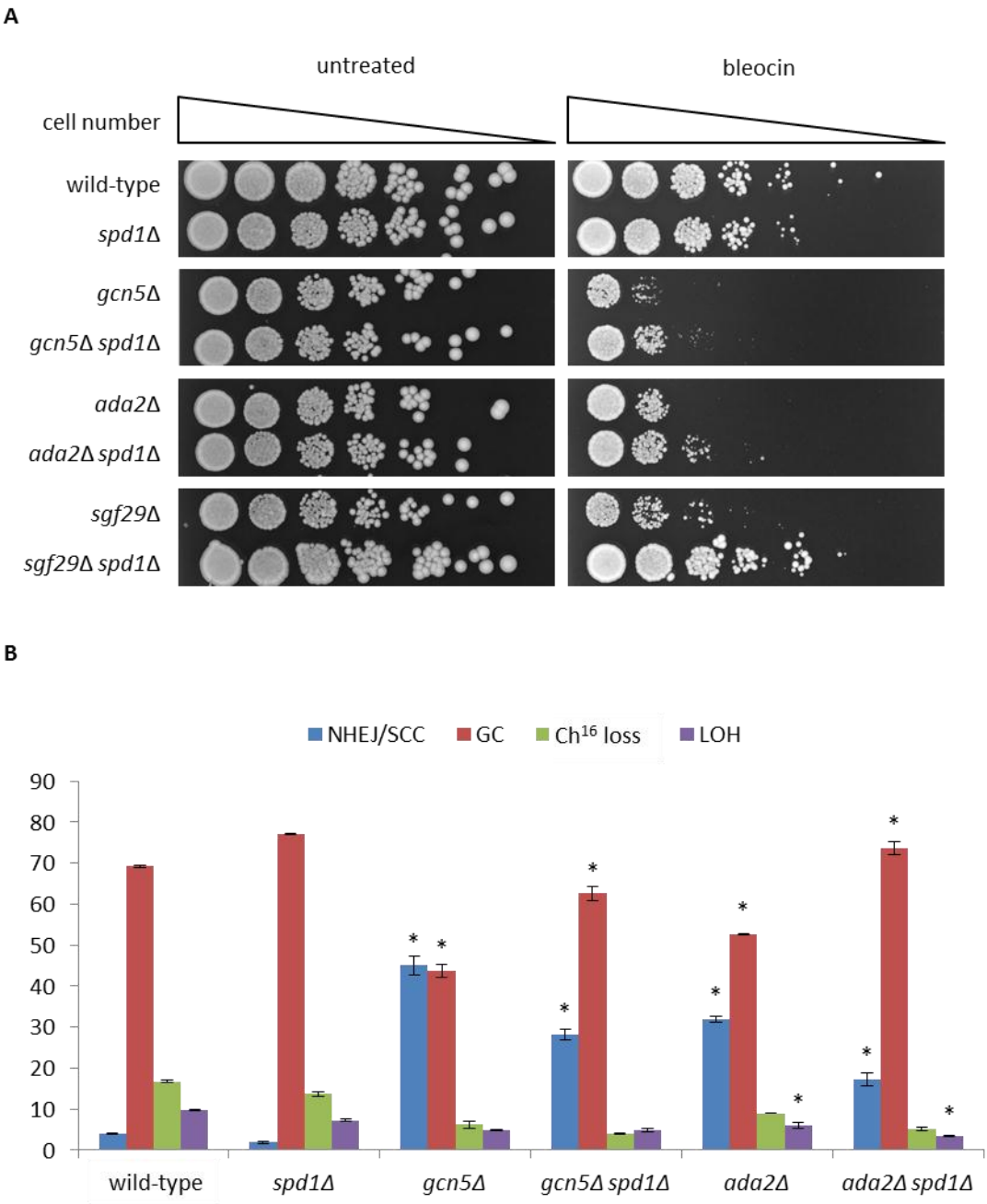


Figure 5.4 Deletion of *spd1*$^{+}$ suppresses the DSB sensitivity and HR defect of Gcn5 HAT module gene deletion strains

(A) Fivefold serial dilutions of wild-type, *spd1*Δ, *gcn5*Δ, *gcn5*Δ *spd1*Δ, *ada2*Δ and *ada2*Δ *spd1*Δ were spotted onto YE6S and YE6S + 0.2 µg/ml bleocin. Serial dilutions were performed using auxotrophic strains.

(B) DSB assay analysis of wild-type and *spd1*Δ, *gcn5*Δ, *gcn5*Δ *spd1*Δ, *ada2*Δ and *ada2*Δ *spd1*Δ. The percentage NHEJ/SCC, GC, LOH and Ch^{16} loss events are shown. Mean values ± standard errors are presented for three repeats. Asterisk (*****) represents a significant difference between the Gcn5 HAT module gene deletion strains and the corresponding *spd1*Δ double deletion strains.

As observed for *ngg1*Δ, *spd1*Δ partially suppressed the DSB repair phenotype of *gcn5*Δ and *ada2*Δ (Figure 5.4.B). Significantly increased levels of GC were observed for *gcn5*Δ *spd1*Δ (62.6%, p = 0.01) and *ada2*Δ *spd1*Δ (73.7%, p = 0.01) compared to the parental deletion strains. Significantly decreased levels of NHEJ/SCC were observed for *gcn5*Δ *spd1*Δ (28.2%, p = 0.03) and *ada2*Δ *spd1*Δ (17.3%, p = 0.03) compared to the parental deletion strains. A significant reduction in the levels of LOH compared to the parental deletion strain was observed for *ada2*Δ *spd1*Δ (3.4%, p = 0.03) but not for *gcn5*Δ *spd1*Δ (4.9%, p = 0.99) compared to the parental deletion strains. No significant change was observed in the levels of LOH for either *gcn5*Δ *spd1*Δ (4.0%, p = 0.09) or *ada2*Δ *spd1*Δ (5.1%, p = 0.31) compared to the parental checkpoint deletion strains.

5.2.3 Deletion of *ngg1*$^+$ and *gcn5*$^+$ decreases cellular nucleotide pools

To confirm a role for the Gcn5 HAT module in DNA damage-induced nucleotide synthesis, log phase cultures of wild-type, *ngg1*Δ and *gcn5*Δ strains were grown in the presence or absence of bleocin to induce DSBs. The levels of nucleotides were measured by HPLC and normalised to wild-type in the absence of bleocin treatment. *ngg1*Δ and *gcn5*Δ showed reduced levels of nucleotides compared to wild-type both in the presence and absence of bleocin (Figure 5.5.A-B).

In the absence of bleocin the levels of dGTP, dTTP and dATP were reduced compared to wild-type in *ngg1*Δ and *gcn5*Δ backgrounds. However, both strains showed similar levels of dCTP to wild-type (Figure 5.5A). In both *ngg1*Δ and *gcn5*Δ backgrounds levels of all four nucleotides increased in response to bleocin treatment however the increase in the levels of dCTP, dGTP and dTTP was less than observed for wild-type (Figure 5.5.B).

Figure 5.5

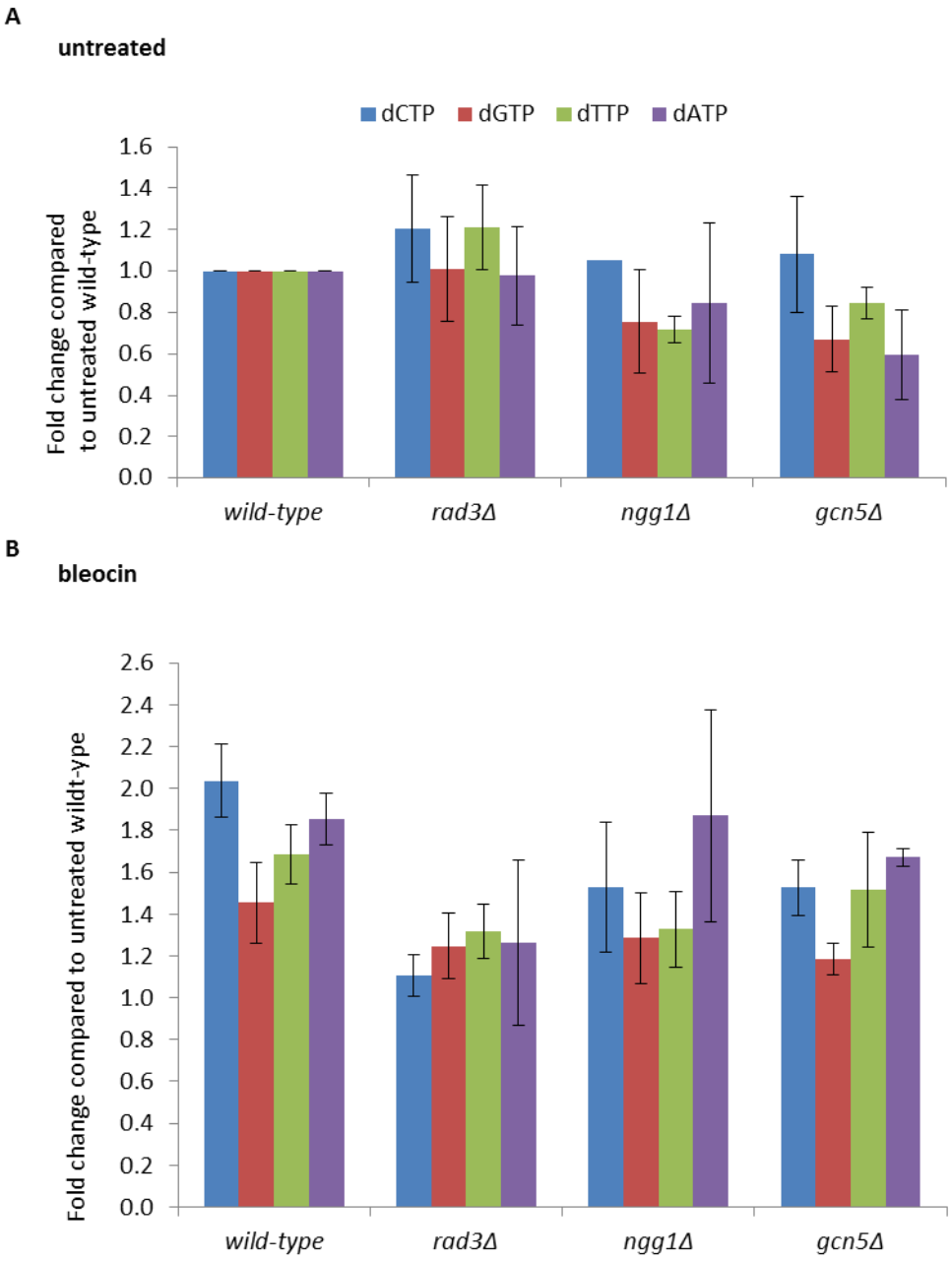


Figure 5.5 Deletion of *ngg1*$^{+}$ and *gcn5*$^{+}$ decreases cellular nucleotide pools

HPLC analysis of dNTP levels in log phase wild-type, *rad3*Δ, *ngg1*Δ and *gcn5*Δ strains grown for 2 hours in **(A)** YE6S or **(B)** 2 µg/ml bleocin. Means fold change compared to wild-type grown in YE6S is presented ± standard errors. A minimum of three independent repeats were performed. Due to detection problems only one dCTP measurement was made for *ngg1*Δ in (A). HPLC analysis was performed by Lisa Folkes (Department of Oncology, University of Oxford).

5.2.4 Exogenous nucleosides suppress the DSB sensitivity of *rad3*Δ, *ngg1*Δ and *gcn5*Δ

Whilst Spd1 is known to act as an inhibitor of RNR activity, it is possible that it performs other functions. It was important to confirm that the suppression of DSB sensitivity by *spd1*Δ observed for Gcn5 HAT module deletion strains was a direct effect of the release of RNR inhibition. To do this the addition of exogenous nucleosides was used to increase the supply of nucleotides independently of *spd1*Δ.

Yeast lack a nucleoside salvage pathway and therefore the ability to efficiently transport exogenous deoxynucleosides (dN) into cells and to convert them into deoxynucleoside monophosphates (dNMP) by phosphorylation. To overcome this, an *S. pombe* strain was used in which the gene encoding human equilibrative nucleoside transporter 1 (hENT1) was integrated into the *ura4* gene (Edgar Hartsuiker, Bangor University). hENT1 allows the passive transport of nucleosides but not nucleotides or bases across the plasma membrane (Griffiths *et al.*, 1997). This transporter has been used in studies with *S. pombe* to transport thymidine and thymidine analogues into cells (Hodson *et al.*, 2003; Hua and Kearsey, 2011; Sivakumar *et al.*, 2004).

Also integrated into the *ura4* gene was *Drosophila melanogaster* deoxynucleoside kinase (*dm*NK). This enzyme phosphorylates of all four deoxynucleosides to the corresponding dNMPs (Johansson *et al.*, 1999; Munch-Petersen *et al.*, 1998). Both genes were expressed from *adh1* promoters allowing constitutive expression in log phase cells.

Strains expressing hENT1 and *dm*NK were subjected to a serial dilution assay. Strains were grown in the presence or absence of 0.5 µg/ml bleocin and also in the presence or absence of 1 µM deoxyadenosine (dA), deoxyguanosine (dG), deoxycytidine (dC) and thymidine (dT).

Expression of hENT1 and *dm*NK in a wild-type background did not affect growth on PMG media (Figure 5.6.A-B) but did confer a slight sensitivity to bleocin which could be suppressed by the addition of 1 µM dN (Figure 5.6.C-D). *rad3*Δ, *gcn5*Δ and *ngg1*Δ were sensitive to bleocin and this was partially suppressed by the addition of 1 µM dN (Figure 5.6.A-D).

5.2.5 Deletion of *ngg1*$^{+}$ does not affect Cdt2 induction in response to DSB

The DNA damage checkpoint is required for DNA damage-induced expression of Cdt2 (Figure 4.5) (Liu *et al.*, 2005; Moss *et al.*, 2010). Cdt2 recruits Spd1 for ubiquitination by the Ddb1-Cul4^{Cdt2} which subsequently results in Spd1 degradation to increase nucleotide pools (Liu *et al.*, 2005). Therefore the DSB sensitivity of *cdt2*Δ, *rad3*Δ and *rad26*Δ can be suppressed by *spd1*Δ (Figure 3.13 and Figure 4.1). In contrast, the suppression of *ngg1*Δ DSB sensitivity was found to be independent of an effect on Cdt2-YFP expression either in the presence or absence of bleocin as observed by western blot (Figure 3.18) or fluorescence microscopy (Figure 3.19.A-B).

5.2.6 Deletion of *ngg1*$^{+}$ does not affect RNR protein levels

In *S. cerevisiae* the SAGA complex is required for expression of *RNR3*, which encodes a subunit of RNR, in response to DNA damage (Zhang *et al.*, 2008). It was investigated whether the *S. pombe* Gcn5 HAT module promotes RNR expression in response to DNA damage. Log phase wild-type and *ngg1*Δ cultures were treated with bleocin and RNR protein levels observed by western blot. In a wild-type background there was no visible change in the levels of Cdc22 tagged with green fluorescent protein (Cdc22-GFP) or Succ22 tagged with cyan fluorescent protein (Suc22-CFP) with up to 4 hours bleocin treatment (Figure 5.7A-B). No difference was observed between the levels of Cdc22-GFP in a wild-type and *ngg1*Δ background either in the presence or absence of bleocin treatment.

Figure 5.6

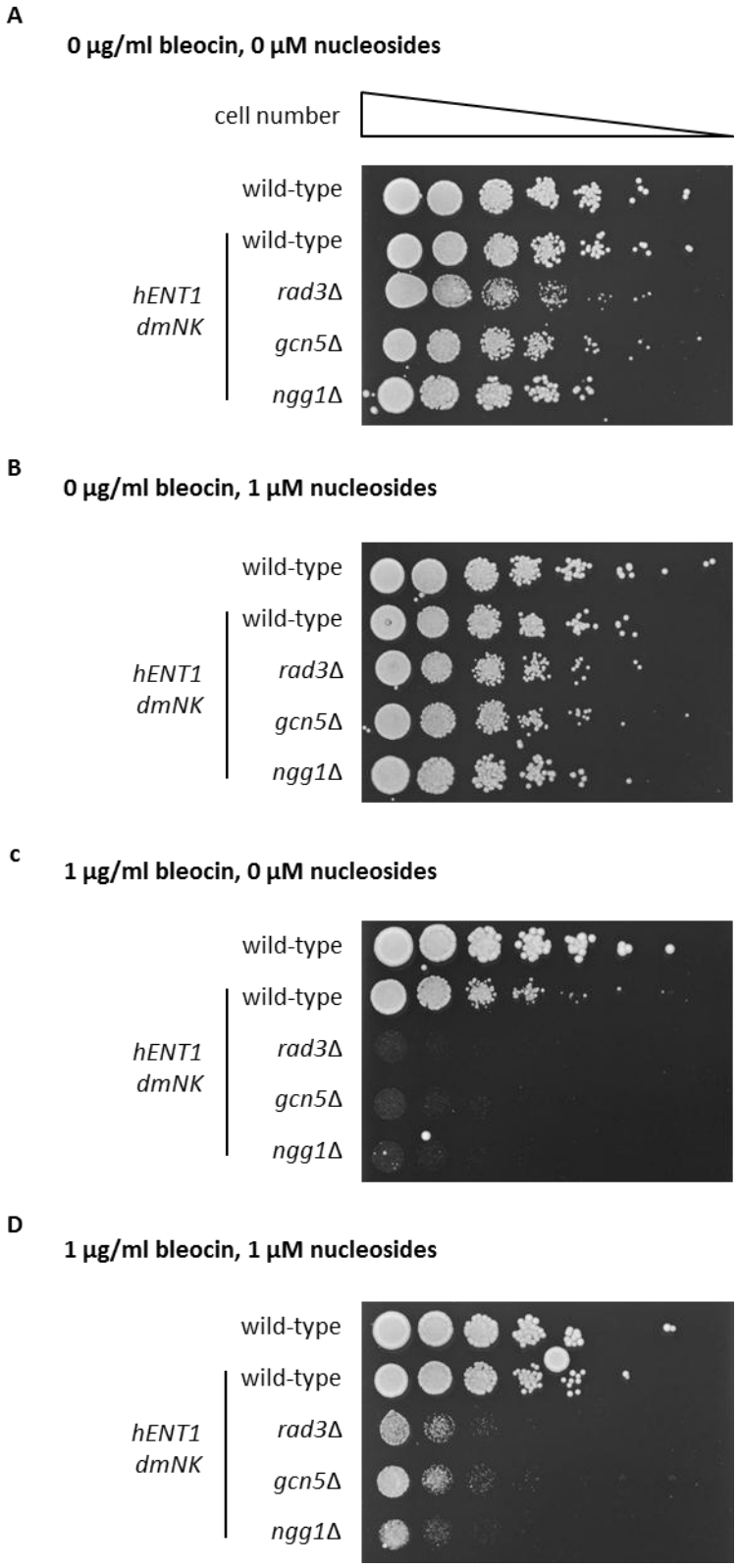


Figure 5.6 Increasing cellular nucleotide pools suppresses the DSB sensitivity of *rad3*Δ, *gcn5*Δ and *ngg1*Δ
Fivefold serial dilutions of wild-type and of wild-type, *rad3*Δ, *gcn5*Δ and *ngg1*Δ strains expressing hENT1 and *dm*NK were spotted onto **(A)** PMG, **(B)** PMG + 1 µM nucleosides, **(C)** PMG + 0.5 µg/ml bleocin. **(D)** PMG + 1 µM nucleosides + 0.5 µg/ml bleocin. Serial dilutions were performed using prototrophic strains. 1 µM nucleosides included dA, dC, dG and dT.

Figure 5.7

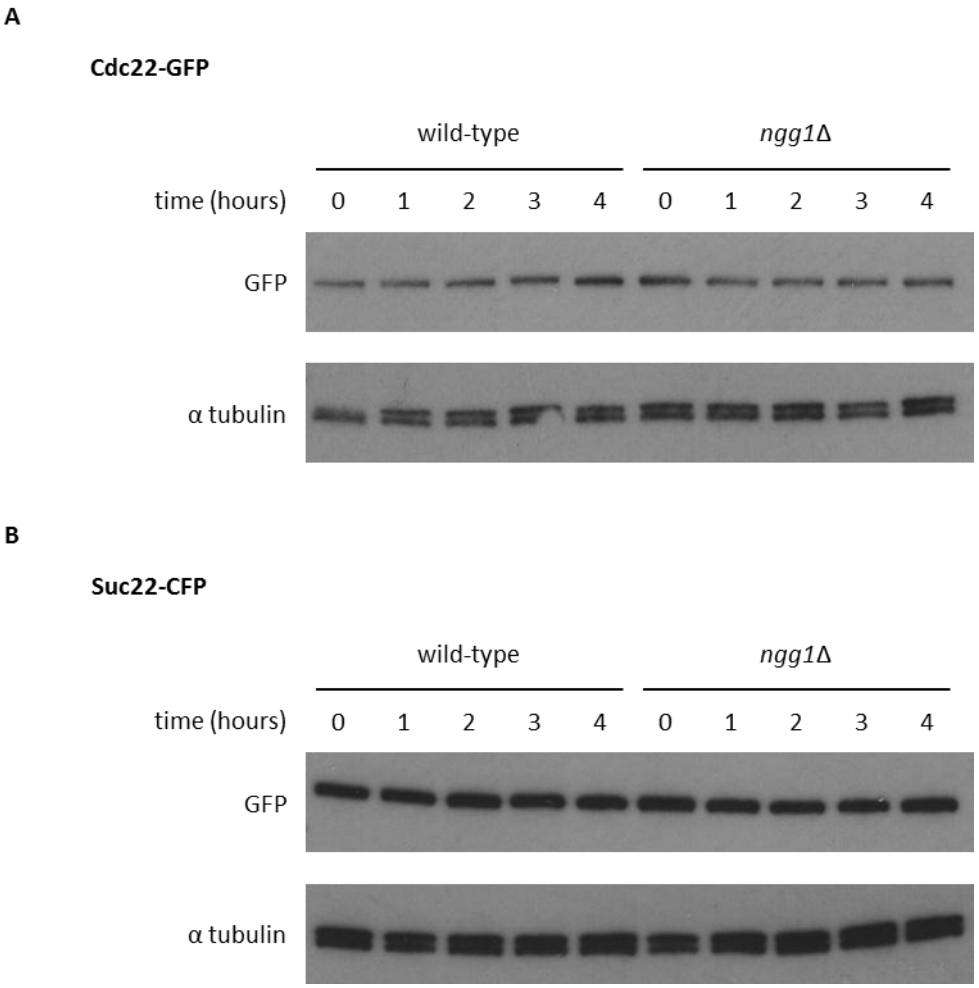


Figure 5.7 Deletion of *ngg1*$^{+}$ does not affect RNR protein levels

Western blot analysis of **(A)** Cdc22-GFP and **(B)** Suc22-CFP levels for wild-type and *ngg1*Δ strains treated with 2 μg/ml bleocin for 4 hours. Cdc22-GFP Suc22-CFP were detected with an anti GFP antibody. An α tubulin loading control was used.

5.2.7 Deletion of *ngg1*$^{+}$ increases repair by NHEJ and SCC

In the DSB assay repair by NHEJ and SCC are indistinguishable as both repair outcomes result in retention of all minichromsome markers (Figure 1.5). Failure to induce a DSB at the *MATa* site of the minichromosome would also result in retention of all markers. As the DSB assay repair profiles of *ngg1*Δ, *gcn5*Δ and *ada2*Δ all demonstrated significant increases in the assay outcome annotated as NHEJ/SCC where all minichromosome markers are retained, it was important to elucidate the cause of this result.

Firstly the contribution of DSB repair by NHEJ to the NHEJ/SCC assay outcome in an *ngg1*Δ background was investigated (Figure 5.8.A). To do this repair by NHEJ was prevented by deleting *ku70*$^{+}$. As expected *ku70*Δ strain had very low levels of NHEJ/SCC, which were significantly reduced compared to wild-type (2.1%, p = 0.02). This was associated with a significant increase in GC (86.7%, p = 0.01) compared to wild-type. No significant change was observed in the levels of Ch^{16} loss or LOH compared to wild-type.

*ngg1*Δ *ku70*Δ had significantly decreased NHEJ/SCC (17.4%, p = 0.04) compared to *ngg1*Δ, indicating that DSB repair by NHEJ was significantly increased in an *ngg1*Δ background compared to wild-type. However, this population was still significantly higher than that observed for *ku70*Δ (p = 0.01). The reduction in NHEJ in *ngg1*Δ *ku70*Δ was associated with a significant increase in GC compared to *ngg1*Δ (72.9%, p = 0.02). No significant changes were observed in the levels of Ch^{16} or LOH compared to *ngg1*Δ (Figure 5.8.A). As *ku70*Δ could not eliminate the population of cells retaining all minichromosome markers in an *ngg1*Δ background multiple causes must be responsible for this assay outcome.

Figure 5.8

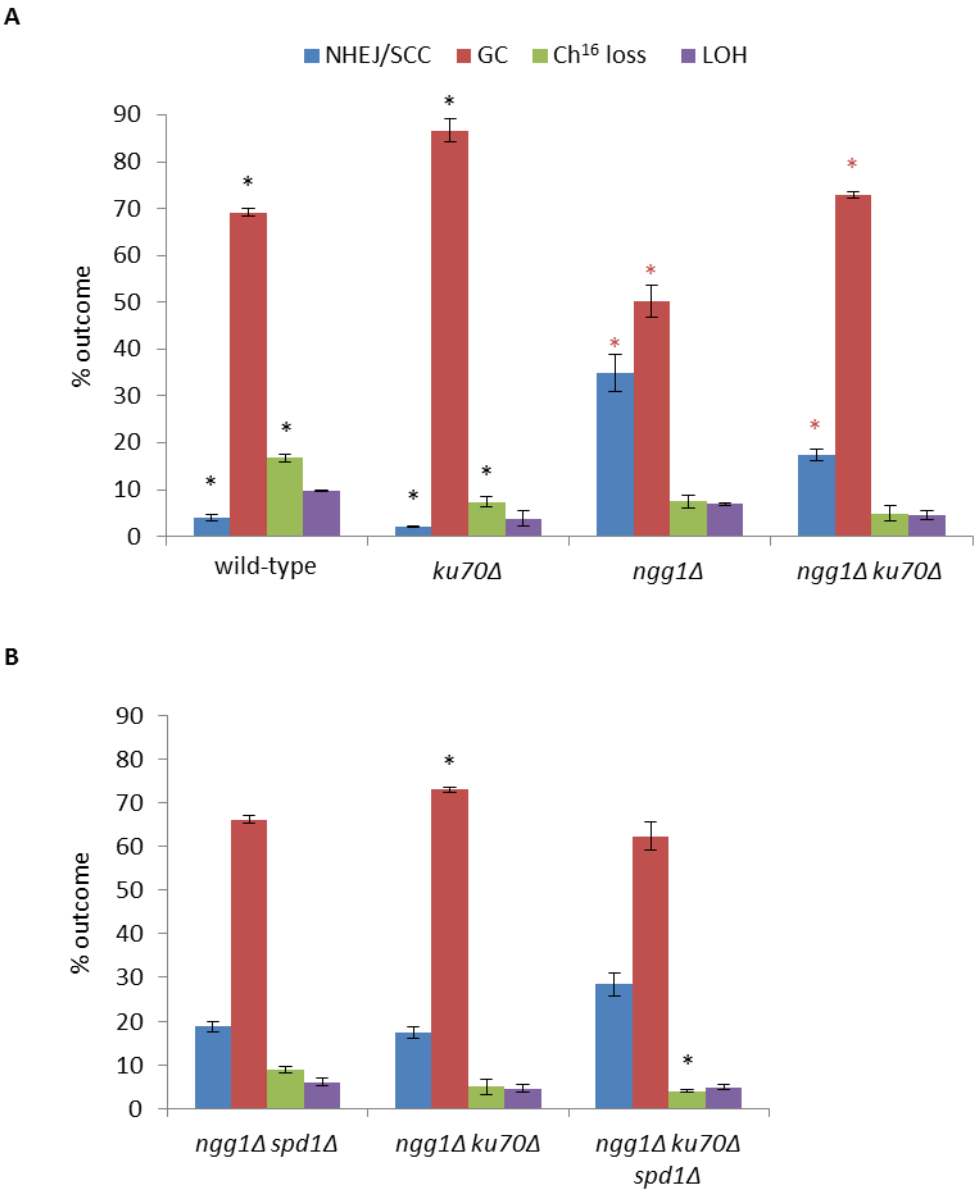


Figure 5.8 Deletion of *ngg1*$^{+}$ increases repair by NHEJ

(A) DSB assay analysis of wild-type, *ku70*Δ, *ngg1*Δ, and *ngg1*Δ *ku70*Δ. The percentage NHEJ/SCC, GC, LOH and Ch^{16} loss events are shown. Mean values ± standard errors are presented for three repeats. Asterisk (*****) in black represents a significant difference between wild-type and *ku70*Δ. Asterisk (*****) in red represents a significant difference between *ngg1*Δ and *ngg1*Δ *ku70*Δ.

(B) DSB assay analysis of wild-type, *ngg1*Δ *spd1*Δ, *ngg1*Δ *ku70*Δ and *ngg1*Δ *spd1*Δ *ku70*Δ. The percentage NHEJ/SCC, GC, LOH and Ch^{16} loss events are shown. Mean values ± standard errors are presented for three repeats. Mean values for *ngg1*Δ *spd1*Δ *ku70*Δ are presented for two independent repeats. Asterisk (*****) represents a significant difference compared to *ngg1*Δ *spd1*Δ.

Interestingly the repair profile of *ngg1*Δ *ku70*Δ resembled that of *ngg1*Δ *spd1*Δ (Figure 5.8.B). The only significant difference was an increase in repair by GC for *ngg1*Δ *ku70*Δ ($p < 0.01$) compared to *ngg1*Δ *spd1*Δ. To investigate the contribution of NHEJ to the NHEJ/SCC repair outcome in an *ngg1*Δ *spd1*Δ background *ngg1*Δ *spd1*Δ *ku70*Δ was subjected to the DSB assay (Figure 5.8.B). No significant change was observed in the levels of NHEJ/SCC (28.5%, $p = 0.05$) compared to *ngg1*Δ *spd1*Δ. This suggests that NHEJ does not significantly contribute to the NHEJ/SCC DSB assay outcome in an *ngg1*Δ *spd1*Δ background. Therefore it is predicted that deletion of *spd1*$^+$ in an *ngg1*Δ background results in a switch in repair pathway choice from NHEJ to GC.

As discussed above, Deletion of *ku70*$^+$ could not eliminate the population of cells retaining all minichromosome markers in an *ngg1*Δ background (Figure 5.8.A). It was investigated whether this population resulted from increased SCC or poor DSB induction. If DSB induction was impaired, it would be predicted that increasing HO endonuclease expression would improve the efficiency of DSB formation and reduce the observed levels of NHEJ/SCC.

In the DSB assay HO is normally expressed from a weak *nmt1* promoter on a REP81X plasmid, which is active in the absence of thiamine. HO was instead expressed from a stronger *nmt1* promoter on a REP41X plasmid (Figure 5.9). This was predicted to increase HO expression. However, as expression from this promoter is leakier, when assessing DSB repair at 48 hours it was necessary to take into account any loss of minichromosome markers observed at 0 hours.

Figure 5.9

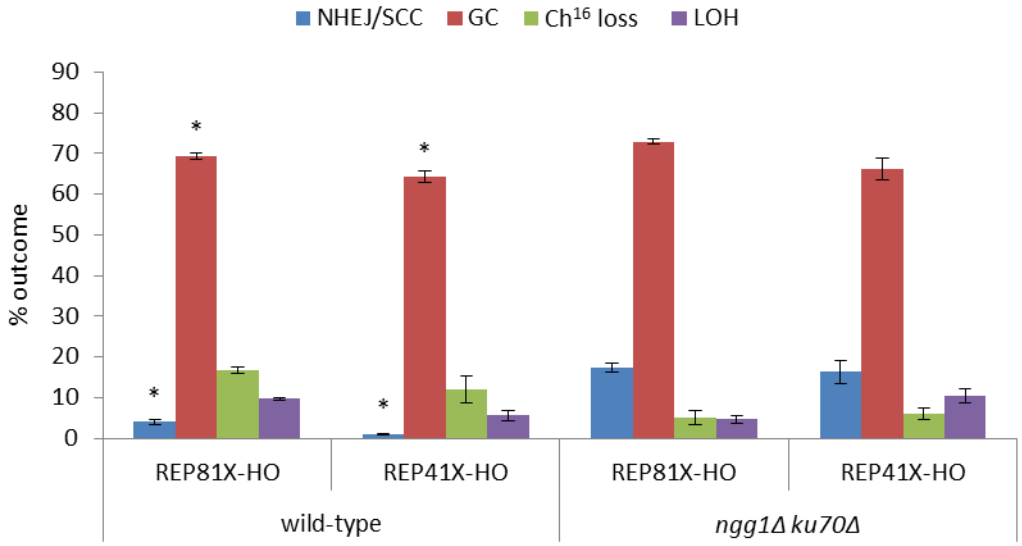


Figure 5.9 Deletion of *ngg1*$^{+}$ does not affect DSB induction

DSB assay analysis of wild-type and *ngg1*Δ *ku70*Δ following 48 hours expression of HO endonuclease from a weak *nmt1* promoter on a REP81X-HO plasmid or from a stronger *nmt1* promoter on a REP41X-HO plasmid. The percentage NHEJ/SCC, GC, LOH and Ch^{16} loss events are shown. Mean values ± standard errors are presented for three repeats. Asterisk (*****) represents a significant difference between the results using REP81X-HO and REP41X-HO in each background.

Expression of HO from a REP41X plasmid in a wild-type background resulted in significantly decreased levels of NHEJ (1.0%, p = < 0.01) and significantly increased levels of GC (64.2%, p = 0.03) compared to wild-type with REP81X-HO. No significant difference was observed between the DSB assay repair profiles of *ngg1*Δ *ku70*Δ strains containing either REP81X-HO or REP41X-HO. This suggests that cutting efficiency was unlikely to be contributing to the DSB repair profile, and instead both NHEJ and SCC contribute to the increased NHEJ/SCC observed for *ngg1*Δ (Figure 5.9).

5.2.8 Deletion of *ngg1*$^{+}$ does not affect the cell cycle during the DSB assay

In the DSB assay *ngg1*Δ demonstrated reduced repair by HR and increased repair by NHEJ and SCC compared to wild-type. A similar DSB repair profile was observed for *gcn5*Δ and *ada2*Δ. In yeast, DSB repair pathway choice is cell cycle regulated. HR is normally restricted to the S and G2 phases of the cell cycle where a sister chromatid can provide a homologous template for repair. In contrast NHEJ can occur in G1 (Aylon *et al.*, 2004; Ferreira and Cooper, 2004; Ira *et al.*, 2004). If loss of Gcn5 HAT module function affected cell cycle progression this could indirectly affect DSB repair pathway choice.

FACS analysis was used to analyse the cell cycle phase of wild-type and *ngg1*Δ cells during the DSB assay. Prior to DSB induction the majority of wild-type and *ngg1*Δ cells had a 2C DNA content (Figure 5.10.A-B, 0 hours). The same was observed following the removal of thiamine (Figure 5.10.A-B, 2 hours and 4 hours), and at time points at which Prudden *et al.* (2003) showed DSB induction and processing to occur in a wild-type background (Figure 5.10.A-B, 20 hours to 32 hours). This suggests Ngg1 does not greatly impact on cell cycle progression during the DSB assay.

Figure 5.10

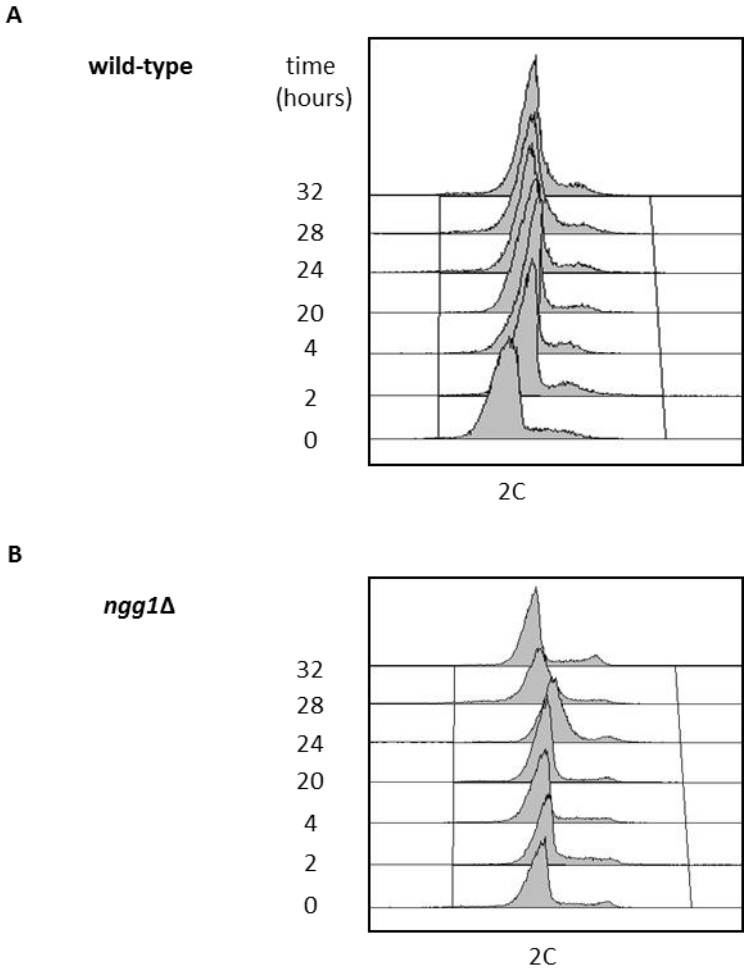


Figure 5.10 The majority of *ngg1*Δ cells are in G2 at the time of DSB induction.

FACS analysis of samples of **(A)** wild-type and **(B)** *ngg1*Δ cells subjected to the DSB assay. Samples were taken at 0 hours, 2 hours, 4 hours, 20 hours, 24 hours, 28 hours and 32 hours following DSB induction.

5.2.9 A redundant role for *gcn5*$^{+}$ in suppressing DSB sensitivity

It is difficult to study the role of HATs in DSB repair because of the functional redundancy which exists between them (Wang *et al.*, 2012). Therefore the effect of *gcn5*Δ on the bleocin sensitivity of other HATs and members of HAT complexes was investigated. The HAT deletion strains were subjected to a serial dilution assay and deletion of *gcn5*$^{+}$ was found to increase the DSB sensitivity of many of these strains (Figure 5.11).

*nto1*Δ, *hat1*Δ and *yaf9*Δ were not bleocin sensitive. In addition to compromising *nto1*Δ growth under control conditions *gcn5*Δ in these backgrounds resulted in greater DSB sensitivity than observed for *gcn5*Δ alone. *naa40*Δ, *eaf6*Δ, *eaf7*Δ and *nrc1*Δ were mildly bleocin sensitive. gcn5Δ compromised *nrc1*Δ growth under control conditions. *gcn5*Δ in these backgrounds also resulted in greater DSB sensitivity than observed for any of the parental strains. *gcn5*Δ did not affect the DNA damage sensitivity of *elp3*Δ or *rtt109*Δ (Figure 5.11). These findings strongly suggest that HATs function redundantly to promote genome stability in response to DNA damage.

Figure 5.11

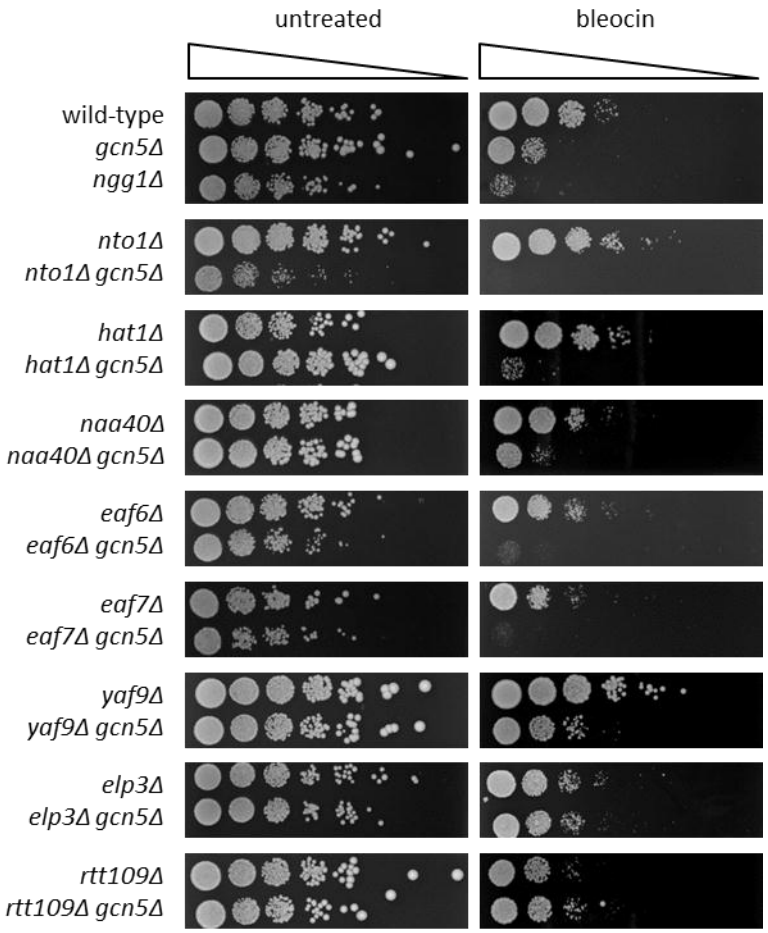


Figure 5.11 Deletion of *gcn5*$^{+}$ increases the DSB sensitivity of other HAT gene deletion strains

Fivefold serial dilutions of wild-type, *spd1*Δ, *gcn5*Δ, *ngg1*Δ, *nto1*Δ, *nto1*Δ *gcn5*Δ, *hat1*Δ, *hat1*Δ *gcn5*Δ, *naa40*Δ, *naa40*Δ *gcn5*Δ, *eaf6*Δ, *eaf6*Δ *gcn5*Δ, *eaf7*Δ, *eaf7*Δ *gcn5*Δ, *yaf9*Δ, *yaf9*Δ *gcn5*Δ, *nrc1*Δ, *nrc1*Δ *gcn5*Δ, *elp3*Δ, *elp3*Δ *gcn5*Δ, *rtt109*Δ and *rtt109*Δ *gcn5*Δ were spotted onto YE6S and YE6S + 0.2 µg/ml bleocin. Serial dilutions were performed using auxotrophic strains. Some of the data presented in this figure has been published in Pai *et al.* (2014).

5.3 DISCUSSION

The results presented in this chapter support a role for the Gcn5 HAT module in promoting efficient HR by promoting nucleotide synthesis. The results are also consistent with the role for the Gcn5 HAT module in promoting HR through chromatin remodelling at the break site as proposed by (Pai *et al.*, 2014). Furthermore a role for nucleotide synthesis is predicted in DSB repair pathway choice and requires further investigation.

5.3.1 A role for the Gcn5 HAT module in DNA damage-induced nucleotide synthesis

Gcn5 HAT module gene deletion strains were sensitive to DSBs (Figure 5.2.A and Figure 5.4.A) and had depleted nucleotide pools both in the presence and absence of DSB (Figure 5.5.A-B). The DNA damage sensitivity of these strains was suppressed by two methods predicted to increase cellular nucleotide pools. Firstly by deleting *spd1*$^{+}$ to release RNR inhibition (Figure 5.2.A and Figure 5.4.A), and secondly by providing a salvage pathway which allows cells to take up and utilise nucleosides added to the media (Figure 5.6). This evidence strongly supports a role for the Gcn5 HAT module in DNA damage-induced nucleotide synthesis. However, the exact mechanism remains elusive. Deletion of *ngg1*$^{+}$ had no detectable effect on RNR protein levels (Figure 5.7). Additionally *ngg1*$^{+}$ was not required for Cdt2 induction in response to DSBs which is required for the degradation of the RNR inhibitor Spd1 (Figure 3.18 and Figure 3.19.A-B).

The DSB sensitivity of Gcn5 HAT module gene deletion strains (Figure 5.2.A and Figure 5.4.A) confirms previous observations for *gcn5*Δ (Pai *et al.*, 2014). This DSB sensitivity would be expected in a strain exhibiting reduced nucleotide pools as nucleotide synthesis is required for efficient gap filling during HR (Moss *et al.*, 2010). This DSB sensitivity appears to be specific to Gcn5 HAT module gene deletion strains as SAGA SPT domain mutants

*spt3*Δ and *spt8*Δ and DUB domain mutant *sgf73*Δ were not identified as DSB sensitive (Appendix V). This supports the functional independence of SAGA complex modules (Lee *et al.*, 2011).

The mechanism by which Gcn5 HAT module promotes nucleotide synthesis remains unclear. The DNA damage checkpoint promotes nucleotide synthesis in response to DNA damage (Huang *et al.*, 1998; Liu *et al.*, 2005; Moss *et al.*, 2010), however *gcn5*Δ cells proficiently arrest in response to DSBs (Deegan, 2012).

In *S. cerevisiae* The SAGA complex is required for transcription of *RNR3* following MMS-induced DNA damage (Zhang *et al.*, 2008). Deletion of *SPT3* or *SPT8* encoding SAGA complex SPT domain components prevented recruitment of TBP to the *RNR3* promoter and had a large effect on mRNA levels. Deletion of *GCN5*, *ADA2* or *NGG1* encoding HAT domain components also decreased *RNR3* expression by 40%. Although TBP recruitment was not affected by loss of HAT domain function, downstream RNAPII recruitment was compromised. This suggested that both histone acetylation and TBP recruitment are both important for *RNR3* expression. *gcn5*Δ *spt3*Δ had a greater effect on *RNR3* expression than either of the single deletion strains.

Previous studies in *S. pombe* and *S. cerevisiae* have monitored changes in RNR expression following DNA damage at the mRNA level. It is possible that changes in transcription of *cdc22*$^{+}$ and *suc22*$^{+}$ in response to bleocin are not translated to the protein level or are masked by the high levels of RNR protein in S phase cells within the sample population. However, it is also possible that DSB induction does not affect RNR levels in *S. pombe*. *cdc22*$^{+}$ is under control of the MBF transcription factor which is activated by the DNA replication checkpoint through Cds1 phosphorylation of the MBF inhibitor Yox1 (Gomez-Escoda *et al.*, 2011).

However, a recent study by Ivanova *et al.* (2013) demonstrated that MBF-dependent transcription was inhibited by the activation of the DNA damage checkpoint through Chk1 phosphorylation of the MBF component Cdc10 resulting in its release from target genes.

In *S. pombe* Gcn5 plays an important role in the transcription of stress response genes. Johnsson *et al.* (2006) performed microarray analysis on wild-type and *gcn5*Δ strains. In rich media *gcn5*Δ altered the expression of less than 1% of genes by more than two fold compared to wild-type. However, under KCl stress, *gcn5*Δ is important for the expression of a subset of stress response genes and subsequently conferred sensitivity to KCl as well as to other stress conditions including heat shock and $CaCl_2$.

A role for Gcn5 in stress adaptation is conserved in other yeast species and dependent on Gcn5 HAT activity (Xue-Franzen *et al.*, 2010). In this respect it would be important to investigate whether the Gcn5 HAT module is required for expression of genes which respond to DNA damage in *S. pombe* including additional genes involved in DNA damage-induced nucleotide synthesis. It would also be important to confirm that Gcn5 HAT activity is required for efficient nucleotide synthesis.

5.3.2 A role for the Gcn5 HAT module in DSB repair pathway choice

In addition to exhibiting DSB sensitivity, *ngg1*Δ, *gcn5*Δ and *ada2*Δ strains all demonstrated a significant switch in DSB repair pathway choice, as observed in the DSB assay. *ngg1*Δ, *gcn5*Δ and *ada2*Δ strains had significantly reduced levels of GC compared to wild-type but this was not associated with increased levels of failed HR (Figure 5.2.B, Figure 5.4.B). Instead significantly increased levels of NHEJ and SCC were observed (Figure 5.8.A). This was not an artefact of reduced DSB induction in an *ngg1*Δ background (Figure 5.9) or an indirect effect of an altered cell cycle in an *ngg1*Δ background (Figure 5.10.A-B).

In yeast, DSB repair pathway choice is cell cycle regulated and therefore changes in the cell cycle progression may affect the balance between HR and NHEJ (Aylon *et al.*, 2004; Ferreira and Cooper, 2004; Ira *et al.*, 2004). The normal cell cycle distribution of *ngg1*Δ cells during the DSB assay is supported by the observations of (Johnsson *et al.*, 2006) showing *gcn5*Δ to have a similar doubling time to wild-type under exponential growth conditions in rich media.

During the writing of this thesis an independent study in the Humphrey laboratory proposed a role for *S. pombe* Gcn5 and Set2-dependent modification of H3K36 in determining repair pathway choice (Pai *et al.*, 2014). The model proposed that Gcn5-dependent H3K36 acetylation results in open chromatin, increased DSB resection and HR. Set2-dependent H3K36 methylation results in closed chromatin, reduced DSB and promotes NHEJ (Figure 5.1). As Ngg1, Ada2 and Sgf29 promote Gcn5 HAT activity (Balasubramanian *et al.*, 2002; Bian *et al.*, 2011), the results presented in this chapter provide further evidence to support the role of H3K36 modification in repair pathway choice.

Nucleotide synthesis is required for efficient post synaptic gap filling during HR. However the Gcn5 HAT deletion strains did not show increased levels of failed HR in the DSB assay compared to wild-type. Therefore the relationship between the DSB sensitivity of *ngg1*Δ and *gcn5*Δ strains and the reduced nucleotide pools in these backgrounds is unclear. It seems likely that there would be greater demand for nucleotides for efficient HR repair when multiple DSBs are inflicted by bleocin compared to a single HO-induced DSB. Modification of H3K36 is cell cycle regulated (Pai *et al.*, 2014). Disruption of this regulation allowing NHEJ during S phase would also be highly toxic to the cell.

5.3.3 Deletion of *spd1*$^+$ suppresses the HR defect of Gcn5 HAT module deletion strains

In addition to suppressing DSB sensitivity, *spd1*Δ partially suppressed the switch in repair pathway choice observed in *ngg1*Δ, *gcn5*Δ and *ada2*Δ backgrounds (Figure 5.2.B and Figure 5.4.B). Interestingly, although the levels of both NHEJ and SCC are significantly elevated in an *ngg1*Δ strain, *spd1*Δ appeared only to decrease the levels of NHEJ (Figure 5.8.B). A hypothesis would be that nucleotide levels regulate DSB repair pathway choice between HR and NHEJ such that HR is promoted when sufficient nucleotides are available for post synaptic gap filling during HR.

It would be important to confirm the switch in DSB repair mechanism is mediated by increased nucleotide pools following deletion of *spd1*$^+$ in an *ngg1*Δ background. To do this a DSB assay strain could be constructed containing the genes encoding hENT1 and *dm*NK (Griffiths *et al.*, 1997; Johansson *et al.*, 1999; Munch-Petersen *et al.*, 1998). This would allow cellular nucleotide pools during the DSB assay to be changed by the addition of nucleosides to the media, thereby facilitating the analysis of nucleotide levels on repair pathway choice more directly.

The initiation of DSB resection represents a commitment to HR (Kakarougkas and Jeggo, 2014; Shibata *et al.*, 2014). Pai *et al.* (2014) showed that a *gcn5*Δ strain had reduced Rad11 and Rad51 foci following bleomycin treatment, suggesting reduced resection. It is predicted that, in addition to Gcn5 acetylation of H3K36 promoting DSB resection by relaxing chromatin, Gcn5-dependent nucleotide synthesis also promotes DSB resection. This may be through an indirect effect on chromatin at the break site or through regulation of the activity of Ctp1 and MRN. In *S. cerevisiae* resection is regulated during the cell cycle by CDK-dependent phosphorylation of Sae2 (Huertas *et al.*, 2008).

The following model is proposed: in response to DSBs in a wild-type background nucleotide synthesis is up-regulated. This promotes DSB resection resulting in a commitment to HR. In a Gcn5 HAT module gene deletion background DSB-induced nucleotide synthesis is reduced compared to wild-type. This inhibits DSB resection and promotes NHEJ. Conversely deletion of *spd1*$^{+}$ in a Gcn5 HAT module gene deletion background partially suppresses the defect in DSB-induced nucleotide synthesis and therefore promotes DSB resection and HR.

This model is supported by significantly decreased NHEJ/SCC and significantly increased GC in a *spd1*Δ deletion background compared to wild-type (Figure 3.20). Deletion of *spd1*$^{+}$ promotes RNR activity (Hakansson *et al.*, 2006a). Reduced NHEJ/SCC and increased GC was also observed following deletion of *spd1*$^{+}$ in *arp42*Δ, *liz1*Δ and V2-53D9 backgrounds (Figure 3.21.D-F). Conversely *rad3*Δ and *rad26*Δ, which have compromised nucleotide synthesis (Moss *et al.*, 2010), showed small but significant increases in NHEJ/SCC compared to wild-type (Figure 4.3). Furthermore, a mutant allele of *rad3* exhibited a larger significant increase in the levels of NHEJ/SCC and reduced levels of HR compared to wild-type (Humphrey laboratory, unpublished results).

However, this prediction is contradicted as no increase in NHEJ is observed in a temperature sensitive *cdc22-m45* background at the semi-permissive temperature when RNR activity is impaired (Moss *et al.*, 2010; Singer and Johnston, 1985). *rad3*Δ, *rad26*Δ, *cdt2*Δ and *ddb1*Δ strains with compromised damage-induced nucleotide synthesis show high levels of failed HR which can be suppressed by deleting *spd1*Δ supporting a predominantly post-synaptic role for nucleotide synthesis in these backgrounds. It is therefore possible that Spd1 may promote HR through an alternative mechanism.

Figure 5.12

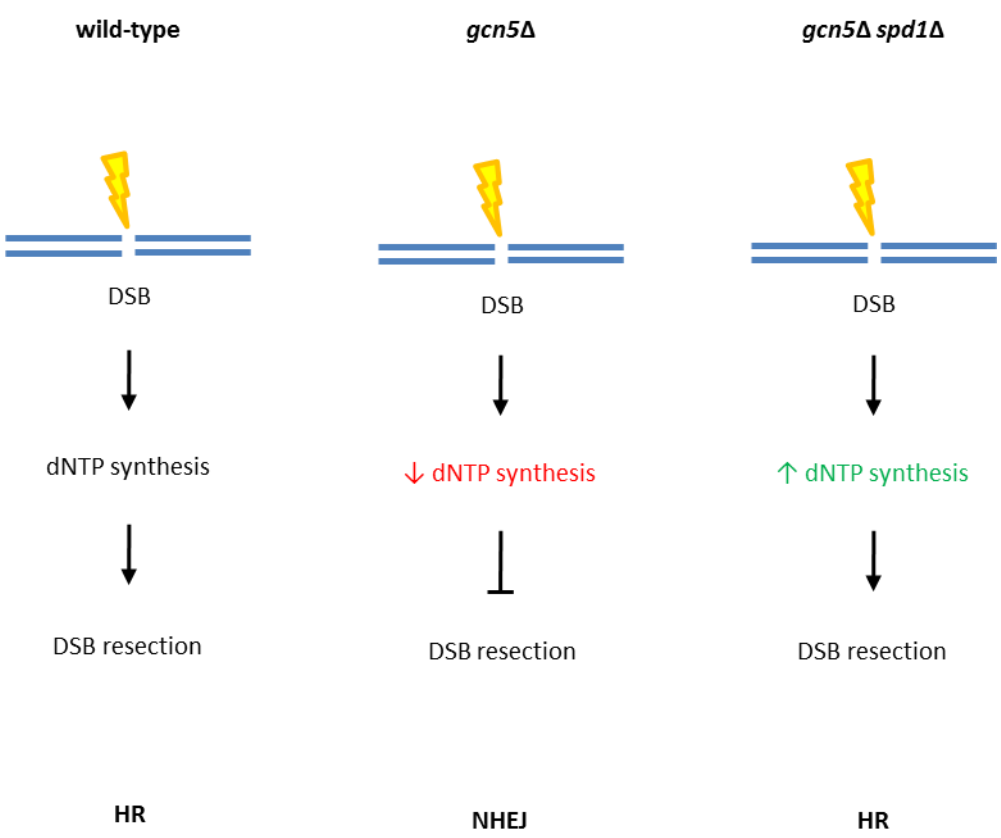


Figure 5.12 Model of DSB repair pathway regulation by nucleotide synthesis

Following DSBs in a wild-type background nucleotide synthesis is up regulated. It is hypothesised that this promotes DSB resection resulting in a commitment to HR. In a Gcn5 HAT module gene deletion background DSB-induced nucleotide synthesis is reduced compared to wild-type. It is hypothesised that this inhibits DSB resection and promotes NHEJ. Conversely deletion of *spd1*$^{+}$ in a Gcn5 HAT module gene deletion background is predicted to suppress the defect in DSB-induced nucleotide synthesis and therefore promotes DSB resection and HR.

5.3.4 Gcn5 and other HATs cooperate to suppress DSB sensitivity

It is difficult to study the role of HATs in DSB repair because of the functional redundancy which exists between them (Wang *et al.*, 2012). In this study it was demonstrated that Gcn5 cooperates with other HAT complexes to suppress sensitivity to DSBs (Figure 5.11). This supports and extends previous observations of roles for these HATs in DSB repair.

Firstly *gcn5*Δ increased the DSB sensitivity of *nto1*Δ. *S. cerevisiae* Nto1 was identified as a component of the NuA3 HAT complex of which Sas3 is the catalytic subunit (Taverna *et al.*, 2006). The *S. pombe* homologue of *S. cerevisiae* Sas3 is Mst2. Wang et al. (2012) previously showed that in *S. pombe* Gcn5 and Mst2 redundantly acetylate H3K14 at sites of DNA damage and that this is required for checkpoint activation. They proposed that H3K14 acetylation may regulate chromatin structure to allow recruitment of Rad3 and subsequent H2A phosphorylation.

Secondly *gcn5*Δ increased the DSB sensitivity of *hat1*Δ. Hat1 acetylates new H4 on K5 and K12 prior to its deposition onto DNA (Tong *et al.*, 2012). *S. pombe hat1*Δ strains are sensitive to MMS suggesting a role in DNA repair (Benson *et al.*, 2007). Human HAT1 is recruited to DSB where it interacts with RAD50 and RAD51 and facilitates efficient HR through histone turnover (Yang *et al.*, 2013).

*gcn5*Δ also increased the DSB sensitivity of *eaf6*Δ, *eaf7*Δ and *yaf9*Δ encoding members of the NuA4 HAT complex (Doyon and Cote, 2004; Mitchell *et al.*, 2008) and *naa40*Δ which co-translationally acetylates H2A and H4 (Hole *et al.*, 2011).

5.4 SUMMARY

In this chapter the role of Ngg1 and other components of the Gcn5 HAT module in nucleotide synthesis and DSB repair was investigated. The results presented provide evidence that:

- The Gcn5 HAT module suppresses DSB sensitivity by promoting nucleotide synthesis.
- The Gcn5 HAT module promotes nucleotide synthesis independently of Cdt2 induction to promote Spd1 degradation and independently of an effect on RNR protein levels.
- The Gcn5 HAT module regulates DSB repair pathway choice between HR and NHEJ by promoting HR. This supports the model proposed by Pai *et al.* (2014).
- Nucleotide pools and Spd1 have predicted roles in DSB repair pathway choice.

Chapter 6 General Discussion

This thesis presents a study to identify and characterise new genes important for HR through roles in damage-induced nucleotide synthesis in *S. pombe*. Such genes are predicted to be essential for the maintenance of genome stability. Candidates were selected using a quantitative, colony-based screen to identify gene deletion strains whose DSB sensitivity was suppressed by deleting the RNR inhibitor *spd1*$^{+}$ to promote nucleotide synthesis (Chapter 3). As a result of the screen, suppression of DSB sensitivity by deletion of *spd1*$^{+}$ was confirmed for 19 gene deletion strains. The genes identified included *ddb1*$^{+}$, *cdt2*$^{+}$, *rad3*$^{+}$ and *csn1*$^{+}$ which have known roles in damage-induced nucleotide synthesis and therefore validate the screen approach (Liu *et al.*, 2005; Moss *et al.*, 2010). The screen led to the further characterisation of a role for the DNA damage checkpoint promoting damage-induced nucleotide synthesis and DSB resection (Chapter 4) and of a role for the Gcn5 HAT protein module in promoting nucleotide synthesis and HR (Chapter 5).

This study has successfully identified a role for a number of genes in DNA damage-induced nucleotide synthesis. These genes can be placed into functional groups based on analysis of the role of these genes in DSB repair (Table 6.1, Groups 1 to 5). The study has also identified a number of genes for which a role in nucleotide synthesis could not be confirmed. However, deletion of *spd1*$^{+}$ can suppress the DSB sensitivity resulting from deletion of these genes (Table 6.1, Groups 6 and 7). The groups of genes identified are discussed in the following sections.

Table 6.1 Summary of Results

	Gene deletion	DSB sens-itive	DSB sensitivity suppressed by *spd1*Δ	DSB repair profile of *sens*Δ strain compared to wild-type	DSB repair profile of *sens*Δ *spd1*Δ compared to *sens*Δ	Damage-induced nucleotide pools vs wild-type	Damage-induced Cdt2 vs wild-type
1	*ddb1*Δ	yes	yes	↓GC ↑Ch^{16} loss	↑GC, ↓Ch^{16} loss	no induction	significant increase
	*cdt2*Δ			↓GC ↑LOH	↑GC		-
2	*csn1*Δ	yes	partially	no change	↑GC ↓Ch^{16} loss ↓NHEJ/SCC ↓LOH	no induction	significant increase ± DSBs
3	*rad3*Δ	yes	partially	↓GC ↑Ch^{16} loss ↑LOH ↑NHEJ/SCC	↑GC ↓Ch^{16} loss ↓LOH ↓NHEJ/SCC	no induction	no induction
	*rad26*Δ				↑GC, ↓LOH	not tested	
4	*rad17*Δ	yes	no	↓GC, ↓Ch^{16} loss, ↑LOH	no change	not tested	no induction
	*rad9*Δ						
	*rad1*Δ						
	*hus1*Δ						
5	*ngg1*Δ	yes	partially	↓GC ↑NHEJ ↑SCC	↑GC ↓NHEJ	reduced	wild-type
	*gcn5*Δ						not tested
	*ada2*Δ					not tested	
	*sgf29*Δ			not tested	not tested		
6	*arp42*Δ	yes	partially	↓GC ↑NHEJ/SCC	↑GC ↓NHEJ/SCC	↓dCTP	wild-type
	V2-53D9					not reduced	
	*liz1*Δ						
7	*pmk1*Δ	yes	partially	↓Ch^{16} loss	no change	↓dCTP	wild-type
	*trm112*Δ		yes	no change		not reduced	reduced
	*swi3*Δ			↑NHEJ/SCC	↓LOH		increase ± DSBs
8	*rpp202*Δ	no	yes	not tested	not tested	reduced	wild-type
	*atp2*Δ	yes				↓dCTP	
	*vps16*Δ					not reduced	
	*trt1*Δ		partially				

Text in grey indicates the data was obtained from Moss *et al.* (2010).

6.1 A role for Csn1 in promoting nucleotide synthesis

Csn1 is a component of the COP9 signalosome previously shown to be required for Spd1 degradation by activating the Ddb1-Cul4^{Cdt2} complex to promote Spd1 ubiquitination (Liu *et al.*, 2003; Mundt *et al.*, 2002). The results presented in this thesis support a role for Csn1 in promoting nucleotide synthesis by this mechanism. A role is also predicted for Csn1 in promoting the degradation of Cdt2. Unexpectedly a *csn1*Δ strain did not show compromised DSB repair by HR. This contrasts with the DSB sensitivity of *csn1*Δ and the HR defect of *ddb1*Δ and *cdt2*Δ strains (Moss *et al.*, 2010). A *csn1*Δ *spd1*Δ strain had a hyper-recombinant phenotype similar to *mrc1*Δ and *cds1*Δ replication checkpoint deletion strains (Blaikley *et al.*, 2014). The relationship between these genes could be further tested by epistasis analysis.

6.2 A role for the DNA damage checkpoint promoting damage-induced nucleotide synthesis and DSB resection

In this study distinct roles were identified for the DNA damage checkpoint in suppressing LOH during HR. *rad3*$^+$, *rad26*$^+$, *rad17*$^+$, *rad9*$^+$, *rad1*$^+$ and *hus1*$^+$ were required for DNA damage-induced nucleotide synthesis through Cdt2 induction to promote Spd1 degradation. This extends previous observations and demonstrates the importance of the DNA damage checkpoint in maintaining genome stability (Blaikley *et al.*, 2014; Moss *et al.*, 2010).

As expected the HR repair defect of *rad3* and *rad26* deletion strains was partially suppressed by *spd1*$^+$ deletion. However, the HR repair defect of *rad17* and 9-1-1 complex gene deletion strains was not suppressed. An additional role was confirmed for Rad17 and the 9-1-1 complex in preventing LOH by promoting Exo1-dependent DSB resection. Subsequent studies have provided evidence that this role is conserved in *S. pombe* at collapsed replication forks (Tsang *et al.*, 2014), in *S. cerevisiae* at uncapped telomeres and *in vitro* with the human homologues (Ngo *et al.*, 2014). It would be interesting in future studies to elucidate the mechanism by which the 9-1-1 complex promotes Exo1-dependent resection.

Related to the findings of this study, Tsang *et al.* (2014) demonstrated that Rad3 inhibits Exo1-dependent resection at collapsed replication forks. In this thesis a role was also identified for Rad3 in inhibiting Exo1 independent extensive resection predicted to be mediated by Rqh1-Dna2. *S. cerevisiae* Mec1, the homologue of *S. pombe* Rad3, is required for the inhibitory phosphorylation of Exo1 (Morin *et al.*, 2008) and also phosphorylates Dna2 in response to DNA damage (Chen *et al.*, 2011). It would be interesting to investigate whether this is a conserved response in *S. pombe*, as this would be consistent with the genetic data.

6.3 A role for Ngg1 and the Gcn5 HAT module promoting nucleotide synthesis and HR

This study identified a role for the *S. pombe* Gcn5 HAT module, consisting of Gcn5, Ngg1, Ada2 and Sgf29, in suppressing DSB sensitivity by promoting nucleotide synthesis. This was independent of an effect on Cdt2 induction or RNR protein levels and contrasts with the requirement of *S. cerevisiae* Gcn5 for the transcription of *RNR3* following DNA damage (Zhang *et al.*, 2008). Gcn5 has a conserved role in the transcription of stress response genes in *S. pombe* and in *S. cerevisiae* (Johnsson *et al.*, 2006; Xue-Franzen *et al.*, 2010). Further studies should utilise microarray analysis to investigate whether *S. pombe* Gcn5 is promoting the expression of other genes required for DNA damage-induced nucleotide synthesis. In human cells the HAT Tip60 is required for the recruitment of RNR to DSBs (Niida *et al.*, 2010). It would be interesting to investigate by ChIP analysis whether *S. pombe* RNR is similarly recruited to DSB and whether this is promoted by Gcn5.

In this study the Gcn5 HAT module was also found to regulate DSB repair pathway choice by promoting HR. Gcn5 HAT module gene deletion strains had reduced levels of DSB repair by HR associated with increased levels of repair by NHEJ. This supports the model proposed by Pai *et al.* (2014) in which Gcn5-dependent H3K36 acetylation at DSBs results in open chromatin, increased DSB resection and HR. DSB resection is recognised as a key step in commitment to HR (Kakarougkas and Jeggo, 2014; Shibata *et al.*, 2014). Pai *et al.* (2014)

showed that a *gcn5*Δ strain had reduced Rad11 and Rad51 foci following DSBs, suggesting reduced resection. A role for Gcn5 in promoting DSB resection could be confirmed with the SSA assay successfully utilised in Chapter 4.

Surprisingly, deletion of *spd1*$^{+}$ in a Gcn5 HAT module deletion background also promoted HR. This predicts a novel role for nucleotide pools in regulating DSB repair pathway choice between HR and NHEJ such that HR is promoted when sufficient nucleotides are available for post synaptic gap filling during HR. The following model is proposed: in response to DSBs in a wild-type background nucleotide synthesis is up regulated. This promotes DSB resection resulting in a commitment to HR. In a Gcn5 HAT module gene deletion background DSB-induced nucleotide synthesis is impaired. This inhibits DSB resection and promotes NHEJ. Conversely deletion of *spd1*$^{+}$ in a Gcn5 HAT module gene deletion background partially suppresses the defect in DSB-induced nucleotide synthesis and therefore promotes DSB resection and HR (Figure 5.12). Nucleotide synthesis may promote DSB resection through an indirect effect on chromatin at the break site or by regulating Ctp1 and MRN activity.

Other groups of deletion strains in Table 6.1 provide evidence to support this model. For example *rad3*Δ and *rad26*Δ which have compromised DSB-induced nucleotide synthesis (Moss *et al.*, 2010) showed small but significant increases in NHEJ/SCC compared to wild-type. Furthermore deletion of *spd1*$^{+}$ in *arp42*Δ, *liz1*Δ and V2-53D9 backgrounds promotes DSB repair by HR and reduces NHEJ. However, *rad3*Δ, *rad26*Δ, *cdt2*Δ and *ddb1*Δ strains with compromised damage-induced nucleotide synthesis show high levels of failed HR which can be suppressed by deleting *spd1*Δ supporting a predominantly post-synaptic role for nucleotide synthesis in these backgrounds. In addition no increase in NHEJ is observed in a

temperature sensitive *cdc22-m45* background when RNR activity is impaired (Moss *et al.*, 2010; Singer and Johnston, 1985).

To test this model it would be important to confirm firstly that deletion of *spd1*$^{+}$ is not indirectly affecting DSB repair by altering cell cycle progression as HR is cell cycle regulated (Huertas *et al.*, 2008; Ira *et al.*, 2004). Secondly it must be independently confirmed that increased nucleotide pools promote HR. The nucleotide salvage pathway constructs presented in Chapter 4 could be utilised in the DSB assay to assess the effect of nucleotides pools on DSB repair more directly (Griffiths *et al.*, 1997; Johansson *et al.*, 1999; Munch-Petersen *et al.*, 1998). However this presents technical difficulties as the assay requires several nucleobases to be added to the media in excess. Alternatively the effect of nucleotide pools on the formation RPA and Rad51 foci following IR induced DSBs could be observed by microscopy as an indicator of DSB repair by HR.

6.4 Deletion of *spd1*$^{+}$ promotes HR in *arp42*Δ, *liz1*Δ and V2-53D9 backgrounds independently of nucleotide synthesis

*arp42*Δ, *liz1*Δ, and V2-53D9 deletion strains were all DSB sensitive and showed, to varying degrees, a switch in DSB repair from HR to NHEJ/SCC in the DSB assay. This was similar to the observations for Gcn5 HAT module deletion strains. However, *arp42*Δ, *liz1*Δ, and V2-53D9 strains did not show substantially reduced damage-induced nucleotide synthesis and so were not selected for more detailed analysis in this study. Despite proficient nucleotide synthesis, *spd1*Δ in these backgrounds suppressed the DSB sensitivity of these strains and promoted HR as observed for the Gcn5 HAT deletion strains. Further validation is required to confirm that these results are not artefacts of an altered cell cycle. Subsequently two models could explain these results. Firstly further elevation of nucleotide pools could alter DSB repair

pathway choice as predicted for the Gcn5 HAT module. Secondly deletion of *spd1*$^+$ may promote HR by an alternative mechanism.

6.5 Deletion of *spd1*$^+$ suppresses DSB sensitivity in *swi3*Δ, *pmk1*Δ, and *trm112*Δ backgrounds independently of nucleotide synthesis

Deletion of *spd1*$^+$ suppressed the DSB sensitivity of *swi3*Δ, *pmk1*Δ, and *trm112*Δ strains. However this was independent of reduced nucleotide pools in these backgrounds, as observd by HPLC analyasis and independent of an effect on HR in the DSB assay. Swi3 is important for the stabilisation of replication forks in response to replication stress (Noguchi *et al.*, 2004; Shimmoto *et al.*, 2009; Tanaka *et al.*, 2010) and so DNA damage during S phase would be predicted to have catastrophic effects in a *swi3*Δ background. Recently a role was identified for Spd1 in promoting replication stress independently of RNR regulation (Fleck *et al.*, 2013). Deletion of *spd1*$^+$ may therefore enable cells to cope with replication stress caused by DNA damage in the absence of Swi3. It would be interesting to investigate roles for *pmk1*$^+$, and *trm112*$^+$ in DNA replication.

6.6 Other candidates identified

Deletion of *spd1*$^+$ suppressed the DSB sensitivity of *rpp202*Δ, *atp2*Δ, *vps16*Δ and *trt1*Δ strains. Further analysis is required to confirm a role for these genes in DSB repair.

The screen also identified a number of deletion strains with increased DSB sensitivity following deletion of *spd1*$^+$ (Appendix V). Analysis of these strains was outside the scope of this thesis, however it would interesting to investigate the cause of this phenotype. As excessive nucleotide levels affect DNA polymerase fidelity leading to increased mutation rates (Chabes *et al*., 2003) a prediction may be that these gene deletion strains already have elevated nucleotide levels or compromised maintenance of genome stability independently of nucleotide synthesis.

6.7 Investigating DSB repair in the context of chromatin

The DSB assay utilised in this thesis allowed DSB repair events at a site-specific DSB to be distinguished and quantified in different genetic backgrounds. Generating the DSB within the context of a non-essential minichromosome also allowed the study of failed repair events, which would normally be fatal to the cell. However this genetic approach could be complemented by biochemical techniques, for example ChIP, allowing analysis of the recruitment of repair proteins to the DSB, in addition to analysis of the chromatin structure at the DSB which represents a barrier to DSB detection and repair (Price and D'Andrea, 2013).

Using Micrococcal nuclease (MNase) digestion it has been demonstrated that *S. pombe gcn5*$^{+}$ is required for a global increase in chromosome accessibility following bleocin treatment (Pai *et al.*, 2014). Furthermore in *S. cerevisiae* ChIP analysis was used to demonstrate that that *S. cerevisiae* Gcn5 is recruited to a HO-induced DNA DSB at the *MAT* locus during HR repair (Tamburini and Tyler, 2005).

In human cells Zinc Finger Nucleases designed to target and cleave specific genomic loci have been used in combination with ChIP analysis to elucidate the chromatin remodelling events which occur following a DSB (Ayrapetov *et al.*, 2014; Urnov *et al.*, 2005; Xu *et al.*, 2012). PARP dependent loading of the kap-1/HP1/suv39h1 complex at the DSB allows suv39h1 to methylate H3K9. This leads to the transient formation of heterochromatin (Ayrapetov *et al.*, 2014). Tip60 binding to H3K9 is required for activation of its HAT activity resulting in H4 and ATM acetylation (Sun *et al.*, 2009). Furthermore, p400 dependent H2AZ exchange onto chromatin occurs at DSBs in regions with low levels of H2AZ resulting in chromatin relaxation. H2AZ exchange is required for Tip60 dependent acetylation of H4 and the recruitment of BRCA1 and Ku70-Ku80 (Xu *et al.*, 2012).

It would be interesting to investigate the effect of deletion of *S. pombe gcn5*$^{+}$ as well as nucleotide pools on the changes in chromatin structure which occur at a DSB and further the impact on the recruitment of DSB repair proteins by ChIP analysis. This analysis requires rapid and synchronous DSB induction which could potentially be achieved using the urg-HO expression system utilised in this thesis (Watson *et al.*, 2011).

Techniques have been developed in *S. cerevisiae* for the detection and analysis of UV induced cyclobutane pyrimidine dimers (CPDs) and their subsequent repair by nucleotide excision repair on a genome wide scale (Teng *et al.*, 2011). This is important to identify differences in repair between genomic loci and to correlate these findings with differences in chromatin structure. Following UV irradiation the DNA is sheered into 200-800 bp fragments. Immunoprecipitation is performed with an antibody which detects CPDs. The genomic location of the CPDs can then be analysed by microarray analysis and refined using mathematical modelling (Teng *et al.*, 2011). This technique can be combined with ChIP-on-Chip analysis of DNA damage induced changes in chromatin structure and recruitment of repair proteins.

A difficulty in adapting the above technique for the analysis of DSB repair is the detection of the sites of DSBs. Iacovoni *et al.* (2010) developed a system to allow the simultaneous study of repair at multiple DSB located within different chromatin contexts distributed across the human genome. The restriction enzyme AsiSI was expressed in human cell lines fused to a modified oestrogen receptor ligand binding domain. Following the addition of 4-OHT the AsiSI fusion protein rapidly translocates to the nucleus where it cleaves an 8 bp recognition sequence in approximately 150 locations to generate DNA DSBs. The knowledge of the exact DNA DSB locations allows the analysis of recruitment of proteins involved in DNA repair and chromatin remodelling to these sites can be monitored over time using ChIP-Seq. This

method was used to demonstrate that transcriptionally active chromatin is preferentially repaired by HR (Aymard *et al.*, 2014). Adaption of the system for use with *S. pombe* could provide insights into how *gcn5*$^{+}$ deletion and nucleotide levels impact on DSB repair at genomic loci in different chromatin regions.

References

Abbas, T., Keaton, M., and Dutta, A. (2013a). Regulation of TGF-β signaling, exit from the cell cycle, and cellular migration through cullin cross-regulation: SCF-FBXO11 turns off CRL4-Cdt2. Cell Cycle *12*, 2175-2182.

Abbas, T., Mueller, A.C., Shibata, E., Keaton, M., Rossi, M., and Dutta, A. (2013b). CRL1-FBXO11 promotes Cdt2 ubiquitylation and degradation and regulates Pr-Set7/Set8-mediated cellular migration. Mol Cell *49*, 1147-1158.

Asakawa, H., Yang, H.J., Yamamoto, T.G., Ohtsuki, C., Chikashige, Y., Sakata-Sogawa, K., Tokunaga, M., Iwamoto, M., Hiraoka, Y., and Haraguchi, T. (2014). Characterization of nuclear pore complex components in fission yeast *Schizosaccharomyces pombe*. Nucleus *5*, 149-162.

Ashton, T.M., Mankouri, H.W., Heidenblut, A., McHugh, P.J., and Hickson, I.D. (2011). Pathways for Holliday junction processing during homologous recombination in *Saccharomyces cerevisiae*. Mol Cell Biol *31*, 1921-1933.

Aylon, Y., and Kupiec, M. (2003). The checkpoint protein Rad24 of *Saccharomyces cerevisiae* is involved in processing double-strand break ends and in recombination partner choice. Mol Cell Biol *23*, 6585-6596.

Aylon, Y., Liefshitz, B., and Kupiec, M. (2004). The CDK regulates repair of double-strand breaks by homologous recombination during the cell cycle. EMBO J *23*, 4868-4875.

Aymard, F., Bugler, B., Schmidt, C.K., Guillou, E., Caron, P., Briois, S., Iacovoni, J.S., Daburon, V., Miller, K.M., Jackson, S.P., and Legube, G. (2014). Transcriptionally active chromatin recruits homologous recombination at DNA double-strand breaks. Nat Struct Mol Biol *21*, 366-374.

Ayrapetov, M.K., Gursoy-Yuzugullu, O., Xu, C., Xu, Y., and Price, B.D. (2014). DNA double-strand breaks promote methylation of histone H3 on lysine 9 and transient formation of repressive chromatin. Proc Natl Acad Sci U S A *111*, 9169-9174.

Bailleul, B., Galiegue, S., and Loucheux-Lefebvre, M.H. (1981). Adducts from the reaction of O,O'-diacetyl or O-acetyl derivatives of the carcinogen 4-hydroxyaminoquinoline 1-oxide with purine nucleosides. Cancer Res *41*, 4559-4565.

Balasubramanian, R., Pray-Grant, M.G., Selleck, W., Grant, P.A., and Tan, S. (2002). Role of the Ada2 and Ada3 transcriptional coactivators in histone acetylation. J Biol Chem *277*, 7989-7995.

Bashkirov, V.I., King, J.S., Bashkirova, E.V., Schmuckli-Maurer, J., and Heyer, W.D. (2000). DNA repair protein Rad55 is a terminal substrate of the DNA damage checkpoints. Mol Cell Biol *20*, 4393-4404.

Begley, T.J., Rosenbach, A.S., Ideker, T., and Samson, L.D. (2002). Damage recovery pathways in *Saccharomyces cerevisiae* revealed by genomic phenotyping and interactome mapping. Molecular cancer research : MCR *1*, 103-112.

Begley, U., Dyavaiah, M., Patil, A., Rooney, J.P., DiRenzo, D., Young, C.M., Conklin, D.S., Zitomer, R.S., and Begley, T.J. (2007). Trm9-catalyzed tRNA modifications link translation to the DNA damage response. Mol Cell *28*, 860-870.

Bennett, C.B., Lewis, L.K., Karthikeyan, G., Lobachev, K.S., Jin, Y.H., Sterling, J.F., Snipe, J.R., and Resnick, M.A. (2001). Genes required for ionizing radiation resistance in yeast. Nat Genet *29*, 426-434.

Benson, L.J., Phillips, J.A., Gu, Y., Parthun, M.R., Hoffman, C.S., and Annunziato, A.T. (2007). Properties of the type B histone acetyltransferase Hat1: H4 tail interaction, site preference, and involvement in DNA repair. J Biol Chem *282*, 836-842.

Beranek, D.T. (1990). Distribution of methyl and ethyl adducts following alkylation with monofunctional alkylating agents. Mutat Res *231*, 11-30.

Bermudez, V.P., Lindsey-Boltz, L.A., Cesare, A.J., Maniwa, Y., Griffith, J.D., Hurwitz, J., and Sancar, A. (2003). Loading of the human 9-1-1 checkpoint complex onto DNA by the checkpoint clamp loader hRad17-replication factor C complex in vitro. Proc Natl Acad Sci U S A *100*, 1633-1638.

Bester, A.C., Roniger, M., Oren, Y.S., Im, M.M., Sarni, D., Chaoat, M., Bensimon, A., Zamir, G., Shewach, D.S., and Kerem, B. (2011). Nucleotide deficiency promotes genomic instability in early stages of cancer development. Cell *145*, 435-446.

Bian, C., Xu, C., Ruan, J., Lee, K.K., Burke, T.L., Tempel, W., Barsyte, D., Li, J., Wu, M., Zhou, B.O., Fleharty, B.E., Paulson, A., Allali-Hassani, A., Zhou, J.Q., Mer, G., Grant, P.A., Workman, J.L., Zang, J., and Min, J. (2011). Sgf29 binds histone H3K4me2/3 and is required for SAGA complex recruitment and histone H3 acetylation. EMBO J *30*, 2829-2842.

Bianchi, V., Pontis, E., and Reichard, P. (1986). Changes of deoxyribonucleoside triphosphate pools induced by hydroxyurea and their relation to DNA synthesis. J Biol Chem *261*, 16037-16042.

Bjorklund, S., Skog, S., Tribukait, B., and Thelander, L. (1990). S-phase-specific expression of mammalian ribonucleotide reductase R1 and R2 subunit mRNAs. Biochemistry *29*, 5452-5458.

Blaikley, E.J., Tinline-Purvis, H., Kasparek, T.R., Marguerat, S., Sarkar, S., Hulme, L., Hussey, S., Wee, B.Y., Deegan, R.S., Walker, C.A., Pai, C.C., Bahler, J., Nakagawa, T., and Humphrey, T.C. (2014). The DNA damage checkpoint pathway promotes extensive resection and nucleotide synthesis to facilitate homologous recombination repair and genome stability in fission yeast. Nucleic Acids Res *42*, 5644-5656.

Blankley, R.T., and Lydall, D. (2004). A domain of Rad9 specifically required for activation of Chk1 in budding yeast. J Cell Sci *117*, 601-608.

Blier, P.R., Griffith, A.J., Craft, J., and Hardin, J.A. (1993). Binding of Ku protein to DNA. Measurement of affinity for ends and demonstration of binding to nicks. J Biol Chem *268*, 7594-7601.

Borgne, A., and Nurse, P. (2000). The Spd1p S phase inhibitor can activate the DNA replication checkpoint pathway in fission yeast. J Cell Sci *113 Pt 23*, 4341-4350.

Botuyan, M.V., Lee, J., Ward, I.M., Kim, J.E., Thompson, J.R., Chen, J., and Mer, G. (2006). Structural basis for the methylation state-specific recognition of histone H4-K20 by 53BP1 and Crb2 in DNA repair. Cell *127*, 1361-1373.

Broadus, M.R., and Gould, K.L. (2012). Multiple protein kinases influence the redistribution of fission yeast Clp1/Cdc14 phosphatase upon genotoxic stress. Mol Biol Cell *23*, 4118-4128.

Brownell, J.E., Zhou, J., Ranalli, T., Kobayashi, R., Edmondson, D.G., Roth, S.Y., and Allis, C.D. (1996). Tetrahymena histone acetyltransferase A: a homolog to yeast Gcn5p linking histone acetylation to gene activation. Cell *84*, 843-851.

Cary, R.B., Peterson, S.R., Wang, J., Bear, D.G., Bradbury, E.M., and Chen, D.J. (1997). DNA looping by Ku and the DNA-dependent protein kinase. Proc Natl Acad Sci U S A *94*, 4267-4272.

Chabes, A., Domkin, V., and Thelander, L. (1999). Yeast Sml1, a protein inhibitor of ribonucleotide reductase. J Biol Chem *274*, 36679-36683.

Chabes, A., Georgieva, B., Domkin, V., Zhao, X., Rothstein, R., and Thelander, L. (2003). Survival of DNA damage in yeast directly depends on increased dNTP levels allowed by relaxed feedback inhibition of ribonucleotide reductase. Cell *112*, 391-401.

Chabes, A., and Thelander, L. (2000). Controlled protein degradation regulates ribonucleotide reductase activity in proliferating mammalian cells during the normal cell cycle and in response to DNA damage and replication blocks. J Biol Chem *275*, 17747-17753.

Chai, B., Huang, J., Cairns, B.R., and Laurent, B.C. (2005). Distinct roles for the RSC and Swi/Snf ATP-dependent chromatin remodelers in DNA double-strand break repair. Genes Dev *19*, 1656-1661.

Chambers, A.L., Brownlee, P.M., Durley, S.C., Beacham, T., Kent, N.A., and Downs, J.A. (2012). The two different isoforms of the RSC chromatin remodeling complex play distinct roles in DNA damage responses. PLoS One *7*, e32016.

Chappell, C., Hanakahi, L.A., Karimi-Busheri, F., Weinfeld, M., and West, S.C. (2002). Involvement of human polynucleotide kinase in double-strand break repair by non-homologous end joining. EMBO J *21*, 2827-2832.

Chen, H., Lisby, M., and Symington, L.S. (2013). RPA coordinates DNA end resection and prevents formation of DNA hairpins. Mol Cell *50*, 589-600.

Chen, J., and Stubbe, J. (2005). Bleomycins: towards better therapeutics. Nat Rev Cancer *5*, 102-112.

Chen, X., Niu, H., Chung, W.H., Zhu, Z., Papusha, A., Shim, E.Y., Lee, S.E., Sung, P., and Ira, G. (2011). Cell cycle regulation of DNA double-strand break end resection by Cdk1-dependent Dna2 phosphorylation. Nat Struct Mol Biol *18*, 1015-1019.

Cope, G.A., Suh, G.S., Aravind, L., Schwarz, S.E., Zipursky, S.L., Koonin, E.V., and Deshaies, R.J. (2002). Role of predicted metalloprotease motif of Jab1/Csn5 in cleavage of Nedd8 from Cul1. Science *298*, 608-611.

Cortez, D., Guntuku, S., Qin, J., and Elledge, S.J. (2001). ATR and ATRIP: partners in checkpoint signaling. Science *294*, 1713-1716.

Cullen, J.K., Hussey, S.P., Walker, C., Prudden, J., Wee, B.Y., Dave, A., Findlay, J.S., Savory, A.P., and Humphrey, T.C. (2007). Break-induced loss of heterozygosity in fission yeast: dual roles for homologous recombination in promoting translocations and preventing de novo telomere addition. Mol Cell Biol *27*, 7745-7757.

D'Angiolella, V., Donato, V., Forrester, F.M., Jeong, Y.T., Pellacani, C., Kudo, Y., Saraf, A., Florens, L., Washburn, M.P., and Pagano, M. (2012). Cyclin F-mediated degradation of ribonucleotide reductase M2 controls genome integrity and DNA repair. Cell *149*, 1023-1034.

Daley, J.M., Gaines, W.A., Kwon, Y., and Sung, P. (2014). Regulation of DNA Pairing in Homologous Recombination. Cold Spring Harbor perspectives in biology, doi 10.1101/cshperspect.a017954 (E-published ahead of print).

Decosterd, L.A., Cottin, E., Chen, X., Lejeune, F., Mirimanoff, R.O., Biollaz, J., and Coucke, P.A. (1999). Simultaneous determination of deoxyribonucleoside in the presence of ribonucleoside triphosphates in human carcinoma cells by high-performance liquid chromatography. Anal Biochem *270*, 59-68.

Deegan, R. (2012). The Role of Histone Modification in DNA Double-Strand Break Repair in *Schizosaccharomyces pombe*. In Chromosome Integrity Group, Gray Institute for Radiation Oncology and Biology, Department of Oncology (Oxford: University of Oxford).

Deem, A., Keszthelyi, A., Blackgrove, T., Vayl, A., Coffey, B., Mathur, R., Chabes, A., and Malkova, A. (2011). Break-induced replication is highly inaccurate. PLoS Biol *9*, e1000594.

Deng, S.K., Gibb, B., de Almeida, M.J., Greene, E.C., and Symington, L.S. (2014). RPA antagonizes microhomology-mediated repair of DNA double-strand breaks. Nat Struct Mol Biol *21*, 405-412.

Deshpande, G.P., Hayles, J., Hoe, K.L., Kim, D.U., Park, H.O., and Hartsuiker, E. (2009). Screening a genome-wide *S. pombe* deletion library identifies novel genes and pathways involved in genome stability maintenance. DNA Repair (Amst) *8*, 672-679.

Dianov, G.L., O'Neill, P., and Goodhead, D.T. (2001). Securing genome stability by orchestrating DNA repair: removal of radiation-induced clustered lesions in DNA. BioEssays : news and reviews in molecular, cellular and developmental biology *23*, 745-749.

Dore, A.S., Kilkenny, M.L., Rzechorzek, N.J., and Pearl, L.H. (2009). Crystal structure of the Rad9-Rad1-Hus1 DNA damage checkpoint complex--implications for clamp loading and regulation. Mol Cell *34*, 735-745.

Downs, J.A., and Jackson, S.P. (2004). A means to a DNA end: the many roles of Ku. Nature reviews Molecular cell biology *5*, 367-378.

Downs, J.A., Lowndes, N.F., and Jackson, S.P. (2000). A role for *Saccharomyces cerevisiae* histone H2A in DNA repair. Nature *408*, 1001-1004.

Doyon, Y., and Cote, J. (2004). The highly conserved and multifunctional NuA4 HAT complex. Current opinion in genetics & development *14*, 147-154.

Du, L.L., Nakamura, T.M., and Russell, P. (2006). Histone modification-dependent and -independent pathways for recruitment of checkpoint protein Crb2 to double-strand breaks. Genes Dev *20*, 1583-1596.

Duda, D.M., Borg, L.A., Scott, D.C., Hunt, H.W., Hammel, M., and Schulman, B.A. (2008). Structural insights into NEDD8 activation of cullin-RING ligases: conformational control of conjugation. Cell *134*, 995-1006.

Dupaigne, P., Le Breton, C., Fabre, F., Gangloff, S., Le Cam, E., and Veaute, X. (2008). The Srs2 helicase activity is stimulated by Rad51 filaments on dsDNA: implications for crossover incidence during mitotic recombination. Mol Cell *29*, 243-254.

Eason, R.G., Pourmand, N., Tongprasit, W., Herman, Z.S., Anthony, K., Jejelowo, O., Davis, R.W., and Stolc, V. (2004). Characterization of synthetic DNA bar codes in *Saccharomyces cerevisiae* gene-deletion strains. Proc Natl Acad Sci U S A *101*, 11046-11051.

Eberharter, A., Sterner, D.E., Schieltz, D., Hassan, A., Yates, J.R., 3rd, Berger, S.L., and Workman, J.L. (1999). The ADA complex is a distinct histone acetyltransferase complex in *Saccharomyces cerevisiae*. Mol Cell Biol *19*, 6621-6631.

Edelstein, A., Amodaj, N., Hoover, K., Vale, R., and Stuurman, N. (2010). Computer control of microscopes using microManager. Curr Protoc Mol Biol *Chapter 14*, Unit14 20.

Edwards, R.J., Bentley, N.J., and Carr, A.M. (1999). A Rad3-Rad26 complex responds to DNA damage independently of other checkpoint proteins. Nat Cell Biol *1*, 393-398.

Elledge, S.J., and Davis, R.W. (1990). Two genes differentially regulated in the cell cycle and by DNA-damaging agents encode alternative regulatory subunits of ribonucleotide reductase. Genes Dev *4*, 740-751.

Ellison, V., and Stillman, B. (2003). Biochemical characterization of DNA damage checkpoint complexes: clamp loader and clamp complexes with specificity for 5' recessed DNA. PLoS Biol *1*, E33.

Falck, J., Coates, J., and Jackson, S.P. (2005). Conserved modes of recruitment of ATM, ATR and DNA-PKcs to sites of DNA damage. Nature *434*, 605-611.

Feng, Z., Scott, S.P., Bussen, W., Sharma, G.G., Guo, G., Pandita, T.K., and Powell, S.N. (2011). Rad52 inactivation is synthetically lethal with BRCA2 deficiency. Proc Natl Acad Sci U S A *108*, 686-691.

Fernandez Sarabia, M.J., McInerny, C., Harris, P., Gordon, C., and Fantes, P. (1993). The cell cycle genes *cdc22*$^{+}$ and *suc22*$^{+}$ of the fission yeast *Schizosaccharomyces pombe* encode the large and small subunits of ribonucleotide reductase. Mol Gen Genet *238*, 241-251.

Ferreira, M.G., and Cooper, J.P. (2004). Two modes of DNA double-strand break repair are reciprocally regulated through the fission yeast cell cycle. Genes Dev *18*, 2249-2254.

Figaro, S., Wacheul, L., Schillewaert, S., Graille, M., Huvelle, E., Mongeard, R., Zorbas, C., Lafontaine, D.L., and Heurgue-Hamard, V. (2012). Trm112 is required for Bud23-mediated methylation of the 18S rRNA at position G1575. Mol Cell Biol *32*, 2254-2267.

Fishman-Lobell, J., and Haber, J.E. (1992). Removal of nonhomologous DNA ends in double-strand break recombination: the role of the yeast ultraviolet repair gene *RAD1*. Science *258*, 480-484.

Fleck, O., Vejrup-Hansen, R., Watson, A., Carr, A.M., Nielsen, O., and Holmberg, C. (2013). Spd1 accumulation causes genome instability independently of ribonucleotide reductase activity but functions to protect the genome when deoxynucleotide pools are elevated. J Cell Sci *126*, 4985-4994.

Fu, D., Brophy, J.A., Chan, C.T., Atmore, K.A., Begley, U., Paules, R.S., Dedon, P.C., Begley, T.J., and Samson, L.D. (2010). Human AlkB homolog ABH8 Is a tRNA methyltransferase required for wobble uridine modification and DNA damage survival. Mol Cell Biol *30*, 2449-2459.

Furnari, B., Blasina, A., Boddy, M.N., McGowan, C.H., and Russell, P. (1999). Cdc25 inhibited in vivo and in vitro by checkpoint kinases Cds1 and Chk1. Mol Biol Cell *10*, 833-845.

Furnari, B., Rhind, N., and Russell, P. (1997). Cdc25 mitotic inducer targeted by Chk1 DNA damage checkpoint kinase. Science *277*, 1495-1497.

Furuya, K., Poitelea, M., Guo, L., Caspari, T., and Carr, A.M. (2004). Chk1 activation requires Rad9 S/TQ-site phosphorylation to promote association with C-terminal BRCT domains of Rad4^{TOPBP1}. Genes Dev *18*, 1154-1164.

Fuzesi-Levi, M.G., Ben-Nissan, G., Bianchi, E., Zhou, H., Deery, M.J., Lilley, K.S., Levin, Y., and Sharon, M. (2014). Dynamic regulation of the COP9 signalosome in response to DNA damage. Mol Cell Biol *34*, 1066-1076.

Garcia, V., Phelps, S.E., Gray, S., and Neale, M.J. (2011). Bidirectional resection of DNA double-strand breaks by Mre11 and Exo1. Nature *479*, 241-244.

Glickman, M.H., Rubin, D.M., Coux, O., Wefes, I., Pfeifer, G., Cjeka, Z., Baumeister, W., Fried, V.A., and Finley, D. (1998). A subcomplex of the proteasome regulatory particle required for ubiquitin-conjugate degradation and related to the COP9-signalosome and eIF3. Cell *94*, 615-623.

Gomez-Escoda, B., Ivanova, T., Calvo, I.A., Alves-Rodrigues, I., Hidalgo, E., and Ayte, J. (2011). Yox1 links MBF-dependent transcription to completion of DNA synthesis. EMBO Rep *12*, 84-89.

Gotter, A.L., Suppa, C., and Emanuel, B.S. (2007). Mammalian TIMELESS and Tipin are evolutionarily conserved replication fork-associated factors. J Mol Biol *366*, 36-52.

Gottlieb, T.M., and Jackson, S.P. (1993). The DNA-dependent protein kinase: requirement for DNA ends and association with Ku antigen. Cell *72*, 131-142.

Grant, P.A., Duggan, L., Cote, J., Roberts, S.M., Brownell, J.E., Candau, R., Ohba, R., Owen-Hughes, T., Allis, C.D., Winston, F., Berger, S.L., and Workman, J.L. (1997). Yeast Gcn5 functions in two multisubunit complexes to acetylate nucleosomal histones: characterization of an Ada complex and the SAGA (Spt/Ada) complex. Genes Dev *11*, 1640-1650.

Green, C.M., Erdjument-Bromage, H., Tempst, P., and Lowndes, N.F. (2000). A novel Rad24 checkpoint protein complex closely related to replication factor C. Curr Biol *10*, 39-42.

Griffiths, D.J., Barbet, N.C., McCready, S., Lehmann, A.R., and Carr, A.M. (1995). Fission yeast *rad17*: a homologue of budding yeast *RAD24* that shares regions of sequence similarity with DNA polymerase accessory proteins. EMBO J *14*, 5812-5823.

Griffiths, M., Beaumont, N., Yao, S.Y., Sundaram, M., Boumah, C.E., Davies, A., Kwong, F.Y., Coe, I., Cass, C.E., Young, J.D., and Baldwin, S.A. (1997). Cloning of a human nucleoside transporter implicated in the cellular uptake of adenosine and chemotherapeutic drugs. Nat Med *3*, 89-93.

Guarino, E., Salguero, I., and Kearsey, S.E. (2014). Cellular regulation of ribonucleotide reductase in eukaryotes. Seminars in cell & developmental biology *30*, 97-103.

Hakansson, P., Dahl, L., Chilkova, O., Domkin, V., and Thelander, L. (2006a). The *Schizosaccharomyces pombe* replication inhibitor Spd1 regulates ribonucleotide reductase activity and dNTPs by binding to the large Cdc22 subunit. J Biol Chem *281*, 1778-1783.

Hakansson, P., Hofer, A., and Thelander, L. (2006b). Regulation of mammalian ribonucleotide reduction and dNTP pools after DNA damage and in resting cells. J Biol Chem *281*, 7834-7841.

Han, T.X., Xu, X.Y., Zhang, M.J., Peng, X., and Du, L.L. (2010). Global fitness profiling of fission yeast deletion strains by barcode sequencing. Genome Biol *11*, R60.

Hanahan, D., and Weinberg, R.A. (2011). Hallmarks of cancer: the next generation. Cell *144*, 646-674.

Hannah, J., and Zhou, P. (2009). Regulation of DNA damage response pathways by the cullin-RING ubiquitin ligases. DNA Repair (Amst) *8*, 536-543.

Harris, P., Kersey, P.J., McInerny, C.J., and Fantes, P.A. (1996). Cell cycle, DNA damage and heat shock regulate *suc22*$^{+}$ expression in fission yeast. Mol Gen Genet *252*, 284-291.

Harris, S., Kemplen, C., Caspari, T., Chan, C., Lindsay, H.D., Poitelea, M., Carr, A.M., and Price, C. (2003). Delineating the position of *rad4*$^{+}$/*cut5*$^{+}$ within the DNA-structure checkpoint pathways in *Schizosaccharomyces pombe*. J Cell Sci *116*, 3519-3529.

Heurgue-Hamard, V., Champ, S., Mora, L., Merkulova-Rainon, T., Kisselev, L.L., and Buckingham, R.H. (2005). The glutamine residue of the conserved GGQ motif in *Saccharomyces cerevisiae* release factor eRF1 is methylated by the product of the *YDR140w* gene. J Biol Chem *280*, 2439-2445.

Heurgue-Hamard, V., Graille, M., Scrima, N., Ulryck, N., Champ, S., van Tilbeurgh, H., and Buckingham, R.H. (2006). The zinc finger protein Ynr046w is plurifunctional and a component of the eRF1 methyltransferase in yeast. J Biol Chem *281*, 36140-36148.

Heyer, W.D., Ehmsen, K.T., and Liu, J. (2010). Regulation of homologous recombination in eukaryotes. Annu Rev Genet *44*, 113-139.

Hodson, J.A., Bailis, J.M., and Forsburg, S.L. (2003). Efficient labeling of fission yeast *Schizosaccharomyces pombe* with thymidine and BUdR. Nucleic Acids Res *31*, e134.

Hofer, A., Crona, M., Logan, D.T., and Sjoberg, B.M. (2012). DNA building blocks: keeping control of manufacture. Critical reviews in biochemistry and molecular biology *47*, 50-63.

Hole, K., Van Damme, P., Dalva, M., Aksnes, H., Glomnes, N., Varhaug, J.E., Lillehaug, J.R., Gevaert, K., and Arnesen, T. (2011). The human N-alpha-acetyltransferase 40 (hNaa40p/hNatD) is conserved from yeast and N-terminally acetylates histones H2A and H4. PLoS One *6*, e24713.

Horigome, C., Oma, Y., Konishi, T., Schmid, R., Marcomini, I., Hauer, M.H., Dion, V., Harata, M., and Gasser, S.M. (2014). SWR1 and INO80 Chromatin Remodelers Contribute to DNA Double-Strand Break Perinuclear Anchorage Site Choice. Mol Cell *55*, 626-639.

Horiuchi, J., Silverman, N., Marcus, G.A., and Guarente, L. (1995). ADA3, a putative transcriptional adaptor, consists of two separable domains and interacts with ADA2 and GCN5 in a trimeric complex. Mol Cell Biol *15*, 1203-1209.

Hua, H., and Kearsey, S.E. (2011). Monitoring DNA replication in fission yeast by incorporation of 5-ethynyl-2'-deoxyuridine. Nucleic Acids Res *39*, e60.

Huang, M., and Elledge, S.J. (1997). Identification of *RNR4*, encoding a second essential small subunit of ribonucleotide reductase in *Saccharomyces cerevisiae*. Mol Cell Biol *17*, 6105-6113.

Huang, M., Zhou, Z., and Elledge, S.J. (1998). The DNA replication and damage checkpoint pathways induce transcription by inhibition of the Crt1 repressor. Cell *94*, 595-605.

Huertas, P., Cortes-Ledesma, F., Sartori, A.A., Aguilera, A., and Jackson, S.P. (2008). CDK targets Sae2 to control DNA-end resection and homologous recombination. Nature *455*, 689-692.

Humphrey, T. (2000). DNA damage and cell cycle control in Schizosaccharomyces pombe. Mutat Res *451*, 211-226.

Iacovoni, J.S., Caron, P., Lassadi, I., Nicolas, E., Massip, L., Trouche, D., and Legube, G. (2010). High-resolution profiling of gammaH2AX around DNA double strand breaks in the mammalian genome. EMBO J *29*, 1446-1457.

Ira, G., Pellicioli, A., Balijja, A., Wang, X., Fiorani, S., Carotenuto, W., Liberi, G., Bressan, D., Wan, L., Hollingsworth, N.M., Haber, J.E., and Foiani, M. (2004). DNA end resection, homologous recombination and DNA damage checkpoint activation require CDK1. Nature *431*, 1011-1017.

Ivanov, E.L., Sugawara, N., Fishman-Lobell, J., and Haber, J.E. (1996). Genetic requirements for the single-strand annealing pathway of double-strand break repair in *Saccharomyces cerevisiae*. Genetics *142*, 693-704.

Ivanova, T., Alves-Rodrigues, I., Gomez-Escoda, B., Dutta, C., DeCaprio, J.A., Rhind, N., Hidalgo, E., and Ayte, J. (2013). The DNA damage and the DNA replication checkpoints converge at the MBF transcription factor. Mol Biol Cell *24*, 3350-3357.

Jackson, S.P., and Bartek, J. (2009). The DNA-damage response in human biology and disease. Nature *461*, 1071-1078.

Jia, X., Weinert, T., and Lydall, D. (2004). Mec1 and Rad53 inhibit formation of single-stranded DNA at telomeres of *Saccharomyces cerevisiae cdc13-1* mutants. Genetics *166*, 753-764.

Johansson, M., van Rompay, A.R., Degreve, B., Balzarini, J., and Karlsson, A. (1999). Cloning and characterization of the multisubstrate deoxyribonucleoside kinase of *Drosophila melanogaster*. J Biol Chem *274*, 23814-23819.

Johnsson, A., Durand-Dubief, M., Xue-Franzen, Y., Ronnerblad, M., Ekwall, K., and Wright, A. (2009). HAT-HDAC interplay modulates global histone H3K14 acetylation in gene-coding regions during stress. EMBO Rep *10*, 1009-1014.

Johnsson, A., Xue-Franzen, Y., Lundin, M., and Wright, A.P. (2006). Stress-specific role of fission yeast Gcn5 histone acetyltransferase in programming a subset of stress response genes. Eukaryot Cell *5*, 1337-1346.

Kakarougkas, A., and Jeggo, P.A. (2014). DNA DSB repair pathway choice: an orchestrated handover mechanism. The British journal of radiology *87*, 20130685.

Kalhor, H.R., and Clarke, S. (2003). Novel methyltransferase for modified uridine residues at the wobble position of tRNA. Mol Cell Biol *23*, 9283-9292.

Kasparek, T. (2013). Identification and Characterisation of Determinants of Genome Stability in Response to a Double-Strand Break. In Gray Institute for Radiation Oncology and Biology, Department of Oncology (University of Oxford).

Kasparek, T.R., and Humphrey, T.C. (2011). DNA double-strand break repair pathways, chromosomal rearrangements and cancer. Seminars in cell & developmental biology *22*, 886-897.

Kent, N.A., Chambers, A.L., and Downs, J.A. (2007). Dual chromatin remodeling roles for RSC during DNA double strand break induction and repair at the yeast *MAT* locus. J Biol Chem *282*, 27693-27701.

Khym, J.X. (1975). An analytical system for rapid separation of tissue nucleotides at low pressures on conventional anion exchangers Clin Chem *21*, 1245-1252.

Kim, D.U., Hayles, J., Kim, D., Wood, V., Park, H.O., Won, M., Yoo, H.S., Duhig, T., Nam, M., Palmer, G., Han, S., Jeffery, L., Baek, S.T., Lee, H., Shim, Y.S., Lee, M., Kim, L., Heo, K.S., Noh, E.J., Lee, A.R., Jang, Y.J., Chung, K.S., Choi, S.J., Park, J.Y., Park, Y., Kim, H.M., Park, S.K., Park, H.J., Kang, E.J., Kim, H.B., Kang, H.S., Park, H.M., Kim, K., Song, K., Song, K.B., Nurse, P., and Hoe, K.L. (2010). Analysis of a genome-wide set of gene deletions in the fission yeast *Schizosaccharomyces pombe*. Nat Biotechnol *28*, 617-623.

Knudson, A.G. (1993). Antioncogenes and human cancer. Proc Natl Acad Sci U S A *90*, 10914-10921.

Koster, D.A., Palle, K., Bot, E.S., Bjornsti, M.A., and Dekker, N.H. (2007). Antitumour drugs impede DNA uncoiling by topoisomerase I. Nature *448*, 213-217.

Langerak, P., Mejia-Ramirez, E., Limbo, O., and Russell, P. (2011). Release of Ku and MRN from DNA ends by Mre11 nuclease activity and Ctp1 is required for homologous recombination repair of double-strand breaks. PLoS Genet *7*, e1002271.

Lasko, D., Cavenee, W., and Nordenskjold, M. (1991). Loss of constitutional heterozygosity in human cancer. Annu Rev Genet *25*, 281-314.

Lawless, C., Wilkinson, D.J., Young, A., Addinall, S.G., and Lydall, D.A. (2010). Colonyzer: automated quantification of micro-organism growth characteristics on solid agar. BMC Bioinformatics *11*, 287.

Lee, H.S., Park, J.H., Kim, S.J., Kwon, S.J., and Kwon, J. (2010). A cooperative activation loop among SWI/SNF, gamma-H2AX and H3 acetylation for DNA double-strand break repair. EMBO J *29*, 1434-1445.

Lee, K.K., Sardiu, M.E., Swanson, S.K., Gilmore, J.M., Torok, M., Grant, P.A., Florens, L., Workman, J.L., and Washburn, M.P. (2011). Combinatorial depletion analysis to assemble the network architecture of the SAGA and ADA chromatin remodeling complexes. Mol Syst Biol *7*, 503.

Lee, Y.D., Wang, J., Stubbe, J., and Elledge, S.J. (2008). Dif1 is a DNA-damage-regulated facilitator of nuclear import for ribonucleotide reductase. Mol Cell *32*, 70-80.

Lehman, J.A., Hoelz, D.J., and Turchi, J.J. (2008). DNA-dependent conformational changes in the Ku heterodimer. Biochemistry *47*, 4359-4368.

Li, B., and Reese, J.C. (2001). Ssn6-Tup1 regulates RNR3 by positioning nucleosomes and affecting the chromatin structure at the upstream repression sequence. J Biol Chem *276*, 33788-33797.

Li, X., Zhang, X.P., Solinger, J.A., Kiianitsa, K., Yu, X., Egelman, E.H., and Heyer, W.D. (2007). Rad51 and Rad54 ATPase activities are both required to modulate Rad51-dsDNA filament dynamics. Nucleic Acids Res *35*, 4124-4140.

Liang, B., Qiu, J., Ratnakumar, K., and Laurent, B.C. (2007). RSC functions as an early double-strand-break sensor in the cell's response to DNA damage. Curr Biol *17*, 1432-1437.

Lieber, M.R. (2010). The mechanism of double-strand DNA break repair by the nonhomologous DNA end-joining pathway. Annual review of biochemistry *79*, 181-211.

Lindsey-Boltz, L.A., Bermudez, V.P., Hurwitz, J., and Sancar, A. (2001). Purification and characterization of human DNA damage checkpoint Rad complexes. Proc Natl Acad Sci U S A *98*, 11236-11241.

Lingaraju, G.M., Bunker, R.D., Cavadini, S., Hess, D., Hassiepen, U., Renatus, M., Fischer, E.S., and Thoma, N.H. (2014). Crystal structure of the human COP9 signalosome. Nature *512*, 161–165.

Liu, C., Poitelea, M., Watson, A., Yoshida, S.H., Shimoda, C., Holmberg, C., Nielsen, O., and Carr, A.M. (2005). Transactivation of *Schizosaccharomyces pombe cdt2*$^{+}$ stimulates a Pcu4-Ddb1-CSN ubiquitin ligase. EMBO J *24*, 3940-3951.

Liu, C., Powell, K.A., Mundt, K., Wu, L., Carr, A.M., and Caspari, T. (2003). Cop9/signalosome subunits and Pcu4 regulate ribonucleotide reductase by both checkpoint-dependent and -independent mechanisms. Genes Dev *17*, 1130-1140.

Liu, J., Doty, T., Gibson, B., and Heyer, W.D. (2010). Human BRCA2 protein promotes RAD51 filament formation on RPA-covered single-stranded DNA. Nat Struct Mol Biol *17*, 1260-1262.

Liu, J., Furukawa, M., Matsumoto, T., and Xiong, Y. (2002a). NEDD8 modification of CUL1 dissociates p120(CAND1), an inhibitor of CUL1-SKP1 binding and SCF ligases. Mol Cell *10*, 1511-1518.

Liu, N., Schild, D., Thelen, M.P., and Thompson, L.H. (2002b). Involvement of Rad51C in two distinct protein complexes of Rad51 paralogs in human cells. Nucleic Acids Res *30*, 1009-1015.

Ljungman, M. (2010). The DNA damage response--repair or despair? Environmental and molecular mutagenesis *51*, 879-889.

Llorente, B., Smith, C.E., and Symington, L.S. (2008). Break-induced replication: what is it and what is it for? Cell Cycle *7*, 859-864.

Lopez-Girona, A., Furnari, B., Mondesert, O., and Russell, P. (1999). Nuclear localization of Cdc25 is regulated by DNA damage and a 14-3-3 protein. Nature *397*, 172-175.

Lowndes, N.F., McInerny, C.J., Johnson, A.L., Fantes, P.A., and Johnston, L.H. (1992). Control of DNA synthesis genes in fission yeast by the cell-cycle gene *cdc10*$^{+}$. Nature *355*, 449-453.

Lundin, C., North, M., Erixon, K., Walters, K., Jenssen, D., Goldman, A.S., and Helleday, T. (2005). Methyl methanesulfonate (MMS) produces heat-labile DNA damage but no detectable in vivo DNA double-strand breaks. Nucleic Acids Res *33*, 3799-3811.

Lyapina, S., Cope, G., Shevchenko, A., Serino, G., Tsuge, T., Zhou, C., Wolf, D.A., Wei, N., and Deshaies, R.J. (2001). Promotion of NEDD-CUL1 conjugate cleavage by COP9 signalosome. Science *292*, 1382-1385.

Lydall, D., and Weinert, T. (1995). Yeast checkpoint genes in DNA damage processing: implications for repair and arrest. Science *270*, 1488-1491.

Ma, Y., Pannicke, U., Schwarz, K., and Lieber, M.R. (2002). Hairpin opening and overhang processing by an Artemis/DNA-dependent protein kinase complex in nonhomologous end joining and V(D)J recombination. Cell *108*, 781-794.

Madrid, M., Soto, T., Khong, H.K., Franco, A., Vicente, J., Perez, P., Gacto, M., and Cansado, J. (2006). Stress-induced response, localization, and regulation of the Pmk1 cell integrity pathway in *Schizosaccharomyces pombe*. J Biol Chem *281*, 2033-2043.

Mahajan, K.N., Nick McElhinny, S.A., Mitchell, B.S., and Ramsden, D.A. (2002). Association of DNA polymerase mu (pol mu) with Ku and ligase IV: role for pol mu in end-joining double-strand break repair. Mol Cell Biol *22*, 5194-5202.

Mahaney, B.L., Meek, K., and Lees-Miller, S.P. (2009). Repair of ionizing radiation-induced DNA double-strand breaks by non-homologous end-joining. Biochem J *417*, 639-650.

Matos, J., and West, S.C. (2014). Holliday junction resolution: regulation in space and time. DNA Repair (Amst) *19*, 176-181.

Matsuoka, S., Ballif, B.A., Smogorzewska, A., McDonald, E.R., 3rd, Hurov, K.E., Luo, J., Bakalarski, C.E., Zhao, Z., Solimini, N., Lerenthal, Y., Shiloh, Y., Gygi, S.P., and Elledge, S.J. (2007). ATM and ATR substrate analysis reveals extensive protein networks responsive to DNA damage. Science *316*, 1160-1166.

Mazauric, M.H., Dirick, L., Purushothaman, S.K., Bjork, G.R., and Lapeyre, B. (2010). Trm112p is a 15-kDa zinc finger protein essential for the activity of two tRNA and one protein methyltransferases in yeast. J Biol Chem *285*, 18505-18515.

Mazin, A.V., Alexeev, A.A., and Kowalczykowski, S.C. (2003). A novel function of Rad54 protein. Stabilization of the Rad51 nucleoprotein filament. J Biol Chem *278*, 14029-14036.

Mine-Hattab, J., and Rothstein, R. (2012). Increased chromosome mobility facilitates homology search during recombination. Nat Cell Biol *14*, 510-517.

Mitchell, L., Lambert, J.P., Gerdes, M., Al-Madhoun, A.S., Skerjanc, I.S., Figeys, D., and Baetz, K. (2008). Functional dissection of the NuA4 histone acetyltransferase reveals its role as a genetic hub and that Eaf1 is essential for complex integrity. Mol Cell Biol *28*, 2244-2256.

Mochida, S., Esashi, F., Aono, N., Tamai, K., O'Connell, M.J., and Yanagida, M. (2004). Regulation of checkpoint kinases through dynamic interaction with Crb2. EMBO J *23*, 418-428.

Monahan, B.J., Villen, J., Marguerat, S., Bahler, J., Gygi, S.P., and Winston, F. (2008). Fission yeast SWI/SNF and RSC complexes show compositional and functional differences from budding yeast. Nat Struct Mol Biol *15*, 873-880.

Moore, J.K., and Haber, J.E. (1996). Cell cycle and genetic requirements of two pathways of nonhomologous end-joining repair of double-strand breaks in *Saccharomyces cerevisiae*. Mol Cell Biol *16*, 2164-2173.

Moreno, S., Klar, A., and Nurse, P. (1991). Molecular genetic analysis of fission yeast *Schizosaccharomyces pombe*. Methods Enzymol *194*, 795-823.

Morin, I., Ngo, H.P., Greenall, A., Zubko, M.K., Morrice, N., and Lydall, D. (2008). Checkpoint-dependent phosphorylation of Exo1 modulates the DNA damage response. EMBO J *27*, 2400-2410.

Morris, S.A., Rao, B., Garcia, B.A., Hake, S.B., Diaz, R.L., Shabanowitz, J., Hunt, D.F., Allis, C.D., Lieb, J.D., and Strahl, B.D. (2007). Identification of histone H3 lysine 36 acetylation as a highly conserved histone modification. J Biol Chem *282*, 7632-7640.

Morrow, D.M., Tagle, D.A., Shiloh, Y., Collins, F.S., and Hieter, P. (1995). *TEL1*, an *S. cerevisiae* homolog of the human gene mutated in ataxia telangiectasia, is functionally related to the yeast checkpoint gene *MEC1*. Cell *82*, 831-840.

Moss, J. (2011). Identification and characterisation of homologous recombination genes in *Schizosaccaromyces Pombe*. In Chromosome Integrity Group, Gray Institute of Radiation Oncology and Biology, Department of Oncology (Oxford: University of Oxford).

Moss, J., Tinline-Purvis, H., Walker, C.A., Folkes, L.K., Stratford, M.R., Hayles, J., Hoe, K.L., Kim, D.U., Park, H.O., Kearsey, S.E., Fleck, O., Holmberg, C., Nielsen, O., and Humphrey, T.C. (2010). Break-induced ATR and Ddb1-Cul4^{Cdt2} ubiquitin ligase-dependent nucleotide synthesis promotes homologous recombination repair in fission yeast. Genes Dev *24*, 2705-2716.

Moynihan, E.B., and Enoch, T. (1999). Liz1p, a novel fission yeast membrane protein, is required for normal cell division when ribonucleotide reductase is inhibited. Mol Biol Cell *10*, 245-257.

Munch-Petersen, B., Piskur, J., and Sondergaard, L. (1998). Four deoxynucleoside kinase activities from *Drosophila melanogaster* are contained within a single monomeric enzyme, a new multifunctional deoxynucleoside kinase. J Biol Chem *273*, 3926-3931.

Mundt, K.E., Liu, C., and Carr, A.M. (2002). Deletion mutants in COP9/signalosome subunits in fission yeast *Schizosaccharomyces pombe* display distinct phenotypes. Mol Biol Cell *13*, 493-502.

Nakamura, T.M., Du, L.L., Redon, C., and Russell, P. (2004). Histone H2A phosphorylation controls Crb2 recruitment at DNA breaks, maintains checkpoint arrest, and influences DNA repair in fission yeast. Mol Cell Biol *24*, 6215-6230.

Namiki, Y., and Zou, L. (2006). ATRIP associates with replication protein A-coated ssDNA through multiple interactions. Proc Natl Acad Sci U S A *103*, 580-585.

Neale, M.J., Pan, J., and Keeney, S. (2005). Endonucleolytic processing of covalent protein-linked DNA double-strand breaks. Nature *436*, 1053-1057.

Nestoras, K., Mohammed, A.H., Schreurs, A.S., Fleck, O., Watson, A.T., Poitelea, M., O'Shea, C., Chahwan, C., Holmberg, C., Kragelund, B.B., Nielsen, O., Osborne, M., Carr, A.M., and Liu, C. (2010). Regulation of ribonucleotide reductase by Spd1 involves multiple mechanisms. Genes Dev *24*, 1145-1159.

Ngo, G.H., Balakrishnan, L., Dubarry, M., Campbell, J.L., and Lydall, D. (2014). The 9-1-1 checkpoint clamp stimulates DNA resection by Dna2-Sgs1 and Exo1. Nucleic Acids Res *42*, 10516-10528.

Nick McElhinny, S.A., and Ramsden, D.A. (2004). Sibling rivalry: competition between Pol X family members in V(D)J recombination and general double strand break repair. Immunological reviews *200*, 156-164.

Nickoloff, J.A., Singer, J.D., and Heffron, F. (1990). In vivo analysis of the *Saccharomyces cerevisiae* HO nuclease recognition site by site-directed mutagenesis. Mol Cell Biol *10*, 1174-1179.

Niida, H., Katsuno, Y., Sengoku, M., Shimada, M., Yukawa, M., Ikura, M., Ikura, T., Kohno, K., Shima, H., Suzuki, H., Tashiro, S., and Nakanishi, M. (2010). Essential role of Tip60-dependent recruitment of ribonucleotide reductase at DNA damage sites in DNA repair during G1 phase. Genes Dev *24*, 333-338.

Nik-Zainal, S., Van Loo, P., Wedge, D.C., Alexandrov, L.B., Greenman, C.D., Lau, K.W., Raine, K., Jones, D., Marshall, J., Ramakrishna, M., Shlien, A., Cooke, S.L., Hinton, J., Menzies, A., Stebbings, L.A., Leroy, C., Jia,

M., Rance, R., Mudie, L.J., Gamble, S.J., Stephens, P.J., McLaren, S., Tarpey, P.S., Papaemmanuil, E., Davies, H.R., Varela, I., McBride, D.J., Bignell, G.R., Leung, K., Butler, A.P., Teague, J.W., Martin, S., Jonsson, G., Mariani, O., Boyault, S., Miron, P., Fatima, A., Langerod, A., Aparicio, S.A., Tutt, A., Sieuwerts, A.M., Borg, A., Thomas, G., Salomon, A.V., Richardson, A.L., Borresen-Dale, A.L., Futreal, P.A., Stratton, M.R., and Campbell, P.J. (2012). The life history of 21 breast cancers. Cell *149*, 994-1007.

Niwa, O., Matsumoto, T., and Yanagida, M. (1986). Construction of a mini-chromosome by deletion and its mitotic and meiotic behavior in fission yeast. Molecular and General Genetics *203*, 397-405.

Noguchi, C., Rapp, J.B., Skorobogatko, Y.V., Bailey, L.D., and Noguchi, E. (2012). Swi1 associates with chromatin through the DDT domain and recruits Swi3 to preserve genomic integrity. PLoS One *7*, e43988.

Noguchi, E., Noguchi, C., Du, L.L., and Russell, P. (2003). Swi1 prevents replication fork collapse and controls checkpoint kinase Cds1. Mol Cell Biol *23*, 7861-7874.

Noguchi, E., Noguchi, C., McDonald, W.H., Yates, J.R., 3rd, and Russell, P. (2004). Swi1 and Swi3 are components of a replication fork protection complex in fission yeast. Mol Cell Biol *24*, 8342-8355.

Oishi, H., Kitagawa, H., Wada, O., Takezawa, S., Tora, L., Kouzu-Fujita, M., Takada, I., Yano, T., Yanagisawa, J., and Kato, S. (2006). An hGCN5/TRRAP histone acetyltransferase complex co-activates BRCA1 transactivation function through histone modification. J Biol Chem *281*, 20-26.

Pai, C.C., Deegan, R.S., Subramanian, L., Gal, C., Sarkar, S., Blaikley, E.J., Walker, C., Hulme, L., Bernhard, E., Codlin, S., Bahler, J., Allshire, R., Whitehall, S., and Humphrey, T.C. (2014). A histone H3K36 chromatin switch coordinates DNA double-strand break repair pathway choice. Nat Commun *5*, 4091.

Paques, F., and Haber, J.E. (1999). Multiple pathways of recombination induced by double-strand breaks in *Saccharomyces cerevisiae*. Microbiol Mol Biol Rev *63*, 349-404.

Patil, A., Dyavaiah, M., Joseph, F., Rooney, J.P., Chan, C.T., Dedon, P.C., and Begley, T.J. (2012). Increased tRNA modification and gene-specific codon usage regulate cell cycle progression during the DNA damage response. Cell Cycle *11*, 3656-3665.

Paull, T.T., and Gellert, M. (1998). The 3' to 5' exonuclease activity of Mre 11 facilitates repair of DNA double-strand breaks. Mol Cell *1*, 969-979.

Pfeiffer, P., Goedecke, W., and Obe, G. (2000). Mechanisms of DNA double-strand break repair and their potential to induce chromosomal aberrations. Mutagenesis *15*, 289-302.

Pickart, C.M., and Eddins, M.J. (2004). Ubiquitin: structures, functions, mechanisms. Biochim Biophys Acta *1695*, 55-72.

Povirk, L.F. (1996). DNA damage and mutagenesis by radiomimetic DNA-cleaving agents: bleomycin, neocarzinostatin and other enediynes. Mutat Res *355*, 71-89.

Pray-Grant, M.G., Schieltz, D., McMahon, S.J., Wood, J.M., Kennedy, E.L., Cook, R.G., Workman, J.L., Yates, J.R., 3rd, and Grant, P.A. (2002). The novel SLIK histone acetyltransferase complex functions in the yeast retrograde response pathway. Mol Cell Biol *22*, 8774-8786.

Price, B.D., and D'Andrea, A.D. (2013). Chromatin remodeling at DNA double-strand breaks. Cell *152*, 1344-1354.

Prudden, J., Evans, J.S., Hussey, S.P., Deans, B., O'Neill, P., Thacker, J., and Humphrey, T. (2003). Pathway utilization in response to a site-specific DNA double-strand break in fission yeast. EMBO J *22*, 1419-1430.

Purushothaman, S.K., Bujnicki, J.M., Grosjean, H., and Lapeyre, B. (2005). Trm11p and Trm112p are both required for the formation of 2-methylguanosine at position 10 in yeast tRNA. Mol Cell Biol *25*, 4359-4370.

Qu, M., Yang, B., Tao, L., Yates, J.R., 3rd, Russell, P., Dong, M.Q., and Du, L.L. (2012). Phosphorylation-dependent interactions between Crb2 and Chk1 are essential for DNA damage checkpoint. PLoS Genet *8*, e1002817.

Raji, H., and Hartsuiker, E. (2006). Double-strand break repair and homologous recombination in *Schizosaccharomyces pombe*. Yeast *23*, 963-976.

Reddy, Y.V., Ding, Q., Lees-Miller, S.P., Meek, K., and Ramsden, D.A. (2004). Non-homologous end joining requires that the DNA-PK complex undergo an autophosphorylation-dependent rearrangement at DNA ends. J Biol Chem *279*, 39408-39413.

Rhind, N., Furnari, B., and Russell, P. (1997). Cdc2 tyrosine phosphorylation is required for the DNA damage checkpoint in fission yeast. Genes Dev *11*, 504-511.

Rhind, N., and Russell, P. (2001). Roles of the mitotic inhibitors Wee1 and Mik1 in the G(2) DNA damage and replication checkpoints. Mol Cell Biol *21*, 1499-1508.

Robinson, J.T., Thorvaldsdottir, H., Winckler, W., Guttman, M., Lander, E.S., Getz, G., and Mesirov, J.P. (2011). Integrative genomics viewer. Nat Biotechnol *29*, 24-26.

Roguev, A., Wiren, M., Weissman, J.S., and Krogan, N.J. (2007). High-throughput genetic interaction mapping in the fission yeast *Schizosaccharomyces pombe*. Nat Methods *4*, 861-866.

Rossi, M., Duan, S., Jeong, Y.T., Horn, M., Saraf, A., Florens, L., Washburn, M.P., Antebi, A., and Pagano, M. (2013). Regulation of the $CRL4^{Cdt2}$ ubiquitin ligase and cell-cycle exit by the SCF^{Fbxo11} ubiquitin ligase. Mol Cell *49*, 1159-1166.

Saha, A., and Deshaies, R.J. (2008). Multimodal activation of the ubiquitin ligase SCF by Nedd8 conjugation. Mol Cell *32*, 21-31.

Sanders, S.L., Jennings, J., Canutescu, A., Link, A.J., and Weil, P.A. (2002). Proteomics of the eukaryotic transcription machinery: identification of proteins associated with components of yeast TFIID by multidimensional mass spectrometry. Mol Cell Biol *22*, 4723-4738.

Sanders, S.L., Portoso, M., Mata, J., Bahler, J., Allshire, R.C., and Kouzarides, T. (2004). Methylation of histone H4 lysine 20 controls recruitment of Crb2 to sites of DNA damage. Cell *119*, 603-614.

Sanso, M., Vargas-Perez, I., Quintales, L., Antequera, F., Ayte, J., and Hidalgo, E. (2011). Gcn5 facilitates Pol II progression, rather than recruitment to nucleosome-depleted stress promoters, in *Schizosaccharomyces pombe*. Nucleic Acids Res *39*, 6369-6379.

Sardana, R., and Johnson, A.W. (2012). The methyltransferase adaptor protein Trm112 is involved in biogenesis of both ribosomal subunits. Mol Biol Cell *23*, 4313-4322.

Seeber, A., Dion, V., and Gasser, S.M. (2013). Checkpoint kinases and the INO80 nucleosome remodeling complex enhance global chromatin mobility in response to DNA damage. Genes Dev *27*, 1999-2008.

Shibata, A., Barton, O., Noon, A.T., Dahm, K., Deckbar, D., Goodarzi, A.A., Lobrich, M., and Jeggo, P.A. (2010). Role of ATM and the damage response mediator proteins 53BP1 and MDC1 in the maintenance of G_2/M checkpoint arrest. Mol Cell Biol *30*, 3371-3383.

Shibata, A., Moiani, D., Arvai, A.S., Perry, J., Harding, S.M., Genois, M.M., Maity, R., van Rossum-Fikkert, S., Kertokalio, A., Romoli, F., Ismail, A., Ismalaj, E., Petricci, E., Neale, M.J., Bristow, R.G., Masson, J.Y., Wyman, C., Jeggo, P.A., and Tainer, J.A. (2014). DNA double-strand break repair pathway choice is directed by distinct MRE11 nuclease activities. Mol Cell *53*, 7-18.

Shimada, K., Nakamura, M., Anai, S., De Velasco, M., Tanaka, M., Tsujikawa, K., Ouji, Y., and Konishi, N. (2009). A novel human AlkB homologue, ALKBH8, contributes to human bladder cancer progression. Cancer Res *69*, 3157-3164.

Shimmoto, M., Matsumoto, S., Odagiri, Y., Noguchi, E., Russell, P., and Masai, H. (2009). Interactions between Swi1-Swi3, Mrc1 and S phase kinase, Hsk1 may regulate cellular responses to stalled replication forks in fission yeast. Genes Cells *14*, 669-682.

Shukla, A., Lahudkar, S., Durairaj, G., and Bhaumik, S.R. (2012). Sgf29p facilitates the recruitment of TATA box binding protein but does not alter SAGA's global structural integrity in vivo. Biochemistry *51*, 706-714.

Singer, R.A., and Johnston, G.C. (1985). Indirect suppression of the *wee1* mutant phenotype in *Schizosaccharomyces pombe*. Exp Cell Res *158*, 533-543.

Sivakumar, S., Porter-Goff, M., Patel, P.K., Benoit, K., and Rhind, N. (2004). In vivo labeling of fission yeast DNA with thymidine and thymidine analogs. Methods *33*, 213-219.

Smith, A.M., Heisler, L.E., Mellor, J., Kaper, F., Thompson, M.J., Chee, M., Roth, F.P., Giaever, G., and Nislow, C. (2009). Quantitative phenotyping via deep barcode sequencing. Genome Res *19*, 1836-1842.

Sorensen, C.S., Hansen, L.T., Dziegielewski, J., Syljuasen, R.G., Lundin, C., Bartek, J., and Helleday, T. (2005). The cell-cycle checkpoint kinase Chk1 is required for mammalian homologous recombination repair. Nat Cell Biol *7*, 195-201.

Spedale, G., Timmers, H.T., and Pijnappel, W.W. (2012). ATAC-king the complexity of SAGA during evolution. Genes Dev *26*, 527-541.

Stephens, P.J., Greenman, C.D., Fu, B., Yang, F., Bignell, G.R., Mudie, L.J., Pleasance, E.D., Lau, K.W., Beare, D., Stebbings, L.A., McLaren, S., Lin, M.L., McBride, D.J., Varela, I., Nik-Zainal, S., Leroy, C., Jia, M., Menzies, A., Butler, A.P., Teague, J.W., Quail, M.A., Burton, J., Swerdlow, H., Carter, N.P., Morsberger, L.A., Iacobuzio-Donahue, C., Follows, G.A., Green, A.R., Flanagan, A.M., Stratton, M.R., Futreal, P.A., and Campbell, P.J. (2011). Massive genomic rearrangement acquired in a single catastrophic event during cancer development. Cell *144*, 27-40.

Stephens, P.J., McBride, D.J., Lin, M.L., Varela, I., Pleasance, E.D., Simpson, J.T., Stebbings, L.A., Leroy, C., Edkins, S., Mudie, L.J., Greenman, C.D., Jia, M., Latimer, C., Teague, J.W., Lau, K.W., Burton, J., Quail, M.A., Swerdlow, H., Churcher, C., Natrajan, R., Sieuwerts, A.M., Martens, J.W., Silver, D.P., Langerod, A., Russnes, H.E., Foekens, J.A., Reis-Filho, J.S., van 't Veer, L., Richardson, A.L., Borresen-Dale, A.L., Campbell, P.J., Futreal, P.A., and Stratton, M.R. (2009). Complex landscapes of somatic rearrangement in human breast cancer genomes. Nature *462*, 1005-1010.

Sterner, D.E., Grant, P.A., Roberts, S.M., Duggan, L.J., Belotserkovskaya, R., Pacella, L.A., Winston, F., Workman, J.L., and Berger, S.L. (1999). Functional organization of the yeast SAGA complex: distinct components involved in structural integrity, nucleosome acetylation, and TATA-binding protein interaction. Mol Cell Biol *19*, 86-98.

Stolz, J., Caspari, T., Carr, A.M., and Sauer, N. (2004). Cell division defects of *Schizosaccharomyces pombe liz1*- mutants are caused by defects in pantothenate uptake. Eukaryot Cell *3*, 406-412.

Sun, Y., Jiang, X., Xu, Y., Ayrapetov, M.K., Moreau, L.A., Whetstine, J.R., and Price, B.D. (2009). Histone H3 methylation links DNA damage detection to activation of the tumour suppressor Tip60. Nat Cell Biol *11*, 1376-1382.

Sung, P. (1997). Function of yeast Rad52 protein as a mediator between replication protein A and the Rad51 recombinase. J Biol Chem *272*, 28194-28197.

Svejstrup, J.Q., Christiansen, K., Gromova, II, Andersen, A.H., and Westergaard, O. (1991). New technique for uncoupling the cleavage and religation reactions of eukaryotic topoisomerase I. The mode of action of camptothecin at a specific recognition site. J Mol Biol *222*, 669-678.

Tamburini, B.A., and Tyler, J.K. (2005). Localized histone acetylation and deacetylation triggered by the homologous recombination pathway of double-strand DNA repair. Mol Cell Biol *25*, 4903-4913.

Tanaka, T., Yokoyama, M., Matsumoto, S., Fukatsu, R., You, Z., and Masai, H. (2010). Fission yeast Swi1-Swi3 complex facilitates DNA binding of Mrc1. J Biol Chem *285*, 39609-39622.

Taricani, L., and Wang, T.S. (2006). Rad4^{TopBP1}, a scaffold protein, plays separate roles in DNA damage and replication checkpoints and DNA replication. Mol Biol Cell *17*, 3456-3468.

Taverna, S.D., Ilin, S., Rogers, R.S., Tanny, J.C., Lavender, H., Li, H., Baker, L., Boyle, J., Blair, L.P., Chait, B.T., Patel, D.J., Aitchison, J.D., Tackett, A.J., and Allis, C.D. (2006). Yng1 PHD finger binding to H3 trimethylated at K4 promotes NuA3 HAT activity at K14 of H3 and transcription at a subset of targeted ORFs. Mol Cell *24*, 785-796.

Teng, Y., Bennett, M., Evans, K.E., Zhuang-Jackson, H., Higgs, A., Reed, S.H., and Waters, R. (2011). A novel method for the genome-wide high resolution analysis of DNA damage. Nucleic Acids Res *39*, e10.

Thelen, M.P., Venclovas, C., and Fidelis, K. (1999). A sliding clamp model for the Rad1 family of cell cycle checkpoint proteins. Cell *96*, 769-770.

Thorvaldsdottir, H., Robinson, J.T., and Mesirov, J.P. (2013). Integrative Genomics Viewer (IGV): high-performance genomics data visualization and exploration. Brief Bioinform *14*, 178-192.

Tinline-Purvis, H., Savory, A.P., Cullen, J.K., Dave, A., Moss, J., Bridge, W.L., Marguerat, S., Bahler, J., Ragoussis, J., Mott, R., Walker, C.A., and Humphrey, T.C. (2009). Failed gene conversion leads to extensive end processing and chromosomal rearrangements in fission yeast. EMBO J *28*, 3400-3412.

Toda, T., Dhut, S., Superti-Furga, G., Gotoh, Y., Nishida, E., Sugiura, R., and Kuno, T. (1996). The fission yeast *pmk1*$^{+}$ gene encodes a novel mitogen-activated protein kinase homolog which regulates cell integrity and functions coordinately with the protein kinase C pathway. Mol Cell Biol *16*, 6752-6764.

Tong, K., Keller, T., Hoffman, C.S., and Annunziato, A.T. (2012). *Schizosaccharomyces pombe* Hat1 (Kat1) is associated with Mis16 and is required for telomeric silencing. Eukaryot Cell *11*, 1095-1103.

Tsang, E., Miyabe, I., Iraqui, I., Zheng, J., Lambert, S.A., and Carr, A.M. (2014). The extent of error-prone replication restart by homologous recombination is controlled by Exo1 and checkpoint proteins. J Cell Sci *127*, 2983-2994.

Tsaponina, O., Barsoum, E., Astrom, S.U., and Chabes, A. (2011). Ixr1 is required for the expression of the ribonucleotide reductase Rnr1 and maintenance of dNTP pools. PLoS Genet *7*, e1002061.

Urnov, F.D., Miller, J.C., Lee, Y.L., Beausejour, C.M., Rock, J.M., Augustus, S., Jamieson, A.C., Porteus, M.H., Gregory, P.D., and Holmes, M.C. (2005). Highly efficient endogenous human gene correction using designed zinc-finger nucleases. Nature *435*, 646-651.

Uziel, T., Lerenthal, Y., Moyal, L., Andegeko, Y., Mittelman, L., and Shiloh, Y. (2003). Requirement of the MRN complex for ATM activation by DNA damage. EMBO J *22*, 5612-5621.

van den Born, E., Vagbo, C.B., Songe-Moller, L., Leihne, V., Lien, G.F., Leszczynska, G., Malkiewicz, A., Krokan, H.E., Kirpekar, F., Klungland, A., and Falnes, P.O. (2011). ALKBH8-mediated formation of a novel diastereomeric pair of wobble nucleosides in mammalian tRNA. Nat Commun *2*, 172.

Vejrup-Hansen, R., Fleck, O., Landvad, K., Fahnoe, U., Broendum, S.S., Schreurs, A.S., Kragelund, B.B., Carr, A.M., Holmberg, C., and Nielsen, O. (2014). Spd2 assists Spd1 in the modulation of ribonucleotide reductase architecture but does not regulate deoxynucleotide pools. J Cell Sci *127*, 2460-2470.

Vermeulen, M., Eberl, H.C., Matarese, F., Marks, H., Denissov, S., Butter, F., Lee, K.K., Olsen, J.V., Hyman, A.A., Stunnenberg, H.G., and Mann, M. (2010). Quantitative interaction proteomics and genome-wide profiling of epigenetic histone marks and their readers. Cell *142*, 967-980.

Walker, J.R., Corpina, R.A., and Goldberg, J. (2001). Structure of the Ku heterodimer bound to DNA and its implications for double-strand break repair. Nature *412*, 607-614.

Wang, Y., Kallgren, S.P., Reddy, B.D., Kuntz, K., Lopez-Maury, L., Thompson, J., Watt, S., Ma, C., Hou, H., Shi, Y., Yates, J.R., 3rd, Bahler, J., O'Connell, M.J., and Jia, S. (2012). Histone H3 lysine 14 acetylation is required for activation of a DNA damage checkpoint in fission yeast. J Biol Chem *287*, 4386-4393.

Watson, A., Mata, J., Bahler, J., Carr, A., and Humphrey, T. (2004). Global gene expression responses of fission yeast to ionizing radiation. Mol Biol Cell *15*, 851-860.

Watson, A.T., Daigaku, Y., Mohebi, S., Etheridge, T.J., Chahwan, C., Murray, J.M., and Carr, A.M. (2013). Optimisation of the *Schizosaccharomyces pombe urg1* expression system. PLoS One *8*, e83800.

Watson, A.T., Werler, P., and Carr, A.M. (2011). Regulation of gene expression at the fission yeast *Schizosaccharomyces pombe urg1* locus. Gene *484*, 75-85.

Wei, N., Tsuge, T., Serino, G., Dohmae, N., Takio, K., Matsui, M., and Deng, X.W. (1998). The COP9 complex is conserved between plants and mammals and is related to the 26S proteasome regulatory complex. Curr Biol *8*, 919-922.

Weinert, T., and Hartwell, L. (1989). Control of G2 delay by the rad9 gene of Saccharomyces cerevisiae. Journal of cell science Supplement *12*, 145-148.

White, J., Li, Z., Sardana, R., Bujnicki, J.M., Marcotte, E.M., and Johnson, A.W. (2008). Bud23 methylates G1575 of 18S rRNA and is required for efficient nuclear export of pre-40S subunits. Mol Cell Biol *28*, 3151-3161.

Wood, V., Harris, M.A., McDowall, M.D., Rutherford, K., Vaughan, B.W., Staines, D.M., Aslett, M., Lock, A., Bahler, J., Kersey, P.J., and Oliver, S.G. (2012). PomBase: a comprehensive online resource for fission yeast. Nucleic Acids Res *40*, D695-699.

Woollard, A., Basi, G., and Nurse, P. (1996). A novel S phase inhibitor in fission yeast. EMBO J *15*, 4603-4612.

Wu, X., and Huang, M. (2008). Dif1 controls subcellular localization of ribonucleotide reductase by mediating nuclear import of the R2 subunit. Mol Cell Biol *28*, 7156-7167.

Xu, Y., Ayrapetov, M.K., Xu, C., Gursoy-Yuzugullu, O., Hu, Y., and Price, B.D. (2012). Histone H2A.Z controls a critical chromatin remodeling step required for DNA double-strand break repair. Mol Cell *48*, 723-733.

Xu, Y.J., Davenport, M., and Kelly, T.J. (2006). Two-stage mechanism for activation of the DNA replication checkpoint kinase Cds1 in fission yeast. Genes Dev *20*, 990-1003.

Xue-Franzen, Y., Johnsson, A., Brodin, D., Henriksson, J., Burglin, T.R., and Wright, A.P. (2010). Genome-wide characterisation of the Gcn5 histone acetyltransferase in budding yeast during stress adaptation reveals evolutionarily conserved and diverged roles. BMC genomics *11*, 200.

Yaneva, M., Kowalewski, T., and Lieber, M.R. (1997). Interaction of DNA-dependent protein kinase with DNA and with Ku: biochemical and atomic-force microscopy studies. EMBO J *16*, 5098-5112.

Yang, X., Li, L., Liang, J., Shi, L., Yang, J., Yi, X., Zhang, D., Han, X., Yu, N., and Shang, Y. (2013). Histone acetyltransferase 1 promotes homologous recombination in DNA repair by facilitating histone turnover. J Biol Chem *288*, 18271-18282.

Yoshida, S.H., Al-Amodi, H., Nakamura, T., McInerny, C.J., and Shimoda, C. (2003). The *Schizosaccharomyces pombe cdt2*$^{+}$ gene, a target of G1-S phase-specific transcription factor complex DSC1, is required for mitotic and premeiotic DNA replication. Genetics *164*, 881-893.

Yue, M., Zeng, L., Singh, A., and Xu, Y. (2014). Rad4 mainly functions in Chk1-mediated DNA damage checkpoint pathway as a scaffold protein in the fission yeast *Schizosaccharomyces pombe*. PLoS One *9*, e92936.

Zaitsevskaya-Carter, T., and Cooper, J.A. (1997). Spm1, a stress-activated MAP kinase that regulates morphogenesis in *S.pombe*. EMBO J *16*, 1318-1331.

Zeng, Y., Forbes, K.C., Wu, Z., Moreno, S., Piwnica-Worms, H., and Enoch, T. (1998). Replication checkpoint requires phosphorylation of the phosphatase Cdc25 by Cds1 or Chk1. Nature *395*, 507-510.

Zeng, Y., and Piwnica-Worms, H. (1999). DNA damage and replication checkpoints in fission yeast require nuclear exclusion of the Cdc25 phosphatase via 14-3-3 binding. Mol Cell Biol *19*, 7410-7419.

Zhang, H., Kruk, J.A., and Reese, J.C. (2008). Dissection of coactivator requirement at *RNR3* reveals unexpected contributions from TFIID and SAGA. J Biol Chem *283*, 27360-27368.

Zhao, X., and Rothstein, R. (2002). The Dun1 checkpoint kinase phosphorylates and regulates the ribonucleotide reductase inhibitor Sml1. Proc Natl Acad Sci U S A *99*, 3746-3751.

Zheng, J., Yang, X., Harrell, J.M., Ryzhikov, S., Shim, E.H., Lykke-Andersen, K., Wei, N., Sun, H., Kobayashi, R., and Zhang, H. (2002). CAND1 binds to unneddylated CUL1 and regulates the formation of SCF ubiquitin E3 ligase complex. Mol Cell *10*, 1519-1526.

Zhou, B.B., and Elledge, S.J. (2000). The DNA damage response: putting checkpoints in perspective. Nature *408*, 433-439.

Zhou, C., Seibert, V., Geyer, R., Rhee, E., Lyapina, S., Cope, G., Deshaies, R.J., and Wolf, D.A. (2001). The fission yeast COP9/signalosome is involved in cullin modification by ubiquitin-related Ned8p. BMC Biochem *2*, 7.

Zou, L., Cortez, D., and Elledge, S.J. (2002). Regulation of ATR substrate selection by Rad17-dependent loading of Rad9 complexes onto chromatin. Genes Dev *16*, 198-208.

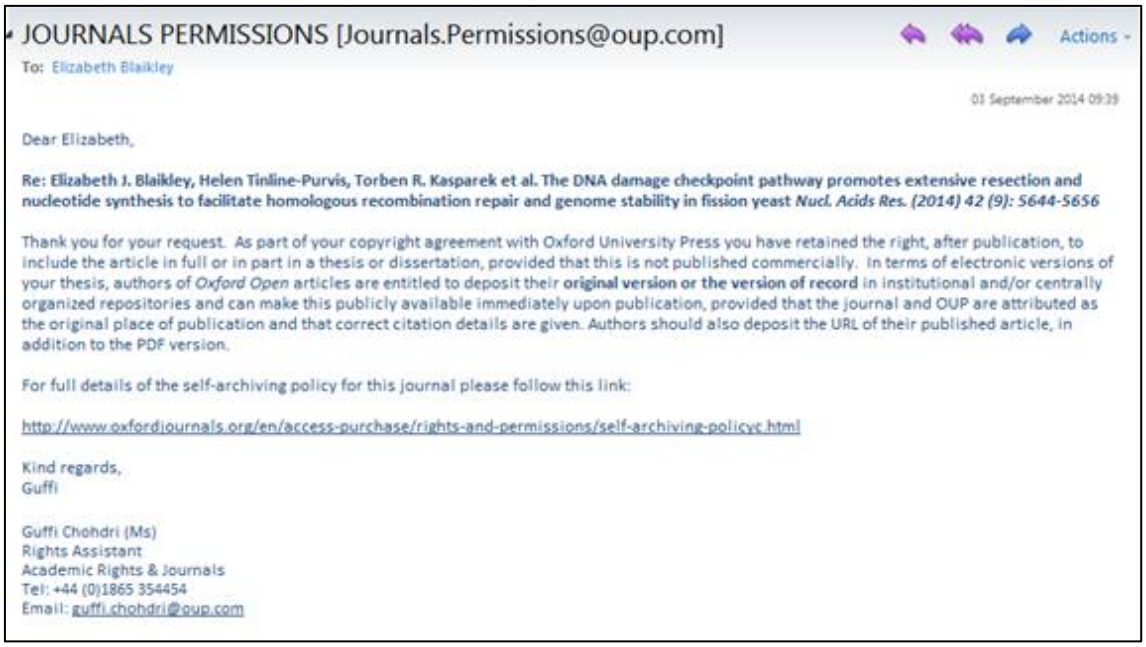
Zou, L., and Elledge, S.J. (2003). Sensing DNA damage through ATRIP recognition of RPA-ssDNA complexes. Science *300*, 1542-1548.

Zou, L., Liu, D., and Elledge, S.J. (2003). Replication protein A-mediated recruitment and activation of Rad17 complexes. Proc Natl Acad Sci U S A *100*, 13827-13832.

Zubko, M.K., Guillard, S., and Lydall, D. (2004). Exo1 and Rad24 differentially regulate generation of ssDNA at telomeres of *Saccharomyces cerevisiae cdc13-1* mutants. Genetics *168*, 103-115.

Appendicies

Appendix I Permissions obtained



JOURNALS PERMISSIONS [Journals.Permissions@oup.com]

Actions

To: Elizabeth Blaikley

03 September 2014 09:39

Dear Elizabeth,

Re: Elizabeth J. Blaikley, Helen Tinline-Purvis, Torben R. Kasparek et al. The DNA damage checkpoint pathway promotes extensive resection and nucleotide synthesis to facilitate homologous recombination repair and genome stability in fission yeast *Nucl. Acids Res. (2014) 42 (9): 5644-5656*

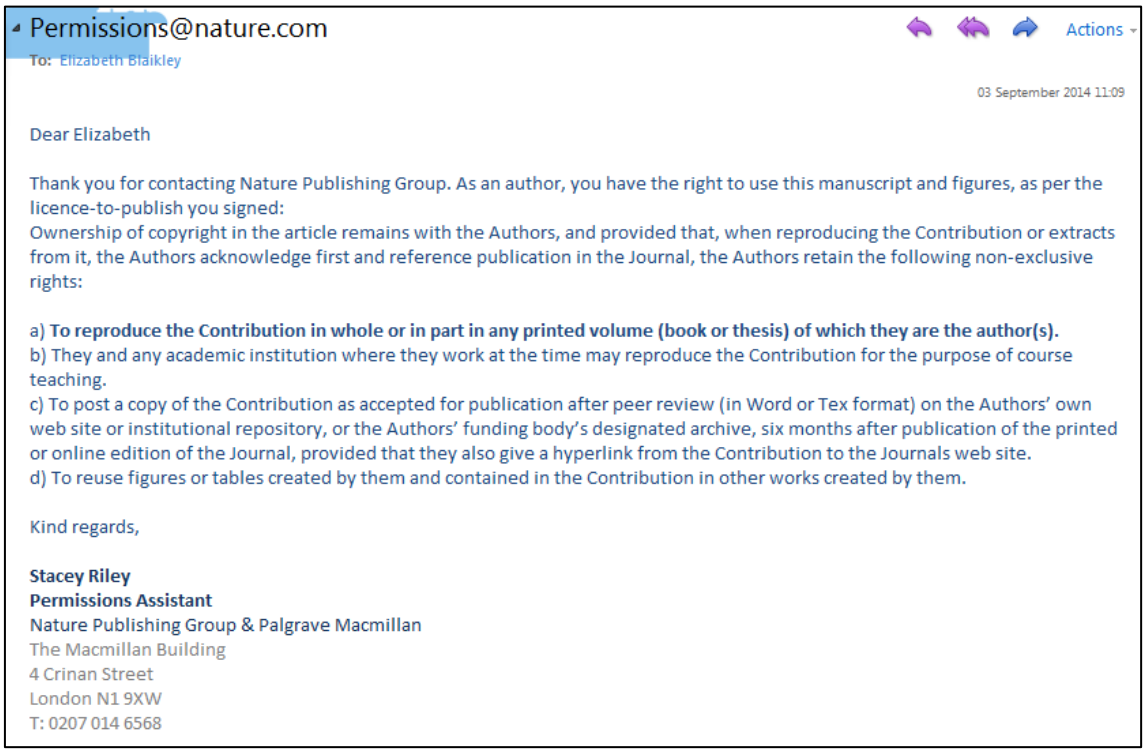
Thank you for your request. As part of your copyright agreement with Oxford University Press you have retained the right, after publication, to include the article in full or in part in a thesis or dissertation, provided that this is not published commercially. In terms of electronic versions of your thesis, authors of *Oxford Open* articles are entitled to deposit their **original version or the version of record** in institutional and/or centrally organized repositories and can make this publicly available immediately upon publication, provided that the journal and OUP are attributed as the original place of publication and that correct citation details are given. Authors should also deposit the URL of their published article, in addition to the PDF version.

For full details of the self-archiving policy for this journal please follow this link:

http://www.oxfordjournals.org/en/access-purchase/rights-and-permissions/self-archiving-policyc.html

Kind regards,
Guffi

Guffi Chohdri (Ms)
Rights Assistant
Academic Rights & Journals
Tel: +44 (0)1865 354454
Email: guffi.chohdri@oup.com



Permissions@nature.com

Actions

To: Elizabeth Blaikley

03 September 2014 11:09

Dear Elizabeth

Thank you for contacting Nature Publishing Group. As an author, you have the right to use this manuscript and figures, as per the licence-to-publish you signed:
Ownership of copyright in the article remains with the Authors, and provided that, when reproducing the Contribution or extracts from it, the Authors acknowledge first and reference publication in the Journal, the Authors retain the following non-exclusive rights:

a) **To reproduce the Contribution in whole or in part in any printed volume (book or thesis) of which they are the author(s).**
b) They and any academic institution where they work at the time may reproduce the Contribution for the purpose of course teaching.
c) To post a copy of the Contribution as accepted for publication after peer review (in Word or Tex format) on the Authors' own web site or institutional repository, or the Authors' funding body's designated archive, six months after publication of the printed or online edition of the Journal, provided that they also give a hyperlink from the Contribution to the Journals web site.
d) To reuse figures or tables created by them and contained in the Contribution in other works created by them.

Kind regards,

Stacey Riley
Permissions Assistant
Nature Publishing Group & Palgrave Macmillan
The Macmillan Building
4 Crinan Street
London N1 9XW
T: 0207 014 6568

Appendix II Oligonucleotide primers used in this study

Number	Homology	Orientation	Sequence	Source
253	uptag	Forward	CGCTCCCGCCTTACTTCGCA	Bioneer
254	uptag	Reverse	GATGTGAGAACTGTATCCTAGCAAG	Bioneer
255	downtag	Forward	TTGCGTTGCGTAGGGGGGAT	Bioneer
256	downtag	Reverse	TGATTTTGATGACGAGCGTAAT	Bioneer
1040	*air1*	Forward	ATTGGCTATCATGAGTGAGC	This study
1037	*alp14*	Forward	TAATGTTAGATTGGGTTGGC	This study
765	*arp42*	Forward	CCACTACTTCAGTACAGCCT	This study
DL29	*cdt2*	Forward	CACTCCGCGAGTTGAGATTG	Bioneer
759	*csn1*	Forward	AGGACCGATCAACTACAAT	This study
782	*hus1*	Forward	GGGTTTTCCAAGGAAGAAGAGGATT	Bioneer
755	*liz1*	Forward	AGAATACAGCGGTTACTCCA	This study
1039	*mms1*	Forward	CTCAGGTAACACTATTCGGC	This study
769	*ngg1*	Forward	ATTACGATGGTTCAGTGAGA	This study
1047	*nse6*	Forward	CAAGGACTTAATCGATCTGC	This study
1048	*nup132*	Forwards	ACAGGCTCGGAGACTGAAAC	This study
761	*pab1*	Forward	ATTAGTGATGCCGTACATTG	This study
753	*pmk1*	Forward	ATCTATAGGTACAGAGGTCCG	This study
781	*rad1*	Forward	ACTCGTCTATTAAGCTTTACGGCTT	Bioneer
779	*rad17*	Forward	CAAAGTCTCTACCTTTAGCTTCCTA	Bioneer
778	*rad26*	Forward	CGTTAAAGCATCTTATATAGCTGCG	Bioneer

Number	Homology	Orientation	Sequence	Source
777	*rad3*	Forward	TCAATCATTATCAGAAACATCCAGCCT	Bioneer
1036	*rad51*	Forward	AGCTTGTCAGACTACGCAAC	This study
780	*rad9*	Forward	ATGTCGGGCAATTACAAGTAATAAA	Bioneer
1046	*rpp202*	Forward	ATTAGATGCCACGTTTATGC	This study
763	*SPBC21C3.12c*	Forward	AATAGGATAGACATACCGGAG	This study
764	*SPBC21C3.12c*	Reverse	TAATGGATCAGACGGTTATG	This study
751	*SPBC557.02c*	Forward	ATGGTCAACAAGTTTCAACTG	This study
752	*SPBC557.02c*	Reverse	TATCTCATCCTGATCACGAG	This study
1043	*SPBC806.05*	Forward	TTAGCAGACGATCACTCGAT	This study
767	*swi3*	Forward	ACGCGTACATAGCTTTCACT	This study
757	*trm112*	Forward	TATCCTATGGTGATGTAGCC	This study
1042	*trt1*	Forward	TCATGAGTTGCTTCAGAACG	This study
1041	*uge1*	Forward	TGTAGGTTGGTAAGTATGCG	This study
1038	*vam7*	Forward	GAGTTGAACATCATGTGTGG	This study
1048	*vps16*	Forward	ACCTATACGTAAACCTGAGG	This study
1044	probe A	Forward	TATTGCTCATCGTCGTCCTTG	A. Watson
1045	probe A	Reverse	TATTGCTCATCGTCGGTCTC	A. Watson
650	probe B	Forward	CTGCAGCAGGCGGCAACGGT	A. Watson
651	probe B	Reverse	GCGATAGCGCCCCTGTGTGT	A. Watson

Appendix III Plasmids used in this study

Number	Name	Insert	Backbone	Source
40	pREP81X	-	pREP81X	F. Osman
28	pREP81X-HO	HO	pREP81X	F. Osman
39	pREP41X	-	pREP41X	Lab stock
206	pREP41X-HO	HO	pREP41X	H. Tinline-Purvis
238	pAW8E-HO	HO	pAW8E	A. Watson

Appendix IV Genetic determinants of site-specific DSB-induced marker loss

Table showing DSB assay results for strains transformed with REP81X-HO plasmids

For each genetic background the assay was repeated using three independent strains, to score approximately 600 colonies per strain. Exceptions were *arp42*Δ *spd1*Δ and *trm112*Δ where two independent strains were used. The mean for the three strains ± the standard error is shown. p values (T test) were calculated compared to wild-type Ch^{16}-RMYAH. A single blank vector control was also analysed in each genetic background to calculate the spontaneous levels of GC, Ch^{16} loss and LOH and was subtracted to give the break-induced values shown

Genetic background	NHEJ /SCC			GC			Ch^{16} loss			LOH		
	Mean	SE	p	Mean	SE	p	Mean	SE	p	Mean	SE	p
wild-type	4.0	0.6	-	69.2	0.8	-	16.8	0.7	-	9.8	0.3	-
spd1Δ	2.0	0.5	0.03	77.1	0.2	0.00	13.7	1.1	0.08	7.3	0.5	0.02
ku70Δ	2.1	0.1	0.02	86.7	2.5	0.01	7.4	1.2	0.00	3.8	1.6	0.07
ada2Δ	31.9	0.8	0.00	52.6	0.1	0.01	9.0	0.0	0.00	6.1	0.9	0.02
ada2Δ spd1Δ	17.3	2.9	0.04	73.7	2.8	0.25	5.1	0.6	0.00	3.4	0.3	0.00
arp42Δ	63.9	4.7	0.01	19.4	0.7	0.00	7.1	2.7	0.06	9.2	2.6	0.86
arp42Δ spd1Δ	42.8	0.3	0.00	39.3	1.3	0.01	12.4	0.1	0.00	5.1	1.0	0.15
csn1Δ	5.9	0.9	0.16	67.0	1.7	0.32	12.9	1.6	0.12	12.8	1.7	0.22
csn1Δ spd1Δ	0.9	0.4	0.00	91.4	1.2	0.00	3.7	0.3	0.00	3.6	0.6	0.00
gcn5Δ	45.1	3.8	0.01	43.7	2.6	0.01	6.2	1.6	0.01	4.9	0.1	0.00
gcn5Δ spd1Δ	28.2	2.4	0.01	62.6	2.9	0.15	4.0	0.4	0.00	4.9	0.6	0.01
hus1Δ	3.4	1.5	0.74	38.1	3.3	0.01	1.4	0.4	0.00	56.6	2.3	0.00
hus1Δ spd1Δ	5.9	4.2	0.71	32.2	4.5	0.01	0.0	0.5	0.00	60.8	0.3	0.00
liz1Δ	21.2	6.4	0.11	61.6	0.2	0.00	11.1	5.2	0.40	6.1	1.4	0.11
liz1Δ spd1Δ	3.6	0.3	0.54	67.5	1.4	0.34	9.3	2.0	0.05	10.7	1.1	0.49
ngg1Δ	34.9	4.0	0.01	50.3	3.4	0.03	7.5	1.4	0.01	7.0	0.3	0.00

Genetic background	NHEJ /SCC			GC			Ch^{16} loss			LOH		
	Mean	SE	p	Mean	SE	p	Mean	SE	p	Mean	SE	p
ngg1Δ ku70Δ	17.4	1.2	0.00	72.9	0.6	0.01	5.0	1.7	0.01	4.6	1.0	0.03
ngg1Δ ku70Δ spd1Δ	28.5	2.7	0.01	62.3	3.2	0.16	4.0	0.4	0.00	4.9	0.6	0.01
ngg1Δ spd1Δ	18.8	1.1	0.00	66.1	0.9	0.04	9.0	0.8	0.00	6.0	0.9	0.04
pmk1Δ	4.8	1.4	0.66	78.9	4.3	0.15	3.3	1.9	0.03	3.8	2.2	0.50
pmk1Δ spd1Δ	4.0	0.2	0.94	81.2	1.7	0.01	4.9	0.1	0.00	8.7	1.7	0.61
rad1Δ	3.4	1.1	0.65	41.1	2.3	0.00	0.2	0.3	0.00	54.8	3.2	0.01
rad1Δ spd1Δ	2.3	0.2	0.03	44.6	3.2	0.01	1.0	0.2	0.00	51.8	3.6	0.01
rad17 spd1Δ	2.9	0.7	0.25	39.2	1.0	0.00	1.3	0.2	0.00	56.6	1.0	0.00
rad17Δ	4.3	0.7	0.75	32.3	2.0	0.00	1.3	0.6	0.00	61.2	2.1	0.00
rad26Δ	7.4	0.8	0.03	15.6	1.7	0.00	38.4	3.4	0.02	36.3	2.3	0.01
rad26Δ spd1Δ	4.0	1.7	0.99	32.4	3.0	0.00	39.6	0.3	0.00	23.4	1.2	0.01
rad3Δ	7.7	0.7	0.01	17.0	1.0	0.00	45.2	2.3	0.00	29.9	2.3	0.01
rad3Δ spd1Δ	1.8	0.5	0.02	36.8	2.9	0.01	39.7	2.5	0.01	20.6	0.8	0.00
rad9Δ	6.6	1.1	0.12	34.7	2.9	0.00	1.0	0.2	0.00	57.4	2.3	0.00
rad9Δ spd1Δ	2.5	0.8	0.20	43.3	4.2	0.02	0.8	0.2	0.00	52.7	3.6	0.01
swi3Δ	7.5	0.4	0.00	57.5	3.0	0.05	20.2	1.2	0.08	12.5	1.6	0.23
swi3Δ spd1Δ	12.0	0.3	0.02	65.7	1.3	0.34	7.8	0.4	0.00	13.3	1.4	0.37
trm112Δ	4.6	0.1	0.19	66.8	0.7	0.19	18.6	0.1	0.25	10.0	0.8	0.19
trm112Δ spd1Δ	4.9	1.2	0.55	63.0	1.4	0.03	20.1	2.0	0.23	11.8	0.8	0.13
V2-53D9	15.3	2.4	0.00	51.0	1.7	0.00	18.4	1.5	0.35	12.9	1.6	0.12
V2-53D9 *spd1Δ*	7.6	1.4	0.56	64.4	0.5	0.70	18.5	1.3	0.98	7.0	2.5	0.31

Table showing DSB assay results for strains transformed with REP41X-HO plasmids

For wild-type the assay was repeated using three independent strains, for *ngg1*Δ *spd1*Δ *ku70*Δ using two independent strains. The ± the standard error is shown. p values (T test) were calculated compared to wild-type Ch^{16}-RMYAH. A single blank vector control was also analysed in each genetic background to calculate the spontaneous levels of GC, Ch^{16} loss and LOH and was subtracted to give the break-induced values shown

Genetic background	NHEJ /SCC			GC			Ch^{16} loss			LOH		
	Mean	SE	p	Mean	SE	p	Mean	SE	p	Mean	SE	p
wild-type	1.0	0.3	-	64.2	1.4	-	12.0	3.3	-	5.6	1.3	-
***ngg1*Δ *ku70*Δ**	16.3	2.7	0.14	66.1	2.7	0.55	6.0	1.5	0.38	10.4	1.8	0.32

Appendix V Results of the screen to identify deletion strains whose DSB sensitivity is suppressed by deleting *spd1*$^{+}$

For details of how the screen was performed see Chapter 3 Section 3.2.3 and Section 3.2.4.

Table of screen results

M refers to the mean result and p refers to the standard error of the mean. The size of *sens*Δ and *sens*Δ *spd1*Δ colonies grown for 48 hours on untreated media or media treated with 0.1 µg/ml bleocin for 48 hours were measured. The experiment was repeated 5 times and anomalous data excluded. Each *sens*Δ colony size is shown as percentage of wild-type for each particular experiment. Each *sens*Δ *spd1*Δ colony size is shown as a percentage *spd1*Δ for each particular experiment. These results were used to calculate the ratios of *sens*Δ *spd1*Δ : *sens*Δ colony size on bleocin treated plates and the ratios of *sens*Δ *spd1*Δ : *sens*Δ colony size on control plates. The difference between the two ratios was then obtained.

rank	strain		*sens*Δ colony size (% wild-type)				*sens*Δ *spd1*Δ colony size (% *spd1*Δ)				ratio (*sens*Δ *spd1*Δ:*sens*Δ)					
	gene deletion	name	untreated		bleocin		untreated		bleocin		untreated		bleocin		difference	
			M	p	Mv	p	M	p	M	p	M	p	M	p	M	p
1	SPBC29A3.14c	*trt1*	65	5	23	5	51	3	63	3	0.80	0.09	2.90	0.48	2.10	0.47
2	SPBC365.14c	*uge1*	63	6	20	5	64	4	45	9	1.04	0.10	2.78	0.71	1.74	0.63
3	SPAC11E3.08c	*nse6*	70	7	27	8	66	3	52	3	0.96	0.11	2.16	0.48	1.20	0.58
4	SPAC1486.01	*sod2*	75	6	62	13	86	5	112	5	1.15	0.07	2.04	0.53	0.89	0.46
5	SPAC222.12c	*atp2*	63	10	43	8	65	4	76	6	1.14	0.17	1.94	0.23	0.80	0.09
6	SPAC17H9.10c	*ddb1*	62	10	37	13	54	4	48	7	0.92	0.14	1.66	0.61	0.74	0.50
7	SPCC594.06c	*vam7*	72	7	49	14	65	2	67	8	0.92	0.09	1.59	0.44	0.67	0.48
8	SPAC806.05		82	1	45	9	57	7	36	5	0.69	0.08	1.35	0.71	0.66	0.69
9	SPBC215.03c	*csn1*	93	6	53	6	68	6	74	11	0.73	0.04	1.39	0.13	0.66	0.11
10	SPAC9E9.08	*rad26*	88	8	45	7	56	2	52	4	0.65	0.08	1.20	0.17	0.55	0.09
11	SPBC119.08	*pmk1*	75	7	56	13	65	4	69	25	0.86	0.04	1.41	0.73	0.55	0.75
12	SPAC664.07c	*rad9*	84	2	36	4	69	2	51	11	0.83	0.04	1.37	0.19	0.54	0.17
13	SPAC824.05	*vps16*	73	7	49	13	80	7	68	3	1.09	0.03	1.63	0.46	0.54	0.46
14	SPAC644.14c	*rad51*	69	5	34	4	46	2	40	1	0.69	0.08	1.20	0.19	0.51	0.11
15	SPAC17H9.19c	*cdt2*	79	9	52	5	52	5	61	1	0.68	0.10	1.19	0.09	0.51	0.02
16	SPBP35G2.08c	*air1*	81	10	43	5	58	3	52	2	0.75	0.12	1.24	0.14	0.49	0.20
17	SPCC895.07	*alp14*	55	17	43	23	31	1	31	4	0.64	0.21	1.12	0.62	0.48	0.41
18	SPBC216.05	*rad3*	87	9	48	4	64	2	59	8	0.75	0.08	1.22	0.09	0.47	0.15
19	SPAC227.07c	*pab1*	77	6	67	13	54	6	72	10	0.73	0.10	1.19	0.23	0.47	0.16
20	SPBC2G2.01c	*liz1*	64	6	31	5	63	9	42	9	1.03	0.17	1.47	0.40	0.44	0.28
21	SPAC3H8.05c	*mms1*	55	5	30	2	38	4	34	4	0.72	0.12	1.15	0.10	0.44	0.04
22	SPBC23G7.15c	*rpp202*	72	8	73	17	56	4	79	5	0.79	0.05	1.21	0.28	0.42	0.23

rank	strain		*sens*Δ colony size (% wild-type)				*sens*Δ *spd1*Δ colony size (% *spd1*Δ)				ratio (*sens*Δ *spd1*Δ:*sens*Δ)					
	gene deletion	name	untreated		bleocin		untreated		bleocin		untreated		bleocin		difference	
			M	p	Mv	p	M	p	M	p	M	p	M	p	M	p
23	SPAC23D3.09	*arp42*	78	16	28	6	46	8	25	10	0.70	0.16	1.09	0.41	0.38	0.31
24	SPBC30D10.04	*swi3*	78	4	58	9	61	3	63	9	0.79	0.03	1.14	0.13	0.36	0.15
25	SPAC31A2.02	*trm112*	47	5	51	10	58	1	75	3	1.25	0.13	1.60	0.32	0.34	0.22
26	SPBC28F2.10c	*kap1*	95	6	62	13	98	5	81	19	1.04	0.07	1.33	0.13	0.29	0.07
27	SPBC21C3.12c		82	4	54	6	83	6	69	6	1.01	0.06	1.30	0.07	0.28	0.11
28	SPAC1952.07	*rad1*	76	7	43	6	55	8	43	10	0.73	0.09	1.01	0.20	0.28	0.11
29	SPBC557.02c		90	8	76	8	71	5	75	6	0.75	0.03	1.01	0.09	0.26	0.09
30	SPBC30D10.13c	*pdb1*	59	6	76	13	51	3	81	6	0.87	0.04	1.13	0.24	0.26	0.26
31	SPBC106.07c		59	7	73	4	32	4	56	9	0.54	0.02	0.78	0.14	0.23	0.13
32	SPAC14C4.13	*rad17*	79	4	43	6	56	3	39	5	0.71	0.04	0.93	0.13	0.22	0.11
33	SPAC823.04	*rrp36*	102	8	75	7	85	7	71	11	0.85	0.10	1.05	0.29	0.20	0.20
34	SPCC1672.06c	*vip1*	75	9	95	16	97	8	132	9	1.29	0.06	1.49	0.28	0.19	0.22
35	SPBP8B7.16c	*dbp2*	83	7	47	11	84	5	65	8	1.07	0.11	1.27	0.09	0.19	0.10
36	SPAC13G7.07	*arb2*	80	9	63	11	37	1	41	4	0.48	0.05	0.66	0.06	0.19	0.07
37	SPAC17H9.03c	*rdl1*	84	7	92	18	85	5	96	10	1.03	0.08	1.21	0.25	0.18	0.28
38	SPAC1952.05	*gcn5*	102	5	80	8	91	6	88	14	0.90	0.07	1.08	0.07	0.18	0.07
39	SPBC28F2.02	*mep33*	83	5	89	13	76	4	99	20	0.92	0.04	1.09	0.11	0.17	0.08
40	SPAC20G4.04c	*hus1*	74	5	46	6	66	2	50	8	0.89	0.05	1.07	0.08	0.17	0.06
41	SPCC1393.11		75	6	86	13	63	6	80	7	0.84	0.03	1.01	0.16	0.17	0.15
42	SPBC1921.07c	*sgf29*	86	7	65	9	65	9	60	9	0.77	0.11	0.94	0.11	0.17	0.07
43	SPAC11G7.04	*ubi1*	69	13	59	7	24	4	32	5	0.38	0.06	0.55	0.07	0.17	0.07
44	SPBC21D10.10	*bdc1*	86	8	82	10	74	8	87	17	0.88	0.09	1.05	0.11	0.17	0.17
45	SPBC1347.01c	*rev1*	78	7	93	15	67	5	83	4	0.86	0.02	1.02	0.22	0.16	0.21
46	SPCC757.12		80	10	105	20	66	3	96	4	0.86	0.09	1.00	0.24	0.14	0.15
47	SPBC28E12.06c	*lvs1*	53	5	56	10	71	1	80	4	1.37	0.13	1.51	0.25	0.14	0.12
48	SPBC1773.11c	*mug89*	91	6	105	19	86	5	99	9	0.96	0.06	1.09	0.23	0.14	0.27
49	SPBC3B8.10c	*nem1*	82	7	79	10	62	3	72	12	0.76	0.03	0.89	0.04	0.13	0.05
50	SPAC2F3.15	*lsk1*	90	7	93	5	57	3	71	3	0.64	0.06	0.77	0.01	0.13	0.07
51	SPCC584.11c	*svf1*	67	5	47	7	50	3	40	7	0.75	0.01	0.88	0.16	0.13	0.17
52	SPBC3D6.10	*apn2*	87	7	88	12	86	4	96	7	1.00	0.03	1.12	0.09	0.12	0.08
53	SPCC61.02	*spt3*	85	7	95	13	59	5	73	5	0.70	0.01	0.82	0.11	0.12	0.10
54	SPBC16G5.06		75	3	82	12	50	7	62	10	0.66	0.07	0.78	0.10	0.12	0.06
55	SPAC144.02	*iec1*	65	7	37	2	55	7	36	8	0.86	0.08	0.97	0.18	0.11	0.15
56	SPCC4G3.14	*mdj1*	89	6	75	6	75	4	69	10	0.85	0.06	0.96	0.18	0.11	0.13
57	SPAC824.02	*bst1*	66	4	56	8	40	5	41	10	0.60	0.06	0.70	0.11	0.10	0.08
58	SPAC17A5.02c	*dbr1*	68	5	69	8	82	1	90	8	1.22	0.10	1.32	0.07	0.10	0.04
59	SPBC9B6.07	*nop52*	65	9	64	9	72	4	73	13	1.20	0.17	1.30	0.34	0.10	0.25
60	SPCC663.03	*pmd1*	88	9	106	4	75	5	103	4	0.87	0.07	0.97	0.03	0.10	0.07
61	SPBC146.11c	*mug97*	65	6	84	14	68	5	95	14	1.05	0.02	1.15	0.07	0.10	0.06
62	SPBC146.13c	*myo1*	73	13	78	5	81	6	105	23	1.25	0.28	1.34	0.22	0.09	0.27
63	SPAC31G5.15	*psd3*	63	4	115	13	46	6	94	12	0.73	0.04	0.82	0.02	0.09	0.04
64	SPCC188.07	*ccq1*	85	11	79	10	74	6	74	15	0.95	0.16	1.04	0.26	0.09	0.17
65	SPAC140.03	*arb1*	55	5	54	7	37	3	40	5	0.67	0.02	0.76	0.11	0.09	0.09

rank	strain		*sens*Δ colony size (% wild-type)				*sens*Δ *spd1*Δ colony size (% *spd1*Δ)				ratio (*sens*Δ *spd1*Δ:*sens*Δ)					
	gene deletion	name	untreated		bleocin		untreated		bleocin		untreated		bleocin		difference	
			M	p	Mv	p	M	p	M	p	M	p	M	p	M	p
66	SPBC16A3.17c		67	5	77	11	71	4	89	14	1.07	0.06	1.16	0.05	0.09	0.02
67	SPBC543.07	*pek1*	105	10	111	18	49	12	58	3	0.47	0.10	0.55	0.09	0.09	0.03
68	SPCC1450.03		86	9	91	11	81	7	91	5	0.94	0.02	1.02	0.09	0.08	0.07
69	SPAC1B1.04c	*pan3*	77	6	135	7	38	7	76	9	0.49	0.06	0.56	0.07	0.07	0.01
70	SPAC1805.14		89	9	86	6	67	2	72	7	0.76	0.06	0.84	0.04	0.07	0.03
71	SPBC713.07c		85	8	89	8	76	5	85	9	0.93	0.11	1.00	0.17	0.07	0.10
72	SPBC18H10.11c	*ppr2*	72	5	94	12	69	4	99	18	0.96	0.04	1.03	0.07	0.07	0.05
73	SPAC30D11.04c	*nup124*	82	9	74	11	75	9	77	13	0.95	0.13	1.02	0.06	0.07	0.14
74	SPAC694.06c	*mrc1*	100	8	106	12	56	6	65	4	0.56	0.08	0.63	0.09	0.07	0.03
75	SPCC1682.12c	*ubp16*	79	6	100	12	55	3	75	9	0.70	0.04	0.76	0.05	0.07	0.04
76	SPBC16E9.18	*psd1*	89	7	69	8	79	6	67	7	0.91	0.10	0.97	0.06	0.07	0.08
77	SPBC3E7.08c	*rad13*	80	7	92	10	51	1	64	4	0.65	0.07	0.72	0.06	0.06	0.01
78	SPCP20C8.01c		70	5	91	8	50	2	70	9	0.72	0.04	0.78	0.11	0.06	0.13
79	SPAC637.06	*gmh5*	54	4	72	12	64	5	85	8	1.18	0.03	1.24	0.21	0.06	0.19
80	SPAC25H1.07	*emc1*	61	4	47	4	54	4	44	5	0.89	0.06	0.95	0.06	0.06	0.07
81	SPAC9G1.07		90	6	85	16	70	3	68	9	0.79	0.05	0.85	0.10	0.06	0.09
82	SPAC13G6.01c	*rad8*	77	9	98	14	49	4	68	4	0.66	0.10	0.71	0.06	0.05	0.04
83	SPBC902.03	*psp7*	76	4	96	5	47	4	64	9	0.62	0.02	0.67	0.10	0.05	0.08
84	SPCC757.09c	*rnc1*	77	5	84	12	51	9	58	10	0.64	0.10	0.69	0.10	0.05	0.03
85	SPBC651.10	*nse5*	86	6	101	15	60	3	77	13	0.70	0.03	0.75	0.04	0.05	0.04
86	SPAC3H5.11		87	6	105	18	60	7	74	9	0.69	0.08	0.74	0.10	0.05	0.02
87	SPBC342.06c	*rtt109*	90	7	102	6	48	5	59	3	0.54	0.08	0.58	0.05	0.04	0.04
88	SPAC18G6.15	*mal3*	75	7	70	5	55	4	54	2	0.74	0.07	0.78	0.05	0.04	0.04
89	SPAPJ696.01c	*vps17*	77	5	99	10	54	4	75	13	0.71	0.03	0.75	0.09	0.04	0.08
90	SPAC4F10.04	*ypa1*	70	4	50	11	54	4	39	8	0.77	0.01	0.81	0.04	0.04	0.04
91	SPCC4G3.11	*mug154*	78	5	86	14	58	3	65	8	0.74	0.01	0.77	0.06	0.03	0.07
92	SPAC637.09		68	6	112	14	53	4	87	10	0.78	0.02	0.81	0.16	0.03	0.17
93	SPAC1F12.09	*gpi17*	86	9	60	11	65	5	46	8	0.80	0.12	0.82	0.12	0.02	0.18
94	SPAC16.01	*rho2*	76	19	69	30	55	4	52	6	0.57	0.06	0.59	0.11	0.02	0.05
95	SPAC16C9.05	*cph1*	72	4	44	5	62	5	39	8	0.87	0.03	0.88	0.14	0.02	0.12
96	SPBC27.06c	*mgr2*	76	4	96	12	65	3	87	19	0.86	0.03	0.88	0.10	0.02	0.08
97	SPCC285.13c	*nup60*	71	6	73	9	62	5	66	14	0.89	0.10	0.90	0.14	0.02	0.05
98	SPAC23C11.04c	*pnk1*	96	10	76	10	66	8	53	10	0.70	0.10	0.71	0.12	0.01	0.02
99	SPAC9.05	*mfh1*	107	6	142	1	51	11	71	25	0.49	0.13	0.50	0.18	0.01	0.05
100	SPBC83.18c	*fic1*	66	4	81	8	65	1	79	4	0.99	0.08	0.99	0.12	0.00	0.06
101	SPAC1F12.06c		88	7	112	10	77	4	97	5	0.88	0.07	0.88	0.06	0.00	0.08
102	SPCC18.09c	*hnt3*	76	7	81	12	59	4	63	8	0.78	0.03	0.78	0.04	0.00	0.04
103	SPBC32F12.07c		106	8	132	19	61	2	75	4	0.58	0.04	0.58	0.05	0.00	0.06
104	SPBPB2B2.10c	*gal7*	78	8	109	11	49	3	69	4	0.65	0.10	0.65	0.07	0.00	0.04
105	SPCC1442.02		84	5	105	21	55	4	64	10	0.65	0.04	0.65	0.10	0.00	0.06
106	SPBC1604.08c	*imp1*	84	8	116	12	53	1	73	3	0.64	0.05	0.64	0.04	0.00	0.02
107	SPBC21H7.04	*dbp7*	91	8	130	9	57	4	82	10	0.63	0.04	0.62	0.04	0.00	0.02
108	SPCC31H12.08c	*ccr4*	59	6	69	6	65	5	76	5	1.15	0.11	1.14	0.17	0.00	0.16

rank	strain		*sens*Δ colony size (% wild-type)				*sens*Δ *spd1*Δ colony size (% *spd1*Δ)				ratio (*sens*Δ *spd1*Δ:*sens*Δ)					
	gene deletion	name	untreated		bleocin		untreated		bleocin		untreated		bleocin		difference	
			M	p	Mv	p	M	p	M	p	M	p	M	p	M	p
109	SPAC16C9.06c	*upf1*	84	9	105	7	65	9	82	12	0.79	0.12	0.78	0.10	-0.01	0.03
110	SPCC970.07c	*raf2*	74	5	80	6	56	0	61	6	0.77	0.06	0.76	0.02	-0.01	0.08
111	SPBC342.03	*gas4*	63	5	102	7	56	3	89	7	0.89	0.03	0.89	0.11	-0.01	0.12
112	SPAC31A2.15c	*dcc1*	79	4	92	14	57	3	65	10	0.72	0.02	0.71	0.04	-0.01	0.03
113	SPAC17H9.08		44	4	76	12	67	4	111	5	1.55	0.05	1.54	0.20	-0.01	0.16
114	SPCC1020.07		86	7	124	10	51	4	73	2	0.61	0.09	0.59	0.05	-0.01	0.05
115	SPBC4F6.06	*kin1*	91	12	106	21	63	11	73	14	0.71	0.10	0.69	0.04	-0.01	0.07
116	SPBC1105.10	*rav1*	89	9	102	7	48	13	55	15	0.54	0.13	0.52	0.12	-0.02	0.07
117	SPCC576.02		71	5	104	7	74	5	107	12	1.04	0.03	1.03	0.05	-0.02	0.08
118	SPAC8C9.12c		59	5	73	9	63	5	78	11	1.08	0.05	1.06	0.02	-0.02	0.08
119	SPBC725.09c	*hob3*	70	7	97	9	63	6	85	7	0.90	0.01	0.88	0.03	-0.02	0.04
120	SPBC1289.14		97	8	94	7	52	7	47	6	0.54	0.05	0.52	0.09	-0.02	0.05
121	SPBC29A10.16c		65	5	94	15	87	3	118	7	1.35	0.06	1.33	0.24	-0.02	0.18
122	SPAC13A11.01c	*rga8*	82	6	106	10	39	4	49	13	0.48	0.02	0.46	0.11	-0.02	0.09
123	SPAC23E2.01	*fep1*	92	8	96	12	54	13	47	6	0.56	0.13	0.54	0.10	-0.02	0.15
124	SPAC25H1.02	*jmj1*	84	6	120	10	50	2	69	4	0.60	0.06	0.58	0.02	-0.02	0.04
125	SPCC74.09	*mug24*	77	5	85	13	53	8	52	9	0.68	0.08	0.65	0.12	-0.02	0.05
126	SPAC56F8.02		88	10	93	8	68	8	70	7	0.77	0.04	0.75	0.03	-0.03	0.01
127	SPAC1A6.03c		82	8	115	14	78	0	107	7	0.98	0.09	0.95	0.09	-0.03	0.01
128	SPAC29B12.06c	*rcd1*	87	5	99	15	72	4	83	19	0.83	0.02	0.81	0.07	-0.03	0.06
129	SPAC23H3.13c	*gpa2*	89	8	112	13	51	6	61	4	0.59	0.11	0.56	0.10	-0.03	0.01
130	SPCC1739.05	*set5*	58	5	84	16	67	3	89	21	1.18	0.12	1.16	0.23	-0.03	0.19
131	SPAC13C5.06c	*mug121*	66	3	106	4	72	3	111	6	1.08	0.02	1.05	0.07	-0.03	0.05
132	SPBC947.08c	*hip4*	87	6	129	15	45	1	63	4	0.52	0.05	0.50	0.04	-0.03	0.02
133	SPBC1105.05	*exg1*	86	9	117	12	56	11	73	13	0.64	0.09	0.61	0.07	-0.03	0.03
134	SPAC110.02	*pds5*	67	4	49	5	49	4	33	2	0.73	0.07	0.70	0.11	-0.03	0.07
135	SPBC839.03c		76	4	75	9	64	3	61	8	0.84	0.02	0.81	0.03	-0.03	0.04
136	SPBC106.10	*pka1*	63	11	86	20	47	5	60	2	0.83	0.23	0.80	0.21	-0.03	0.02
137	SPAC664.01c	*swi6*	81	6	108	8	49	8	64	18	0.61	0.08	0.57	0.12	-0.03	0.05
138	SPAC227.17c		81	5	115	15	76	6	100	13	0.96	0.14	0.92	0.24	-0.04	0.11
139	SPBC902.02c	*ctf18*	84	8	104	11	59	6	70	12	0.71	0.04	0.67	0.04	-0.04	0.04
140	SPAC1486.04c	*alm1*	73	9	83	16	84	3	89	9	1.19	0.10	1.15	0.24	-0.04	0.15
141	SPCC23B6.05c	*ssb3*	68	4	69	10	64	3	64	11	0.94	0.05	0.91	0.04	-0.04	0.03
142	SPAC1783.07c	*pap1*	90	7	113	10	52	2	60	4	0.58	0.03	0.54	0.02	-0.04	0.02
143	SPAC22H12.04c	*rps102*	113	8	144	7	66	5	79	5	0.59	0.02	0.55	0.03	-0.04	0.03
144	SPCP31B10.05	*tdp1*	86	8	98	13	69	2	75	7	0.83	0.07	0.79	0.06	-0.04	0.06
145	SPBC12C2.02c	*ste20*	75	5	98	6	55	2	68	2	0.74	0.03	0.70	0.03	-0.04	0.02
146	SPCP1E11.04c	*pal1*	60	5	99	5	47	9	73	12	0.77	0.10	0.73	0.11	-0.04	0.01
147	SPBC725.12	*nbl1*	86	7	108	9	56	4	65	4	0.66	0.03	0.61	0.06	-0.04	0.05
148	SPBC342.05	*crb2*	73	5	105	8	53	6	71	4	0.72	0.07	0.68	0.04	-0.05	0.03
149	SPAC6B12.02c	*mus7*	109	10	147	13	63	3	79	2	0.59	0.06	0.54	0.05	-0.05	0.05
150	SPAC15A10.03c	*rad54*	60	9	12	6	34	3	10	6	0.57	0.03	0.53	0.27	-0.05	0.30
151	SPAC25B8.05	*deg1*	76	5	115	19	47	3	65	10	0.62	0.04	0.57	0.04	-0.05	0.04

rank	strain		*sens*Δ colony size (% wild-type)				*sens*Δ *spd1*Δ colony size (% *spd1*Δ)				ratio (*sens*Δ *spd1*Δ:*sens*Δ)					
	gene deletion	name	untreated		bleocin		untreated		bleocin		untreated		bleocin		difference	
			M	p	Mv	p	M	p	M	p	M	p	M	p	M	p
152	SPAPB1A10.09	*ase1*	80	5	97	13	69	3	83	17	0.88	0.07	0.83	0.09	-0.05	0.03
153	SPAC688.10	*rev3*	83	6	116	14	50	3	63	2	0.61	0.04	0.56	0.05	-0.05	0.05
154	SPAC1006.03c	*red1*	69	4	107	9	39	3	55	8	0.57	0.06	0.52	0.09	-0.05	0.10
155	SPBC365.06	*pmt3*	97	8	110	8	73	4	77	2	0.76	0.04	0.71	0.05	-0.05	0.03
156	SPAC6F12.09	*rdp1*	80	4	69	7	45	6	36	3	0.58	0.10	0.53	0.07	-0.05	0.05
157	SPCC11E10.06c	*elp4*	71	5	94	15	62	2	78	13	0.88	0.04	0.83	0.03	-0.05	0.06
158	SPAC694.04c		74	6	100	9	67	2	85	5	0.92	0.06	0.87	0.07	-0.06	0.04
159	SPCC584.01c		60	5	76	17	38	3	43	6	0.64	0.04	0.59	0.08	-0.06	0.06
160	SPBC16A3.03c	*lyn1*	76	5	100	12	71	8	89	10	0.96	0.14	0.90	0.06	-0.06	0.11
161	SPBC1778.09		94	9	132	21	61	6	76	6	0.65	0.06	0.59	0.06	-0.06	0.07
162	SPAC8E11.02c	*rad24*	100	10	122	11	61	1	67	3	0.62	0.06	0.56	0.03	-0.06	0.05
163	SPBC25H2.09		65	4	101	8	72	3	105	4	1.12	0.03	1.05	0.05	-0.06	0.04
164	SPAC19B12.04	*rps3001*	79	6	107	7	54	2	68	5	0.70	0.07	0.63	0.00	-0.07	0.07
165	SPAC1610.02c		86	4	113	11	69	2	85	12	0.80	0.03	0.74	0.04	-0.07	0.03
166	SPAC1002.14	*itt1*	87	7	118	11	61	1	75	3	0.71	0.04	0.64	0.04	-0.07	0.05
167	SPAC1834.12	*pex7*	87	6	127	8	70	4	94	6	0.81	0.05	0.74	0.03	-0.07	0.04
168	SPCC553.01c	*dbl2*	93	5	92	11	65	3	57	7	0.70	0.06	0.63	0.06	-0.07	0.06
169	SPAC821.05		77	5	87	7	81	7	88	12	1.07	0.12	1.00	0.10	-0.07	0.08
170	SPCC188.02	*par1*	80	11	119	7	65	2	90	6	0.83	0.08	0.76	0.05	-0.07	0.05
171	SPBC27.02c	*ask1*	94	10	110	7	70	6	74	2	0.75	0.02	0.68	0.03	-0.07	0.01
172	SPBC16C6.03c		72	6	90	9	69	3	82	13	0.98	0.09	0.91	0.09	-0.07	0.06
173	SPBC1A4.02c	*leu1*	69	4	115	5	53	2	80	6	0.77	0.02	0.70	0.04	-0.07	0.05
174	SPCC2H8.05c	*dbl1*	74	6	91	9	64	4	75	13	0.88	0.08	0.81	0.08	-0.07	0.04
175	SPCP25A2.02c	*rhp26*	64	5	99	6	81	3	119	7	1.27	0.05	1.20	0.06	-0.07	0.00
176	SPBC20F10.07		97	6	120	19	78	5	90	15	0.81	0.04	0.74	0.02	-0.07	0.04
177	SPBC3B8.02	*php5*	60	6	93	8	73	1	108	4	1.25	0.13	1.18	0.06	-0.07	0.17
178	SPCC1753.02c	*git3*	105	11	126	26	79	6	82	2	0.78	0.13	0.70	0.15	-0.07	0.11
179	SPBC26H8.05c	*pph3*	91	8	148	8	52	5	73	11	0.57	0.01	0.49	0.08	-0.07	0.08
180	SPAC9G1.05	*aip1*	75	8	121	18	51	4	75	9	0.70	0.13	0.63	0.08	-0.08	0.05
181	SPCC417.02	*dad5*	77	6	103	12	70	4	85	10	0.91	0.05	0.83	0.04	-0.08	0.05
182	SPBC27B12.11c	*pho7*	99	9	128	7	74	3	88	5	0.77	0.07	0.69	0.03	-0.08	0.05
183	SPBC1105.04c	*cbp1*	70	4	101	14	46	3	57	2	0.66	0.08	0.59	0.07	-0.08	0.04
184	SPBC25H2.08c	*mrs2*	75	5	128	4	73	5	115	6	0.98	0.02	0.90	0.02	-0.08	0.03
185	SPBC15C4.04c		75	7	106	15	67	3	84	5	0.90	0.05	0.82	0.07	-0.08	0.05
186	SPAC2E1P3.04	*cao1*	103	8	146	8	66	3	83	8	0.65	0.07	0.57	0.04	-0.08	0.03
187	SPCC594.02c		58	7	58	7	53	8	46	8	0.92	0.10	0.84	0.17	-0.08	0.07
188	SPBC56F2.08c		63	3	81	7	54	2	63	7	0.85	0.03	0.77	0.04	-0.08	0.04
189	SPAC17G8.14c	*pck1*	71	6	111	9	52	6	71	10	0.72	0.03	0.64	0.07	-0.08	0.07
190	SPBC11B10.07c	*ivn1*	107	9	144	6	79	4	97	5	0.76	0.07	0.68	0.04	-0.08	0.06
191	SPCC4G3.15c	*not2*	99	9	134	11	81	7	100	16	0.83	0.08	0.74	0.07	-0.08	0.09
192	SPAC18G6.02c	*chp1*	80	6	100	9	61	6	69	12	0.79	0.10	0.70	0.14	-0.08	0.09
193	SPBC651.09c	*prf1*	83	12	109	12	57	2	68	3	0.72	0.10	0.64	0.08	-0.08	0.14
194	SPCC1259.03	*rpa12*	65	6	100	11	80	3	114	6	1.24	0.08	1.16	0.09	-0.08	0.01

rank	strain		*sens*Δ colony size (% wild-type)				*sens*Δ *spd1*Δ colony size (% *spd1*Δ)				ratio (*sens*Δ *spd1*Δ:*sens*Δ)					
	gene deletion	name	untreated		bleocin		untreated		bleocin		untreated		bleocin		difference	
			M	p	Mv	p	M	p	M	p	M	p	M	p	M	p
195	SPBC839.05c	*rps1701*	63	3	95	15	50	3	64	7	0.79	0.04	0.70	0.08	-0.09	0.05
196	SPBC1604.03c		68	5	111	9	93	1	144	8	1.39	0.10	1.30	0.08	-0.09	0.03
197	SPBC21C3.18	*spo4*	87	8	130	12	51	5	65	4	0.59	0.02	0.50	0.02	-0.09	0.03
198	SPAC20H4.07	*rad57*	91	9	110	19	70	5	75	9	0.78	0.06	0.69	0.03	-0.09	0.06
199	SPAC23C11.14	*zhf1*	98	7	141	8	65	6	82	3	0.68	0.08	0.59	0.01	-0.09	0.07
200	SPAC1002.15c	*pcm5*	65	11	66	10	49	5	51	7	0.91	0.32	0.82	0.09	-0.09	0.24
201	SPAPB1E7.06c	*eme1*	63	5	116	12	42	3	68	7	0.68	0.09	0.59	0.06	-0.09	0.06
202	SPCC1450.02	*bdf1*	74	9	56	6	62	7	42	4	0.84	0.00	0.75	0.01	-0.09	0.01
203	SPAC222.08c		48	4	80	14	32	2	45	7	0.67	0.05	0.58	0.05	-0.09	0.03
204	SPCC895.05	*for3*	80	8	109	9	65	3	80	4	0.83	0.06	0.73	0.03	-0.09	0.05
205	SPBC2G2.13c	*dcd1*	75	9	98	14	72	4	90	17	1.00	0.08	0.91	0.07	-0.09	0.05
206	SPAPB2B4.04c	*pmc1*	81	6	126	9	68	3	94	4	0.85	0.03	0.75	0.04	-0.09	0.02
207	SPAC732.02c		69	6	106	8	76	3	107	2	1.11	0.07	1.01	0.06	-0.09	0.02
208	SPAC4F10.19c		70	5	87	9	72	4	84	15	1.06	0.11	0.96	0.11	-0.09	0.08
209	SPBC19C7.12c	*omh1*	73	5	92	12	57	3	64	8	0.79	0.03	0.69	0.03	-0.10	0.05
210	SPAC4H3.05	*srs2*	84	6	111	18	69	3	83	15	0.84	0.06	0.75	0.06	-0.10	0.03
211	SPAC19G12.13c	*poz1*	67	4	93	12	71	5	88	7	1.06	0.06	0.96	0.06	-0.10	0.09
212	SPCC330.02	*rhp7*	82	9	116	16	60	3	73	6	0.74	0.06	0.64	0.03	-0.10	0.04
213	SPAC12G12.12		100	4	135	15	70	2	80	5	0.70	0.02	0.60	0.03	-0.10	0.03
214	SPBC2G2.14	*csi1*	72	7	90	12	57	3	62	1	0.81	0.11	0.71	0.08	-0.10	0.03
215	SPBC691.04		61	3	84	10	70	4	86	5	1.14	0.04	1.04	0.12	-0.10	0.10
216	SPAC13C5.04		82	6	88	13	65	4	63	11	0.81	0.07	0.71	0.05	-0.10	0.03
217	SPBC1718.07c	*zfs1*	78	10	89	8	79	7	80	11	1.08	0.16	0.98	0.21	-0.10	0.09
218	SPAC22F3.10c	*gcs1*	76	2	118	9	31	3	34	5	0.41	0.02	0.30	0.06	-0.11	0.06
219	SPBC21B10.03c	*ath1*	76	5	68	7	66	5	51	3	0.88	0.04	0.77	0.09	-0.11	0.13
220	SPAC23H3.06	*apl6*	89	7	108	4	67	9	68	9	0.74	0.06	0.64	0.11	-0.11	0.06
221	SPBC1861.03	*mak10*	106	8	148	17	81	4	100	17	0.77	0.03	0.66	0.03	-0.11	0.05
222	SPCC794.09c	*tef101*	69	4	113	6	42	4	57	8	0.61	0.03	0.51	0.07	-0.11	0.05
223	SPAC1A6.09c	*lag1*	69	3	108	4	69	7	95	13	0.98	0.05	0.88	0.10	-0.11	0.06
224	SPAC11E3.04c	*ubc13*	53	5	79	11	77	1	103	5	1.49	0.14	1.37	0.24	-0.11	0.11
225	SPAC22F8.11	*plc1*	84	7	126	16	62	0	80	13	0.74	0.05	0.63	0.02	-0.11	0.04
226	SPBC776.15c	*kgd2*	103	7	150	21	85	4	104	7	0.83	0.08	0.72	0.11	-0.11	0.16
227	SPCC18B5.06	*erf1*	73	5	99	16	65	2	77	13	0.91	0.05	0.79	0.07	-0.11	0.03
228	SPCC162.10	*ppk33*	94	9	123	8	66	2	74	4	0.71	0.06	0.60	0.02	-0.11	0.05
229	SPCC126.04c	*sgf73*	92	7	151	16	69	4	96	10	0.75	0.05	0.64	0.02	-0.11	0.05
230	SPBC31F10.15c	*atp15*	56	3	109	8	30	2	44	7	0.53	0.05	0.41	0.08	-0.11	0.05
231	SPCC188.10c		80	6	117	14	75	4	95	10	0.95	0.07	0.83	0.09	-0.11	0.08
232	SPAC6B12.08	*mug185*	62	4	74	12	50	5	50	6	0.81	0.10	0.70	0.08	-0.12	0.05
233	SPCC576.13	*swc5*	78	6	113	9	57	1	69	4	0.74	0.05	0.62	0.03	-0.12	0.06
234	SPAC19B12.06c		65	5	98	6	61	3	81	7	0.95	0.05	0.83	0.05	-0.12	0.08
235	SPCC126.08c		94	6	126	11	65	2	72	2	0.69	0.03	0.58	0.03	-0.12	0.04
236	SPBC577.10	*pre3*	76	7	104	16	88	6	105	12	1.19	0.15	1.07	0.17	-0.12	0.10
237	SPBC1E8.03c		79	4	106	11	84	5	101	11	1.08	0.09	0.96	0.08	-0.12	0.09

rank	strain		*sens*Δ colony size (% wild-type)				*sens*Δ *spd1*Δ colony size (% *spd1*Δ)				ratio (*sens*Δ *spd1*Δ:*sens*Δ)					
	gene deletion	name	untreated		bleocin		untreated		bleocin		untreated		bleocin		difference	
			M	p	Mv	p	M	p	M	p	M	p	M	p	M	p
238	SPAC3G6.06c	*rad2*	77	6	118	7	88	5	121	7	1.14	0.04	1.02	0.07	-0.12	0.06
239	SPCC126.13c		65	8	94	17	78	5	96	19	1.26	0.14	1.14	0.23	-0.12	0.15
240	SPBC23E6.08	*sat1*	76	6	37	4	67	4	30	8	0.89	0.05	0.77	0.12	-0.12	0.12
241	SPAC29B12.08	*clr5*	77	5	93	14	89	4	97	17	1.16	0.06	1.03	0.06	-0.12	0.02
242	SPAC144.06	*apl5*	74	5	82	12	81	5	81	14	1.11	0.04	0.98	0.07	-0.13	0.04
243	SPBC16C6.04	*dbi6*	93	7	123	8	79	4	91	7	0.87	0.07	0.74	0.06	-0.13	0.05
244	SPAC6F6.01	*cch1*	96	9	115	13	64	3	64	11	0.68	0.06	0.55	0.04	-0.13	0.06
245	SPAPB1A11.01	*mfc1*	79	7	109	11	83	5	102	10	1.08	0.12	0.95	0.07	-0.13	0.09
246	SPBC27.08c	*sua1*	71	5	121	7	47	7	63	8	0.65	0.05	0.52	0.05	-0.13	0.01
247	SPBC56F2.05c		83	7	119	22	74	4	90	15	0.91	0.05	0.78	0.06	-0.13	0.03
248	SPBC25H2.10c		69	7	93	12	64	2	76	11	0.95	0.08	0.81	0.02	-0.14	0.09
249	SPAC12B10.12c	*rhp41*	74	8	109	13	53	7	64	9	0.72	0.04	0.59	0.04	-0.14	0.01
250	SPBC14C8.17c	*spt8*	87	6	136	25	72	6	93	19	0.84	0.08	0.71	0.10	-0.14	0.06
251	SPBC725.10		75	8	106	12	63	2	76	7	0.85	0.08	0.71	0.01	-0.14	0.08
252	SPAC4G8.05	*ppk14*	85	6	113	7	56	7	61	11	0.67	0.09	0.53	0.07	-0.14	0.03
253	SPAC19B12.10	*sst2*	78	5	109	8	60	2	71	18	0.78	0.08	0.64	0.12	-0.14	0.04
254	SPAC9.02c		66	6	77	8	77	4	82	13	1.19	0.09	1.05	0.07	-0.14	0.08
255	SPAC15E1.02c		63	4	110	6	82	3	128	8	1.31	0.06	1.16	0.02	-0.14	0.06
256	SPAC1071.02	*mms19*	61	3	115	22	20	10	24	21	0.33	0.16	0.18	0.15	-0.15	0.01
257	SPAC1783.02c	*vps66*	77	5	119	6	66	6	84	10	0.85	0.04	0.70	0.08	-0.15	0.05
258	SPAC1002.03c	*gls2*	69	5	88	12	73	2	81	7	1.08	0.06	0.93	0.05	-0.15	0.09
259	SPCC1020.11c	*ecm6*	64	4	43	6	56	8	32	9	0.87	0.07	0.72	0.15	-0.15	0.12
260	SPCC645.05c	*myo2*	76	7	104	13	82	5	96	7	1.12	0.12	0.97	0.11	-0.15	0.16
261	SPBC19G7.18c		70	5	94	11	70	4	84	19	1.02	0.09	0.87	0.10	-0.15	0.06
262	SPAC328.10c	*rps502*	67	5	110	12	51	6	68	15	0.76	0.11	0.61	0.09	-0.15	0.02
263	SPAC9E9.13	*wos2*	74	6	107	14	62	4	75	10	0.85	0.04	0.70	0.04	-0.15	0.06
264	SPCC188.13c	*dcr1*	77	9	105	5	51	5	55	7	0.67	0.02	0.52	0.06	-0.15	0.06
265	SPAC57A7.12	*pdr13*	64	7	106	8	65	2	93	3	1.04	0.08	0.89	0.04	-0.15	0.05
266	SPBC2F12.12c	*cay1*	70	6	123	9	70	2	106	5	1.02	0.08	0.87	0.02	-0.15	0.06
267	SPAC24H6.03	*cul3*	87	9	127	13	65	7	75	9	0.75	0.03	0.59	0.02	-0.16	0.05
268	SPBC19C2.14	*smd3*	80	5	68	6	51	9	34	16	0.63	0.08	0.47	0.22	-0.16	0.17
269	SPBC26H8.12		42	1	61	3	67	7	86	9	1.59	0.20	1.43	0.19	-0.16	0.06
270	SPBC691.05c		62	5	102	10	87	5	127	7	1.42	0.04	1.25	0.08	-0.16	0.04
271	SPBC215.08c	*arg4*	67	6	105	12	77	2	105	12	1.16	0.08	0.99	0.03	-0.17	0.05
272	SPAC4D7.06c		67	6	126	8	58	5	88	8	0.87	0.02	0.70	0.05	-0.17	0.06
273	SPBC13E7.08c	*leo1*	68	4	110	4	100	1	145	5	1.49	0.09	1.32	0.01	-0.17	0.08
274	SPAC15A10.06		80	8	119	16	83	4	101	7	1.04	0.06	0.87	0.06	-0.17	0.03
275	SPBC21B10.10	*rps402*	77	6	107	9	70	8	80	16	0.95	0.15	0.78	0.17	-0.18	0.04
276	SPAC1F3.10c	*39722*	75	6	120	7	89	4	122	8	1.20	0.05	1.02	0.01	-0.18	0.05
277	SPBC543.03c	*pku80*	77	4	115	16	47	3	50	7	0.62	0.03	0.44	0.03	-0.18	0.02
278	SPAC1F3.02c	*mkh1*	80	5	92	6	58	5	50	8	0.72	0.04	0.54	0.07	-0.18	0.07
279	SPAC4F10.18	*nup37*	88	7	123	16	76	4	88	16	0.90	0.10	0.70	0.06	-0.19	0.07
280	SPAC17G8.05	*med20*	67	4	87	6	77	5	84	3	1.18	0.14	0.99	0.08	-0.19	0.10

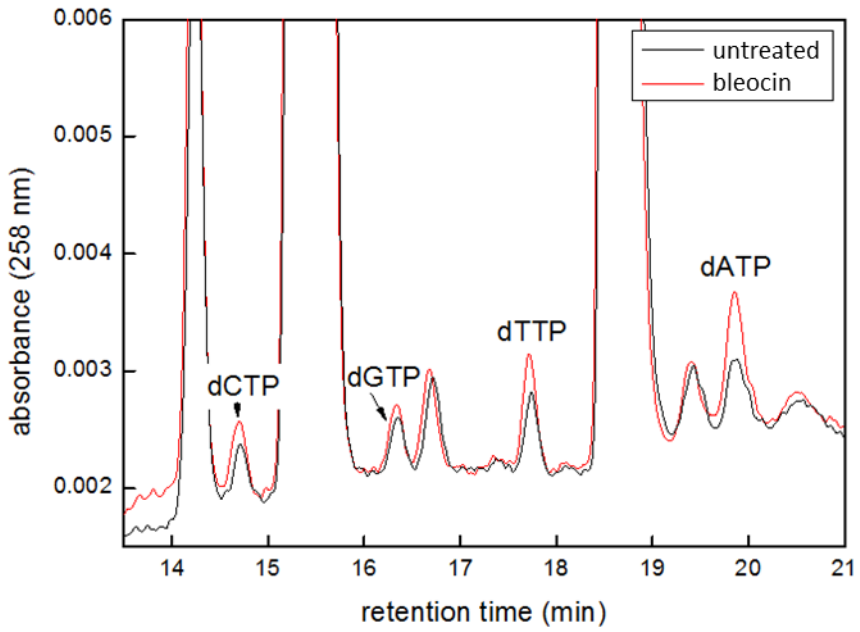
rank	strain		*sens*Δ colony size (% wild-type)				*sens*Δ *spd1*Δ colony size (% *spd1*Δ)				ratio (*sens*Δ *spd1*Δ:*sens*Δ)					
	gene deletion	name	untreated		bleocin		untreated		bleocin		untreated		bleocin		difference	
			M	p	Mv	p	M	p	M	p	M	p	M	p	M	p
281	SPAC513.03	*mfm2*	55	2	91	18	60	7	73	10	1.08	0.12	0.88	0.16	-0.20	0.05
282	SPBC17G9.07	*rps2402*	66	7	96	7	60	4	72	12	0.97	0.14	0.77	0.13	-0.20	0.05
283	SPCC1739.06c		83	6	135	14	41	5	40	8	0.49	0.04	0.29	0.04	-0.20	0.02
284	SPCC18B5.11c	*cds1*	80	5	117	17	72	7	82	8	0.91	0.08	0.71	0.03	-0.21	0.12
285	SPAC1805.07c	*dad2*	61	4	79	8	69	3	77	15	1.15	0.07	0.95	0.10	-0.21	0.04
286	SPBC31F10.09c	*nut2*	56	7	61	5	37	4	29	5	0.67	0.11	0.46	0.05	-0.21	0.07
287	SPAC8C9.10c	*rpp14*	74	6	108	16	79	6	96	20	1.08	0.10	0.87	0.07	-0.22	0.04
288	SPCC550.12	*arp6*	86	6	152	7	63	6	77	6	0.73	0.02	0.51	0.02	-0.22	0.03
289	SPAC1071.07c	*rps1502*	59	2	94	3	58	6	72	8	0.99	0.07	0.76	0.06	-0.23	0.08
290	SPAC31G5.18c	*sde2*	82	6	125	13	97	2	116	8	1.20	0.06	0.94	0.05	-0.26	0.09
291	SPBC428.08c	*clr4*	66	6	111	14	50	6	54	6	0.76	0.07	0.49	0.02	-0.26	0.07
292	SPAC17C9.13c	*cut8*	99	5	146	5	86	5	89	5	0.88	0.08	0.61	0.03	-0.27	0.07
293	SPBC24C6.10c	*dip1*	50	4	127	16	53	1	101	8	1.07	0.10	0.80	0.04	-0.27	0.08
294	SPBC36.04	*cys11*	64	4	107	10	33	3	26	8	0.51	0.02	0.24	0.07	-0.27	0.06
295	SPAC1687.12c	*coq4*	44	2	51	2	23	3	12	1	0.52	0.09	0.24	0.02	-0.28	0.07
296	SPAC1527.02	*sft2*	57	3	62	4	53	5	40	13	0.92	0.05	0.63	0.20	-0.29	0.19
297	SPAC4G9.16c	*rpl901*	79	5	112	14	68	7	66	14	0.88	0.11	0.58	0.07	-0.30	0.04
298	SPAC823.05c	*tlg2*	72	5	42	6	41	1	11	8	0.57	0.02	0.27	0.18	-0.30	0.20
299	SPBC660.14	*mik1*	67	6	132	13	69	3	103	21	1.06	0.09	0.75	0.09	-0.32	0.11
300	SPAC3A12.13c		40	3	70	3	60	1	80	5	1.50	0.13	1.15	0.01	-0.35	0.15
301	SPAC26H5.05	*mga2*	71	14	84	14	43	2	26	7	0.65	0.11	0.30	0.04	-0.35	0.15
302	SPBC4F6.10	*vps901*	102	7	27	6	74	8	10	5	0.74	0.10	0.34	0.18	-0.40	0.18
303	SPCC364.03	*rpl1702*	42	3	77	11	54	6	61	9	1.34	0.19	0.81	0.08	-0.53	0.23
304	SPAC25A8.01c	*fft3*	81	7	165	12	82	1	73	7	1.03	0.08	0.45	0.05	-0.59	0.03

Table of strains excluded from the screen

gene deletion	name	reason for exclusion
SPCC576.12c	*mhf2*	strain could not be woken from the V1 or V2 Bioneer *S. pombe* haploid deletion libraries
SPCC553.04	*cyp9*	
SPCC1259.08		
SPCC18.06c	*caf1*	
SPAC29A4.16	*hal1*	
SPBC32F12.01c	*css1*	
SPAC17G6.04c	*cpp1*	
SPBPB2B2.08		
SPAC3C7.03c	*rhp55*	*sens*Δ *spd1*Δ strain could not be isolated
SPCC1393.10	*ctr4*	
SPCC1682.15	*mug122*	
SPBC31F10.10c		
SPBP8B7.28c	*stc1*	
SPAC3H8.10	*spo20*	

gene deletion	name	reason for exclusion
SPAC4D7.03	*pop2*	
SPAC1142.07c	*vps32*	
SPAC19G12.08	*scs7*	
SPCC126.15c	*sec65*	
SPAC31A2.11c	*cuf1*	
SPAC1782.05	*ypa2*	
SPAC20H4.02	*dsc3*	*sens*Δ *spd1*Δ strain did not grow during the screen
SPAC29B12.04	*snz1*	
SPAC227.01c	*erd1*	
SPCC306.06c		
SPBC27B12.06	*gpi13*	
SPBC56F2.11	*met6*	
SPBC2A9.08c	*sec22*	
SPBC649.03	*rhp14*	
SPAC4D7.11	*dsc4*	
SPAC13C5.07	*rad32*	*sens*Δ strain did not grow during the screen
SPCC825.03c	*psy1*	
SPBC409.15	*tsr1*	
SPAC13A11.04c	*ubp8*	
SPBC2D10.18	*abc1*	
SPCC777.13	*vps35*	
SPAC8C9.03	*cgs1*	
SPBC21.02	*rtc5*	*sens*Δ and *sens*Δ *spd1*Δ strains did not grow during the screen
SPBC947.02	*alp2*	
SPCC338.16	*pof3*	
SPAC4C5.02c	*ryh1*	
SPAC13G6.14	*aps1*	
SPCC338.08	*ctp1*	
SPBC25D12.06		
SPAC29B12.05c		
SPAC31A2.13c	*sft1*	anomalous results excluded
SPAC11G7.02	*pub1*	
SPCP1E11.05c	*are2*	
SPAC27F1.08	*pdt1*	
SPBC1773.12		

Appendix VI HPLC analysis of wild-type in the presence or absence of DNA damage



This figure was provided by Lisa Folkes (Department of Oncology, University of Oxford). Chromatogram showing the output of HPLC analysis of dNTP levels for a wild-type strain grown in the presence (red) or absence (black) of 2µg/ml bleocin for 2 hours.

Appendix VII Publications

Blaikley, E.J., Tinline-Purvis, H., Kasparek, T.R., Marguerat, S., Sarkar, S., Hulme, L., Hussey, S., Wee, B.Y., Deegan, R.S., Walker, C.A., Pai, C.C., Bahler, J., Nakagawa, T., and Humphrey, T.C. (2014). The DNA damage checkpoint pathway promotes extensive resection and nucleotide synthesis to facilitate homologous recombination repair and genome stability in fission yeast. Nucleic Acids Res *42*, 5644-5656.

URL: http://nar.oxfordjournals.org/content/42/9/5644.long

Pai, C.C., Deegan, R.S., Subramanian, L., Gal, C., Sarkar, S., Blaikley, E.J., Walker, C., Hulme, L., Bernhard, E., Codlin, S., Bahler, J., Allshire, R., Whitehall, S., and Humphrey, T.C. (2014). A histone H3K36 chromatin switch coordinates DNA double-strand break repair pathway choice. Nat Commun *5*, 4091

URL: http://www.nature.com/ncomms/2014/140609/ncomms5091/full/ncomms5091.html

Pai, C.C., Blaikley, E.J., Humphrey, T., (2014) The DNA Double-Strand Break Repair Assay. The Laboratory Manual on Fission Yeast Methodology, Cold Spring Habor [IN PRESS]